

AT&T

July–August 1985 Vol. 64 No. 6 Part 1

TECHNICAL
JOURNAL

A JOURNAL OF THE AT&T COMPANIES

Digital Data Transmission

Single-Tone Location

Indoor Wireless Communication

Speech Modeling and Processing

EDITORIAL BOARD

	M. IWAMA, <i>Board Chairman</i> ¹	
S. M. BAUMAN ²	P. A. GANNON ⁴	J. S. NOWAK ¹
W. F. BRINKMAN ³	W. R. HARLIN ⁵	L. C. SEIFERT ⁶
J. CHERNAK ¹	T. J. HERR ⁴	W. E. STRICH ⁷
M. F. COCCA ¹	D. M. HILL ⁵	J. W. TIMKO ¹
B. R. DARNALL ¹	D. HIRSCH ²	V. A. VYSSOTSKY ¹
A. FEINER ²	S. HORING ¹	J. H. WEBER ⁸

¹ AT&T Bell Laboratories ² AT&T Information Systems ³ Sandia National Laboratories
⁴ AT&T Network Systems ⁵ AT&T Technology Systems ⁶ AT&T Technologies
⁷ AT&T Communications ⁸ AT&T

EDITORIAL STAFF

P. WHEELER, <i>Managing Editor</i>	A. M. SHARTS, <i>Assistant Editor</i>
L. S. GOLLER, <i>Assistant Editor</i>	B. VORCHHEIMER, <i>Circulation</i>

AT&T TECHNICAL JOURNAL (ISSN 8756-2324) is published ten times each year by AT&T, 550 Madison Avenue, New York, NY 10022; C. L. Brown, Chairman of the Board; L. L. Christensen, Secretary. The Computing Science and Systems section and the special issues are included as they become available. Subscriptions: United States—1 year \$35; foreign—1 year \$45.

Payment for foreign subscriptions or single copies must be made in United States funds, or by check drawn on a United States bank and made payable to the AT&T Technical Journal, and sent to AT&T Bell Laboratories, Circulation Dept., Room 1E335, 101 J. F. Kennedy Pky, Short Hills, NJ 07078.

Back issues of the special, single-subject supplements may be obtained by writing to the AT&T Customer Information Center, P.O. Box 19901, Indianapolis, Indiana 46219, or by calling (800) 432-6600. Back issues of the general, multisubject issues may be obtained from University Microfilms, 300 N. Zeeb Road, Ann Arbor, Michigan 48106.

Single copies of material from this issue of the Journal may be reproduced for personal, noncommercial use. Permission to make multiple copies must be obtained from the Editor.

Printed in U.S.A. Second-class postage paid at Short Hills, NJ 07078 and additional mailing offices. Postmaster: Send address changes to the AT&T Technical Journal, Room 1E335, 101 J. F. Kennedy Pky, Short Hills, NJ 07078.

Copyright © 1985 AT&T.

AT&T TECHNICAL JOURNAL

VOL. 64

JULY-AUGUST 1985

NO. 6, PART 1

Copyright © 1985 AT&T. Printed in U.S.A.

Digital Transmission Over Cross-Coupled Linear Channels	1147
J. Salz	
Tone Location by Cyclotomic Filters	1161
D. Hertz, R. P. Kurshan, D. Malah, and J. T. Peoples	
Performance of Nondiversity Receivers for Spread Spectrum in Indoor Wireless Communications	1181
M. Kavehrad	
Recognition of Isolated Digits Using Hidden Markov Models With Continuous Mixture Densities	1211
L. R. Rabiner, B.-H. Juang, S. E. Levinson, and M. M. Sondhi	
Maximum-Likelihood Estimation for Mixture Multivariate Stochastic Observations of Markov Chains	1235
B.-H. Juang	
Some Properties of Continuous Hidden Markov Model Representations	1251
L. R. Rabiner, B.-H. Juang, S. E. Levinson, and M. M. Sondhi	
Variable-Length Packetization of μ-Law PCM Speech	1271
R. Steele and F. Benjamin	
PAPERS BY AT&T BELL LABORATORIES AUTHORS	1293

Digital Transmission Over Cross-Coupled Linear Channels

By J. SALZ*

(Manuscript received January 14, 1985)

For a multiuser data communications system operating over a mutually cross-coupled linear channel with additive noise sources, we determine the following: (1) a linear cross-coupled receiver processor (filter) that yields the least-mean-squared error between the desired outputs and the actual outputs, and (2) a cross-coupled transmitting filter that optimally distributes the total available power among the different users, as well as the total available frequency spectrum. The structure of the optimizing filters is similar to the known 2×2 case encountered in problems associated with digital transmission over dually polarized radio channels.

I. INTRODUCTION

A variety of communication channels can be modeled as multi-input, multi-output, mutually cross-coupled linear networks with additive noise sources. A few examples of communications systems operating over such channels are dually polarized radio systems, frequency/time-division multiplexing with crosstalk, cordless PBXs, spread-spectrum multiuser systems, and multisensor radar/sonar systems. In many applications it is beneficial to design cross-coupled transmitters and receivers that take advantage of the inherent mutual interferences. The chief purpose of this paper is to explore these issues from a theoretical point of view.

The general problem we address follows. We consider an N input-

* AT&T Bell Laboratories.

Copyright © 1985 AT&T. Photo reproduction for noncommercial use is permitted without payment of royalty provided that each reproduction is done without alteration and that the Journal reference and copyright notice are included on the first page. The title and abstract, but no other portions, of this paper may be copied or distributed royalty free by computer-based and other information-service systems without further permission. Permission to reproduce or republish any other portion of this paper must be obtained from the Editor.

port, N output-port, linear transmission channel characterized by an $N \times N$ complex matrix frequency transfer function, $C(\omega)$, where the entries in $C(\omega)$, $C_{ij}(\omega)$, $i, j = 1 \dots N$, represent the transfer characteristics from input i to output j . Digital data signals $D_i(t)$, $i = 1 \dots N$ are intended for simultaneous transmission over this medium. The general problem we address is as follows: how does one jointly optimize the $2N^2$ entries of cross-coupled linear receiving and transmitting matrix filters when the performance criterion is total Mean-Squared Error (MSE) subject to a constraint on the total average transmitted power? The general setup is shown schematically in Fig. 1.

This paper includes generalizations to $N(N \geq 2)$ dimensions of earlier work dealing with digital data transmission over dually polarized radio channels.^{1,2} As far as can be determined, these generalizations have not been reported in the open literature. We found, however, two early papers^{3,4} dealing with multi-input, multi-output, communications that might be of interest to the reader in connection with our problem. For additive Gaussian noise sources the Shannon capacity of the type of channel considered here has also been determined.⁵

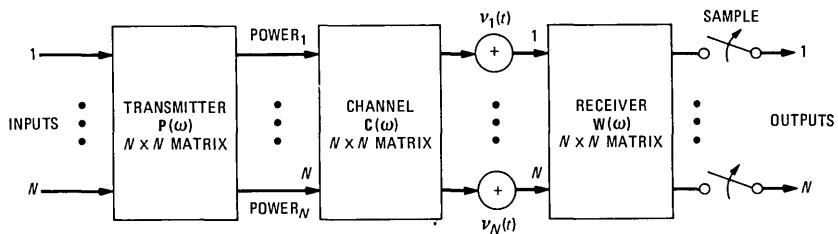
After formulating the problem in the next section, we derive the optimal matrix receiving filter structure and provide a closed-form formula for the least MSE. In Section IV we address and solve the optimum transmitter problem, while the last section has our concluding remarks.

II. PROBLEM FORMULATION

Consider a linear communications medium characterized by N^2 (N is an arbitrary integer) real impulse response functions,

$$h_{lj}(t) = \int_{-\infty}^{\infty} H_{lj}(\omega) e^{i\omega t} \frac{d\omega}{2\pi}, \quad l, j = 1, 2 \dots N, \quad (1)$$

where $H_{lj}(\omega)$, $l, j = 1 \dots N$ are the complex frequency transfer characteristics from input l to output j . The representation in (1) characterizes a linear medium with N inputs and N outputs where



Σ POWER = CONSTANT

Fig. 1—Multi-input, multi-output data communications.

$h_{lj}(t)$ is interpreted as the output of the j th medium when the l th input is a unit impulse. More compactly, let $\mathbf{h}(t)$ represent the $N \times N$ impulse response matrix with entries $h_{lj}(t)$. Now the diagonal entries stand for the direct-channel impulse responses, while the off-diagonal terms are the cross-interference impulse responses.

In the present situation we have in mind that N real data signals,

$$D_l(t) = \sum_n a_n^{(l)} g(t - nT), \quad l = 1 \dots N, \quad (2)$$

where $\{a_n^{(l)}\}$ are the data symbols, are intended for simultaneous transmission over the N channels. Mutual dispersive cross coupling, intersymbol interference, and noise distort these signals, and the purpose here is to devise transmitting and receiving processors to mitigate against these interferences.

The present model also accommodates bandpass coherent data signals in which case (2) represents the baseband-equivalent signals with complex data symbols. In our general formulation, however, we can get by with only real data symbols since complex numbers are isomorphic to 2×2 real matrices.*

Returning to the general formulation, the N data sequences are now represented by the column vectors

$$\mathbf{A}_n = \begin{bmatrix} a_n^{(1)} \\ \vdots \\ a_n^{(N)} \end{bmatrix}, \text{ all } n,$$

and the data signal is thus represented by an N -dimensional vector,

$$\mathbf{D}(t) = \sum_n \mathbf{A}_n g(t - nT). \quad (3)$$

Consequently, the channel output signal can be represented as the vector time function,

$$\mathbf{S}(t) = \sum_n \mathbf{H}(t - nT) \mathbf{A}_n, \quad (4)$$

where the matrix $\mathbf{H}(t)$ is the convolution

$$\mathbf{H}(t) = \int_{-\infty}^{\infty} g(t - \tau) \mathbf{h}(\tau) d\tau, \quad (5)$$

and the $N \times N$ matrix $\mathbf{h}(t)$ has entries defined in (1).

For the sake of clarity, we restrict our treatment to $N \times N$ transmitter and receiver filters, while we recognize applications where it

* References 1 and 2 exploit this isomorphism effectively in the treatment of quadrature amplitude modulated systems over bandpass channels.

would be necessary to handle nonsquare matrices. This does not, however, restrict our approach, as will become evident.

Proceeding with the analysis, we presume that a noise vector $\nu(t)$ is added to (4) and the sum signal is passed through an $N \times N$ matrix receiver filter denoted by $\mathbf{W}(t)$. A representative sample of the output vector taken at $t = 0$ (without loss of generality) yields

$$\mathbf{S}_0 = \mathbf{U}_0\mathbf{A}_0 + \sum_{\substack{n \\ n \neq 0}} \mathbf{U}_n\mathbf{A}_n + \nu_0, \quad (6)$$

where

$$\mathbf{U}_n = \int_{-\infty}^{\infty} \mathbf{W}(-\tau)\mathbf{H}(\tau - nT)d\tau$$

and

$$\nu_0 = \int_{-\infty}^{\infty} \mathbf{W}(-\tau)\nu(\tau)d\tau.$$

We now regard the vector $\tilde{\mathbf{S}}_0$ [a suitably quantized version of \mathbf{S}_0 in (6)] as an estimate of the data vector \mathbf{A}_0 . Thus the system designer has the freedom to choose the receiver matrix $\mathbf{W}(t)$ and a transmitting filter (yet unspecified) to make $\tilde{\mathbf{S}}_0$ as close as possible, in some reasonable sense, to the desired quantity. While the most objective sense in which this can be made close to \mathbf{A}_0 is

$$\text{probability } [\tilde{\mathbf{S}}_0 \neq \mathbf{A}_0] < \delta$$

for a given δ , it is not a mathematically tractable quantity to work with, and therefore a simpler cost function is sought. As is well known, the probability of error cannot be expressed exactly even when the added noise is assumed to be Gaussian—a difficulty caused by the presence of intersymbol and cross-channel interference. Here we employ a simple cost-function, least-mean-squared error between \mathbf{S}_0 and \mathbf{A}_0 . This criterion, which lends itself to mathematical analysis, can also be used to upper bound the probability of error when the added noise is Gaussian.

Returning to the mathematical problem at hand, we thus define the error vectors ϵ as the difference between \mathbf{S}_0 , eq. (6), and the desired data vector \mathbf{A}_0 . The total Mean-Squared Error ($\overline{\text{MSE}}$) then is

$$\overline{\text{MSE}} = \mathbf{E}\{\epsilon^+\epsilon\} = \text{tr}[\mathbf{E}\{\epsilon\epsilon^+\}], \quad (7)$$

where

$$\epsilon = (\mathbf{U}_0 - \mathbf{I})\mathbf{A}_0 + \sum_{\substack{n \\ n \neq 0}} \mathbf{U}_n\mathbf{A}_n + \nu_0. \quad (8)$$

In (7) tr stands for the trace of a matrix, † the complex conjugate transpose, and $E(\cdot)$ the mathematical expectation with respect to all random variables.

Without loss of generality, we assume that the data symbols as well as the vector sequences \mathbf{A}_n are independent and identically distributed, as are the added noise components in $\nu(t)$. With these assumptions the detailed evaluation of (7) becomes

$$\begin{aligned} \text{MSE} = \frac{\overline{\text{MSE}}}{\sigma_d^2} = & \text{tr} \left[\mathbf{I} - 2 \int_{-\infty}^{\infty} \mathbf{W}(-\tau) \mathbf{H}(\tau) \mathbf{d}\tau \right. \\ & + \sigma^2 \int_{-\infty}^{\infty} \mathbf{W}(-\tau) \mathbf{W}^\dagger(-\tau) \mathbf{d}\tau \\ & \left. + \sum_{\substack{n \\ n \neq 0}} \int_{-\infty}^{\infty} \mathbf{W}(-\tau) \mathbf{H}(\tau - nT) \mathbf{d}\tau \int_{-\infty}^{\infty} \mathbf{H}^\dagger(\tau - nT) \mathbf{W}^\dagger(-\tau) \mathbf{d}\tau \right], \quad (9) \end{aligned}$$

where

$$E\{\mathbf{A}_n \mathbf{A}_n^\dagger\} = \sigma_d^2 \mathbf{I},$$

$$E\{\nu(t) \nu^\dagger(t)\} = N_0 \mathbf{I},$$

and

$$\sigma^2 = \frac{N_0}{\sigma_d^2}.$$

Recall that when the data symbols $\{a_n^{(l)}\}$ take on values, $\pm 1 \pm 3 \pm \dots \pm (L-1)$, $E\{a_n^{(l)}\} = \sigma_d^2 = L^2 - 1/3$.

In the next section (9) is first minimized with respect to the class of all $N \times N$ real matrices for a given channel matrix \mathbf{H} and parameter σ^2 , and in Section IV it is further minimized with respect to the admissible class of transmitter filters.

III. THE RECEIVER OPTIMIZATION PROBLEM

It turns out that the mathematical machinery used in the selection of the optimum $N \times N$, $\mathbf{W}(t)$, is the same as that for the 4×4 case developed in Ref. 2, so here we only briefly review the approach.

Proceeding with the optimization problem, replace $\mathbf{W}(t)$ by

$$(\mathbf{W}_0)_{ij} + (\zeta \eta)_{ij}, \quad i, j = 1, \dots, N, \quad (10)$$

where η_{ij} are arbitrary functions of τ , and set

$$\frac{\partial}{\partial \zeta_{ij}} (\text{MSE}) = [\mathbf{0}]_{ij}$$

at $\zeta_{ij} = 0$, $i, j = 1, \dots, N$.

Now compute

$$\begin{aligned} \frac{\partial}{\partial \xi_{ij}} (\text{MSE}) = \text{tr} \left[-2 \int_{-\infty}^{\infty} \eta_{ij}^0(\tau) \mathbf{H}(\tau) \mathbf{d}\tau + 2\sigma^2 \int_{-\infty}^{\infty} \mathbf{W}_0(-\tau) \eta_{ji}^0(\tau) \mathbf{d}\tau \right. \\ \left. + 2 \sum_{\substack{n \\ n \neq 0}} \int_{-\infty}^{\infty} \mathbf{W}_0(\tau) \mathbf{H}(\tau - nT) \mathbf{d}\tau \int_{-\infty}^{\infty} \mathbf{H}^\dagger(\tau - nT) \eta_{ji}^0(\tau) \mathbf{d}\tau \right] = 0, \end{aligned}$$

$$i, j = 1, \dots, N, \quad (11)$$

where the matrices, η_{ij}^0 , $i, j = 1, \dots, N$ have the entry $\eta_{ij}(\tau)$ in the ij th position and zero everywhere else. By a direct computation of the trace in eq. (11), one obtains

$$\begin{aligned} - \int_{-\infty}^{\infty} (\mathbf{H}(\tau))_{ji} \eta_{ij}(\tau) \mathbf{d}\tau + \sigma^2 \int_{-\infty}^{\infty} (\mathbf{W}(-\tau))_{ij} \eta_{ij}(\tau) \mathbf{d}\tau \\ + \sum_{\substack{n \\ n \neq 0}} \int_{-\infty}^{\infty} [\mathbf{H}(\tau - nT) \mathbf{U}_n^\dagger]_{ji} \eta_{ij}(\tau) \mathbf{d}\tau = 0, \quad i, j = 1, \dots, N. \end{aligned} \quad (12)$$

Since eq. (12) must hold for all functions, $\eta_{ij}(\tau)$, we obtain the matrix integral equation that must be satisfied by the optimum matrix $\mathbf{W}_0(\tau)$,

$$\sigma^2 \mathbf{W}_0(-\tau) = \mathbf{H}^\dagger(\tau) - \sum_{\substack{n \\ n \neq 0}} \mathbf{U}_n \mathbf{H}^\dagger(\tau - nT), \quad (13)$$

where \mathbf{U}_n is given in eq. (6) with $\mathbf{W}(\tau)$ replaced by $\mathbf{W}_0(\tau)$. Structurally, $\mathbf{W}_0(\tau)$ consists of an $N \times N$ matrix-matched filter followed by a matrix-tapped delay line with matrix-tap coefficients \mathbf{U}_n .

An explicit formula for the least MSE is now possible to obtain by first post-multiplying eq. (13) by $\mathbf{W}_0^\dagger(-\tau)$, integrating, and then comparing the result with eq. (9). The result is

$$\text{MSE}_0 = \text{tr}[\mathbf{I} - \mathbf{U}_0], \quad (14)$$

where \mathbf{U}_0 is obtained by solving a set of infinite linear equations obtained by first post-multiplying eq. (13) by $\mathbf{H}(\tau - kT)$ and then integrating. These operations yield the equations

$$\begin{aligned} \sigma^2 \mathbf{U}_k &= \mathbf{R}_k - \sum_{\substack{n \\ n \neq 0}} \mathbf{U}_n \mathbf{R}_{k-n}, \quad \text{all } k \\ &= \mathbf{R}_{-k}^\dagger, \end{aligned} \quad (15)$$

where

$$\mathbf{R}_k = \int_{-\infty}^{\infty} \mathbf{H}^\dagger(\tau) \mathbf{H}(\tau - kT) \mathbf{d}\tau. \quad (16)$$

The matrix convolutional equation, (15), is easy to solve by Fourier series methods. Thus, inserting the solution of \mathbf{U}_0 , obtained from (15), into (14), we get

$$\text{MSE}_0 = \frac{1}{2\pi} \int_{-\pi}^{\pi} \text{tr} \left[\mathbf{I} + \frac{\mathbf{R}(\omega)}{\sigma^2} \right]^{-1} \mathbf{d}\omega, \quad (17)$$

where

$$\mathbf{R}(\omega) = \sum_k \mathbf{R}_k e^{i\omega kT}$$

and

$$\begin{aligned} \mathbf{R}_k &= \frac{T}{2\pi} \int_{-\pi/T}^{\pi/T} \mathbf{R}(\omega) e^{-i\omega kT} \mathbf{d}\omega, \\ &= \int_{-\infty}^{\infty} \mathbf{H}^\dagger(\tau) \mathbf{H}(\tau - kT) \mathbf{d}\tau \end{aligned} \quad (18)$$

[from (16)].

Now the matrix frequency transfer characteristic is, by definition,

$$\tilde{\mathbf{H}}(\omega) = \int_{-\infty}^{\infty} \mathbf{H}(t) e^{i\omega t} \mathbf{d}t,$$

and, by Parseval's theorem, (18) is put into the form

$$\begin{aligned} \mathbf{R}_k &= \frac{1}{2\pi} \int_{-\infty}^{\infty} \tilde{\mathbf{H}}^\dagger(\omega) \tilde{\mathbf{H}}(\omega) e^{-i\omega kT} \mathbf{d}\omega \\ &= \frac{1}{2\pi} \int_{-\pi/T}^{\pi/T} \sum_k \tilde{\mathbf{H}}^\dagger \left(\omega - \frac{2\pi k}{T} \right) \tilde{\mathbf{H}} \left(\omega - \frac{2\pi k}{T} \right) e^{-i\omega kT} \mathbf{d}\omega. \end{aligned} \quad (19)$$

From this and (18) we determine

$$\mathbf{R}(\omega) = \frac{1}{T} \sum_k \tilde{\mathbf{H}}^\dagger \left(\omega - \frac{2\pi k}{T} \right) \tilde{\mathbf{H}} \left(\omega - \frac{2\pi k}{T} \right), \quad (20)$$

which is the matrix-folded, or aliased, channel spectrum.

In the next section we further minimize MSE, eq. (17), with respect to the transmitter matrix filter.

IV. TRANSMITTER OPTIMIZATION

The general optimization problem with the inclusion of the aliases, eq. (20), appears to be extremely complicated to solve,* and therefore

* We refer the interested reader to Ref. 6, where a similar optimization problem is solved without having to make the bandlimited assumption.

we shall assume that the transmitter filter is strictly bandlimited to the Nyquist frequency, π/T . So, without excess bandwidth, (20) reduces to

$$\mathbf{R}(\omega) = \frac{1}{T} \tilde{\mathbf{H}}^\dagger(\omega) \tilde{\mathbf{H}}(\omega), \quad (21)$$

and since the transmitter matrix filter is in cascade with the channel filter, we can write

$$\tilde{\mathbf{H}}(\omega) = \mathbf{C}(\omega) \mathbf{P}(\omega). \quad (22)$$

Equation (2) now becomes

$$\mathbf{R}(\omega) = \frac{1}{T} \mathbf{P}^\dagger(\omega) \mathbf{C}^\dagger(\omega) \mathbf{C}(\omega) \mathbf{P}(\omega), \quad (23)$$

where $\mathbf{C}(\omega)$ is the transmission medium frequency transfer characteristic and $\mathbf{P}(\omega)$ represents the $N \times N$ matrix transmitting filter frequency characteristics.

Note that the average total transmitted power is proportional to

$$\int_{-\pi/T}^{\pi/T} \text{tr}[\mathbf{P}^\dagger(\omega) \mathbf{P}(\omega)] d\omega,$$

and therefore the quantity we wish to minimize with respect to $\mathbf{P}(\omega)$ is, from (17) and (23),

$$F = \int_{-\pi/T}^{\pi/T} \text{tr} \left[\mathbf{I} + \frac{1}{\sigma^2 T} \mathbf{P}^\dagger(\omega) \mathbf{C}^\dagger(\omega) \mathbf{C}(\omega) \mathbf{P}(\omega) \right]^{-1} d\omega + \lambda \int_{-\pi/T}^{\pi/T} \text{tr}[\mathbf{P}^\dagger(\omega) \mathbf{P}(\omega)] d\omega, \quad (24)$$

where λ is a Lagrange multiplier to be determined from the power constraint.

Since for each value of ω , $\mathbf{C}^\dagger \mathbf{C}$ is hermitian, nonnegative definite, it can be diagonalized by a unitary matrix ψ ,

$$\mathbf{C}^\dagger(\omega) \mathbf{C}(\omega) = \psi^\dagger(\omega) \Lambda(\omega) \psi(\omega), \quad (25)$$

where $\Lambda(\omega)$ is the diagonal matrix with entries, $\lambda_1 \dots \lambda_N$, the eigenvalues of $\mathbf{C}^\dagger \mathbf{C}$. By letting $\mathbf{G} = \psi \mathbf{P}$, $\mathbf{Q} = \mathbf{G} \mathbf{G}^\dagger$, and scaling the eigenvalues by $1/\sigma^2 T$, (24) is put into the form

$$F = \int_{-\pi/T}^{\pi/T} \text{tr}\{(\mathbf{I} + \mathbf{Q} \Lambda)^{-1} + \lambda \mathbf{Q}\} d\omega, \quad (26)$$

where we have used an innocuous result,

$$\text{tr}[\mathbf{I} + \mathbf{A} \mathbf{B}]^{-1} = \text{tr}[\mathbf{I} + \mathbf{B} \mathbf{A}]^{-1},$$

for any matrices \mathbf{A} and \mathbf{B} . (The spectrum of \mathbf{AB} is the same as that of \mathbf{BA} .)

We now seek a minimum over all possible matrices \mathbf{Q} such that

$$\int_{-\pi/T}^{\pi/T} \text{tr}[\mathbf{I} + \bar{\mathbf{Q}}\mathbf{\Lambda}]^{-1} \mathbf{d}\omega = \min_{\mathbf{Q}} \int_{-\pi/T}^{\pi/T} \text{tr}[\mathbf{I} + \mathbf{Q}\mathbf{\Lambda}]^{-1} \mathbf{d}\omega \quad (27)$$

subject to $\int_{-\pi/T}^{\pi/T} \text{tr}\mathbf{Q}\mathbf{d}\omega = \text{constant}$.

Since $\mathbf{\Lambda}$ is real and nonnegative we define

$$\mathbf{M}(\omega) = \mathbf{\Lambda}^{1/2}(\omega)\mathbf{Q}(\omega)\mathbf{\Lambda}^{1/2}(\omega), \quad (28)$$

which is again diagonalized by unitary matrices $\mathbf{U}(\omega)$,

$$\mathbf{M} = \mathbf{U}\text{diag}(\delta_1 \dots \delta_N)\mathbf{U}^\dagger, \quad (29)$$

where $\delta_1 \dots \delta_N$ are now the eigenvalues of \mathbf{M} . Let the diagonal elements of \mathbf{M} be $d_1 \dots d_N$. We then obtain from (29)

$$d_i = \sum_{n=1}^N \delta_n |U_{in}|^2, \quad i = 1 \dots N. \quad (30)$$

This relationship is now used to prove that (27) is achieved when $\bar{\mathbf{Q}}$ is diagonal. Since the integrand in (27) is positive, it suffices to minimize the integral point by point.

Let \mathbf{S}_d be the diagonal matrix formed from \mathbf{M} by setting all off-diagonal entries to zero. From the definition of the trace we write

$$\text{tr}[\mathbf{I} + \mathbf{M}]^{-1} = \sum_{n=1}^N \frac{1}{1 + \delta_n}$$

and

$$\text{tr}[\mathbf{I} + \mathbf{S}_d]^{-1} = \sum_{n=1}^N \frac{1}{1 + d_n}.$$

If diagonal $\bar{\mathbf{Q}}$ renders the smallest trace, it must be shown that

$$\sum_{n=1}^N \frac{1}{1 + d_n} \leq \sum_{n=1}^N \frac{1}{1 + \delta_n}. \quad (31)$$

The proof of (31) is facilitated by the observation from (29) and (30) that

$$|U_{in}| \geq 0, \quad i, n = 1 \dots N$$

and

$$\sum_{i=1}^N |U_{in}|^2 = \sum_{n=1}^N |U_{in}|^2 = 1.$$

These are precisely the necessary and sufficient conditions that $2N$

numbers $\{d_i, \delta_i\}$ be related such that for any continuous convex function $\Phi(x)$ one has

$$\Phi(d_1) + \dots + \Phi(d_N) \leq \Phi(\delta_1) + \dots + \Phi(\delta_N). \quad (32)$$

(See Theorems 13 and 14 in Ref. 7, pp. 30–1.) Since only the diagonal entries in \mathbf{Q} enter into the constraint, this result proves our assertion.

During the course of this research I discussed this assertion with my colleague Hans Witsenhausen, who supplied an elegant proof using Schur transformations. With his permission I reproduce his note to me in the Appendix.

Once we establish the fact that the optimum matrix \mathbf{Q} is diagonal, we note from the definition that

$$\mathbf{Q} = \mathbf{G}\mathbf{G}^\dagger = \psi\mathbf{P}\mathbf{P}^\dagger\psi^\dagger = \text{diagonal}, \quad (33)$$

and since its entries are nonnegative, the form of the optimum transmitter matrix is immediate,

$$\begin{aligned} \mathbf{P}_0(\omega) &= \psi^\dagger(\omega)\mathbf{Q}^{1/2}(\omega)\mathbf{S}(\omega), & |\omega| \leq \frac{\pi}{T} \\ &= [\mathbf{0}], & \text{elsewhere,} \end{aligned} \quad (34)$$

where $\mathbf{S}(\omega)$ is an arbitrary unitary matrix. Thus, there are an infinite number of $\mathbf{P}(\omega)$'s that yield minimum mean-squared error while yielding a fixed amount of total average transmitted power.

The additional problem of determining the optimum values of the diagonal elements q_n in \mathbf{Q} is now easy since (26) can now be written as

$$F = \sum_{n=1}^N \int_{-\pi/T}^{\pi/T} \left[\frac{1}{1 + \lambda_n(\omega)q_n(\omega)} + \lambda q_n(\omega) \right] \mathbf{d}\omega, \quad (35)$$

which is easily minimized with respect to the positive quantities $\{q_n(\omega)\}$ using standard calculus of variation techniques, and the Lagrange multiplier is determined from the given power constraint. The minimization of (35) follows the same procedure as in the $N = 2$ case, treated in detail in Ref. 1.

V. CONCLUSIONS

Fallouts from solving some very special problems associated with digital communications over dually polarized radio channels yielded general results applicable to a wide range of communications situations. It appears that the class of minimization problems encountered in our formulations are well known to the mathematicians; if the engineers could only ask the right questions.

From a mathematical point of view, the optimum overall system has an end-to-end equivalent diagonal characterization. Once this diagonal

(direct) structure is determined, all other problems reduce to the well-known scalar case.

From an engineering point of view the optimum filter structures may provide valuable insights to the design of signal processors in the multiuser communications environment.

REFERENCES

1. N. Amitay and J. Salz, "Linear Equalization Theory in Digital Data Transmission Over Dually Polarized Fading Radio Channels," *AT&T Bell Lab. Tech. J.*, **63**, No. 10 (December 1984), pp. 2215-59.
2. M. Kavehrad and J. Salz, private communication.
3. H. P. Kramer and M. V. Mathews, "A Linear Coding for Transmitting a Set of Correlated Signals," *IRE Trans. Inform. Theory*, *IT-2* (September 1956), pp. 41-6.
4. R. J. Pilc, "The Optimum Linear Modulator for a Gaussian Source Used With A Gaussian Channel," *B.S.T.J.*, **48**, No. 9 (November 1969), pp. 3075-89.
5. L. H. Brandenberg and A. D. Wyner, "Capacity of the Gaussian Channel With Memory: The Multivariate Case," *B.S.T.J.*, **53**, No. 5 (May-June 1974), pp. 745-78.
6. H. S. Witsenhausen, "A Determinant Maximization Problem Occurring in the Theory of Data Communication," *SIAM J. Appl. Math.*, **29**, No. 3 (November 1975), pp. 515-22.
7. E. F. Beckenbach and Richard Bellman, *Inequalities*, Berlin, Heidelberg, New York: Springer-Verlag, 1965, pp. 30-1.
8. A. W. Marshall and I. Olkin, *Inequalities: Theory of Majorization and Its Applications*, New York: Academic, 1979.

APPENDIX

Yet Another Trace Minimization Problem

By H. S. Witsenhausen

Let (Ω, B, μ) be a measure space, and for each $\omega \in \Omega$ let $\Lambda(\omega)$ be an $N \times N$ diagonal matrix with real positive integrable diagonal entries.

Let \mathbf{Q} denote a measurable function from Ω to nonnegative definite hermitian matrices, subject to

$$\int \text{tr} \mathbf{Q}(\omega) \cdot d\mu(\omega) = c. \quad (36)$$

One seeks the minimum, over all such \mathbf{Q} of

$$\int \text{tr}(\mathbf{I} + \mathbf{Q}(\omega)\Lambda(\omega))^{-1} \cdot d\mu(\omega). \quad (37)$$

This problem is easily handled when \mathbf{Q} is diagonal. The purpose of this Appendix is to show that the minimization can be reduced to this case.

Let \mathbf{Q}^d denote the diagonal matrix obtained from \mathbf{Q} by replacing all off-diagonal elements by zero.

Theorem: If $\mathbf{Q}(\cdot)$ satisfies the conditions of the problem, then $\mathbf{Q}^d(\cdot)$ also does and gives (37) no higher value.

Proof: Obviously, \mathbf{Q}^d is hermitian, nonnegative definite and gives the same value in (36). Now (37) can be written

$$\int \text{tr}(\mathbf{I} + M(\omega))^{-1} \cdot d\mu(\omega), \quad (38)$$

where

$$\mathbf{M}(\omega) = \Lambda^{1/2}(\omega)\mathbf{Q}(\omega)\Lambda^{1/2}(\omega) \quad (39)$$

is hermitian, nonnegative definite.

We have

$$\mathbf{M}^d(\omega) = \Lambda^{1/2}(\omega)\mathbf{Q}^d(\omega)\Lambda^{1/2}(\omega). \quad (40)$$

Thus it is enough to show that (38) cannot increase when \mathbf{M} is replaced by \mathbf{M}^d , which we show for each fixed ω .

Let $\lambda_1, \dots, \lambda_n$ be the eigenvalues of \mathbf{M} , and let d_1, \dots, d_n be the diagonal entries of M that are the eigenvalues of \mathbf{M}^d .

$$\text{tr}(\mathbf{I} + \mathbf{M})^{-1} = \sum_{i=1}^n \frac{1}{1 + \lambda_i}. \quad (41)$$

$$\text{tr}(\mathbf{I} + \mathbf{M}^d)^{-1} = \sum_{i=1}^n \frac{1}{1 + d_i}. \quad (42)$$

The right side of (41) is a convex symmetric function of $(\lambda_1, \dots, \lambda_n)$. Hence it is Schur convex. (That is, $f(\mathbf{S}\boldsymbol{\lambda}) \leq f(\boldsymbol{\lambda})$ for doubly stochastic \mathbf{S} .)

As observed by Schur, from the unitary relationship of \mathbf{M} with its diagonal form

$$\mathbf{M} = \mathbf{U} \text{diag}(\lambda_1, \dots, \lambda_n)\mathbf{U} \quad (43)$$

(see Ref. 8), it follows that

$$\mathbf{d} = \mathbf{S}\boldsymbol{\lambda} \quad (44)$$

with doubly stochastic $\mathbf{S}(S_{ij} = |u_{ij}|^2)$.

Thus,

$$\sum_{i=1}^n \frac{1}{1 + d_i} \leq \sum_{i=1}^n \frac{1}{1 + \lambda_i}, \quad (45)$$

which was to be proved.

These two quantities, sometimes referred to as efficiency indices, will be used to compare the performance of the various equalization methods.

AUTHOR

Jack Salz, B.S.E.E., 1955, M.S.E., 1956, and Ph.D. (Electrical Engineering), 1961, University of Florida; AT&T Bell Laboratories, 1961—. Mr. Salz first worked on the electronic switching system. Since 1968 he has supervised a group engaged in theoretical studies in data communications and is currently a member of the Network Systems Research Department. During the academic year 1967–68, he was on leave as Professor of Electrical Engineering at the University of Florida. He was a visiting lecturer at Stanford University in Spring 1981 and a visiting MacKay Lecturer at the University of California, at Berkeley, in Spring 1983.

Tone Location by Cyclotomic Filters

By D. HERTZ,* R. P. KURSHAN,† D. MALAH,* and
J. T. PEOPLES‡

(Manuscript received July 11, 1984)

In this paper we present a tone location system that estimates the frequency of an input tone through additions and comparisons alone. The system uses “cyclotomic” filters (which operate without multiplications), requiring fewer operations than with a conventional Discrete Fourier Transform (DFT) entailing multiplications. In the system presented here, an input tone is first transformed to yield two quadrature tones, which are then digitized. Processing occurs in successive stages at successively reduced sampling rates. During each decimation stage, the system is configured to provide symmetric coverage of a subband in which the tone has been located at the previous stage. Simulations demonstrate that for the case studied, an input signal-to-noise ratio (SNR_i) in excess of 10 dB yields an output signal-to-noise ratio (SNR_o) that is close (within 0.3 dB) to the maximum attainable SNR_o , where SNR_o is measured in terms of the reduction in frequency uncertainty. Enhanced resolution is demonstrated at the expense of the number of computations, while holding the number of decimation stages constant, by using small DFTs in place of the cyclotomic filters. This method still utilizes fewer computations than a conventional DFT (with the same number of frequency cells), with approximately the same performance in the case of low noise. Thus, this alternative method is useful when circumstances prohibit using a single, large DFT.

* Technion-Israel Institute of Technology, Haifa, Israel. This paper is derived from the M.Sc. thesis of D. Hertz, published in 1979, written under the direction of D. Malah and R. P. Kurshan (while the latter was visiting the Technion in 1976–7). Part of the work was completed while D. Malah was visiting AT&T Bell Laboratories in 1979–81. † AT&T Bell Laboratories. ‡ AT&T Bell Laboratories; present affiliation Bell Communications Research, Inc.

Copyright © 1985 AT&T. Photo reproduction for noncommercial use is permitted without payment of royalty provided that each reproduction is done without alteration and that the Journal reference and copyright notice are included on the first page. The title and abstract, but no other portions, of this paper may be copied or distributed royalty free by computer-based and other information-service systems without further permission. Permission to reproduce or republish any other portion of this paper must be obtained from the Editor.

I. INTRODUCTION

In many diverse applications, it is necessary to detect and locate a signal appearing within selected frequency bands, particularly a signal comprised of a single tone. This is tantamount to estimating the frequency of a tone that may appear randomly in any band. Such detection and estimation are generally accomplished in conventional analog systems, using a bank of filters tuned to different, narrowband portions of the spectrum or using a single filter that is effectively swept across the bands of interest. Associated with such techniques, however, are the usual problems of analog processors, including unpredictability due to inherent variability of system components. A discrete-time technique is described by Cappelini et al.,^{1,2} wherein a given frequency band is partitioned into subbands for detection purposes. The partition into subbands is achieved through a decimation approach, using a single, fixed, low-pass digital filter at each decimation stage. In a variety of applications, however, when it is known that the given input signal contains, at most, a single spectral line in the frequency range of interest (e.g., in M-ary FSK demodulation³ and Touch-Tone telephony⁴), this method possesses inherent disadvantages. First, since general filtering is effected at each decimation stage, numerous multiplications and additions must be performed during the filtering operations of each stage. Second, a large amount of memory is required to store samples from the geometrically increasing number of iterated signals. These disadvantages are substantially reduced with a Cyclotomic Tone Location System (CTLS).⁵⁻⁸ Only the CTLS of Ref. 5 is presented here, since it is simpler than the CTLS of Refs. 6 through 8, and we wish to apply this same idea to a DFT Tone Location System (FTLS) as well, described in Section IV. The FTLS, as compared with conventional DFT implementations,^{9,10} trades performance in the presence of noise for reduced implementational complexity.

The CTLS incorporates digital filters utilizing additions alone, thereby eliminating the customary computational load associated with multiplications. Figure 1 is a block diagram of the CTLS. Referring to Fig. 1, the input tone, comprising, say, a single frequency located randomly within a band 0 to $f_s/4$, is first transformed by the Hilbert network to yield a complex tone composed of two tones in quadrature relationship. These two tones correspond to phase-shifted versions of the input tone. The complex tone is initially sampled by the digitizer at a rate of f_s and stored in the buffer. Then, the complex tone and its frequency-shifted versions, from the frequency-shifting unit, are processed by the first-order recursive filter unit. The filters are derived from the set of cyclotomic filters and have only a single resonance in the frequency range up to one-half the sampling rate. The filters are

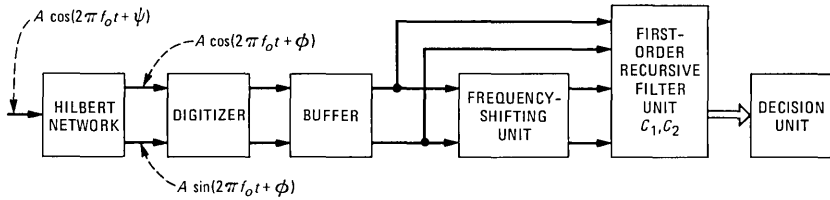


Fig. 1—Block diagram of the CTLS.

arranged so that the resonances associated with the filters and frequency-shifted versions symmetrically cover a band of frequencies including the input tone frequency. Location of the subband containing the tone is achieved in the decision unit by comparing the magnitudes of the various filter outputs to each other after a fixed number of samples have been processed.

It is assumed from here on that *the tone is known to be present*. The problem of detecting the presence of a tone will be commented on later in this paper. The CTLS locates the tone using a multistage process. At the first stage, using the first-order recursive filter unit, which symmetrically covers the band $(0, f_s/4)$, the CTLS unambiguously locates the tone either in $(0, f_s/8)$ or in $(f_s/8, f_s/4)$. Once the tone has been located within a single subband, sampling rate reduction, or decimation, by a factor of two is effected.

This particular choice of the sampling rate reduction ratio and subband width precludes additional spectral lines from appearing within the subband containing the tone. The filters are now reconfigured at the reduced sampling rate to again achieve symmetrical placement of the filter resonances across the previously isolated subband of width $f_s/8$ containing the tone. The process of frequency shifting and filtering by the array is then repeated.

The frequency subbands utilized for resolution at the output of this second stage are each of width $f_s/16$. Again, the subband containing the tone is isolated, and another decimation stage is effected. The processing continues in this manner until the desired frequency resolution has been achieved. Moreover, a minor modification to the CTLS enables the system to test for a tone in any one of the other three bands [rather than $(0, f_s/4)$], i.e., $[kf_s/4, (k + 1)f_s/4]$, $k = 1, 2, 3$, provided k is known to the CTLS.

The FTLS is an extension of the CTLS in the following way. Basically, the input tone to the FTLS is comprised of a frequency, located randomly within the band 0 to $f_s/2$, and is converted to a complex tone. The quadrature tones are both initially sampled at a rate of f_s , and then N samples of the complex tone are processed by an M -point DFT ($M = 2^m$, $N < M$ is mandatory, and the N samples

are padded by $M - N$ zeros). The modulus of the M -point DFTs are further processed. As in the CTLS, the processing is done in successive stages at successively reduced sampling rates. During each decimation stage, the system is configured to provide symmetric coverage of a subband in which the tone has been located in the previous stage.

At each decimation stage the pertinent band is partitioned into $M/2$ subbands [with S stages the initial band will be partitioned into $(M/2)^S$ bands]. A minor modification to the FTLS enables the system to test for a tone in the other band, i.e., $(f_s/2, f_s)$, provided the FTLS knows in which of the two subbands the tone is present. For $N = 2, 3$, and $M = 4$ this reduces to a CTLS, except for the sampling rate, which is now halved.

The organization of the paper is as follows: Section II presents basic relations and a detailed description of the CTLS; Section III gives simulation results associated with the CTLS; Section IV presents a detailed description of the FTLS; and Section V presents the conclusions.

II. CTLS OPERATION PRINCIPLES

For clarity of exposition, we first present an overview of the properties of the first-order recursive filters utilized here. Next, we discuss in detail the time-domain and frequency-domain characteristics of one first-order filter (designated C_1), treated as exemplary of the remaining filters of interest (designated C_2 , C_{4p} , and C_{4m}), to illustrate fundamental concepts helpful to fully comprehend the overall CTLS. Finally, we describe the technique for exploiting the properties of the individual filters to form a composite tone detection system.

2.1 Cyclotomic filters

The properties of the cyclotomic filters discussed herein are presented in greater detail in Kurshan and Gopinath¹¹ and Hertz.⁸ Cyclotomic filters are a class of digital filters having only poles in the transfer function and, moreover, each pole lies on the unit circle. This means that the filters are inherently unstable and are not suitable for conventional filtering operations, which require the processing of numerous sequential samples. In fact, these filters behave more like resonators and it is this property that can be beneficially utilized for tone detection. The salient advantage of this type of resonating filter is that the filters of primary interest exhibit nonzero coefficient values $(\pm 1, \pm j)$ having a modulus of one. This implies that multiplications of samples by filter coefficients reduce to simple addition, subtraction, and signal interchange operations and, significantly, arithmetic errors such as round-off and truncation errors are eliminated.

A cyclotomic filter may be described in terms of a linear recursion

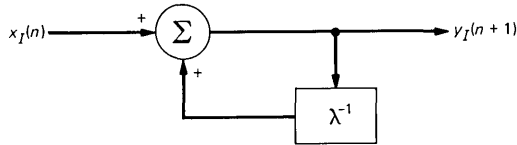


Fig. 2—Cyclotomic digital filter C_1 in block diagram form.

relation whose characteristic polynomial is a cyclotomic polynomial. For example, for a first-order digital filter represented by the Linear Difference Equation (LDE)

$$y_I(n + 1) = y_I(n) + x_I(n), \quad (1)$$

where $x_I(n)$ and $y_I(n)$ are inphase input and output sequence elements, respectively, corresponding to the n th sample, then the characteristic equation is given by the polynomial $\lambda - 1$ (as derived from $y_I(n + 1) - y_I(n) = 0$). This polynomial is cyclotomic and has the designation $C_1(\lambda)$ (or C_1 for simplicity): $C_1(\lambda) = \lambda - 1$. Similarly, the cyclotomic polynomial $C_2(\lambda) = \lambda + 1$ yields a digital filter described by the LDE

$$y_I(n + 1) = -y_I(n) + x_I(n). \quad (2)$$

Other filters of special interest include two first-order, complex filters derived as the roots of the second-order cyclotomic polynomial $C_4(\lambda) = \lambda^2 + 1$. These filters also have roots on the unit circle and are given by (with $j = \sqrt{-1}$) $C_{4p}(\lambda) = \lambda - j$ and $C_{4m}(\lambda) = \lambda + j$; they have the following LDE representations, respectively:

$$y_I(n + 1) = jy_I(n) + x_I(n) \quad (3)$$

and

$$y_I(n + 1) = -jy_I(n) + x_I(n). \quad (4)$$

Figure 2 depicts the C_1 digital filter in block diagram form. Similar block diagrams can be derived for the other first-order filters.

2.2 Filter characteristics

To elucidate the desired characteristics obtained by combining cyclotomic-derived filters into a system architecture, we first present the response of a general filter to an input tone having a randomly distributed phase component. The input tone is presumed to have the analog form $A\cos(2\pi ft + \varphi)$, where φ is the random phase variable, A is the amplitude, and f is the tone frequency.

The impulse response sequence of the general recursive filter is represented by $\{h(k)\}$, where $k \geq 0$. The output sequence elements may then be obtained from the convolutional relationship

$$y_I(n) = \sum_{k=0}^n x_I(k)h(n-k), \quad (5)$$

where $\{x_I(k)\}$ is the input tone sequence obtained by sampling $A\cos(2\pi ft + \varphi)$, $t \geq 0$, at the rate f_s , that is,

$$x_I(k) = A\cos(kv + \varphi), \quad k \geq 0, \quad (6)$$

where

$$\nu = 2\pi f/f_s. \quad (7)$$

Substituting (6) into (5) gives

$$y_I(n) = \sqrt{\alpha_n^2 + \beta_n^2} \cos \left[\tan^{-1} \left(\frac{\beta_n}{\alpha_n} \right) + \varphi \right], \quad (8)$$

where

$$\alpha_n = \operatorname{Re} \left[\sum_{k=0}^n A e^{jk\nu} h(n-k) \right], \quad (9)$$

$$\beta_n = \operatorname{Imag} \left[\sum_{k=0}^n A e^{jk\nu} h(n-k) \right], \quad (10)$$

and the operators denoted "Re" and "Imag" produce the real and imaginary parts of the bracketed part of eqs. (9) and (10), respectively.

Since φ occurs randomly within the interval $(0, 2\pi)$, comparison of $|y_I(n)|$ to a threshold may yield deleterious results due to the dependence of y_n on φ . However, by utilizing the first-order filters in pairs (either actually or on a time-shared basis), the undesirable modulation effects of the random phase component may be eliminated.

This is achieved by forming a new sample sequence $\{x_Q(k)\}$, found by sampling the quadrature tone $A\sin(2\pi ft + \varphi)$, which may be derived through a Hilbert transform operation on the original or inphase input tone. The new sequence elements are given by

$$x_Q(k) = A\sin(kv + \varphi), \quad k \geq 0. \quad (11)$$

If $\{x_Q(k)\}$ is processed by a recursive filter identical to the one that processes $\{x_I(k)\}$, then the new output sequence $\{y_Q(n)\}$ has elements

$$y_Q(n) = \sqrt{\alpha_n^2 + \beta_n^2} \sin \left[\tan^{-1} \left(\frac{\beta_n}{\alpha_n} \right) + \varphi \right]. \quad (12)$$

A squaring operation on both eqs. (8) and (12), followed by a summation and square-root operation, yields an output $\sqrt{\alpha_n^2 + \beta_n^2}$, which is independent of φ .

For future discussion, it is convenient, as exemplified by the form of eqs. (9) and (10), to define a complex input tone having sample

values $Ae^{j(k\nu+\varphi)}$, and a corresponding output sequence $\{z_n\}$ having complex element values

$$z_n = \sum_{k=0}^n Ae^{j(k\nu+\varphi)}h(n-k). \quad (13)$$

The magnitude or modulus of each element of $\{z_n\}$ is then given by

$$|z_n| = \left| \sum_{k=0}^n Ae^{jk\nu}h(n-k) \right| = \sqrt{\alpha_n^2 + \beta_n^2}. \quad (14)$$

As hereinafter utilized, the two-filter device characterized by substantially identical filters C_i ($i = 1, 2, 4p$ or $4m$), which processes inphase and quadrature samples of an input signal in pairs, is a basic or fundamental element of the CTLS.

Whereas the above discussion has focused primarily on sequence domain manipulations, it is helpful to visualize these manipulations in the frequency domain. Moreover, whereas the discussion was couched in terms of generalized impulse responses, particularly pertinent to the subsequent discussion are the frequency domain responses of filters C_1 , C_2 , C_{4p} , and C_{4m} . The filter C_1 , having impulse elements $h(n) = 1$, $n \geq 0$, is treated as exemplary.

Utilizing now the notation $z(C_1, n, \nu)$ to distinguish sequence elements of $\{z_n\}$ so as to explicitly set forth the dependence upon C_1 , n and ν , we obtain the following by substituting $h(n) = 1$ into eq. (14):

$$|z(C_1, n, \nu)| = A \left| \sum_{k=0}^n e^{jk\nu} \right|$$

or

$$|z(C_1, n, \nu)| = A \left| \frac{\sin\left(\frac{n+1}{2}\nu\right)}{\sin\frac{\nu}{2}} \right|. \quad (15)$$

In addition, because the impulse response of C_2 is $(-1)^n$, $n \geq 0$,

$$|z(C_2, n, \nu)| = |z(C_1, n, \nu + \pi)|. \quad (16)$$

Figure 3 shows plots of $|z(C_1, n, \nu)|$ and $|z(C_2, n, \nu)|$ over the range (0 to π) for $n = 3$, that is, four samples corresponding to $n = 0, 1, 2$, and 3 have been processed. The resonating feature of the filters is apparent. Filter C_1 is symmetric with respect to $\nu = 0$, whereas C_2 is symmetric about $\nu = \pi$, and both are periodic with period 2π . Since $\nu = 2\pi f/f_s$, $\nu = \pi$ corresponds to a frequency f , which is one-half the sampling rate. Although the filter response has been illustrated with four samples, the filter may also be operated with two, three, five, six,

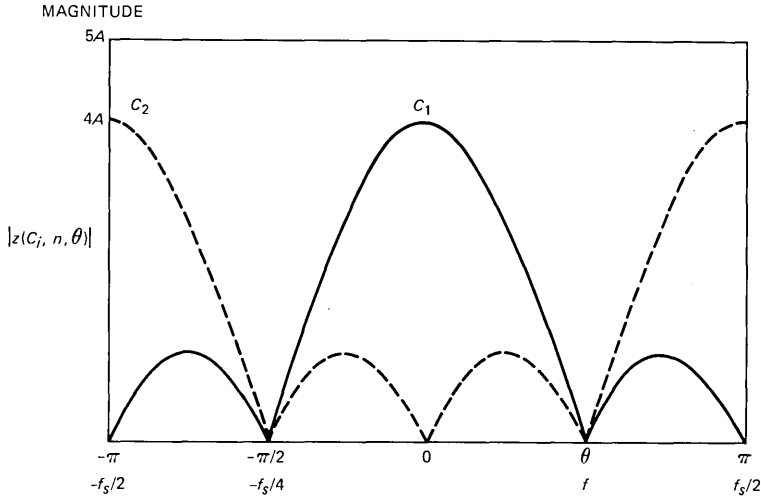


Fig. 3—Responses of filter pairs C_1 and C_2 , each processing real and imaginary sampled tones in parallel, over the range from 0 to one-half of the sampling rate with $N = 4$ samples.

or seven samples. If more than seven samples are used, the main lobes of adjacent filter responses do not intersect. In fact, simulations reveal some enhancement in the signal-to-noise performance when more than four (but fewer than seven) samples are processed.

In a similar manner, the following relations may also be derived:

$$|z(C_{4p}, n, \nu)| = A \left| \frac{\sin \left[\left(\frac{n+1}{2} \right) \left(\nu - \frac{\pi}{2} \right) \right]}{\sin \left[\frac{\left(\nu - \frac{\pi}{2} \right)}{2} \right]} \right| \quad (17)$$

and

$$|z(C_{4m}, n, \nu)| = A \left| \frac{\sin \left[\left(\frac{n+1}{2} \right) \left(\nu + \frac{\pi}{2} \right) \right]}{\sin \left[\frac{\left(\nu + \frac{\pi}{2} \right)}{2} \right]} \right| \quad (18)$$

Because of the manner in which C_{4p} and C_{4m} are related to C_1 ,

$$\left| z \left(C_{4p}, n, \nu + \frac{\pi}{2} \right) \right| = \left| z \left(C_{4m}, n, \nu - \frac{\pi}{2} \right) \right| = |z(C_1, n, \nu)| \quad (19)$$

Figure 4 shows plots of $|z(C_{4p}, n, \nu)|$ and $|z(C_{4m}, n, \nu - \pi)|$ for the same parameters as Fig. 3. Since cyclotomic filters have poles on the unit circle, their responses blow up. However, they can be used only because the input signal is time limited, hence the composite response due to the sinusoidal input can be examined and leads to eqs. (15) through (18).

From the plots of Figs. 3 and 4, we conclude that the filter response from each two-filter device comprising identical filters $C_i (i = 1, 2, 4p$ or $4m)$ has only a single resonance in the frequency range up to one-half of the sampling frequency. The CTLS exploits these filter pairs by covering the frequency band from 0 to $f_s/2$ (ν from 0 to π) in symmetric fashion. Such an arrangement is depicted in Fig. 5a. Since C_{4p} and C_{4m} are merely frequency-shifted versions of C_1 and it appears that C_{4p} and C_{4m} require complex manipulations, it is important to determine if a modified, real sequence can serve as an input to a C_1 filter to produce an output equivalent to a C_{4p} or C_{4m} filter output.

Phase shifting by $\pm\pi/2$ in the frequency domain is equivalent to introducing modulation factors in the sequence (sampled time) domain of the form $\{e^{\pm jk\pi/2}\}$. Thus, if the complex input sequence is modified by the modulation sequence, a new sequence having element values

$$Ae^{j[k(\nu \pm \pi/2) + \varphi]} \tag{20}$$

gives rise to an output corresponding to C_{4p} or C_{4m} , as appropriate. The inphase and quadrature sequences associated with this complex input sequence become, respectively,

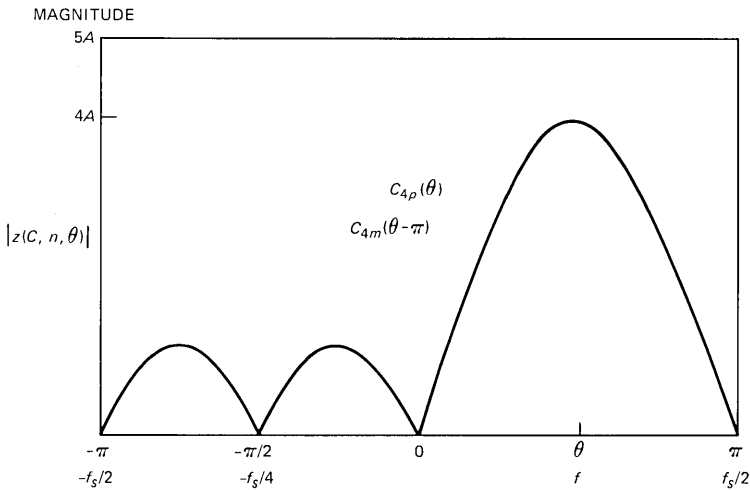


Fig. 4—Responses of complex, recursive filter pairs C_{4p} and C_{4m} in the same scale and over the same range of frequency as in Fig. 3.

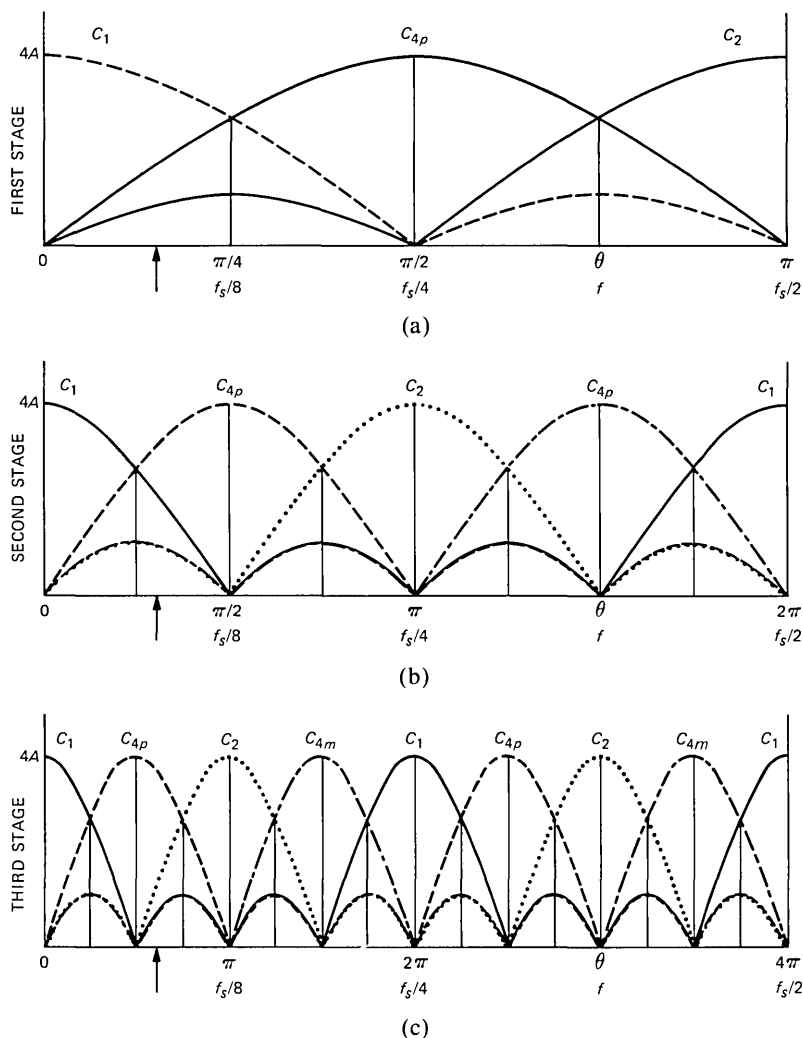


Fig. 5—(a) Arrangement of three first-order recursive filters that cover the frequency band from 0 to one-half of the sampling rate. (b) Arrangement of four recursive filters that cover the band from 0 to one-half of the initial sampling rate and are symmetric over the four subbands shown in Fig. 5a. (c) Arrangement of eight recursive filters that cover the band from 0 to one-half of the initial sampling rate and are symmetric over the eight subbands shown in Fig. 5b.

$$A \cos(k\nu + \varphi) \cos(k\pi/2) \mp A \sin(k\nu + \varphi) \sin(k\pi/2) \quad (21)$$

and

$$A \sin(k\nu + \varphi) \cos(k\pi/2) \pm A \cos(k\nu + \varphi) \sin(k\pi/2). \quad (22)$$

Since k is a nonnegative integer, the shifted inphase sequence reduces

to a sequence that is periodic of period four having element values for $k = 0, 1, 2$ and 3 of [from eq. (21)]:

$$\begin{aligned} &A \cos(k\nu + \varphi); \mp A \sin(k\nu + \varphi); \\ &\quad - A \cos(k\nu + \varphi); \pm A \sin(k\nu + \varphi). \end{aligned} \quad (23)$$

Similarly, the shifted quadrature sequence has elements for $k = 0, 1, 2, 3$ [from eq. (22)] of:

$$\begin{aligned} &A \sin(k\nu + \varphi); \pm A \cos(k\nu + \varphi); \\ &\quad - A \sin(k\nu + \varphi); \mp A \cos(k\nu + \varphi). \end{aligned} \quad (24)$$

Examination of eqs. (23) and (24) suggests that the operation of normalized frequency shifting by $\pm\pi/2$, rather than occurring through frequency-domain manipulations, may be straightforwardly implemented in the sequence or sample domain merely by interchanging and changing signs of the inphase and quadrature inputs to a filter pair, when appropriate. Because of the form of eq. (20), such an implementation may be referred to as a modulus-one multiplier ($j^{\pm k}$) or frequency shifter.

Figure 6 is a block diagram of the modulus-one multiplier for the case of a $-\pi/2$ frequency shift (C_{4p}). The inputs to this unit are the original inphase and quadrature sequence elements. The operations of sign changing and line interchanging occur within this unit, as depicted for $k = 0, 1, \dots, 4, \dots$. The frequency-shifted, inphase, and quadrature sequence elements, respectively, are fed to two identical C_1 filters whose outputs are squared, summed, and square rooted. Finally, this unit provides the response described above by C_{4p} . Note that the operations needed to compute the modulus $\sqrt{x^2 + y^2}$ can be simplified

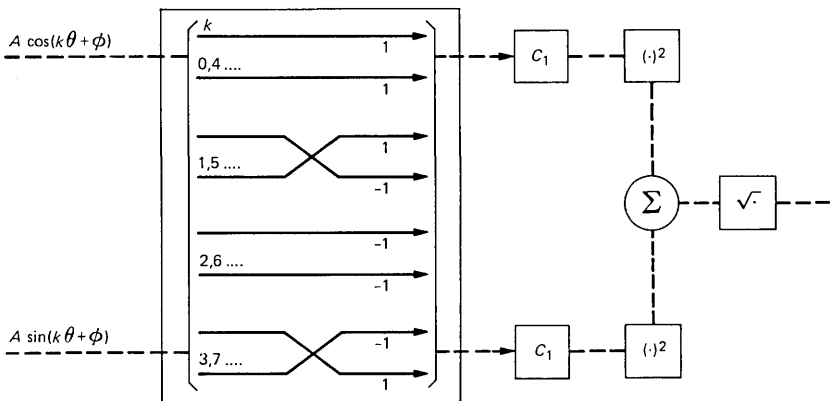


Fig. 6—Block diagram of a modulus-one multiplier for the case of a $-\pi/2$ frequency shift (C_{4p}).

by using known approximations to the modulus (see Refs. 12 through 14). An example is the one given by

$$\sqrt{x^2 + y^2} \approx \text{Max}(|x|, |y|) + \alpha \text{Min}(|x|, |y|). \quad (25)$$

α is a scalar multiplier. In Refs. 5 through 7 we used $\alpha = 0.25$, so that multiplication by α corresponds to two shift operations. The choice of $\alpha = 0.25$ causes only a small degradation in performance, as has been noted in simulations.

Figures 5b and 5c depict how each of the two subbands in the range 0 to $\pi/2$ of Fig. 5a may be further partitioned to isolate the tone of interest. Basically, the subbands are subdivided into second-stage subbands by reducing the sampling rate and reconfiguring the filter array within each subband of interest. For instance, the first-stage subband labeled C_1 in Fig. 5a has been subdivided by reducing the sampling rate by a factor of two and covering the old subband by C_1, C_{4p} , which effects two second-stage subbands symmetrically dispersed across the original subband. Further sampling rate reduction by a factor of two results in the partition of Fig. 5c. The configuration and covering of Fig. 5b occurs within each subband during each stage of decimation after the first stage.

To understand how the given input tone can be isolated by processing with consecutive stages of decimation, the steps in processing a single tone of frequency f_0 are now considered. For the complex tone initially sampled at a rate f_s , spectral lines occur in the digital spectrum at $f_0 + kf_s$, $k = 0, \pm 1, \dots$. The sampling rate is chosen so that the tone falls within the range 0 to $f_s/4$ ($0 < f_0 < f_s/4$); thus the tone may be unambiguously determined to fall within one of the subbands or cells $(0, f_s/8)$ or $(f_s/8, f_s/4)$, by processing the outputs from the filter array or bank configured as C_1, C_{4p} . This is basically accomplished by comparing each filter output to another.

If the complex tone samples are now decimated by a factor of two, that is, only every second value from the original set of samples is retained, then spectral lines appear at $f_0 + kf_s/2$, $k = 0, \pm 1, \dots$. By selecting the 2:1 ratio between initial sampling rate and reduced sampling rate, and by selecting cell widths of $f_s/8$ for the first stage of sampling, no additional spectral components fall within the original subband containing baseband spectral line f_0 . This is true, even though aliasing occurs, because the judicious selection of cell width and reduced sampling rate precludes aliased spectral lines from appearing in the subband containing the spectral line of interest.

The process described with respect to the decimation by a factor of two may continue until the desired resolution (final cell width) is achieved. In Figs. 5a through c three stages of processing are exemplified. The tone will thus be resolved to a cell of width $f_s/32$.

For example, say that $2(f_s/32) \leq f_0 \leq 3(f_s/32)$ (see also the arrows in Figs. 5a through c). At the first stage (Fig. 5a), the output of C_1 is compared to the output of C_{4p} ; since " $|C_1| > |C_{4p}|$ " it is concluded that the tone is located in $0 \leq f_0 \leq f_s/8$. At the second stage (Fig. 5b), the output of C_1 is compared to the output of C_{4p} , and since " $|C_1| < |C_{4p}|$ " it is concluded that the tone is in $f_s/4 \leq f_0 \leq f_s/8$. At the final stage, stage three (Fig. 5c), the output of C_{4p} is compared to the output of C_2 , and since " $|C_{4p}| > |C_2|$ " it is concluded that the tone is in $f_s/16 \leq f_0 \leq 3f_s/32$, which is the correct presumed tone's location.

From the description with respect to the band from 0 to $f_s/4$, it is also apparent that a tone in the bands $(kf_s/4, (k+1)f_s/4)$, $k = 1, 2, 3$ could be processed in an analogous manner, provided k is known to the CTLS and only a single tone is present.

III. CTLS PERFORMANCE

In the previous section only the principles of operation of the CTLS were presented, and no consideration was given to the presence of noise in which the tone is usually embedded.

To combat the noise we propose two methods, based on soft decision and hard decision, respectively. To examine the performance of the CTLS, computer simulations were performed. In the simulations the location of the tone was initially set in the interval $(0, f_s/4)$ and was resolved by the CTLS into one of 64 cells. In each experiment 256 complex data words were processed. At each stage, the filters were operated for a small number of samples ($2 \leq N \leq 7$) as compared with the number of data words (256). Therefore, the filter operation was repeated at each stage (without overlapping the data), exhausting the data.

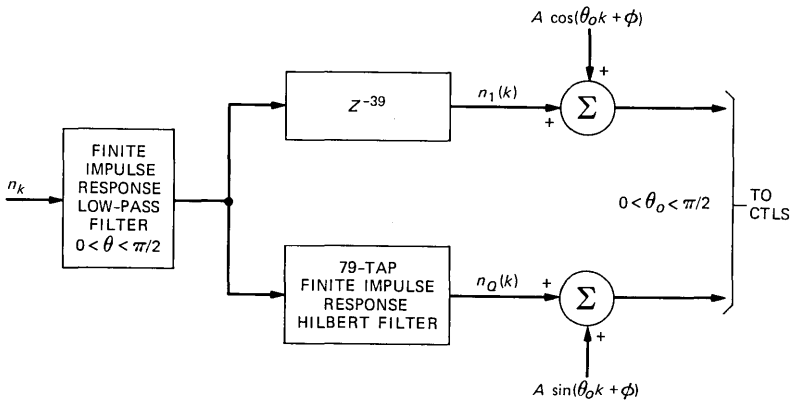


Fig. 7—Block diagram of the configuration for generating the input noisy tone to the CTLS.

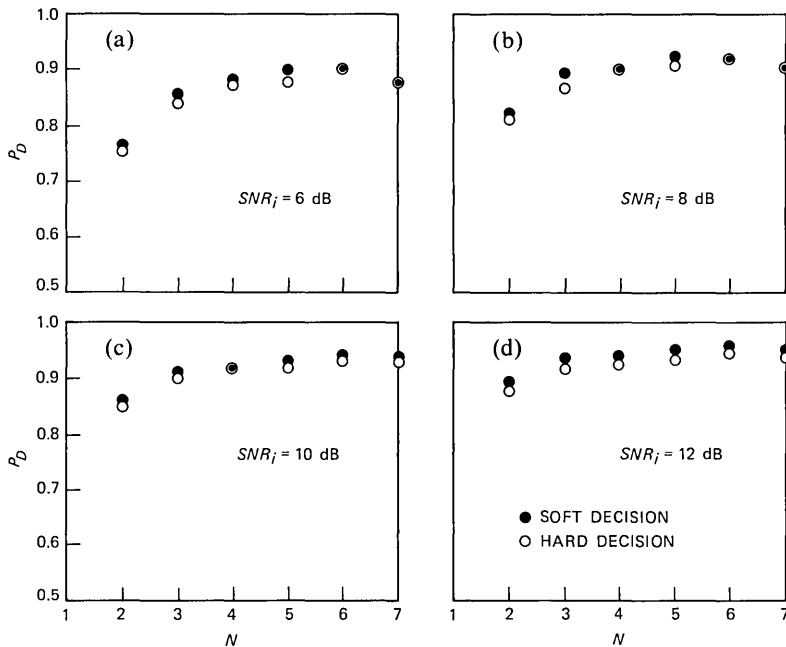


Fig. 8—Probability of correct tone location vs. number of samples; the filters are operated at different input SNR_i values.

With the hard-decision method, the CTLS uses (at each stage) the maximal output of the filters (over all repetitions). With the soft-decision method, the average (over all repetitions) of the filter's output at each stage is used.

Figure 7 is a block diagram of the operations carried out to generate the noisy complex digital tone that was fed to the CTLS. $\{n_k\}$ is a zero mean white ($E\{n_k n_j\} = \sigma^2 \delta_{kj}$) Gaussian sequence, which was low-pass filtered to eliminate out-of-band noise.

The simulations were carried out for different values of SNR_i (6, 8, 10, 12 dB):

$$SNR_i \triangleq \frac{A^2}{E\{n_I^2(k) + n_Q^2(k)\}}, \quad (26)$$

where E denotes the expectation operator. Figure 8(a through d) presents simulation results for the probability of locating the input tone in the correct cell as a function of the number of samples for which the filters are operated ($2 \leq N \leq 7$).

Another performance measure used in our simulations is the output signal-to-noise ratio (SNR_o), which gives the reduction in frequency uncertainty,¹⁰ that is,

$$SNR_o = \frac{\text{var}(\nu_o)}{\text{var}(\nu_o - \hat{\nu}_o)}. \quad (27)$$

In (27) ν_o denotes the uniformly distributed input-normalized frequency (in the range 0 to $\pi/2$), and $\hat{\nu}_o$ is its estimate at cell width.

It is known¹⁰ that when no errors are made in assigning the input signal to a cell, then

$$\max SNR_o = (N_c - 1)^2, \quad (28)$$

which gives 36.12 dB for $N_c = 64$, that is, 64 cells. Figure 9(a through d) shows the computer simulation results obtained for SNR_o as a function of the number of samples at which the filters were operated ($2 \leq N \leq 7$), at different SNR_i values (in the range of 6 to 12 dB).

From the simulation results in Figs. 8 and 9, we conclude the following:

1. The soft-decision method is superior to the hard-decision method.
2. The filters should operate with $N = 6$ samples.

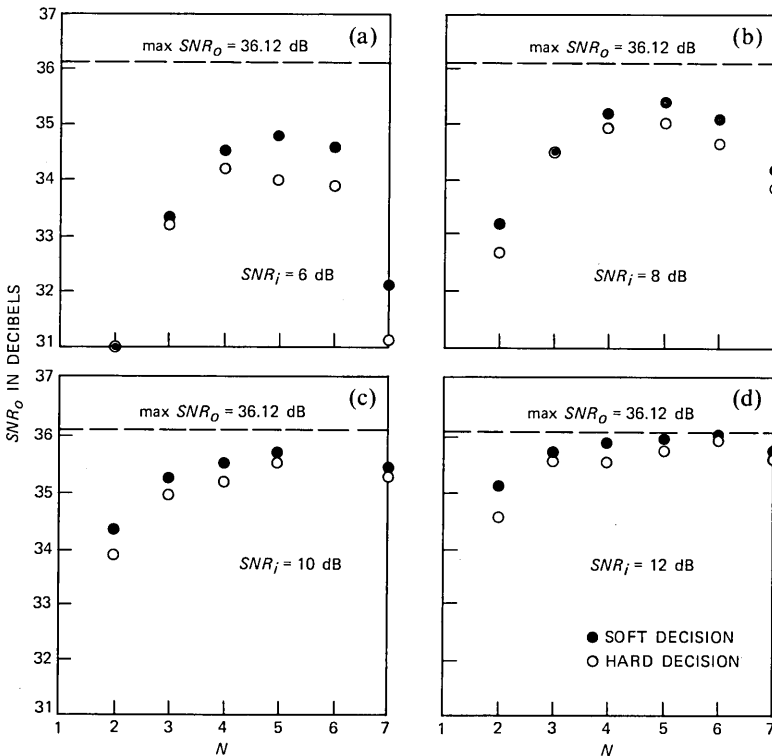


Fig. 9—Output signal to noise ratio (SNR_o) vs. number of samples; the filters are operated at different input SNR_i values.

3. For $SNR_i \geq 10$ dB and in conjunction with (1) and (2), the probability of locating the tone in the correct cell is in excess of 95 percent, and SNR_o is smaller than $\max SNR_o$ by less than 0.3 dB.

IV. DFT TONE LOCATION SYSTEM

In this section we present the DFT Tone Location System (FTLS). Let $\{x_i\}_{i=0}^{N-1}$ be N samples of the complex tone; then

$$X_k = DFT\{x_i\} = \sum_{i=0}^{N-1} x_i e^{-j\frac{2\pi}{M}ki}, \quad (29)$$

i.e., $x_i = 0$ for $i = N, N + 1, \dots, M - 1$ ($M > N$ is mandatory), and

$$A_k = |X_k|, \quad k = 0, 1, \dots, M - 1. \quad (30)$$

It can be easily demonstrated that

$$A_k = |y_{N-1}(k)|, \quad (31)$$

where

$$y_{l+1}(k) = e^{j\frac{2\pi}{M}k} y_l(k) + x_l, \quad (32)$$

$$y_0(k) = 0, \quad l = 0, 1, \dots, N - 1.$$

Therefore, $z(C_i, N - 1, \nu)$, $i = 1, 2, 4p, 4m$ [see eqs. (15) through (18)] are merely particular samples of A_k , i.e., $A_0, A_{M/2}, A_{M/4}, A_{3M/4}$. Similar to the derivations of (15) through (18), we get

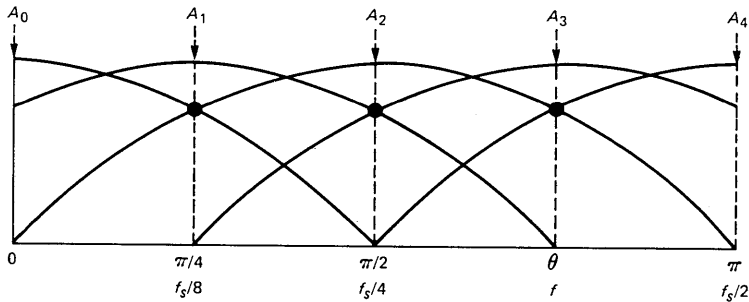
$$A_k = A \left| \frac{\sin \left[\frac{N}{2} \left(\nu - \frac{2\pi}{M} k \right) \right]}{\sin \frac{1}{2} \left(\nu - \frac{2\pi}{M} k \right)} \right|, \quad (33)$$

where A and ν are the tone's amplitude and normalized frequency, respectively.

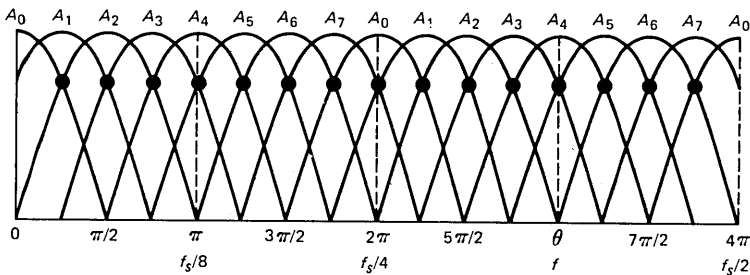
The operation principles of the FTLS are now explained. The input tone, which is comprised of a frequency located randomly within the band 0 to $f_s/2$, is converted into a complex tone. The quadrature tones are both initially sampled at a rate of f_s and then N samples of the complex tone are processed by an M -point DFT ($M = 2^m$, $N < M$, and the N samples are padded by $M - N$ zeros). The modulus of the M -point DFTs are further processed so that the resonances associated with the DFT cover a band of frequencies, including the tone frequency, in symmetric fashion. Location of the subband containing the tone is achieved by finding the maximal modulus of the first $(M/2) + 1$ even (counting from zero) DFT points, A_{2k} say, and then,

if $2k \neq 0, M/2$, comparing A_{2k-1} and A_{2k+1} . The technique is exemplified in Figs. 10a and b for $M = 8$ and $N = 4$.

In the FTLS the above procedure (at stage 1) partitions the initial band $(0, f_s/2)$ to $M/2$ subbands, each of width $(f_s/2)/(M/2)$, and the tone lies unambiguously within one of the $M/2$ subbands because of oversampling. Once a tone has been located within the confines of a subband, sampling rate reduction or decimation by a factor of $M/2$ is effected. Although the tone is now undersampled, judicious choice of sampling rate reduction ratio and subband width precludes additional spectral lines from appearing within the subband containing the tone. At the reduced sampling rate again (as before), N samples of the complex tone are processed by an M -point DFT. The moduli of the M -point DFT are further processed to again achieve a symmetrical placement of the DFT's resonances across the subband of width $(f_s/2)/(M/2)$ containing the tone. Now, if in the previous stage the tone has been located in an even subband (starting with the zeroth cell), find the maximal value of $\{A_0, A_2, \dots, A_{M/2}\}$; otherwise, find the maximal value of $\{A_{M/2}, A_{M/2+2}, \dots, A_{M-2}, A_0\}$, say A_{2k} , and compare



(a)



(b)

Fig. 10—Operation of the FTLS for $M=8$, $N=4$: (a) first stage, and (b) second stage.

A_{2k-1} with A_{2k+1} (provided that $k \neq 0, M/2$, for both cases). Now (after stage 2) the tone is located in a subband of width $(f_s/2)/(M/2)^2$. This process may be repeated until, finally, at the last stage, say S , the frequency subbands utilized for resolving the tone are each of width $(f_s/2)/(M/2)^S$. Note that at each stage only the even DFT coefficients and two odd DFT coefficients are needed. Moreover, a minor modification to the FTLS enables the system to test for a tone in the other band, i.e., $(f_s/2, f_s)$, provided the FTLS knows in which of the two subbands the single tone is present. Also, for $N = 2, 3$ and $M = 4$ we have a FTLS that resembles the CTLS, except for the sampling rate, which is now halved.

It should be noted that the relation $M > N$ is mandatory, and ensures that comparisons between the pertinent A_i 's will be within their main lobes. Note that the ideas to combat noise presented in Section III for the CTLS pertain as well to the FTLS.

Now the FTLS is exemplified by choosing $M = 8$ and $N = 4$. Referring to Fig. 10, A_0 through A_7 are obtained from four samples of the complex tone [see (30)]. Dividing the band 0 to π into four subbands is carried out as follows:

1. The maximal value of $\{A_0, A_2, A_4\}$ is computed. From the result we decide in which of the three subbands $(0, \pi/4)$, $[\pi/4, (3\pi)/4]$, $[(3\pi)/4, \pi]$ the tone is present. If the tone is not in the subband $[\pi/4, (3\pi)/4]$, we continue to the next stage (Fig. 10b); otherwise we

2. Compare A_1 and A_3 , and accordingly find in which of the two subbands, $(\pi/4, \pi/2)$ or $[\pi/2, (3\pi)/4]$, comprising the subband $[\pi/4, (3\pi)/4]$ the tone is present. Now Fig. 10b depicts how each of the four subbands in the range 0 to π of Fig. 10a may be further partitioned to isolate the tone of interest. Basically the subbands are subdivided into second-stage subbands by reducing the sampling rate by a factor of $M/2 = 4$. Now if the tone is present in an even (counting from 0) subband, $(0, \pi/4)$ or $[\pi/2, (3\pi)/4]$, find the maximal value of $\{A_0, A_2, A_4\}$. Otherwise (i.e., the tone is present in one of the odd subbands $(\pi/4, \pi/2)$ or $[(3\pi)/4, \pi]$), find the maximal value of $\{A_4, A_6, A_8\}$. If the even or odd subband output amplitude A_0 or A_4 is maximal, then continue to stage 3. If the maximal value is A_2 (even case) or A_6 (odd case), then compare A_1 with A_3 or A_5 with A_7 , respectively. Now the tone has been located within a subband of width $(f_s/2)/(8/2)^2 = f_s/32$, and the processing continues in this manner until the desired frequency resolution is achieved.

V. CONCLUSION

We have presented two methods of tone location (CTLS and FTLS) as an alternative to conventional DFT. For a given requirement of N_C frequency resolution cells, a conventional DFT, which is a maximum-

likelihood estimator, uses a single transform of size N_C requiring $(N_C/2)\log_2(N_C)$ multiplications, which are the main computational burden. The associated complexity of such multiplication is eliminated in the CTLS, using a decimation scheme involving filters that have coefficients $\pm 1, \pm j$, i.e., multiplier-less digital filters. For the same number of resolution cells, computational complexity is significantly reduced, at the expense of increased frequency uncertainty as a function of increasing noise. This uncertainty is decreased in the FTLS, where the cyclotomic filters of the CTLS are replaced with small DFTs (which can be repeated several times at each decimation stage). While this improved performance is at the expense of increased computational complexity (compared to the CTLS), and the resulting system does not have the optimal performance of a single DFT, the FTLS can nonetheless be preferable over a single DFT when the size of the latter makes it impractical to implement. To obtain N_C frequency resolution cells by using the FTLS in S stages, one M -point DFT is sufficient at each stage, and we have the relationship $N_C = (M/2)^S$. Hence, using the FTLS, $M = 2^{\sqrt[S]{N_C}}$, and $S(M/2)\log_2(M)$ multiplications are sufficient for locating the tone. For example, suppose $N_C = 4096$ and $S = 4$; then $M = 16$, and the conventional DFT requires 24,576 multiplications, whereas the FTLS requires only 128 multiplications.

It follows from the simulations of the CTLS that the soft-decision method should be preferred and the filters should be operated for $N = 6$ samples. For input signal-to-noise ratios in excess of 10 dB the output signal-to-noise ratios differ from the maximal output signal-to-noise ratio by less than 0.3 dB. Finally, note that tone presence can be determined by comparing the filter outputs in the first stage to an appropriate threshold value (see Refs. 11 and 15 and the references therein).

REFERENCES

1. V. Cappelini, "Digital Filtering With Sampled Signal Spectrum Frequency Shift," *Proc. IEEE*, 57 (February 1969), pp. 241-2.
2. V. Cappelini, R. L. Emiliani, and A. Gabbanini, "A Special Purpose On-Line Processor for Bandpass Analysis," *IEEE Trans. Audio Electroacoust.*, AU-18 (June 1970), pp. 188-94.
3. J. M. Wozencraft and I. M. Jacobs, "Principles of Communication Engineering," New York: Wiley, 1967, pp. 642-5.
4. B. Gopinath and R. P. Kurshan, "A Touch-Tone Receiver-Generator With Digital Channel Filters," *B.S.T.J.*, 55 (April 1976), pp. 455-67.
5. D. Hertz, R. P. Kurshan, and D. Malah, "Multiple Tone Detector and Locator," U.S. Patent 4,361,875, issued November 30, 1982.
6. R. P. Kurshan and D. Malah, "Broadband Cyclotomic Tone Detector," U.S. Patent 4,333,156, issued June 1, 1982.
7. D. Hertz, R. P. Kurshan, and D. Malah, "Cyclotomic Tone Detector and Locator," U.S. Patent 4,348,735, issued September 1982.
8. D. Hertz, "Digital Cyclotomic Filters and Their Applications to Signal Processing," M.Sc. Thesis, Technion-Israel Institute of Technology, June 1979.

9. D. C. Rife and R. R. Boorstyn, "Single-Tone Parameter Estimation From Discrete-Time Observations," *IEEE Trans. Inform. Theory*, *IT-20* (September 1974), pp. 591-8.
10. L. C. Palmer, "Coarse Frequency Estimation Using the DFT," *IEEE Trans. Inform. Theory*, *IT-20* (January 1974), pp. 104-9.
11. R. P. Kurshan and B. Gopinath, "Digital Single Tone Generator-Detectors," *B.S.T.J.*, *55* (April 1976), pp. 469-96.
12. M. Onoe, "Fast Amplitude Approximation Yielding Either Exact Mean or Minimum Deviation for Quadrature Pairs," *Proc. IEEE*, *60* (July 1972), pp. 921-2.
13. A. Filip, "Linear Approximation to $\sqrt{x^2 + y^2}$ Having Equiripple Error Characteristics," *IEEE Trans. Audio Electroacoust.*, *AU-21* (December 1973), pp. 554-6.
14. D. F. Freeman, "Equal Ripple Approximation for Envelope Detection," *IEEE Trans. Acoust., Speech, and Signal Processing*, *ASSP-26*, No. 3 (June 1978), pp. 254-6.
15. J. G. Gander, "A Pattern Recognition Approach to Tone Detection," *Signal Processing*, *1*, No. 1 (January 1979), pp. 65-81.

AUTHORS

David Hertz, B.Sc. and M.Sc. (Electrical Engineering), Technion-Israel Institute of Technology, Haifa, in 1975 and 1979, respectively. He is now completing his work towards the Ph.D. degree in electrical engineering at Technion. He holds two patents with coauthors and his research interests are in digital signal processing and control theory.

Robert P. Kurshan, Ph.D. (Mathematics), 1968, University of Washington; Krantzberg Chair for Visiting Scientists, Technion, Haifa, Israel, 1976-1977; AT&T Bell Laboratories, 1968—. Mr. Kurshan is a member of the Mathematics Research Center. His current interests include formal development, specification, and analysis of distributed systems such as communication protocols.

David Malah, B.S. and M.S. (Electrical Engineering), Technion-Israel Institute of Technology, in 1964 and 1967, respectively; Ph.D. (Electrical Engineering), 1971, University of Minnesota; University of New Brunswick, Canada N.B., 1970-72; sabbatical leave, Bell Laboratories, 1979-81; Technion-Israel Institute of Technology, 1972—. At Technion-Israel Institute of Technology, he is Associate Professor of Electrical Engineering. From 1975 to 1979, and since 1981, Mr. Malah has been in charge of the Signal Processing Laboratory at Technion-Israel and is involved in research on speech and image communications, and digital signal processing techniques.

John T. Peoples, B.S.E.E., 1963, University of Detroit, M.S.E.E., 1965, and Ph.D. (Electrical Engineering), 1971, New York University; J.D., 1981, Seton Hall Law School; AT&T Bell Laboratories, 1963-1983. Present affiliation Bell Communications Research, Inc. Mr. Peoples has worked on circuit analysis and synthesis algorithms, modulation techniques, and digital signal processing methods. He is presently Attorney, Intellectual Property Matters. He holds seven U.S. patents. Senior Member, IEEE; member, Tau Beta Pi, Eta Kappa Nu. Admitted before the U.S. Supreme Court; Court of Appeals for the Federal Circuit; New Jersey Federal District Court; and New Jersey Supreme Court. Registered patent attorney in the U.S. and Canada. Member, American Bar Association; American Intellectual Property Law Association; New Jersey Bar Association; and New Jersey Patent Law Association.

Performance of Nondiversity Receivers for Spread Spectrum in Indoor Wireless Communications

By M. KAVEHRAD*

(Manuscript received December 14, 1984)

In this work we have considered direct-sequence spread-spectrum transmission for indoor wireless communications. We have modeled the indoor communications medium, which is a multipath fading channel, by a discrete set of Rayleigh faded paths. We have proposed new analytical techniques to evaluate the probability of error for the receiver terminals studied in this work. Numerical results reveal that, for the nondiversity receivers considered here, Rayleigh fading is very hostile to this form of modulation/multiple-access technique. The results also indicate that either some form of operation to prevent Rayleigh fading or diversity operation to counteract Rayleigh fading is required.

I. INTRODUCTION

A principal purpose of this paper is to evaluate the performance of a direct-sequence Spread-Spectrum Multiple-Access (SSMA) system using Binary Phase Shift Keying (BPSK) modulation for Indoor Wireless Communications (IWC).

In the past decade there has been increased interest in a class of multiple-access techniques known as Code Division Multiple Access (CDMA) in which the mode of access is due primarily to coding by spread-spectrum sequences. In contrast with traditional time- and

* AT&T Bell Laboratories.

Copyright © 1985 AT&T. Photo reproduction for noncommercial use is permitted without payment of royalty provided that each reproduction is done without alteration and that the Journal reference and copyright notice are included on the first page. The title and abstract, but no other portions, of this paper may be copied or distributed royalty free by computer-based and other information-service systems without further permission. Permission to reproduce or republish any other portion of this paper must be obtained from the Editor.

frequency-division multiple access, these techniques do not require accurate time or frequency coordination among the transmitters in the system. This feature makes CDMA very attractive for IWC applications, because, as described later, an IWC takes place in a severe multipath fading environment. However, the cost of the ease of access is the increased channel bandwidth required by spread-spectrum codes. The bandwidth spreading leads to a low spectral energy density level, which is an advantage in military communications in hostile environments. It also offers the possibility of reusing overcrowded radio frequency bands, as recently studied by the Federal Communications Commission.¹

SSMA is a common form of CDMA in which every user is assigned a code sequence modulated onto a carrier signal according to the user's digital information. A high-rate code, that is, many code chips per data bit, spreads the bandwidth of the information signal. Frequency-hopped²⁻⁴ and phase-modulated SSMA⁵ are two forms of SSMA. The latter, also known as direct-sequence spread-spectrum multiple access, is what we concern ourselves with in this work, for its multiple-access capability and ease of implementation.

Since in direct-sequence SSMA the entire channel bandwidth is available to all users of the system at all times, the code sequence applied by each user in spreading the information band must have low cross-correlation properties in order to achieve a low level of mutual interference among the users. Several classes of code sequences suitable for this application have been presented by Sarwate and Pursely.⁶ A class of these codes that are employed in our work is the well-known Gold sequences, which possess the low cross-correlation properties required in multiple-access applications.

The chief purpose of this paper is to assess the communication performance of a direct-sequence SSMA system in the presence of multipath fading that is a characteristic of IWC. Our criterion of merit is average probability of error as a function of signal-to-noise ratio.

There is a sizable literature relating to the effects of multiple-access interference on the performance of a direct-sequence SSMA, among which are Refs. 7 through 12. All of these consider the communication channel to be a single path with no fading. In IWC applications, because of the existence of many reflectors and scatterers, multipath fading is severe. Preliminary impulse response measurements inside office buildings indicate the severity of multipath fades.^{13,14} Hence, the attempt in this work is to incorporate multipath fading effects in the analysis of average probability of error of direct-sequence SSMA. Among the limited number of articles relating to the effects of multipath fading on the performance of direct-sequence SSMA is the work by G. Turin¹⁵ that examines the structure of a number of receivers for

mobile digital radio. However, the computer simulation results in Ref. 15 are restricted to the behavior of a single transmitter-receiver pair, and therefore, no multiple-access interference is taken into account. References 16 through 18 consider fading links, although Ref. 17 specifies single-tone, rather than multiple-access, interference. However, almost all studies have used measures other than average error rate in their evaluation. Reference 18 presents a simplified analysis by invoking the Gaussian assumption for the composite multiple-access interference distribution previously addressed in papers by Yao⁹ and Mazo.¹⁰ We avoid any argument about the validity and range of accuracy of the Gaussian assumption. In this work, unlike in Ref. 18, we make no assumption about the distribution of the composite multiple-access interference. By employing moment-generating techniques, we evaluate the average probability of error in the presence of multipath fading. In this evaluation we apply the numerical Gauss quadrature integration.¹⁹ Specifically, our work extends the work in Ref. 12 to channels with multipath fading.

In Section II we begin with a description of the SSMA system and the channel model. We then derive the conditional error probability. Evaluation of average error probability by the moment-generating approach is described in Section III. Numerical results are discussed in Section IV. Finally, a summary and conclusions are presented in the last section of the paper.

II. THE MODEL AND THEORETICAL DEVELOPMENTS

2.1 System model

Consider the direct-sequence SSMA transmission system model for K users depicted in Fig. 1. The k th user's information signal $b_k(t)$ is a sequence of rectangular pulses taking on values from the set $\{\pm 1\}$ over a T -seconds time interval. Hence,

$$b_k(t) = \sum_{j=-\infty}^{\infty} b_j^k P_T(t - jT), \quad (1)$$

where b_j^k represents the k th user data at the j th timing interval and $P_T(\cdot)$ is a rectangular waveform of T -seconds duration. The k th user is assigned a code waveform $a_k(t)$ that consists of a periodic sequence of rectangular chips taking on values from the set $\{\pm 1\}$ each of duration T_c seconds. If a_i^k represents the i th-chip value of the k th user, then,

$$a_k(t) = \sum_{i=-\infty}^{\infty} a_i^k P_{T_c}(t - iT_c). \quad (2)$$

We assume each user code sequence has a period of $N = T/T_c$. That is, there is one period of code sequence per data bit.

After spreading the information bandwidth to N times its original value, by modulo-2 adding the direct-sequence code to the data signal and biphasic modulating the result onto the carrier signal, $A\cos(\omega_c t + \theta_k)$ — where A is the carrier level, ω_c is the nominal carrier frequency, and θ_k is the carrier phase that is assumed to be uniformly distributed between 0 and 2π —the transmitted signal of the k th user becomes

$$S_k(t) = Aa_k(t)b_k(t)\cos(\omega_c t + \theta_k), \quad k = 1, 2, \dots, K. \quad (3)$$

2.2 Transmission channel model

In spread-spectrum transmission over multipath fading channels, if the spread bandwidth of the transmitted signal exceeds the coherence bandwidth of the channel, where the latter is proportional to the inverse of the channel maximum multipath delay spread, the multipath components can be resolved into a discrete number of Rayleigh faded paths. The number of resolved paths depends on the channel multipath spread and the spreading bandwidth of the signal, as discussed by Proakis.²⁰ We assume that the IWC channel for the desired transmitter and receiver ($k = 1$) depicted in Fig. 1 can be represented by an L -paths Rayleigh fading model where a single transmitted pulse is received via L -paths at the random time instants t_l , $l = 1, \dots, L$. We assume t_l is uniformly distributed over one bit period, i.e., over $(0, T)$. This is ensured by signaling at baseband at a rate less than the channel coherence bandwidth. Hence, intersymbol interference is negligible

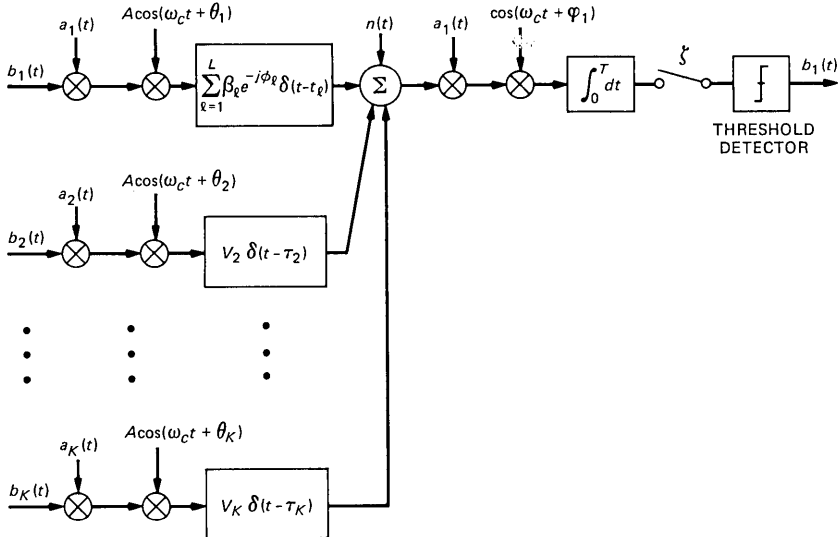


Fig. 1—System model.

here. Therefore, the low-pass equivalent impulse response of the passband channel, $h(t)$, can be represented by

$$h(t) = \sum_{l=1}^L \beta_l \delta(t - t_l) e^{j\phi_l}, \quad (4)$$

where $\delta(\cdot)$ is the Kronecker delta, β_l is a Rayleigh distributed random path gain, and ϕ_l is the random path phase, uniformly distributed between 0 and 2π . It is further assumed that all the parameters of all paths are identically distributed over their specified range. These assumptions are also related to G. Turin's¹⁵ description of a discrete multipath fading environment. As stated earlier, the L -paths model stems from the fact that spread-spectrum signaling with a transmitted signal bandwidth much wider than the coherence bandwidth of the multipath fading channel enables the multipath components to be resolved. Therefore, the channel seems to be fading-frequency selective to the signal. In eq. (4) all the variables are time invariant.

To keep the analysis tractable we further assume that the k th interfering user of the multiple-access system is linked to the receiver of Fig. 1 via a single Rayleigh fading path with a uniformly distributed random delay τ_k ranging from zero to one bit period, T . The conclusions will reveal that there is no loss in generality in making such an assumption. Since our chief aim is to show what is not possible, more elaborate models incorporating more noise sources could only strengthen our conclusions.

Since τ_k and t_l are independent, the model results in a Rayleigh faded interfering user sequence being received asynchronously compared with the desired user sequence at the receiver in Fig. 1. In our formulation we specify the Rayleigh distributed path gain of the interfering users by V_k , $k = 2, \dots, K$. Therefore, as depicted in Fig. 1, the received signal for the fading model described above is given by

$$\begin{aligned} r(t) = & A \sum_{l=1}^L \beta_l a_1(t - t_l) b_1(t - t_l) \cos(\omega_c t - \omega_c t_l + \phi_l + \theta_1) \\ & + A \sum_{k=2}^K V_k a_k(t - \tau_k) b_k(t - \tau_k) \cos(\omega_c t - \omega_c \tau_k + \theta_k) + n(t), \quad (5) \end{aligned}$$

where $n(t)$ is white Gaussian noise with double-sided spectral density of $N_0/2$ level and θ_1 can be assumed to be zero with no loss of generality.

The desired receiver is assumed to coherently recover the carrier phase and delay lock to the first arriving desired signal. Therefore, after (1) the correlation operation that collapses the wideband coded signal into a narrowband modulated signal and (2) the demodulation process, a signal sample at the receiver low-pass filter output can be expressed as

$$\xi = \int_0^T r(t)a_1(t)\cos(\omega_c t)dt; \quad (6)$$

or, using eq. (5) we have

$$\begin{aligned} \xi = & \frac{A}{2} \sum_{l=1}^L \beta_l \int_0^T a_1(t-t_l)b_1(t-t_l)a_1(t)\cos(\psi_l)dt \\ & + \frac{A}{2} \sum_{k=2}^K V_k \int_0^T a_k(t-\tau_k)b_k(t-\tau_k)a_1(t)\cos(\Theta_k)dt + \eta, \quad (7) \end{aligned}$$

where η is a sample of the Gaussian noise with zero mean and $(N_0T)/4$ variance, $\psi_l = \phi_l - \omega_c t_l$ and $\Theta_k = \theta_k - \omega_c \tau_k$.

2.3 Detection problem and average error probability

The assumption of phase and delay locking of the receiver to the first desired modulated signal that is received enables one to rewrite eq. (7) as

$$\begin{aligned} \xi = & \beta_1 \frac{A}{2} \int_0^T a_1^2(t)b_1(t)dt \\ & + \frac{A}{2} \sum_{l=2}^L \beta_l \int_0^T a_1(t-t_l)b_1(t-t_l)a_1(t)\cos(\psi_l)dt \\ & + \frac{A}{2} \sum_{k=2}^K V_k \int_0^T a_k(t-\tau_k)b_k(t-\tau_k)a_1(t)\cos(\Theta_k)dt + \eta. \quad (8) \end{aligned}$$

We notice that from eq. (1),

$$b_1(t) = \sum_{j=-\infty}^{\infty} b_j^1 P_T(t-jT), \quad (9)$$

and therefore, eq. (8) can be expressed as

$$\begin{aligned} \xi = & \beta_1 \frac{AT}{2} b_0^1 + \frac{A}{2} \sum_{l=2}^L \beta_l [b_{-1}^1 R_{1,1}(t_l) + b_0^1 \hat{R}_{1,1}(t_l)]\cos(\psi_l) \\ & + \frac{A}{2} \sum_{k=2}^K V_k [b_{-1}^k R_{k,1}(\tau_k) + b_0^k \hat{R}_{k,1}(\tau_k)]\cos(\Theta_k) + \eta, \quad (10) \end{aligned}$$

where b_0^1 represents the information bit being detected and b_{-1}^1 is the preceding bit, which, due to the channel delay spread, affects the detection of b_0^1 received on the first path between the desired transmitter and receiver.

In eq. (10),

$$R_{1,1}(t_l) = \int_0^{t_l} a_1(t-t_l)a_1(t)dt \quad (11)$$

and

$$\hat{R}_{1,1}(t_l) = \int_{t_l}^T a_1(t - t_l)a_1(t)dt$$

are partial autocorrelation functions of the regenerated desired code at the receiver, that is, $a_1(t)$ with its delayed version received via the l th Rayleigh faded path, namely, $a_1(t - t_l)$. We note that the coded sequence received via the first path between the transmitter and receiver of Fig. 1 is fully correlated with the regenerated sequence $a_1(t)$, owing to the delay locking operation introduced at the receiver. Also, due to the asynchronous arrival of the interfering user's code, eq. (10) contains partial cross correlations of the regenerated sequence, $a_1(t)$, and a delayed version of the interfering codes defined by

$$R_{k,1}(\tau_k) = \int_0^{\tau_k} a_k(t - \tau_k)a_1(t)dt \quad (12)$$

and

$$\hat{R}_{k,1}(\tau_k) = \int_{\tau_k}^T a_k(t - \tau_k)a_1(t)dt.$$

In the second term of eq. (10), if the polarity of the two adjacent data bits b_{-1}^1 and b_0^1 happens to be the same, the sum of the two partial autocorrelations turns into a full autocorrelation with the same polarity as b_0^1 . This could have been useful if the path phase were known. However, due to the random path phase, the second term in eq. (10) only adds to the channel noise. In general, signals delayed by amounts outside $\pm T_c$ seconds about a correlation peak in the correlation of $a_1(t)$ are attenuated by an amount determined by the processing gain of the code, that is, $N = T/T_c$. To assess the degree of degradation that is due to modulated partial correlation, in a separate case, we postulate having off periods of a T -second period between information bits, which forces to zero the undesired term containing b_{-1}^1 in eq. (10). Analysis of this case is presented in Appendix A, and associated numerical results are given in Section 4.2.

For now, we return to our normal transmission policy, where no off period is allowed between adjacent information bits.

The objective of the detector is to compare the received sample in eq. (10) with a preset threshold in order to make a decision on the polarity of the data bit being detected, that is, b_0^1 .

Now the detector makes a wrong decision if ξ is negative while $b_0^1 = +1$, or if ξ is positive and $b_0^1 = -1$. We note that during the detection interval of b_0^1 the other three data bits in eq. (10), namely, b_{-1}^1 , b_{-1}^k , and b_0^k , $k \neq 1$, can independently take on $\{\pm 1\}$. Hence, the conditional

probability of error is expressed by

$$P_{e|\beta_1, x_1, x_2, z} = \frac{1}{2} P_r \left\{ \beta_1 \frac{AT}{2} + \frac{AT}{2} (x_1 + z) + \eta < 0 \mid b_0^1 = +1 \right\} + \frac{1}{2} P_r \left\{ -\beta_1 \frac{AT}{2} + \frac{AT}{2} (x_2 + z) + \eta > 0 \mid b_0^1 = -1 \right\}, \quad (13)$$

where

$$x_1 = \sum_{l=2}^L \frac{\beta_l}{T} \{b_{-1}^l R_{l,1}(t_l) + \hat{R}_{l,1}(t_l)\} \cos(\psi_l), \quad (14)$$

$$x_2 = \sum_{l=2}^L \frac{\beta_l}{T} \{b_{-1}^l R_{l,1}(t_l) - \hat{R}_{l,1}(t_l)\} \cos(\psi_l), \quad (15)$$

and

$$z = \sum_{k=2}^K \frac{V_k}{T} \{b_{-1}^k R_{k,1}(\tau_k) + b_0^k \hat{R}_{k,1}(\tau_k)\} \cos(\Theta_k). \quad (16)$$

We can rewrite eq. (13) as

$$P_{e|\beta_1, x_1, x_2, z} = \frac{1}{4} \left\{ \operatorname{erfc} \left[\frac{\beta_1 \frac{AT}{2} + \frac{AT}{2} (x_1 + z)}{\sigma\sqrt{2}} \right] + \operatorname{erfc} \left[\frac{\beta_1 \frac{AT}{2} - \frac{AT}{2} (x_2 + z)}{\sigma\sqrt{2}} \right] \right\}, \quad (17)$$

where

$$\operatorname{erfc}(\mu) = \frac{2}{\sqrt{\pi}} \int_{\mu}^{\infty} e^{-y^2} dy \quad (18)$$

and σ is the standard deviation of the Gaussian noise. We notice that variables x_1 and x_2 in eq. (17) are in a conjugate form and have identical even moments. This is because the data symbols have zero mean; therefore, all the odd moments of x_1 and x_2 are zero. As a result, all the cross-product terms in the derivation of the even moments become zero. It is then easy to see that the even moments of x_1 and x_2 are identical. Now, to evaluate the average error probability—as will be explained in the next section—we apply the moments of the interference terms along with the numerical Gauss quadrature integration.¹⁹ It is not too difficult, then, to observe that instead of using eq. (17) we can use the following:

$$P_{e|\beta_1,x,z} = \frac{1}{2} \operatorname{erfc} \left\{ \frac{\frac{AT}{2} [\beta_1 - (x + z)]}{\sigma\sqrt{2}} \right\}, \quad (19)$$

where x in this equation can be either x_1 or x_2 . In other words, both eqs. (17) and (19) will result in the same average error probability under evaluation by moment-generating functions.

Also, recalling

$$\sigma = \frac{\sqrt{N_0 T}}{2} \quad (20)$$

and observing the bit energy,

$$E_b = \frac{A^2 T}{2}, \quad (21)$$

we can express eq. (19) as

$$P_{e|\beta_1,x,z} = \frac{1}{2} \operatorname{erfc} \left\{ \sqrt{\frac{E_b}{N_0}} [\beta_1 - (x + z)] \right\}. \quad (22)$$

If instead of a sample value of a Rayleigh random variable in eq. (22) we had a constant value of d_0 , then eq. (22) would become

$$P_{e|x,z} = \frac{1}{2} \operatorname{erfc} \left\{ \sqrt{\frac{E_b}{N_0}} [d_0 - (x + z)] \right\}. \quad (23)$$

Now, in the absence of any multipath fading and multiple-access interference, $d_0 = 1$, and this equation becomes

$$P_e = \frac{1}{2} \operatorname{erfc} \left(\sqrt{\frac{E_b}{N_0}} \right), \quad (24)$$

which is the well-known²⁰ performance of a coherently demodulated BPSK signal.

In the Rayleigh fading case the actual received signal-to-noise ratio is

$$\gamma = \beta_1^2 \frac{E_b}{N_0}, \quad (25)$$

and its average is

$$\gamma_0 = E\{\beta_1^2\} \frac{E_b}{N_0}, \quad (26)$$

where $E\{\cdot\}$ denotes the expected value. Since β_1 is Rayleigh distributed, γ has an exponential density. Hence,

$$P_{e|x,z} = \int_0^\infty P_{e|\beta_1,x,z} p(\gamma) d\gamma, \quad (27)$$

where

$$p(\gamma) = \frac{1}{\gamma_0} e^{-\gamma/\gamma_0} \quad (28)$$

and

$$P_{e|x,z} = \frac{1}{2\gamma_0} \int_0^\infty \operatorname{erfc} \left\{ \sqrt{\gamma} - \sqrt{\frac{E_b}{N_0}} (x+z) \right\} e^{-\gamma/\gamma_0} d\gamma. \quad (29)$$

This may be integrated by parts if we apply the following change of variable:

$$t = \sqrt{\gamma} - \sqrt{\frac{E_b}{N_0}} (x+z);$$

and after some manipulations it results in

$$P_{e|x,z} = \frac{1}{2} \left\{ \operatorname{erfc} \left[-\sqrt{\frac{E_b}{N_0}} (x+z) \right] - \frac{\sqrt{\gamma_0}}{\sqrt{\gamma_0+1}} \exp \left[\frac{-\frac{E_b}{N_0} (x+z)^2}{\gamma_0+1} \right] \cdot \operatorname{erfc} \left[-\frac{\sqrt{\gamma_0}}{\sqrt{\gamma_0+1}} (x+z) - \sqrt{\frac{E_b}{N_0}} \right] \right\}. \quad (30)$$

Interested readers are referred to Appendix B for a detailed derivation of eq. (30) (also see Ref. 21). We notice that in the absence of multiple-access interference and a single-path fading of the desired signal, eq. (30) becomes

$$P_e = \frac{1}{2} \left[1 - \frac{\sqrt{\gamma_0}}{\sqrt{\gamma_0+1}} \right], \quad (31)$$

which is the ideal performance of a single-path Rayleigh fading channel.²⁰

Now using Gauss Quadrature integration¹⁹ the average probability of error can be obtained numerically, by averaging the conditional

probability of eq. (30) over the interference term, $x + z$. This is accomplished by first evaluating the $N_m = 2N_c + 1$ moments of $x + z$, which are applied in evaluation of the N_c weights and nodes of the Quadrature Rule.¹⁹ Hence, the average probability of error is

$$P_e = \frac{1}{2} \sum_{j=1}^{N_c} W_j \left\{ \operatorname{erfc} \left(- \sqrt{\frac{E_b}{N_0}} \zeta_j \right) - \frac{\sqrt{\gamma_0}}{\sqrt{\gamma_0 + 1}} \exp \left[- \frac{E_b}{N_0} \frac{\zeta_j^2}{\gamma_0 + 1} \right] \operatorname{erfc} \left(- \zeta_j \sqrt{\frac{E_b}{N_0}} \frac{\sqrt{\gamma_0}}{\sqrt{\gamma_0 + 1}} \right) \right\}, \quad (32)$$

where W_j 's and ζ_j 's are the N_c weights and nodes of the Quadrature Rule.¹⁹ A detailed formulation of this is given in Appendix C. By the same token, the average probability of error in eq. (23) becomes

$$P_e = \frac{1}{2} \sum_{j=1}^{N_c} W_j \operatorname{erfc} \left\{ \sqrt{\frac{E_b}{N_0}} (d_0 - \zeta_j) \right\}. \quad (33)$$

III. MOMENT-GENERATING APPROACH

The average probability of error expression in eqs. (32) and (33) assumes $2N_c + 1$ moments of random variable $(x + z)$, which is a function of independent random parameters: β_l , t_l , τ_k , ψ_l , Θ_k , and b_i^k .

Furthermore, x and z are independent and symmetrically distributed; hence the odd moments of $(x + z)$ are all zero. Therefore, having the even moments of x and z , one can determine the moments of $(x + z)$ using the simple binomial rule, that is,

$$E\{(x + z)^m\} = \sum_{i=0}^m \binom{m}{i} E\{x^i\} \cdot E\{z^{m-i}\}. \quad (34)$$

In this section we derive the moments of z , and by similarity we deduce the moments of x .

Since

$$z = \sum_{k=2}^K z_k,$$

where

$$z_k = \frac{V_k}{T} \{b_{-1}^k R_{k,1}(\tau_k) + b_0^k \hat{R}_{k,1}(\tau_k)\} \cos \Theta_k,$$

then,

$$E\{z_k^{2m}\} = \frac{1}{T^{2m}} E\{V_k^{2m}\} \cdot E\{[\cos \Theta_k]^{2m} \cdot [b_{-1}^k R_{k,1}(\tau_k) + b_0^k \hat{R}_{k,1}(\tau_k)]^{2m}\}. \quad (35)$$

To evaluate the second expectation of the right-hand side of eq. (35), since Θ_k is an independent random variable, we can deal with it separately.

That is, we first can evaluate

$$E\{\{\cos \Theta_k\}^{2m}\} = \frac{\binom{2m}{m}}{4^m}$$

and then find the second expectation of eq. (35) as

$$\begin{aligned} H &= \frac{\binom{2m}{m}}{4^m} E\{\{b_{-1}^k R_{k,1}(\tau_k) + b_0^k \hat{R}_{k,1}(\tau_k)\}^{2m}\} \\ &= \frac{\binom{2m}{m}}{4^m} \cdot \frac{1}{T} \cdot \int_0^T [b_{-1}^k R_{k,1}(\tau_k) + b_0^k \hat{R}_{k,1}(\tau_k)]^{2m} d\tau_k, \end{aligned}$$

where the expectation in H is over the random delay τ_k .

Now we can expand the latter integral over N chips period. Hence,

$$H = \frac{\binom{2m}{m}}{4^m} \cdot \frac{1}{T} \sum_{n=0}^{N-1} \int_{nT_c}^{(n+1)T_c} [b_{-1}^k R_{k,1}(\tau_k) + b_0^k \hat{R}_{k,1}(\tau_k)]^{2m} d\tau_k.$$

We can then use the standard notations of Pursley⁷ to evaluate the correlation functions. This is accomplished by assuming rectangular chips and noting that for any $0 \leq nT_c \leq \tau \leq (n+1)T_c \leq T$, as shown by Pursley,⁷

$$\begin{cases} R_{k,1}(\tau) = A_{n_{k,1}} T_c + B_{n_{k,1}}(\tau - nT_c) \\ \hat{R}_{k,1}(\tau) = \hat{A}_{n_{k,1}} T_c + \hat{B}_{n_{k,1}}(\tau - nT_c) \end{cases} \quad (36)$$

where

$$\begin{cases} A_{n_{k,1}} = C_{k,1}(n - N) \\ B_{n_{k,1}} = C_{k,1}(n + 1 - N) - C_{k,1}(n - N), \\ \hat{A}_{n_{k,1}} = C_{k,1}(n) \quad k = 1, 2, \dots, K \\ \hat{B}_{n_{k,1}} = C_{k,1}(n + 1) - C_{k,1}(n) \end{cases} \quad (37)$$

where the discrete aperiodic cross-correlation term $C_{k,1}(\cdot)$ is related to chip sequences a_j^k and a_j^1 via

$$C_{k,1}(n) = \begin{cases} \sum_{j=0}^{N-1-n} a_j^k a_{j+n}^1 & 0 \leq n \leq N-1 \\ \sum_{j=0}^{N-1+n} a_{j-n}^k a_j^1 & -(N-1) \leq n \leq 0 \\ 0 & \text{else} \end{cases} \quad (38)$$

Therefore, H becomes

$$H = \frac{1}{T} \frac{\binom{2m}{m}}{4^m} \sum_{n=0}^{N-1} \sum_{r=0}^m \binom{2m}{2r} \cdot \int_{nT_c}^{(n+1)T_c} [A_{n,k,1} T_c + B_{n,k,1} (\tau_k - nT_c)]^{2r} \cdot [\hat{A}_{n,k,1} T_c + \hat{B}_{n,k,1} (\tau_k - nT_c)]^{2(m-r)} d\tau_k. \quad (39)$$

Notice that in deriving eq. (39), because of the even moments, b_{-1}^k and b_0^k are averaged to one. Now in eq. (39), by changing $\tau_k - nT_c$ to WT_c , H becomes

$$H = \frac{T_c^{2m+1}}{T} \frac{\binom{2m}{m}}{4^m} \sum_{n=0}^{N-1} \sum_{r=0}^m \binom{2m}{2r} \cdot \left\{ \int_0^1 [A_{n,k,1} + B_{n,k,1} W]^{2r} \cdot [\hat{A}_{n,k,1} + \hat{B}_{n,k,1} W]^{2(m-r)} dW \right\}. \quad (40)$$

Therefore, to determine H we have to solve

$$\Gamma_{m,r,n} = \int_0^1 [A_{n,k,1} + B_{n,k,1} W]^{2r} \cdot [\hat{A}_{n,k,1} + \hat{B}_{n,k,1} W]^{2(m-r)} dW. \quad (41)$$

This can be done recursively, using integration by parts, and the result is

$$\Gamma_{m,r,n} = \sum_{i=0}^{2r} (-1)^i \frac{(B_{n,k,1})^i}{(\hat{B}_{n,k,1})^{i+1}} \cdot \frac{1}{(i+1)} \cdot \frac{\binom{2r}{i}}{(2(m-r)+i+1)} \cdot \frac{1}{i+1} \cdot \{(A_{n,k,1} + B_{n,k,1})^{2r-i} \cdot (\hat{A}_{n,k,1} + \hat{B}_{n,k,1})^{2(m-r)+i+1} - (A_{n,k,1})^{2r-i} \cdot (\hat{A}_{n,k,1})^{2(m-r)+i+1}\}. \quad (42)$$

A detailed derivation of $\Gamma_{m,r,n}$ is included in Appendix D. For H in eq. (40) we now have

$$H = \frac{T_c^{2m+1}}{T} \frac{\binom{2m}{m}}{4^m} \sum_{n=0}^{N-1} \sum_{r=0}^m \binom{2m}{2r} \Gamma_{m,r,n},$$

and for $E\{z_k^{2m}\}$ in eq. (35),

$$E\{z_k^{2m}\} = \frac{\binom{2m}{m}}{4^m} E\{V_k^{2m}\} \cdot \frac{1}{N^{2m+1}} \sum_{n=0}^{N-1} \sum_{r=0}^m \binom{2m}{2r} \Gamma_{m,r,n}. \quad (43)$$

We notice that for a Rayleigh distributed V_k ,²²

$$E\{V_k^{2m}\} = 2^m \cdot \nu_{0k}^m (m!), \quad (44)$$

where $\nu_{0k} = E\{V_k^2/2\}$ is the average strength of the Rayleigh faded path associated with the k th interfering user. Note that assuming equal average strength cochannel interferers under a fixed total interference power corresponds to a maximum average probability of error in digital communications. Therefore, the results are conservative with respect to this assumption.

To find the moments of

$$z = \sum_{k=2}^K z_k,$$

we can use a three-step method prescribed in Ref. 12, where from the cumulants of random variable z_k , $\gamma_m(z_k)$, the moments of z are arrived at. This simple algorithm is outlined below.

The first step is to find

$$M_{2m} = E\{z_k^{2m}\}$$

and then

$$\gamma_{m+1}(z_k) = M_{m+1}(z_k) - \sum_{r=0}^{m-1} \binom{m}{r} \gamma_{r+1}(z_k) \cdot M_{m-r}(z_k)$$

with

$$\gamma_1(z_k) = M_1(z_k) = 0. \quad (45)$$

The second step is to find

$$\gamma_m(z) = \sum_{k=2}^K \gamma_m(z_k). \quad (46)$$

The third step is to find

$$M_{m+1}(z) = \gamma_{m+1}(z) + \sum_{r=0}^{m-1} \binom{m}{r} \gamma_{r+1}(z) \cdot M_{m-r}(z)$$

with

$$M_1(z) = \gamma_1(z). \quad (47)$$

As stated earlier, we can use a similar method to find the moments of x . Recall that

$$x = \sum_{l=2}^L x_l,$$

where

$$x_l = \frac{\beta_l}{T} \{b_{-1}^1 R_{1,1}(\tau_l) + b_0^1 \hat{R}_{1,1}(\tau_l)\} \cos(\psi_l)$$

and that use of the technique given above to find the moments of z yields

$$E\{x_l^{2m}\} = \frac{\binom{2m}{m}}{4^m} E\{\beta_l^{2m}\} \cdot \frac{1}{N^{2m+1}} \sum_{n=0}^{N-1} \sum_{r=0}^m \binom{2m}{2r} \Delta_{m,r,n}, \quad (48)$$

where

$$\begin{aligned} \Delta_{m,r,n} = & \sum_{i=0}^{2r} (-1)^i \frac{(B_{n_{1,1}})^i}{(\hat{B}_{n_{1,1}})^{i+1}} \cdot \frac{1}{(i+1)} \\ & \cdot \frac{\binom{2r}{i}}{\binom{2(m-r)+i+1}{i+1}} \cdot \{(A_{n_{1,1}} + B_{n_{1,1}})^{2r-i} \\ & \cdot (\hat{A}_{n_{1,1}} + \hat{B}_{n_{1,1}})^{2(m-r)+i+1} - (A_{n_{1,1}})^{2r-i} \cdot (\hat{A}_{n_{1,1}})^{2(m-r)+i+1}\} \end{aligned} \quad (49)$$

and

$$E\{\beta_l^{2m}\} = 2^m \rho_{0l}^m \cdot (m!),$$

where ρ_{0l} is the average strength of the l th path. Again, as stated earlier, equal partitioning of interferers' strength for a fixed total cochannel interference power corresponds to a maximum average error probability.

Having the moments of x_l we can find the moments of x by a similar method, as described for z . Once the moments of x and z are available, we can use their independence property and solve for the moments of $(x+z)$.

IV. DISCUSSION OF NUMERICAL RESULTS

In this section the average probability of error as a function of signal-to-noise ratio is evaluated for various channel configurations.

We will first discuss our spread-spectrum code-generation method, and then we will exhibit and discuss the behavior of the average probability of error.

4.1 Code-generation method

Pseudonoise (PN) sequence codes applied in our numerical evaluations are Gold sequences⁶ obtained from multiplying two primitive polynomials,

$$h_1(x) = x^7 + x^3 + 1 \quad (50)$$

and

$$h_2(x) = x^7 + x^3 + x^2 + x + 1, \quad (51)$$

represented by octal numbers 211 and 217, respectively. Hence, the resulting sequence is

$$h(x) = x^{14} + x^9 + x^8 + x^6 + x^5 + x^4 + x^2 + x + 1, \quad (52)$$

represented by 41567, in octal notation.

The number of shift register stages required to generate the codes from $h_1(x)$ and $h_2(x)$ is $n = 7$, and the codes period is $N = 2^n - 1 = 127$.

To find the actual codes, we used initial loadings of Ref. 23. These initial loadings are shown to generate a class of Gold codes known as Auto-Optimal with Least Sidelobe Energy (AO/LSE). In general, with a generator polynomial of the form

$$h(x) = h_0x^n + h_1x^{n-1} + \dots + h_{n-1}x + h_n$$

and for an initial loading of

$$\underline{\alpha}_0 = (\alpha_0, \alpha_1, \dots, \alpha_{n-1}),$$

we can use the following recursive formula to generate the codes:

$$\alpha_{j+n} = h_1\alpha_{j+n-1} \oplus \dots \oplus h_{n-1}\alpha_{j+1} \oplus h_n\alpha_j, \quad j \geq 0, \quad (53)$$

where \oplus stands for modulo-2 addition. Notice that in eq. (53) for simplicity we have represented the chips by α instead of α_i^k as introduced in eq. (2). The generated codes have three-valued autocorrelation function sidelobes and a three-valued cross correlation taking on values from the set $\{+15, -1, -17\}$.

In our numerical evaluation we used ten initial loadings.²³ Hence, this covers generating ten periodic code sequences for a hypothetical community of users sharing the common channel band on a spread-spectrum multiple-access basis. Once the code sequences are obtained, we compute the partial correlation coefficients of eq. (37), which are

used in conjunction with eqs. (35) and (48) in finding the moments of x and z as described in Section 3.1.

4.2 Numerical results

In what follows we assume the signal communicated between the desired transmitter/receiver pair is received via up to ten distinguishable paths, that is, L in eq. (4) is assumed to be deterministic and at most equal to ten. Also, unless otherwise specified, we assume the transmitters maintain some form of average power control so that the signals from different transmitters arrive at the receivers with the same average power. This kind of average power control in a wireless PBX application is not too difficult, because the users are connected via a star network.

We consider two separate cases:

Case 1—Suppose a terminal in the IWC environment can be moved slightly so that in the case of strong fading of the acquired path, another path, hopefully stronger, can be acquired and then the terminal remains stationary. In this case, if there is not much movement in the channel environment, one may assume β_1 is fixed and perhaps set β_1 to some constant value, d_0 , and use eq. (33) to evaluate the error probability.

Case 2—All the desired signals arriving via different paths at the receiver have Rayleigh distributed random gains. This is a scenario in which the transmitter terminals are mobile and multipath gains are Rayleigh with respect to geographic position of the terminals. Therefore we have to use eq. (32) to compute the average error probability.

In all our computations 15 moments of $(x + z)$ were found to be quite adequate in accurately computing the average error probability. All the average path gains between the desired transmitter and receiver, ρ_{0_i} 's, were assumed to be equal. This assumption also applies to the average path gain of the links between the $K - 1$ interfering transmitters and the receiver, ν_{0_k} 's. As stated earlier, this assumption will result in conservative average error probability values for a fixed total interference power.

Figure 2 depicts the average error probability as a function of both average faded and unfaded signal-to-noise ratio corresponding to Case 1. In the same figure, performance of an ideal coherent BPSK demodulator is shown. In Fig. 2 we observe two sets of results of eq. (33) corresponding to two different values of d_0 . Note that all the interferers are Rayleigh faded with a hypothetical average strength of -14 dB. For $d_0 = 1$, that is, when the desired signal is 14 dB stronger than each interfering signal, the solid curves in Fig. 2 exhibit the performance. The difference in the average strength can be provided by "capture." That is, it can be due to a shorter distance or a higher transmitted

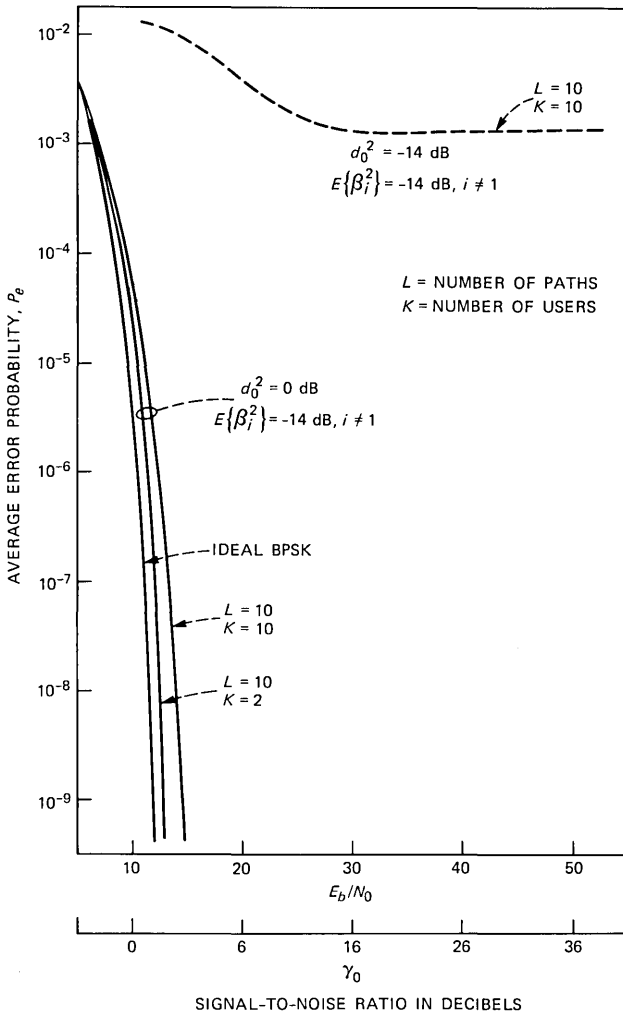


Fig. 2—Error rate performance for a fixed acquired path gain and Rayleigh interferers.

power. As can be observed, the multiple-access interference for at least up to 10 active users can be tolerated, and at an average error probability of 10^{-10} only about 2-dB signal-to-noise ratio degradation is experienced relative to the ideal situation. Therefore the receiver offers an acceptable performance as long as it is operated with capture. Next we demonstrate the performance for when the desired signal is also 14-dB faded, as the interferers are. This is shown by the dashed curve in Fig. 2. As observed, the performance in this scenario is unacceptable.

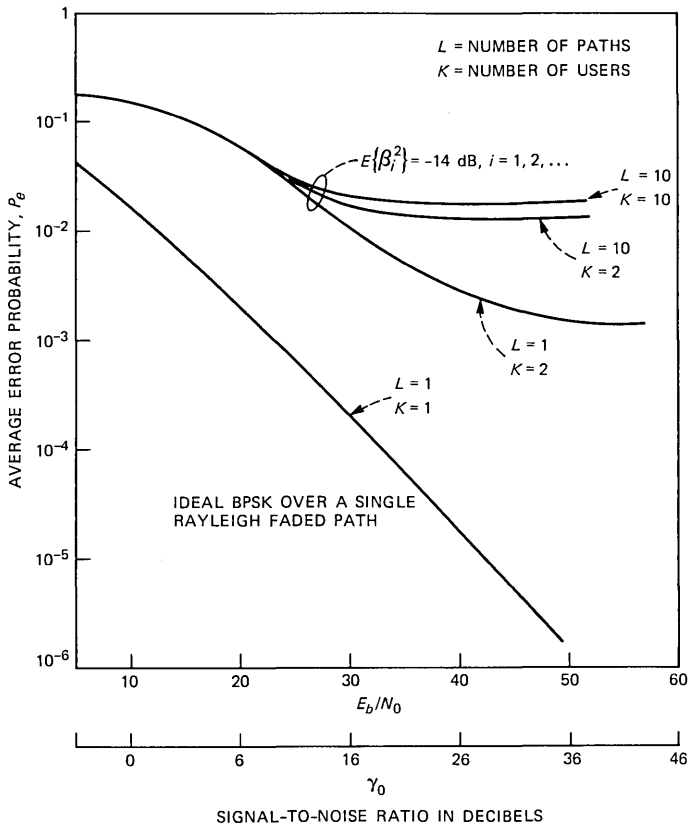


Fig. 3—Error rate performance for Rayleigh acquired path gain and Rayleigh interferers.

We now consider Case 2, where the terminals are to be mobile and the receiver is to cope with the first received Rayleigh faded path it acquires. The average probability of error as a function of faded and unfaded signal-to-noise ratio is depicted in Fig. 3. Again the hypothetical average path strength on all the Rayleigh faded paths was taken to be -14 dB. As can be observed, a simple correlation receiver that is not equipped with any diversity means or error correction capability exhibits a poor performance for the Gold sequences adopted in this work. Needless to say, the ideal performance of such a receiver in the absence of any multiple-access interference—but with a single Rayleigh faded path—is poor to begin with, as depicted in Fig. 3. Comparing the dashed curve of Fig. 2 and the curve in Fig. 3 corresponding to the same parameters reveals that the performance in the latter case is much worse than the former because of the Rayleigh gain of the acquired path, as expected. In a multiple-access environ-

ment when a transmitter and a receiver are communicating, as soon as a second transmitted signal comes on the air, the Rayleigh faded path between the interfering transmitter and the desired receiver can be stronger than the one between this receiver and the desired transmitter. This creates a near-far situation owing to the Rayleigh fading channel model. We notice that the degradation between the case of having only 2 or 10 active users is insignificant in this case, since the initial jump in error probability is large with just two users. Such a large jump, as will be seen later, is due to the insufficient processing gain provided by the $N = 127$ period codes for a Rayleigh channel. To improve this situation, longer sequences and/or diversity means are desired. The aforementioned numerical results assume $L = 10$ fading paths of equal average strength between the desired transmitter and receiver. Evidently, the finite cross correlation among the codes, although small in magnitude, can cause cochannel interference limitation due to the Rayleigh fading nature of the environment. Therefore, as the thermal noise tends to zero, the average error probability saturates to an unacceptable value. To gain some insight into this problem, we consider the following example.

Assume that we have a system of two users where there is a single Rayleigh faded path between the desired transmitter/receiver pair and that there is also a single Rayleigh faded path between the interfering transmitter and the desired receiver. A sample of the received signal after correlation and filtering is

$$\xi = \beta \frac{AT}{2} b_0^1 + \frac{AT}{2} \frac{v}{T} [b_{-1}^2 R_{2,1}(\tau) + b_0^2 \hat{R}_{2,1}(\tau)] \cos(\Theta) + \eta, \quad (54)$$

where β and v are Rayleigh gains of the desired and interfering paths, τ is the relative uniform delay experienced by the interferer, and Θ is the relative interferer path phase uniformly distributed over 0 and 2π . Denote

$$u = \frac{1}{T} [b_{-1}^2 R_{2,1}(\tau) + b_0^2 \hat{R}_{2,1}(\tau)] \cos(\Theta). \quad (55)$$

From eq. (30) the average error probability conditioned on u and v is

$$P_{e|u,v} = \frac{1}{2} \left\{ \operatorname{erfc} \left[-uv \sqrt{\frac{E_b}{N_0}} \right] - \frac{\sqrt{\gamma_0}}{\sqrt{\gamma_0 + 1}} \exp \left[\frac{-\frac{E_b}{N_0} u^2 v^2}{\gamma_0 + 1} \right] \right. \\ \left. \cdot \operatorname{erfc} \left[-\frac{\sqrt{\gamma_0}}{\sqrt{\gamma_0 + 1}} uv \sqrt{\frac{E_b}{N_0}} \right] \right\}, \quad (56)$$

where

$$\gamma_0 = E\{\beta^2\} \frac{E_b}{N_0}.$$

Let

$$\psi = u^2 v^2 \frac{E_b}{N_0}.$$

Then,

$$\psi_0 = E\{u^2\} \cdot E\{v^2\} \frac{E_b}{N_0}.$$

We assume that v and β have the same mean-square value, that is,

$$\gamma_0 = E\{v^2\} \frac{E_b}{N_0}$$

and

$$\psi_0 = \gamma_0 E\{u^2\}. \quad (57)$$

Denote

$$\epsilon = E\{u^2\},$$

and average the conditional error probability of eq. (56) with respect to v . That is, evaluate

$$P_{e|u} = \frac{1}{\psi_0} \int_0^\infty P_{e|u,v} e^{-(\psi)/(\psi_0)} d\psi. \quad (58)$$

This amounts to

$$P_{e|u} = \frac{1}{2} + \frac{1}{2} \frac{\epsilon \sqrt{\gamma_0}}{\sqrt{1 + \epsilon^2 \gamma_0}} - \frac{\sqrt{\gamma_0(\gamma_0 + 1)}}{\epsilon^2 \gamma_0 + \gamma_0 + 1} + \frac{\sqrt{\gamma_0(\gamma_0 + 1)}}{2(\epsilon^2 \gamma_0 + \gamma_0 + 1)} \left\{ 1 - \frac{\epsilon \gamma_0}{\sqrt{\epsilon^2 \gamma_0^2 + \epsilon \gamma_0 + \gamma_0 + 1}} \right\}. \quad (59)$$

Notice that when $\epsilon = 0$, that is, when there is no interferer, this is the standard Rayleigh faded channel performance.

If we average eq. (59) with respect to Θ and τ and let $\gamma_0 \rightarrow \infty$, we get

$$\begin{aligned} \lim_{\gamma_0 \rightarrow \infty} P_e &= \frac{1}{12N^3} \sum_{n=0}^{N-1} [C_{1,2}^2(n+1-N) + C_{1,2}^2(n-N) \\ &\quad + C_{1,2}(n+1-N)C_{1,2}(n-N) + C_{1,2}^2(n+1) \\ &\quad + C_{1,2}^2(n) + C_{1,2}(n+1)C_{1,2}(n)], \quad (60) \end{aligned}$$

where $C_{1,2}(\cdot)$ represents the aperiodic cross correlation of eq. (38). The sum in eq. (60) has been approximated by Pursely.⁷ When we use his approximation the saturation level of the probability of error in the absence of thermal noise is

$$\lim_{\gamma_0 \rightarrow \infty} P_e \approx \frac{1}{6N}, \quad (61)$$

where N is the period of Gold sequences applied here. Therefore, as observed earlier, we can reduce the saturation level by increasing N . In Fig. 4 the average probability of error is depicted for the case in this example. As one can observe, the moment approach yields the same saturation level in the probability of error as predicted by eq. (61).

Finally, as discussed earlier in Section 2.3, we consider the case of having an off period of a T-second period between the adjacent information intervals in order to avoid partial correlation interference from an adjacent bit. In terms of efficiency this is obviously equivalent to reducing the data rate by a factor of 2. The formulation for this case is in Appendix A, and the results for Case 2, where there is no unfaded path available between the transmitter and the receiver, is depicted in Fig. 5. As observed, the return in performance is negligible compared with the results in Fig. 3. To be more specific, the average

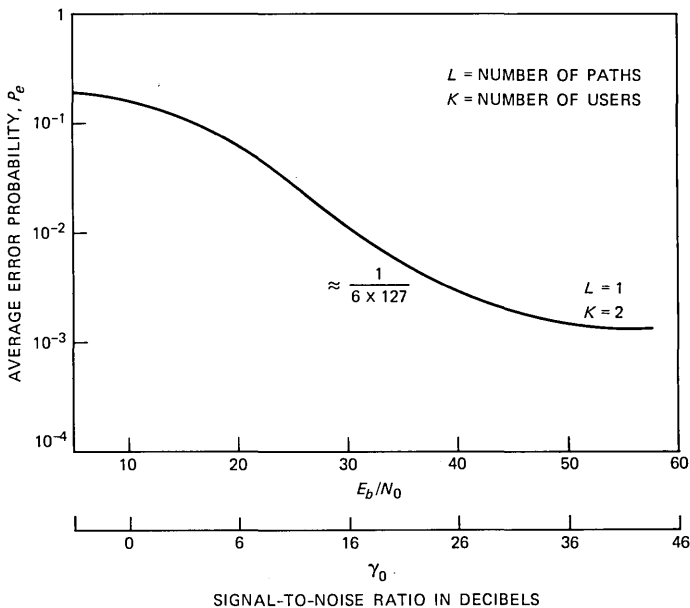


Fig. 4—Error rate performance of two-users system example.

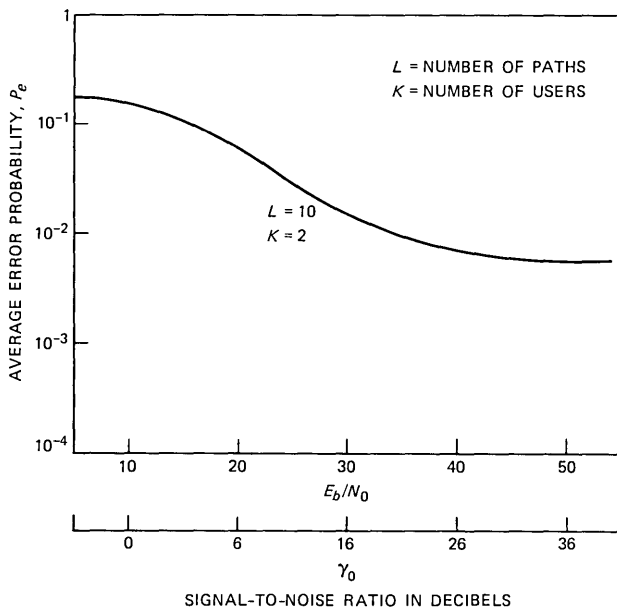


Fig. 5—Error rate performance without adjacent bit overlap.

error probability at large signal-to-noise ratios improves almost by a factor of 2. This improvement can intuitively be predicted considering that the cause, that is, partial correlation interference, is only due to an adjacent bit overlap.

Again the average path strength of all the Rayleigh faded paths in Figs. 4 and 5 was assumed to be -14 dB.

Therefore, without some form of diversity or error-correction coding, the situation as described in Case 2 is hopeless. Of course, other multiple-access fading environments would suffer similar penalties in performance if the access orthogonality could not be maintained. For example, in Frequency-Division Multiple Access (FDMA), any spectral overlap caused by imperfect filtering of adjacent frequency slots can create a similar situation. The same can be said about Time-Division Multiple Access (TDMA), if burst modems used in this application introduce any interburst interference. Consequently, regardless of the mode of access, to overcome the Rayleigh fading in IWC applications a diversity of some form seems necessary.

V. SUMMARY AND CONCLUSIONS

Current work reported herein extends previous results⁷⁻¹⁸ in the following respects. Analysis of the average error probability for Direct-Sequence Spread-Spectrum Multiple Access (DS-SSMA) is extended

to include the effects of multipath fading, typically experienced in an IWC environment.

For spread-spectrum transmission the IWC environment may be modeled by a discrete number of resolved paths with each path having a Rayleigh distributed gain, a uniformly distributed phase, and a uniformly distributed delay that can vary from zero to one information symbol period. The latter assumption is made to ensure having a negligible amount of intersymbol interference. We assume a coherent receiver that uses *no diversity information* to detect the transmitted symbol. We use average probability of error in our performance evaluation. The method of moments is applied to multipath and multiple-access interference, and Gauss quadrature integration is used in the error probability evaluation.

From our numerical work, exhibited in a sequence of graphs, we draw the following conclusions:

1. If a non-Rayleigh faded path exists in an IWC environment, a simple receiver can operate with DS-SSMA in a capture mode with a graceful performance degradation caused by multiple-access interference.

2. If all the discrete paths have Rayleigh gains and guaranteed low average error probability is expected at all times, the simple non-diversity coherent receiver considered in this work will not be able to cope with the Rayleigh channel fading with spread-spectrum codes of period $N = 127$. Therefore some form of diversity seems absolutely necessary. Otherwise, very long code sequences are needed to decrease the error probability of the interference-limited system.

3. The results of this work indicate that in the absence of diversity even small amounts of multiple-access interference can be harmful in a Rayleigh fading IWC environment. Therefore, if a channelized access such as frequency-division or time-division multiple access is to be employed, then careful channelization, that is, tight filtering in the case of FDMA and isolated transmitted bursts in the TDMA case, is necessary to maintain a low probability of error, given that the synchronization problem of a channelized access in a multipath environment can be solved.

VI. ACKNOWLEDGMENT

Discussions with D. J. Goodman, P. McLane, L. Milstein of the University of California at San Diego, A. A. M. Saleh, and Carl-Erik Sundberg were extremely valuable during the course of this work.

REFERENCES

1. Further Notice of Inquiry and Notice of Proposed Rulemaking, "Authorization of

- Spread Spectrum and Other Wideband Emissions Not Presently Provided for in the FCC Rules and Regulations," May 21, 1984.
2. G. R. Cooper and R. W. Nettleton, "A Spread-Spectrum Technique for High-Capacity Mobile Communications," *IEEE Trans. Veh. Technol.*, VT-27 (November 1978), pp. 264-75.
 3. P. S. Henry, "Spectrum Efficiency of a Frequency-Hopped-DPSK Spread-Spectrum Mobile Radio System," *IEEE Trans. Veh. Technol.*, VT-28 (November 1979), pp. 327-32.
 4. O. C. Yue, "Spread-Spectrum Mobile Radio 1977-1982," *IEEE Trans. Veh. Technol.*, VT-32, No. 1 (February 1983), pp. 98-105.
 5. R. C. Dixon, *Spread Spectrum Systems*, New York: Wiley, 1976.
 6. D. V. Sarwate and M. B. Pursley, "Cross-Correlation Properties of Pseudorandom and Related Sequences," *Proc. IEEE*, 68 (May 1980), pp. 598-619.
 7. M. B. Pursley, "Performance Evaluation for Phase-Coded Spread-Spectrum Multiple Access Communication—Part I: System Analysis," *IEEE Trans. Commun.*, COM-25 (August 1977), pp. 795-9.
 8. M. B. Pursley and D. V. Sarwate, "Performance Evaluation for Phase Coded Spread-Spectrum Multiple Access Communication—Part II: Code Sequence Analysis," *IEEE Trans. Commun.*, COM-25 (August 1977), pp. 800-3.
 9. K. Yao, "Error Probability of Asynchronous Spread-Spectrum Multiple Access Communication Systems," *IEEE Trans. Commun.*, COM-25 (August 1977), pp. 803-9.
 10. J. E. Mazo, "Some Theoretical Observations on Spread-Spectrum Communications," *B.S.T.J.*, 58, No. 9 (November 1979), pp. 2013-23.
 11. R.-H. Dou and L. B. Milstein, "Error Probability Bounds and Approximations for DS Spread-Spectrum Communication Systems With Multiple Tone or Multiple Access Interference," *IEEE Trans. Commun.*, COM-32 (May 1984), pp. 493-502.
 12. D. Laforgia, A. Luvison, and V. Fingarelli, "Bit Error Rate Evaluation for Spread-Spectrum Multiple Access Systems," *IEEE Trans. Commun.*, COM-32 (June 1984), pp. 660-9.
 13. S. E. Alexanders, "Radio Propagation Within Buildings at 900 MHz," *Electron. Lett.*, 19 (September 1983), pp. 913-4.
 14. D. Cox, "Universal Portable Radio Communications," *Proc. Nat. Commun. Forum* (September 1984), pp. 169-74.
 15. G. L. Turin, "Introduction to Spread-Spectrum Anti-Multipath Techniques and Their Application to Urban Digital Radio," *Proc. IEEE*, 68 (March 1980), pp. 328-53.
 16. D. E. Borth and M. B. Pursley, "Analysis of Direct-Sequence Spread-Spectrum Multiple-Access Communication Over Rician Fading Channels," *IEEE Trans. Commun.*, COM-27 (October 1979), pp. 1566-77.
 17. L. B. Milstein and D. L. Schilling, "Performance of a Spread-Spectrum System Operating Over a Frequency-Selective Fading Channel in the Presence of Tone Interference," *IEEE Trans. Commun.*, COM-30 (January 1982), pp. 240-7.
 18. G. L. Turin, "The Effects of Multipath and Fading on the Performance of Direct-Sequence CDMA Systems," *IEEE Trans. Veh. Technol.*, VT-33 (August 1984), pp. 213-9.
 19. G. H. Golub and J. H. Welsch, "Calculations of Gauss Quadrature Rules," *Math. Comput.*, 26 (April 1969), pp. 221-30.
 20. J. G. Proakis, *Digital Communications*, New York: McGraw-Hill, 1983.
 21. E. W. Ng and M. Geller, "A Table of Integrals of the Error Functions," *J. Res. NBS*, 73B (January-March 1969), pp. 1-20.
 22. A. Papoulis, *Probability, Random Variables, and Stochastic Processes*, New York: McGraw-Hill, 1965, p. 148.
 23. H. F. A. Roefs and M. B. Pursley, "Correlation Parameters of Random Sequences and Maximal Length Sequences for Spread-Spectrum Multiple-Access Communications," *IEEE Trans. Commun.*, COM-27 (October 1979), pp. 1597-604.

APPENDIX A

Performance Evaluation in the Absence of Partial Correlation

Consider the case of having T-seconds off periods between adjacent information bits. The decision variable of eq. (10) is changed to

$$\xi = \beta_1 \frac{AT}{2} b_0^1 + \frac{AT}{2} \sum_{l=2}^L \frac{\beta_l}{T} b_0^1 \hat{R}_{1,1}(t_l) \cos(\psi_l) + \frac{AT}{2} \sum_{k=2}^K \frac{V_k}{T} b_0^k \hat{R}_{k,1}(\tau_k) \cos(\Theta_k) + \eta. \quad (62)$$

So now

$$x = \sum_{l=2}^L \frac{\beta_l}{T} \hat{R}_{1,1}(t_l) \cos(\psi_l) \quad (63)$$

and

$$z = \sum_{k=2}^K \frac{V_k}{T} \hat{R}_{k,1}(\tau_k) \cos(\Theta_k). \quad (64)$$

To find the moments of x and z we follow a method similar to the one in Section III:

$$E\{x_l^{2m}\} = \frac{1}{T^{2m+1}} (2^m)(\rho_{0l}^m)(m!) \frac{\binom{2m}{m}}{4^m} \sum_{n=0}^{N-1} \int_{nT_c}^{(n+1)T_c} \hat{R}_{1,1}^{2m}(t) dt, \quad (65)$$

where

$$x_l = \frac{\beta_l}{T} b_0^1 \hat{R}_{1,1}(t_l) \cos(\psi_l) \quad (66)$$

and

$$\hat{R}_{1,1}(t_l) = \hat{A}_{n_{1,1}} T_c + \hat{B}_{n_{1,1}}(t_l - nT_c). \quad (67)$$

After proper change of variables we can define

$$H = T_c^{2m+1} \sum_{n=0}^{N-1} \int_0^1 [\hat{A}_{n_{1,1}} + \hat{B}_{n_{1,1}} x]^{2m} dx \quad (68)$$

$$= \frac{1}{(2m+1)} \cdot \frac{1}{\hat{B}_{n_{1,1}}} \{[\hat{A}_{n_{1,1}} + \hat{B}_{n_{1,1}}]^{2m+1} - [\hat{A}_{n_{1,1}}]^{2m+1}\}. \quad (69)$$

Hence,

$$E\{x_l^{2m}\} = 2^m \cdot \rho_{0l}^m \cdot (m!) \cdot \frac{\binom{2m}{m}}{4^m} \cdot \frac{1}{N^{2m+1}} \sum_{n=0}^{N-1} \Gamma_{m,n},$$

where

$$\Gamma_{m,n} = \frac{1}{2m+1} \cdot \frac{1}{\hat{B}_{n_{1,1}}} \{[\hat{A}_{n_{1,1}} + \hat{B}_{n_{1,1}}]^{2m+1} - [\hat{A}_{n_{1,1}}]^{2m+1}\}; \quad (70)$$

from here on the problem is identical to the one solved in Section III.

APPENDIX B

Integration of Conditional Error Probability

Denote

$$\Gamma_0 = -(x + z) \sqrt{E_b/N_0} \tag{71}$$

and

$$I = \frac{1}{2\gamma_0} \int_0^\infty \operatorname{erfc}(\sqrt{\gamma} + \Gamma_0) e^{-\gamma/\gamma_0} d\gamma. \tag{72}$$

Letting $\sqrt{\gamma} + \Gamma_0 = t$ we have

$$I = -\frac{1}{2} \int_{\Gamma_0}^\infty \frac{-2(t - \Gamma_0)}{\gamma_0} \operatorname{erfc}(t) e^{-(1/\gamma_0)(t-\Gamma_0)^2} dt. \tag{73}$$

Now we integrate by parts in eq. (73) to get

$$I = \frac{1}{2} \operatorname{erfc}(\Gamma_0) - \frac{1}{\sqrt{\pi}} \int_{\Gamma_0}^\infty e^{-(1/\gamma_0)(t-\Gamma_0)^2} e^{-t^2} dt. \tag{74}$$

Furthermore,

$$\begin{aligned} \int_{\Gamma_0}^\infty e^{-(1/\gamma_0)(t-\Gamma_0)^2} e^{-t^2} dt \\ = e^{-\Gamma_0^2/(\gamma_0+1)} \int_{\Gamma_0}^\infty e^{-\{[(\sqrt{\gamma_0+1}/\sqrt{\gamma_0})t - [\Gamma_0/\sqrt{\gamma_0(\gamma_0+1)}]]\}^2} dt, \end{aligned} \tag{75}$$

and making the change of variable

$$x = \sqrt{\frac{\gamma_0 + 1}{\gamma_0}} t - \frac{\Gamma_0}{\sqrt{\gamma_0(\gamma_0 + 1)}}$$

in the integral in eq. 75, we get

$$\frac{\sqrt{\pi}}{2} e^{-\Gamma_0^2/(\gamma_0+1)} \frac{\sqrt{\gamma_0}}{\sqrt{\gamma_0 + 1}} \operatorname{erfc} \left(\Gamma_0 \sqrt{\frac{\gamma_0}{\gamma_0 + 1}} \right). \tag{76}$$

Using this result in eq. (76) in the second term in eq. (74) gives

$$\begin{aligned} I = \frac{1}{2} \left\{ \operatorname{erfc}(\Gamma_0) - \frac{\sqrt{\gamma_0}}{\sqrt{\gamma_0 + 1}} \right. \\ \left. \cdot \exp \left(-\frac{\Gamma_0^2}{\gamma_0 + 1} \right) \operatorname{erfc} \left(\Gamma_0 \frac{\sqrt{\gamma_0}}{\sqrt{\gamma_0 + 1}} \right) \right\}, \end{aligned} \tag{77}$$

which is the desired result in eq. (30).

APPENDIX C

Formulation of Gauss Quadrature Rules From the Moments of $(x + z)$

Denote the first $N_m = 2N_c + 1$ moments of $(x + z)$ by the sequence $\{\mu_n\}$, $n = 0, 1, 2, \dots, 2N_c$. In the problem at hand the random variables are evenly distributed. Therefore, as previously stated, the odd moments are all zero.

Let $\mathbf{M} = [m_{ij}]$, $i, j = 1, 2, \dots, 2N_c + 1$, be the Gram matrix of the system with

$$m_{ij} = \mu_{i+j-2}. \quad (78)$$

Thus,

$$\mathbf{M} = \begin{bmatrix} 1 & 0 & \mu_2 & 0 & \cdot & \cdot & \cdot & \mu_{N_c} \\ 0 & \mu_2 & 0 & \cdot & \cdot & \cdot & \cdot & 0 \\ \mu_2 & 0 & \mu_4 & \cdot & \cdot & \cdot & \cdot & \mu_{N_c+2} \\ 0 & \cdot \\ \cdot & \cdot \\ \cdot & \cdot \\ \cdot & \cdot \\ \mu_{N_c} & \cdot & \cdot & \cdot & \cdot & \cdot & \cdot & \mu_{2N_c} \end{bmatrix}, \quad (79)$$

where $\mu_0 = 1$. Also, let $\mathbf{M} = \mathbf{R}^T \mathbf{R}$ be the Cholesky decomposition of \mathbf{M} , where \mathbf{T} represents the transpose matrix with

$$r_{ii} = \left(m_{ii} - \sum_{k=1}^{i-1} r_{ki}^2 \right)^{1/2} \quad (80)$$

and

$$r_{ij} = \left(m_{ij} - \sum_{k=1}^{i-1} r_{ki} r_{kj} \right) / r_{ii}, \quad i < j. \quad (81)$$

Because all the odd moments are zero, it follows that $r_{ij} = 0$ when $(i + j)$ is odd. We now have an upper triangular matrix $\mathbf{R} = [r_{ij}]$, $i, j = 1, 2, \dots, N_c + 1$. The matrix is used to calculate a set of numbers $\{\delta_j\}$, $j = 1, 2, \dots, N_c$, where

$$\delta_j = \frac{r_{j+1j+1}}{r_{jj}}. \quad (82)$$

Now we construct a tridiagonal matrix \mathbf{J} as follows:

$$\mathbf{J} = \begin{bmatrix} 0 & \delta_1 & 0 & \cdot & \cdot & \cdot & 0 \\ \delta_1 & 0 & \delta_2 & \cdot & \cdot & \cdot & 0 \\ 0 & \delta_2 & 0 & \cdot & \cdot & \cdot & 0 \\ \cdot & \cdot & \cdot & \cdot & \cdot & \cdot & \cdot \\ \cdot & \cdot & \cdot & \cdot & \cdot & \cdot & \cdot \\ \cdot & \cdot & \cdot & \cdot & \cdot & \cdot & \cdot \\ \cdot & \cdot & \cdot & \cdot & \cdot & \cdot & \delta_{N_c-1} \\ \cdot & \cdot & \cdot & \cdot & \delta_{N_c-1} & 0 & \cdot \end{bmatrix}, \quad (83)$$

where \mathbf{J} is an $N_c \times N_c$ matrix.

By finding the eigenvalues and eigenvectors of the matrix \mathbf{J} , it is possible to arrive at the weights and nodes of the quadrature rule. Let the eigenvalue equation be

$$\mathbf{J}\tilde{q}_j = \lambda_j \tilde{q}_j. \quad (84)$$

Then the quadrature rule for the sequence (W_j, ζ_j) in eq. (32) is given by the set of numbers $\{q_{1j}^2, \lambda_j\}, j = 1, 2, \dots, N_c$, where q_{1j}^2 is the square of the first element of the eigenvector \tilde{q}_j , and λ_j is an eigenvalue in eq. (84). Hence, if the first $2N_c + 1$ moments are calculated, then the resulting quadrature rule will contain N_c weights and nodes.

APPENDIX D

Evaluation of Even Moments

Consider the integral

$$I_0 = \int_0^1 (a + bx)^n \cdot (c + dx)^m dx. \quad (85)$$

This integral can be expanded to

$$I_0 = \left[\frac{(a + b)^n (c + d)^{m+1}}{d(m + 1)} - \frac{a^n c^{m+1}}{d(m + 1)} \right] - \frac{nb}{d(m + 1)} \int_0^1 (a + bx)^{n-1} \cdot (c + dx)^{m+1} dx, \quad (86)$$

where we now have to solve for

$$I_1 = \int_0^1 (a + bx)^{n-1} \cdot (c + dx)^{m+1} dx. \quad (87)$$

If we integrate by parts in eq. (87) and substitute the result into eq. (86), we find that

$$I_0 = \sum_{i=0}^n (-1)^i \frac{b^i}{d^{i+1}} \cdot \frac{1}{(i + 1)} \cdot \frac{\binom{n}{i}}{\binom{m + i + 1}{i + 1}} \cdot [(a + b)^{n-i} (c + d)^{m+i+1} - a^{n-i} c^{m+i+1}]. \quad (88)$$

In the problem considered in the main body of the paper,

$$a = A_n, \quad b = B_n, \quad c = \hat{A}_n, \quad \text{and} \quad d = \hat{B}_n.$$

Thus, I_0 takes the form

$$I_0 = \Gamma_{m,r,n} = \sum_{i=0}^{2r} (-1)^i \frac{(B_n)^i}{(\hat{B}_n)^{i+1}} \cdot \frac{1}{(i+1)} \cdot \frac{\binom{2r}{i}}{\binom{2(m-r)+i+1}{i+1}} \cdot \{(A_n + B_n)^{2r-i} \cdot (\hat{A}_n + \hat{B}_n)^{2(m-r)+i+1} - A_n^{2r-i} \cdot \hat{A}_n^{2(m-r)+i+1}\}. \quad (89)$$

AUTHOR

Mohsen Kavehrad, B.S. (Electrical Engineering), 1973, Tehran Polytechnic Institute; M.S. (Electrical Engineering), 1975, Worcester Polytechnic Institute; Ph.D. (Electrical Engineering), 1977, Polytechnic Institute of New York; Fairchild Industries, 1977–1978; GTE, 1978–1981; on the faculty of Northeastern University, 1981–1984; AT&T Bell Laboratories, 1981—. At AT&T Bell Laboratories Mr. Kavehrad is a member of the Communications Methods Research Department at Crawford Hill Laboratory, Holmdel, New Jersey. His research interests are digital communications and computer networks. He is a Technical Editor for the IEEE Communications Magazine. He established and was the Chairman of the IEEE Communications Chapter of New Hampshire in 1984. Member, IEEE, Sigma Xi.

Recognition of Isolated Digits Using Hidden Markov Models With Continuous Mixture Densities

By L. R. RABINER, B.-H. JUANG, S. E. LEVINSON, and
M. M. SONDHI*

(Manuscript received November 15, 1984)

In this paper we extend previous work on isolated-word recognition based on hidden Markov models by replacing the discrete symbol representation of the speech signal with a continuous Gaussian mixture density. In this manner the inherent quantization error introduced by the discrete representation is essentially eliminated. The resulting recognizer was tested on a vocabulary of the ten digits across a wide range of talkers and test conditions and shown to have an error rate comparable to that of the best template recognizers and significantly lower than that of the discrete symbol hidden Markov model system. We discuss several issues involved in the training of the continuous density models and in the implementation of the recognizer.

I. INTRODUCTION

In the literature a wide variety of approaches have been proposed to recognize isolated words, based on standard statistical-pattern-recognition techniques.¹⁻⁶ The most successful of these has been the template-based recognizer approach, which uses Dynamic Programming (DP) as the method for comparing patterns. Although the template-based approach using DP has been very successful, alternative recognition strategies have been studied because of

* Authors are employees of AT&T Bell Laboratories.

Copyright © 1985 AT&T. Photo reproduction for noncommercial use is permitted without payment of royalty provided that each reproduction is done without alteration and that the Journal reference and copyright notice are included on the first page. The title and abstract, but no other portions, of this paper may be copied or distributed royalty free by computer-based and other information-service systems without further permission. Permission to reproduce or republish any other portion of this paper must be obtained from the Editor.

1. The high computational cost of the DP approach;
2. The difficulties in extending the DP recognition paradigm to more difficult problems—e.g., connected words, continuous speech;
3. The desire to use a robust parametric model, rather than the nonparametric template, to represent the speech;
4. The desire to use speech units other than words in some circumstances—e.g., syllables, demisyllables, phonemes.

For one or more of the above reasons, several different approaches have been proposed, such as using Vector Quantization (VQ) in the DP computation,⁴ using word-based vector quantization to eliminate the DP processing,⁵ using VQ as a front-end preprocessor,⁷ and using Hidden Markov Models (HMMs) to represent the speech signal.^{6,8-11} Although the VQ-based recognizers have performed very well in isolated-word recognition tasks, and have significantly reduced the computational costs, they have done very little to alleviate the difficulties in extending template-based approaches to large vocabulary connected and continuous speech recognition applications. As such, the HMM recognizer has been and will continue to be of great interest both because of its potential low cost, and because it is a parametric model of the speech signal that can model various events (phonemes, syllables, etc.) in the speech signal.

Although HMMs have been used in a wide variety of speech systems,^{6,8-11} our experience with their application to speech recognition systems has been considerably less than with that of template-based approaches. Hence each new experiment using HMMs gives us a better understanding of the strengths and weaknesses of such models as applied to different speech recognition tasks. In particular, in our own work, we have been studying how to apply HMMs in isolated-word, speaker-independent speech recognition applications over dialed-up telephone lines. In a previous investigation,⁶ we studied HMMs based on observations consisting of discrete symbols from a finite alphabet (i.e., vector-quantized LPC vectors from a fixed-size code book). Work performed at IBM,¹² CMU,⁹ and more recently at Phillips¹³ has used continuous HMMs where it was assumed that all parameters of interest had Gaussian distributions.

The HMMs to be discussed in this paper are based on continuous, mixture density models of the distribution of Linear Predictive Coefficient (LPC)-derived parameter vectors (e.g., cepstral vectors, log-area ratio vectors, etc.). We have devised training procedures for obtaining maximum-likelihood estimates of the parameters of the mixture distribution. We have applied the models to the problem of recognizing isolated digits. Our results show that the average error rates of such HMM recognizers are essentially identical to those of the best template approaches using DP methods, and considerably

lower than those of an HMM recognizer with a discrete symbol VQ front end.

This paper is organized as follows. In Section II we present the continuous mixture density model. We show how we obtain the maximum-likelihood estimates of the model parameters from a training set of data, and how the overall recognition system is implemented. In Section III we describe a series of experimental evolutions of the recognizer and present results on HMM systems with several different sets of parameters. In Section IV we discuss the results and relate them to earlier work with template-based approaches. We also discuss computational aspects of the system in this section. Finally, in Section V we summarize our results.

II. THE CONTINUOUS MIXTURE DENSITY HMM

Figure 1 shows the type of HMM we are considering here. It is based upon a left-to-right Markov chain that starts in state 1 and ends in state N . The observed signal is assumed to be a stochastic function of the state sequence of the Markov chain. The state sequence itself is unobservable (hidden). The goal is to choose the parameters of the HMM to optimally match the observed characteristics of a given signal.

The parameters that characterize the HMM of Fig. 1 are

1. N , the number of states in the model.
2. $A = [a_{ij}]$, $1 \leq i, j \leq N$, the state transition matrix, where a_{ij} is the probability of making a transition from state i to state j . As shown in Fig. 1b, for left-to-right models we use the constraint $a_{ij} = 0, j < i, j > i + 2$.
3. B , the observation probability function.

If we assume that the signal to be represented by the HMM consists of a sequence of observation vectors $\mathbf{O} = \{O_1, O_2, \dots, O_T\}$, where each O_i is a vector that characterizes the signal at time $t = i$, then we can consider two types of observation probability functions, namely, discrete and continuous. For the discrete type we replace O_i by one of M

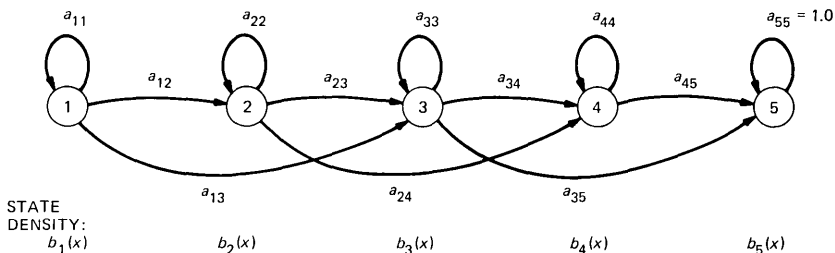


Fig. 1—Representation of a left-to-right hidden Markov model with five states.

possible symbols (via some type of VQ) such that the distortion in quantizing O_i is minimum. Let j be the state at time t . Then $B = [b_{jk}]$, $1 \leq j \leq N$, $1 \leq k \leq M$ is the probability of observing symbol k , in state j .

In the continuous case we have the probability density function $B = \{b_j(\mathbf{x})\}$, $1 \leq j \leq N$, where $b_j(\mathbf{x})d\mathbf{x}$ is the probability that the vector O_t lies between \mathbf{x} and $\mathbf{x} + d\mathbf{x}$. The types of density functions allowed for $b_j(\mathbf{x})$, for which a reestimation algorithm exists, include strictly log-concave densities,¹⁴ elliptically symmetric densities,¹⁵ and, more recently, mixtures of strictly log-concave or elliptically symmetric densities.¹⁶ In this paper we will consider Gaussian mixture densities of the form

$$b_j(\mathbf{x}) = \sum_{k=1}^M c_{jk} \mathcal{N}(\mathbf{x}, \mu_{jk}, \mathbf{U}_{jk}), \quad (1)$$

where $\mathcal{N}(\mathbf{x}, \mu, \mathbf{U})$ denotes a D -dimensional normal density function of mean vector μ and covariance matrix \mathbf{U} .

To summarize the discussion above, a complete specification of a continuous mixture density HMM requires choosing values (and/or parameter estimates) for the following:

- N —number of states in the model
- M —number of mixtures
- D —number of dimensions in each vector
- $A = [a_{ij}]$ —state transition matrix
- $C = [c_{jk}]$ —mixture gain matrix
- $\mu = [\mu_{jkd}]$ —means of the mixture components
- $\mathbf{U} = [\mathbf{U}_{jkde}]$ —covariance matrices of the mixture components.

For the work to be presented here, we have chosen $N = 5$ states on the basis of previous studies with discrete symbol models.⁶ Also, our signal observation vectors (e.g., cepstral vectors, log-area ratios, etc.) are derived from the LPC vector of an eighth-order model of the speech signal.

2.1 Training the HMM

For each word, v , in a vocabulary of V words ($V = 10$ for the digits), an HMM is designed; i.e., the set of parameters above is estimated from a training set of data representing multiple occurrences of the vocabulary word by a wide range of talkers. Since a convergent reestimation procedure exists for the continuous mixture model,¹⁶ it is, in theory, possible to randomly choose initial values for each of the model parameters (subject to the stochastic constraints) and let the reestimation procedure determine the optimum (maximum-likelihood) values. However, experience with the reestimation procedure¹⁷ has

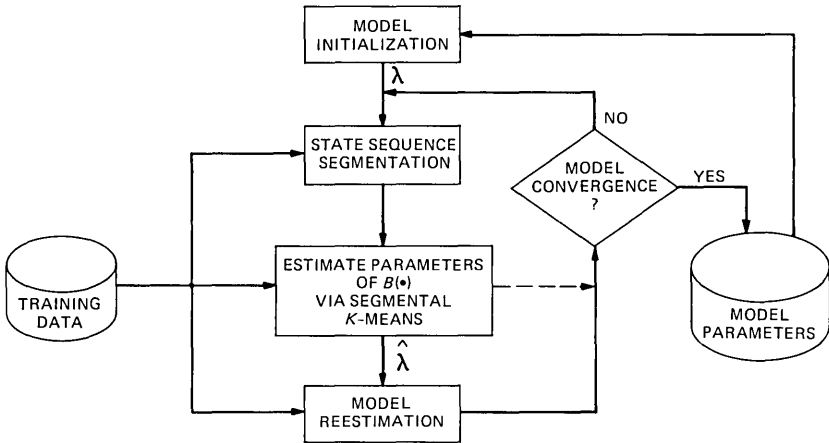


Fig. 2—The training procedure used to estimate parameter values for the optimal continuous mixture density fit to a finite number of observation sequences.

shown that the maximum-likelihood estimates of the means, μ , are quite sensitive to the initial estimate. Hence a procedure for providing good initial estimates of μ for each mixture and each state was required.

Based on previous experience with a K -means iterative procedure for clustering data,¹⁸ a procedure for obtaining model parameter estimates was devised and is shown in Fig. 2. (The analysis used to give the LPC-derived vectors is reviewed in Section 2.2.) We assume a training set of data consisting of Q sequences of observations, where each sequence, $\mathbf{O}^i = \{O_1^i, O_2^i, \dots, O_{T_i}^i\}$, $1 \leq i \leq Q$, is the set of vectors (observations) constituting a single occurrence of the word. The total observation vector is $\mathbf{O} = \{\mathbf{O}^1 \mathbf{O}^2 \dots \mathbf{O}^Q\}$. The first step in the training procedure is to choose an initial model estimate. This initial estimate (unlike the one required for reestimation) can be chosen randomly, or on the basis of any good initial guess. (The procedure to be described here works well for a wide range of initial guesses.)

We denote the N states in the HMM as q_i , $1 \leq i \leq N$. The second step in the training procedure is to segment each word occurrence, \mathbf{O}^i , into states based on the current model, λ . This segmentation is achieved by finding the optimum state sequence, via the Viterbi algorithm, and then backtracking along the optimal path. This procedure is illustrated in Fig. 3, which shows a log-energy plot, an accumulated log-likelihood plot, and a state segmentation for one occurrence of the digit six. Figure 3 shows that the states correspond roughly to the sounds in the word six.

The result of segmenting each of the Q training sequences is, for each of the N states, a set of the observations that occur within each state q_i according to the current model. Since the assumed distribution

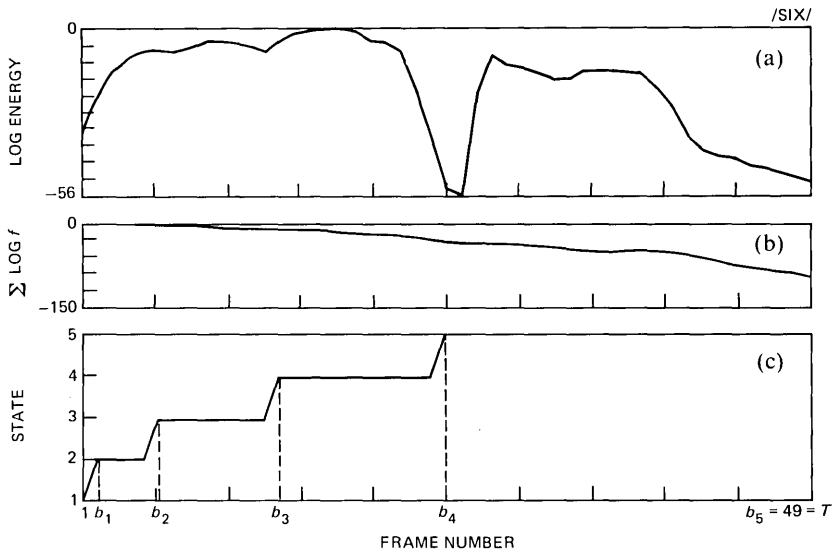


Fig. 3—Plots of (a) log energy, (b) accumulated log likelihood, and (c) state assignment for one occurrence of the word six.

of the observations, within the j th state, is $b_j(\mathbf{x})$, a comparison can be made of the marginal distributions $b_j(\mathbf{x}) |_{\mathbf{x}=\{\dots x_n \dots\}}$ against a histogram of the actual observations (i.e., vectors assigned to that state). Such a comparison is given in Fig. 4 for a $D = 9$ dimensional representation with $M = 5$ mixtures. (The covariance matrices are assumed to be diagonal in this example.) The nine dimensions consist of the eight dimensions of a cepstral representation, and the normalized log energy as the ninth parameter. The results in Fig. 4 are for the first state of the digit 0. The need for values of $M > 1$ is seen in the histogram of the first parameter (the first cepstral component), which is inherently multimodal; similarly, the second, fourth, and eighth cepstral parameters show the need for more than a single Gaussian to provide good fits. Many of the other parameters appear to be well fitted by a single Gaussian curve; however, in some cases even $M = 5$ mixtures do not provide a very good fit.

Following the segmentation into states of all Q training sequences, a segmental K -means procedure is used to cluster the vectors in each state, q_i , into a set of M clusters (to do this we use a Euclidean distortion metric and a VQ design algorithm). From the clustering, an updated set of model parameters is derived as follows:

$$\hat{c}_{jk} = \text{Number of vectors classified in cluster } k \text{ of the } j\text{th state} \\ \text{divided by the number of vectors in state } j$$

$$\hat{\mu}_{jkd} = d\text{th component of the sample mean of the vectors classified} \\ \text{in cluster } k \text{ of state } j$$

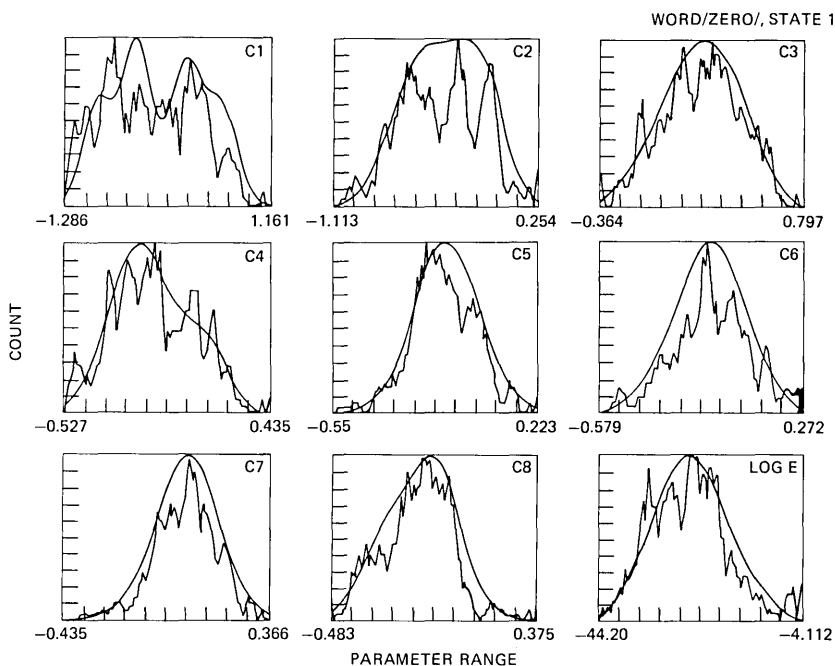


Fig. 4—Comparison of estimated density (jagged contour) and model density (smooth contour) for each of the nine components of the representation vector (eight cepstral components, one log-energy component) for state 1 of the digit zero.

$\hat{U}_{jkr s} = (r, s)$ th component of the sample covariance matrix of the vectors classified in cluster k of state j .

The state transition matrix coefficients, a_{ij} , are not changed according to this procedure. The new model, $\hat{\lambda} = (A, \hat{B}, \hat{\mu}, \hat{U})$, is obtained from the updated estimates \hat{B} , $\hat{\mu}$, and \hat{U} , and the original A matrix. At this point the formal reestimation procedure is used to reestimate optimal values (in a maximum-likelihood sense) of *all* model parameters. The resulting model is then compared to the previous model (by computing a distance score that reflects the statistical similarity of the HMMs¹⁹). If the model distance score exceeds a threshold, then the old model, λ , is replaced by the new model, $\hat{\lambda}$ (the result of reestimation), and the overall training loop is repeated. If the model distance score falls below the threshold, then model convergence is assumed and the final model parameters are saved.

As an alternative to using the sample means, $\hat{\mu}_{jkd}$, and sample covariance matrix, $\hat{U}_{jkr s}$ (which are the maximum-likelihood estimates for a Gaussian distribution), we also investigated a method of fitting a single Gaussian distribution to an observed histogram within each cluster of each state. For the case when \hat{U} is diagonal, a histogram

with NB bins is made for each component of the vector, and the model parameters (i.e., μ and σ) are chosen so as to minimize the cost function

$$\rho = \sum_{i=1}^{NB} \frac{(\hat{h}_i - h_i)^2}{h_i},$$

where h_i is the observed frequency of occurrence in the i th bin, and \hat{h}_i is the corresponding model estimate for that bin. The minimization for the two-parameter case (i.e., μ and σ) can be trivially carried out by several different procedures.

For the case when \hat{U} is a full covariance matrix, the histogram-fitting procedure could, in principle, be extended to D -dimensional histograms with correlated components. However, the amount of training data available was insufficient for the number of parameters being fitted. Instead, the histogram-fitting procedure that we used was as follows. The sample covariance matrix, \hat{U} , was estimated from the training data (as above), and decomposed as

$$\hat{U} = T' \Lambda T,$$

where Λ is a diagonal matrix. The original vectors, c , were transformed by the relation $w = Tc$. In this manner the components of w were uncorrelated with diagonal correlation matrix Λ ; hence the histogram-fitting procedure, described above, could be used along each transformed dimension separately. In practice we have found that the transformation to uncorrelated components and the Gaussian fitting gave somewhat better model parameter estimates than the sample estimates for the full covariance case.

Since the steps of segmenting the training sequences into states and clustering the vectors via a VQ clustering procedure are relatively inexpensive (in a computational sense), and reestimation is an exceedingly costly procedure, a practical implementation of the training procedure of Fig. 2 is to bypass the step of model reestimation until local model convergence is obtained, and then apply the reestimation procedure at the final step. This procedure works well in practice, particularly when used for left-to-right models where the sequential characteristics of the process are of vital importance.

2.2 The HMM recognizer

Once the HMMs have been trained on each vocabulary word, the recognition strategy is straightforward. Figure 5 shows a block diagram of the recognizer. The speech signal, $s(n)$, for the unknown word is first analyzed using an eighth-order LPC analysis. The speech sampling rate is 6.67 kHz, and overlapping sections of 45 ms of speech are analyzed every 15 ms to give a set of eight LPC coefficients. An LPC transformation algorithm is used to convert the LPC representation

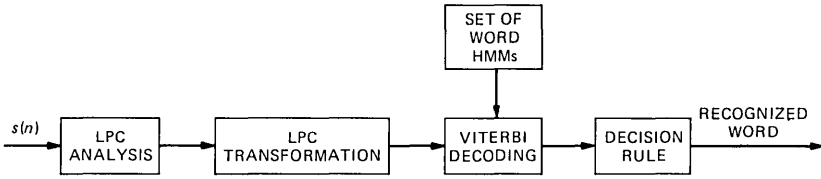


Fig. 5—Block diagram of the HMM recognizer based on continuous mixture densities.

to the desired one for the recognizer. In particular we have considered the following possibilities:

1. LPC-derived cepstrum of eighth-order (the zeroth-order term is not used)
2. LPC-derived log-area ratios
3. Autocorrelation coefficients normalized by energy
4. Residual normalized autocorrelation coefficients
5. Autocorrelation of LPC coefficients.

The vector representation used in training is the one used in the recognizer.

The next step in recognition is to find the optimum state sequence corresponding to the HMM for each vocabulary word, λ^v , $1 \leq v \leq V$, and compute the log-likelihood score for the optimal path. The decision rule assigns the unknown word to the vocabulary word whose model has the highest log-likelihood score.

The optimum path is obtained by the well-known Viterbi algorithm,²⁰ which can be compactly stated as:

1. Initialization— $\delta_1(1) = \log[b_1(O_1)]$
 $\delta_1(i) = -\infty \quad i \neq 1$
2. Recursion $-\delta_t(j) = \max_{j-2 \leq i \leq j} \{\delta_{t-1}(i) + \log a_{ij}\} + \log[b_j(O_t)]$,
 $2 \leq t \leq T, \quad 1 \leq j \leq N$
3. Termination— $\log f = \delta_T(N)$.

2.3 Incorporation of duration into the recognizer

Inherently, each state in the HMM has a geometric duration probability. Thus, a state j , with a probability a_{jj} of returning to itself, has a state duration probability of

$$p_j(\ell) = (1 - a_{jj})a_{jj}^{\ell-1},$$

where ℓ is the number of frames occurring in state j . Experience has shown that exponentials are not good models for state duration probabilities. Thus, we have considered two alternative ways of incorporating state duration information in the recognizer, namely, modification of the scoring procedure to include an internal duration model, and application of a post-processing duration model on the maximum-

likelihood state sequence as determined by the Viterbi algorithm. In either case, in the training phase, we estimate a state duration probability of the form

$$p_j(\ell/T) = \text{probability of being in state } j \text{ for exactly } (\ell/T) \text{ of the word, where } T \text{ is the number of frames in the word and } \ell \text{ is the number of frames spent in state } j.$$

The quantity ℓ/T , which ranges from 0 to 1, is the normalized duration within a given state. For each word, and for each state, the quantity $p_j(\ell/T)$ is estimated (via a simple counting procedure on the training sequences) for 25 values of ℓ/T from 0 to 1.

The state duration probability, $[p_j(\ell)$ or $p_j(\ell/T)]$, is not estimated as part of the training procedure, but instead is computed directly from the training sequences based on the models obtained from the training procedure. Hence the estimates of $p_j(\ell/T)$ are strictly heuristic ones, not maximum-likelihood estimates. Unfortunately, direct reestimation of the maximum-likelihood estimate of $p_j(\ell/T)$ is, at present, totally impractical both because of the excessive computation required, and because of the sparsity of training data for estimating the increased number of model parameters.

A typical set of histograms of $p_j(\ell/T)$ for a five-state model for the word six is shown in Fig. 6. Although the states are hidden, examination of the results of segmentation of typical utterances (of the word six) into states shows that the first two states are essentially the initial /s/, the third state is a transition to the vowel /i/, the fourth state is the vowel, and the fifth state is the stop and the final fricative /s/. As seen from Fig. 6, the average duration of the first state is generally very brief; the second and third states have somewhat longer average durations; the fourth state has a well-defined peak in the density with an average duration of about 20 percent of the word; the final state (the stop plus the fricative) has an average duration of about 50 percent of the word.

For scoring a given observation sequence using the internal duration model, the recursion step of the Viterbi procedure is modified to the form

$$\delta_t(j) = \max_{j-2 \leq i \leq j-1} \max_{0 \leq \ell/T \leq 1.0} \left\{ \delta_{t-\ell}(i) + \log a_{ij} + \alpha \log p_j(\ell/T) + \sum_{\tau=1}^{\ell} \log [b_j(O_{t-\tau})] \right\}. \quad (2)$$

Note that in eq. (2) the duration term appears only when the state changes. Furthermore, a multiplier factor α on the log-duration probability is used to adjust the importance of the duration part of the scoring.

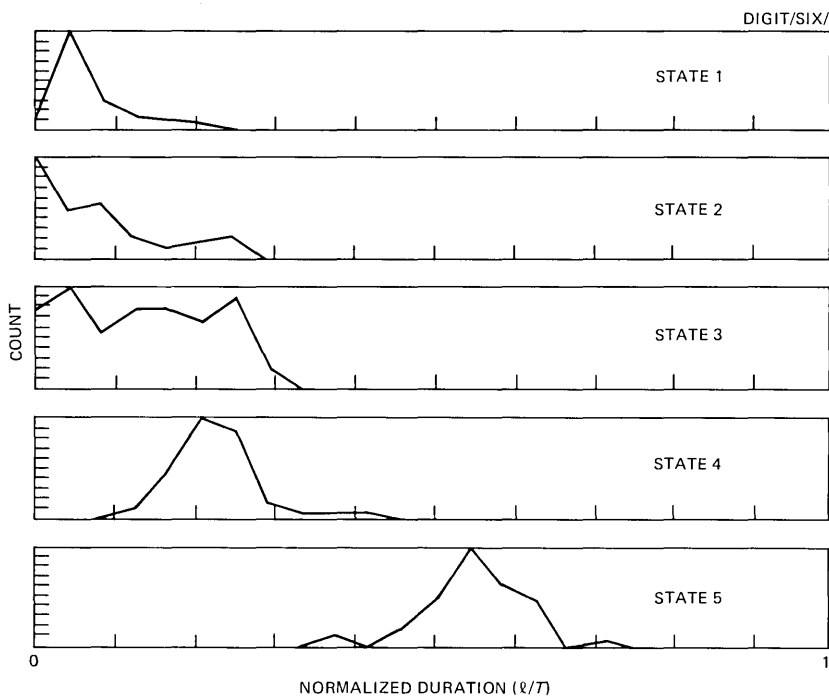


Fig. 6—Histograms of the normalized duration density for the five states of the digit six.

The implementation of the recursion of eq. (2) is considerably more costly than the implementation of the standard Viterbi recursion, since the values $\delta_{t-\ell}(i)$ must be retained for a large range of ℓ values, and since the $\sum \log[b_j(O_{t-\tau})]$ computation must be repeatedly done during each iteration. In practice we have measured an increase of 15 to 20 times in computation for the internal duration model over the standard Viterbi algorithm. For these reasons we have also considered a much simpler post-processor duration model in which the original Viterbi alignment is performed, the maximum-likelihood state sequence is determined, and the duration of each state is obtained via a backtracking procedure. The post-processor then increments the log-likelihood score by the log-duration probabilities (suitably weighted again) to give:

$$\log \hat{f} = \log f + \alpha \sum_{j=1}^N \log[p_j(\ell_j/T)], \quad (3)$$

where ℓ_j/T is the normalized time spent in state j along the optimal alignment path.

The incremental cost of the computation for the post-processor

duration model is essentially negligible, and we will see in Section III that it works as well or better than the internal duration model discussed above.

III. EXPERIMENTAL EVALUATION

To evaluate the performance of the HMM recognizer with the mixture density representation, a series of experiments were run in which several parameters of the models were varied. All evaluations were performed on a database of isolated digits recorded over standard dialed-up telephone lines. Four sets of spoken digits were used. These consisted of the following:

DIG 1—100 talkers (50 male, 50 female), one replication of each digit by each talker.²¹ These recordings have been used as a training set in a wide variety of evaluations of isolated-word recognizers at AT&T Bell Laboratories. The nominal bandwidth of these recordings was 100 to 3200 Hz.

DIG 2—Same 100 talkers and recording conditions as DIG 1; recordings made several weeks later than those of DIG 1.

DIG 3—100 new talkers (50 male, 50 female), one averaged occurrence of each digit by each talker obtained from averaging a pair of robust tokens of the digit.^{22,23} The transmission conditions (i.e., analog front end, filter cutoff frequencies, etc.) differed slightly from those used in recording the DIG 1 and DIG 2 databases.

DIG 4—A second group of 100 new talkers (50 male, 50 female), 20 recordings of each digit by each talker.²⁴ A random sampling of one of the recordings of each digit by each talker was used. The transmission conditions differed substantially from those used in recording the other databases. The nominal bandwidth of these recordings was 200 to 3200 Hz.

Thus, each of the four sets of digits contained 1000 digits. For training the models, only the digits in set DIG 1 or set DIG 4 were used; for testing and evaluating the performance of the recognizer, each of the four sets of digits was used.

3.1 Pilot recognition experiments to determine representation

A series of pilot experiments was run to determine a good set of parameters for use in the HMM recognizer. The five parameter sets (transformations of the LPC parameters) mentioned in Section 2.2 were studied. Results indicated that the best performance was obtained from the cepstral parameters; however, almost the same performance was obtained from the log-area ratio parameters. The remaining three parameter sets—i.e., energy-normalized autocorrelations, residual-normalized autocorrelations, and autocorrelation of LPC coeffi-

cients—all gave significantly poorer performance. This was due to the use of a Euclidean distance metric in the clustering part of the training procedure. Each of the poor representations had the property that one or more of the coefficients in the vector contributed significantly more variance in the distance calculation than the remaining coefficients; hence a large sensitivity to the details of the training set resulted, and very poor estimates of the means and covariances of the parameters were obtained. Such problems could have been alleviated by replacing the Euclidean distance metric with a covariance weighted metric; however, we did not do this because of the greatly increased computational burden.

As a result of the pilot experiment, the parameter set chosen was an eighth-order cepstral vector with the option of appending a peak-normalized log energy as a ninth component of the vector.

3.2 Diagonal versus full covariance matrices

Two forms for the \mathbf{U} matrices of eq. (1) were considered, namely, diagonal matrices (with assumed zero correlation between components of the representation), and full covariance matrices. The advantage of the diagonal covariance matrix is that the computation of $b_j(\mathbf{x})$ reduces to a simple sum of products of Gaussians, whereas for a full covariance matrix the computation of $b_j(\mathbf{x})$ requires a matrix multiply. The disadvantage of the diagonal covariance matrix representation is that, in general, for correlated vector components, a larger value of M (the number of mixtures) is needed to give an adequate model than for a full covariance matrix representation. Neither representation has any particular advantage in terms of ease of making initial estimates or ease of reestimation.

A series of recognition tests was run with diagonal covariance matrices using $M = 1, 3,$ and $5,$ and full covariance matrices using $M = 1$ only. The results showed that performance with the full covariance matrix with $M = 1$ was better than that obtained using only the diagonal covariance matrix with $M = 1$ and $3,$ and comparable to the performance with $M = 5.$ Hence, in all subsequent recognition tests we will consider both diagonal and full covariance models.

3.3 Applicability of word clustering to model generation

In the model training procedure all 100 tokens of each word were used to derive a single HMM for the word. In earlier work, with template-based approaches,²¹ it was shown how word clustering techniques could be used to design a set of templates to represent a broad population of talkers. Thus, one question of interest was whether the word clustering procedure could be combined with the model generation technique to give more than one HMM per word with better

performance than the single HMM system. This idea was tested as follows. First, a single HMM per word was created on training set DIG 1; next the two-cluster-per-word template set was used to partition the 100-token training set into two groups. For each group a single HMM was created; hence a total of two HMMs per word was used in the performance evaluation. The potential disadvantage of this procedure should be clear, namely, that the training data per model available for estimating HMM parameters is half that used for the single model case. Hence there is a good possibility of obtaining less reliable estimates of the model parameters.

This procedure could be continued as above for three or more template solutions; however, experience indicated that a two-model solution was about the limit for 100 training tokens. Beyond this point the unreliability of the estimates was the dominant factor.

Results of a formal series of experiments with each of the four test sets and with one and two models per word are given in Table I, which shows average digit error rates for both diagonal covariance models (part a), and full covariance models (part b) using normalized log-energy and cepstral coefficients, and with the post-processor duration model. For the diagonal covariance models, the results show that for the reference set (DIG 1), the average error rate was essentially 0 for both one- and two-model-per-word systems. For the test set DIG 2 the average error rate for the two-model-per-word system was slightly smaller (by 0.4 percent) than for the one-model-per-word system. For the test sets DIG 3 and DIG 4, the average error rate for the two-model-per-word system was 1 percent smaller than for the one-model-per-word system. Overall, averaged across the three independent test sets, the two-model-per-word system had a 0.7 percent smaller error rate than the one-template-per-word system. This difference, although small, is significant at the 95-percent level for a test with 4000 digits.

Table I—Comparison of performance of HMM recognizer with one and two models per word*

Number of Models per Word	Average Digit Error Rate (%)				Test Set Average
	DIG 1	DIG 2	DIG 3	DIG 4	
(a) Diagonal covariance models, $M = 5$ mixtures					
1	0.2	1.1	3.9	5.2	3.4
2	0.1	0.7	2.8	4.2	2.67
(b) Full covariance models, $M = 1$ mixture					
1	0.2	0.9	2.9	4.7	2.83
2	0.2	0.6	2.2	4.7	2.5

* Both energy and duration were used in the evaluation. The training set was DIG 1.

For the full covariance models, the improvement in performance in going from one to two models per digit was smaller than that obtained in the diagonal covariance case. On average, the improvement in error rate was only 0.33 percent, and for two of the four sets (the training set DIG 1, and the testing set DIG 4) there was no improvement in performance with two models per digit. Thus, for the full covariance models a single model per word was adequate for the data.

3.4 Effects of different number of mixtures

Using the two-model-per-word system for the diagonal covariance case, the number of mixtures, M , was varied from 1 to 7, in steps of two, to see the effects on recognition performance. The results of these tests on the four-digit databases are given in Table IIa. The results show an improvement in performance from an average test set digit error rate of 3.57 percent for $M = 1$ down to an average test set digit error rate of 2.57 percent for $M = 5$; results for $M = 7$ show a slight increase in average test set digit error rate to 2.97 percent. This increase in error rate for the $M = 7$ case is primarily due to a 0.8-percent increase in error rate for test set DIG 4. This result seems to indicate that no real improvement in modeling the statistics of the observations is obtained with $M = 7$; instead, a somewhat broader range for fitting incorrect words is achieved, thereby raising the error rate on DIG 4. Based on the results of Table II, a value of $M = 5$ was deemed most appropriate for the recognizer.

Another test was run for the diagonal covariance case, in which the value of M was made variable with each state of the model. The chosen value was based on the average distortion in the initial modeling section of the training loop. Thus, large values of M (on the order of

Table II—Comparison of performance of HMM recognizer with different values of M^*

M	Average Digit Error Rate (%)				Test Set Average
	DIG 1	DIG 2	DIG 3	DIG 4	
(a) Results on diagonal covariance models for two models per digit					
1	1.1	1.3	3.2	6.2	3.57
3	0.2	1.1	4.1	5.2	3.47
5	0.1	0.7	2.8	4.2	2.57
7	0.0	0.8	3.1	5.0	2.97
(b) Results on full covariance models for one model per digit					
1	0.2	0.9	2.9	4.7	2.83
2	0.0	1.2	6.0	5.3	4.17

* Both energy and duration were used in the evaluation. Training set was DIG 1.

10 to 15) were required for some states, whereas very small values of M (1 to 2) were required for others. Recognition tests using the variable M models gave very poor results (i.e., error rates considerably higher than those for fixed M models). An analysis of the errors showed a greater increase in the likelihood for incorrect models than for the correct model. Hence we concluded that variable M models were not a viable alternative for HMM recognizers.

Using the one-model-per-word system for the full covariance case, a similar test was performed in which values of 1 and 2 were used for M . The results, listed in Table IIb, show a degradation in performance from an average test set digit error rate of 2.83 percent for $M = 1$ to an average test set digit error rate of 4.17 percent for $M = 2$. Most of the increase in error rate occurs for test set DIG 3, where the error rate increases by 3.1 percent. This result again indicates that a single full covariance matrix provides an adequate fit to the training data, and that increases in M primarily decrease the amount of training data per model and therefore lead to poorer parameter estimates and worse recognition performance.

3.5 Effects of energy and duration

To study the effects of including energy in the signal representation, and of including the duration model in the testing, a series of recognition runs were made with the $M = 5$, diagonal covariance, two-model-per-word system, and the $M = 1$, full covariance, two-model-per-word system. The results of these recognition tests are given in Table III. The duration model was implemented as a post-processor computation in all cases.

Table III—Comparison of performance of HMM recognizer with and without energy and with and without duration model (training set was DIG 1)

Condition	Average Digit Error Rate (%)				Test Set Average
	DIG 1	DIG 2	DIG 3	DIG 4	
(a) Results on diagonal covariance models, $M = 5$, with two models per digit					
No energy, no duration model	0.3	2.5	4.3	8.0	4.93
Energy, no duration model	0.3	0.9	2.5	5.5	2.97
No energy, duration model	0.1	1.3	3.3	5.4	3.33
Energy, duration model	0.1	0.7	2.8	4.2	2.57
(b) Results on full covariance models, $M = 1$, with two models per digit					
No energy, no duration model	0.2	2.0	2.8	7.0	3.93
Energy, no duration model	0.2	1.2	2.1	4.4	2.57
No energy, duration model	0.3	1.3	3.0	5.9	3.4
Energy, duration model	0.2	0.6	2.2	4.7	2.5

The results show clearly that the addition of either energy or duration uniformly improves the performance of the HMM recognizer, although energy is more important than duration for the full covariance models. Furthermore, the combination of both energy and duration model yields better performance than either factor individually. The biggest improvements in performance were obtained for test sets DIG 3 and DIG 4, where the transmission characteristics of the speech were different from those of DIG 1 and DIG 2. In these cases the addition of energy and duration model makes the system more robust because these features are, for the most part, insensitive to differences in transmission conditions.

3.6 Comparison of internal duration model and post-processor duration model

The next set of experiments compared the two different implementations of the duration model, namely, the internal duration model and the post-processor duration model. In both cases the same (suboptimal) state-duration probability density function was used, with a multiplier of $\alpha = 3.0$. (This factor was optimized based on preliminary experimentation.) The results of the two runs are given in Table IV.

The results show that the performance of the HMM recognizer with the post-processor duration model was uniformly slightly better than for the recognizer with the internal duration model. Across the three test sets the improvement in performance was about 0.9 percent, and for the two data sets with different transmission conditions (DIG 3 and DIG 4), the improvement was 0.9 percent and 1.7 percent, respectively. In addition, the computational load was between one and two orders of magnitude lower for the post-processor duration model than for the internal duration model. Hence the results given in Table IV strongly justify the use of the "suboptimal" post-processor duration model as an alternative to using the inherent exponential distributions for each state. The major problem with the use of any duration model is the difficulty of making reliable estimates of the density function

Table IV—Comparison of performance of HMM recognizer with two types of duration models*

Duration Model	Average Digit Error Rate (%)				Test Set Average
	DIG 1	DIG 2	DIG 3	DIG 4	
Internal in Viterbi search	0.2	0.9	3.7	5.9	3.5
Post-processor	0.1	0.7	2.8	4.2	2.57

* Results given on diagonal covariance models, $M = 5$, with two models per digit, and with energy used as a feature. Training set was DIG 1.

from a finite training set of observations (as is invariably the case for most speech processing applications). However, the improvements in performance obtained from using the duration model more than justify its use in the HMM recognizer.

3.7 Effects of different training sets

The last set of experiments investigated the effects of different training sets on the overall recognizer performance. The results of these experiments are given in Table V, which shows average test set digit error rate as a function of training set, model type, and number of models per digit. (All models used both energy and the post-processor duration model.) The results of Table V show that when the set DIG 4 was used as the training set, the performance among all four test sets was more uniform than when the set DIG 1 was used as the training set. The results also show that with a single model per digit, the performance with the DIG 4 training models was comparable or better than the performance of the DIG 1 training models with two models per digit. Thus the use of the slightly narrower bandwidth training data led to models that were more robust to small differences in recording conditions than those obtained from the broader bandwidth training data.

IV. DISCUSSION

4.1 General results

In the previous sections we have proposed and tested an HMM isolated-word recognizer that uses a continuous mixture density model for the probability densities of the feature vector. Based on experimentation with the recognizer, in a speaker-independent mode, using a vocabulary of ten digits, the following general results were obtained:

1. The proposed model training procedure, with an iterative K -means loop for estimating initial values for the means and covariances

Table V—Comparison of performance of the recognizer as a function of the training set, model type, and number of models per digit*

Training Set	Model Type	Number of Models per Digit	Average Digit Error Rate (%)				Test Set Average
			DIG 1	DIG 2	DIG 3	DIG 4	
DIG 1	Diagonal covariance	2	0.1	0.7	2.8	4.2	2.57
DIG 1	Full covariance	2	0.2	0.6	2.2	4.7	2.5
DIG 4	Diagonal covariance	1	2.5	2.4	2.8	0.5	2.57
DIG 4	Full covariance	1	2.5	1.7	2.1	0.8	2.1
DIG 4	Full covariance	2	2.3	2.2	2.1	0.5	2.2

* All models used both energy and the post-processor duration model.

of the components of the mixture model, works extremely well in practice and was able to converge to a local maximum of the likelihood function in a small number of iterations (typically 2 to 4 in most cases).

2. Several speech parameters (most notably the set of cepstral parameters and the set of log-area ratios) are well represented by the continuous mixture density, and give good recognition performance in the HMM recognizer. Other speech parameters (e.g., energy-normalized autocorrelation parameters, residual-normalized autocorrelation parameters, etc.) are not well represented by the continuous mixture density, and give relatively poor performance in the HMM recognizer when a Euclidean distance measure was used.

3. Mixture models with diagonal covariance matrices need a somewhat larger number of mixtures (typically, $M = 3$ to 5) than mixture models with full covariance matrices ($M = 1$) in order to give the same performance.

4. Combining the techniques of clustering and HMM model building can lead to small improvements in the performance of the HMM recognizer.

5. The addition of a word-normalized energy contour (as an extra dimension to the feature vector) uniformly improves performance of the HMM recognizer and makes it more robust to differences in talker populations and transmission conditions.

6. The addition of duration information, on a state-by-state basis, into the HMM recognizer uniformly improves performance and increases robustness of the recognizer to different talkers and transmission conditions.

7. The combination of normalized energy and duration information works better than either factor alone in the HMM recognizer.

8. Word models with variable number of mixture densities per state (based on clustering distortion statistics) yield significantly worse performance than models with a fixed number of mixture densities per state.

9. The duration model of the HMM recognizer can be conveniently (and suboptimally) implemented as a post-processor to the Viterbi decoding procedure. In practice the performance of this system is actually better (somewhat) than the recognizer with the duration model built into the Viterbi decoding procedure.

The above results are one measure of the success achieved by the continuous mixture density HMM recognizer. Another way of measuring the success is to compare the current performance results with those of alternative recognition systems based on templates²¹ and based on discrete densities (i.e., VQ symbols).⁶ Such a comparison is given in Table VI for the case when the data of set DIG 1 was used as

Table VI—Comparison of performance of three types of recognizers on the digits database*

Type of Recognizer	Average Digit Error Rate (%)				Test Set Average
	DIG 1	DIG 2	DIG 3	DIG 4	
HMM—Continuous density	0.1	0.7	2.8	4.2	2.57
HMM—Discrete density	—	2.9	—	—	—
DTW—Templates	0.0	0.6	2.7	3.9	2.4

* Training set was DIG 1.

the training set. For the discrete density HMM recognizer, results are given only for the DIG 2 data set where the performance is significantly worse than that of the HMM recognizer with a continuous mixture density. For the template-based Dynamic Time Warping (DTW) recognizer, the results, based on the latest clustering procedure,²⁵ are comparable to those of the continuous density HMM recognizer. Since the template-based DTW recognizer has been studied for about ten years and has been highly optimized in its performance, the equality between the HMM recognizer and the DTW recognizer, at least for the digits vocabulary, is highly significant.

4.2 Computational considerations

To calculate the computation required in the HMM recognizer, and to contrast it with that required by the DTW recognizer, we must define the following:

- N = Number of states in HMM model
- M = Number of mixture densities per state
- D = Dimensionality of vectors in signal representation
- T = Average number of frames (observations) per word
- R = Number of HMMs per word
- V = Number of words in vocabulary
- Q = Number of templates per word in DTW system
- P = Order of LPC analysis.

The computation for the HMM recognizer, in the Viterbi decoding algorithm, is

$$C_V = R \cdot V \cdot N \cdot T \cdot C_b,$$

where C_b is the computation required to evaluate the mixture density $b_j(\mathbf{x})$. Assuming that multiplications, divisions, exponentiation, and logarithms all take a single multiply-add time (somewhat optimistic calculations), then

$$C_b \approx 3DM \text{ *, + } \quad (\text{diagonal covariance})$$

or $C_b \approx D^2 M^* \cdot +$ (full covariance)

and

$$C_V = 3D \cdot M \cdot R \cdot V \cdot N \cdot T^* \cdot + \quad (\text{diagonal covariance})$$

or $C_v = D^2 M \cdot R \cdot V \cdot N \cdot T^* \cdot +$ (full covariance).

The standard DTW recognizer requires

$$C_{DTW} = Q \cdot V \cdot \frac{T^2}{3} \cdot (p + 1)^* \cdot + \cdot$$

Hence the ratio of C_V to C_{DTW} is

$$\text{RATIO} = \frac{C_V}{C_{DTW}} = \frac{3DMRN}{Q \frac{T}{3} (p + 1)} \quad (\text{diagonal covariance})$$

or

$$\text{Ratio} = \frac{D^2 MRN}{Q \frac{T}{3} (p + 1)} \quad (\text{full covariance}).$$

If we choose typical values of $N = 5$, $M = 5$, $D = 9$, $T = 40$, $R = 2$, $V = 10$, $Q = 12$, $p = 8$, for the diagonal covariance case, we get

$$\text{RATIO} = 15/16,$$

and using $R = 1$, $M = 1$ for the full covariance case we get

$$\text{RATIO} = 9/32,$$

i.e., the computation of the HMM recognizer is essentially that of the DTW recognizer for the diagonal covariance case, and about one-quarter that of the DTW recognizer for the full covariance case. This situation is very different from the discrete symbol HMM recognizer, where the computation was an order of magnitude smaller than that of the DTW recognizer. The problem with the continuous mixture density recognizer is the $b_j(\mathbf{x})$ computation, which is extremely expensive, especially for values of $M > 1$.

V. SUMMARY

In this paper we have extended our experimental investigations of HMM recognizers to include the case where the density function for the observations in each state is represented by a continuous mixture of Gaussian variables. We have shown how the parameters of such a

signal representation can be optimally estimated (in a maximum-likelihood sense) from a finite training set of data, and have given a simple way of implementing the training procedure based on a K -means iteration. We have tested the HMM recognizer, in a speaker-independent mode, on a vocabulary of the ten digits, and shown that the error rate of the system is smaller than that obtained from the discrete density (VQ-based) HMM recognizer, and comparable to that of the multiple template-based DTW recognizer.

REFERENCES

1. F. I. Itakura, "Minimum Prediction Residual Principle Applied to Speech Recognition," *IEEE Trans. Acoust., Speech, and Signal Proc.*, *ASSP-23*, No. 1 (February 1975), pp. 67-72.
2. G. M. White and R. B. Neely, "Speech Recognition Experiments With Linear Prediction, Bandpass Filtering, and Dynamic Programming," *IEEE Trans. Acoust., Speech, and Signal Proc.*, *ASSP-24*, No. 2 (April 1976), pp. 183-8.
3. G. R. Doddington and T. B. Schalk, "Speech Recognition: Turning Theory to Practice," *IEEE Spectrum*, *18* (September 1981), pp. 26-32.
4. K. Shikano, "Spoken Word Recognition Based Upon Vector Quantization of Input Speech," *Trans. Comm. Speech Res.* (December 1982), pp. 473-80.
5. J. E. Shore and D. K. Burton, "Discrete Utterance Speech Recognition Without Time Alignment," *IEEE Trans. Inform. Theory*, *IT-29*, No. 4 (July 1983), pp. 473-91.
6. L. R. Rabiner, S. E. Levinson, and M. M. Sondhi, "On the Application of Vector Quantization and Hidden Markov Models to Speaker-Independent, Isolated Word Recognition," *B.S.T.J.*, *62*, No. 4 (April 1983), pp. 1075-105.
7. K. C. Pan, F. K. Soong, and L. R. Rabiner, "A Vector Quantization Based Preprocessor for Speaker Independent Isolated Word Recognition," *Trans. Acoust., Speech, and Signal Proc.*, *ASSP-33*, No. 3 (June 1985).
8. A. B. Poritz, "Linear Predictive Hidden Markov Models and the Speech Signal," *Proc. IEEE, ICASSP '82*, Paris, France (May 1982), pp. 1291-4.
9. J. K. Baker, "The Dragon System—An Overview," *IEEE Trans. Acoust., Speech, and Signal Proc.*, *ASSP-23*, No. 1 (February 1975), pp. 24-9.
10. L. R. Bahl, F. Jelinek, and R. L. Mercer, "A Maximum Likelihood Approach to Continuous Speech Recognition," *IEEE Trans. Pattern Analysis and Machine Intelligence, PAMI-5*, No. 2 (March 1983), pp. 179-90.
11. R. Billi, "Vector Quantization and Markov Source Models Applied to Speech Recognition," *Proc. IEEE, ICASSP '82*, Paris, France (May 1982), pp. 574-7.
12. F. Jelinek, "Continuous Speech Recognition by Statistical Methods," *Proc. IEEE*, *64* (April 1976), pp. 532-56.
13. H. Bourlard, C. J. Wellekins, and H. Ney, "Connected Digit Recognition Using Vector Quantization," *Proc. IEEE, ICASSP '84*, San Diego, Calif. (March 1984), pp. 26.10.1-4.
14. L. E. Baum, T. Petrie, G. Soules, and N. Weiss, "A Maximization Technique Occurring in the Statistical Analysis of Probabilistic Functions of Markov Chains," *Ann. Math. Stat.*, *41* (1970), pp. 164-71.
15. L. R. Liporace, "Maximum Likelihood Estimation for Multivariate Observations of Markov Sources," *IEEE Trans. Inform. Theory*, *IT-28* (September 1982), pp. 729-34.
16. B.-H. Juang, S. E. Levinson, and M. M. Sondhi, "Maximum Likelihood Estimation for Multivariate Normal Mixture Observations of Markov Chains," *IEEE Int. Symp. Inform. Theory*, Brighton, England, June 23-28, 1985.
17. L. R. Rabiner, B.-H. Juang, S. E. Levinson, and M. M. Sondhi, "Some Properties of Continuous Hidden Markov Model Representations," *AT&T Tech. J.*, *64*, No. 6 (July-August 1985), pp. 1251-70.
18. Y. Linde, A. Buzo, and R. M. Gray, "An Algorithm for Vector Quantization," *IEEE Trans. Commun.*, *COM-28*, No. 1 (January 1980), pp. 84-95.
19. B.-H. Juang and L. R. Rabiner, "A Probabilistic Distance Measure for Hidden Markov Models," *AT&T Tech. J.*, *64*, No. 2, Part 1 (February 1985), pp. 391-408.
20. A. J. Viterbi, "Error Bounds for Convolutional Codes and an Asymptotically

- Optimum Decoding Algorithm," IEEE Trans. Inform. Theory, *IT-13* (April 1967), pp. 260-9.
21. L. R. Rabiner, S. E. Levinson, A. E. Rosenberg, and J. G. Wilpon, "Speaker Independent Recognition of Isolated Words Using Clustering Techniques," IEEE Trans. Acoust., Speech, and Signal Proc., *ASSP-27*, No. 4 (August 1979), pp. 336-49.
 22. L. R. Rabiner and J. G. Wilpon, "A Simplified Robust Training Procedure for Speaker Trained, Isolated Word Recognition Systems," J. Acoust. Soc. Am., *68*, No. 5 (November 1980), pp. 1271-6.
 23. J. G. Wilpon, L. R. Rabiner, and A. Bergh, "Speaker Independent Isolated Word Recognition Using a 129-Word Airline Vocabulary," J. Acoust. Soc. Am., *72*, No. 2 (August 1982), pp. 390-6.
 24. A. E. Rosenberg, K. L. Shipley, and D. E. Bock, "A Speech Data Base Facility Using a Computer Controlled Cassette Tape Deck," J. Acoust. Soc. Am., Suppl. 1, *72* (Fall 1982), p. 580.
 25. J. G. Wilpon and L. R. Rabiner, "A Modified *K*-Means Clustering Algorithm for Use in Speaker Independent Isolated Word Recognition," Trans. Acoust., Speech, and Signal Proc., *ASSP-33*, No. 3 (June 1985).

AUTHORS

Biing-Hwang Juang, B.Sc. (Electrical Engineering), 1973, National Taiwan University, Republic of China; M.Sc. and Ph.D. (Electrical and Computer Engineering), University of California, Santa Barbara, 1979 and 1981, respectively; Speech Communications Research Laboratory (SCRL), 1978; Signal Technology, Inc., 1979-1982; AT&T Bell Laboratories, 1982; AT&T Information Systems Laboratories, 1983; AT&T Bell Laboratories, 1983—. Before joining AT&T Bell Laboratories, Mr. Juang worked on vocal tract modeling at Speech Communications Research Laboratory, and on speech coding and interference suppression at Signal Technology, Inc. Presently, he is a member of the Acoustics Research Department, where he is researching speech communications techniques and stochastic modeling of speech signals.

Stephen E. Levinson, B.A. (Engineering Sciences), 1966, Harvard; M.S. and Ph.D. (Electrical Engineering), University of Rhode Island, Kingston, Rhode Island, 1972 and 1974, respectively; General Dynamics, 1966-1969; Yale University, 1974-1976; AT&T Bell Laboratories, 1976—. From 1966 to 1969, Mr. Levinson was a design engineer at Electric Boat Division of General Dynamics in Groton, Connecticut. From 1974 to 1976, he held a J. Willard Gibbs Instructorship in Computer Science at Yale University. In 1976, he joined the technical staff at AT&T Bell Laboratories, where he is pursuing research in the areas of speech recognition and cybernetics. In 1984 he held a visiting fellowship in the Engineering Department at Cambridge University. Member, Association for Computing Machinery, editorial board of *Speech Technology*; fellow, Acoustical Society of America, senior member, IEEE; associate editor, *IEEE Transactions on Acoustics, Speech and Signal Processing*; vice chairman, ASSP technical committee on speech.

Lawrence R. Rabiner, S.B. and S.M., 1964, Ph.D., 1967 (Electrical Engineering), The Massachusetts Institute of Technology; AT&T Bell Laboratories, 1962—. From 1962 through 1964, Mr. Rabiner participated in the cooperative plan in electrical engineering at AT&T Bell Laboratories. He worked on digital circuitry, military communications problems, and problems in binaural hearing. Currently, he is engaged in research on speech communications and digital signal processing techniques. He is coauthor of *Theory and Application of Digital Signal Processing* (Prentice-Hall, 1975) and *Digital*

Processing of Speech Signals (Prentice-Hall, 1978). Former President, IEEE, ASSP Society; former Associate Editor, ASSP Transactions; former member, Technical Committee on Speech Communication; Member, IEEE Proceedings Editorial Board, Eta Kappa Nu, Sigma Xi, Tau Beta Pi, The National Academy of Engineering. Fellow, Acoustical Society of America, IEEE.

Man Mohan Sondhi, B.Sc. (Physics), Honours degree, 1950, Delhi University, Delhi, India, D.I.I.Sc. (Communications Engineering), 1953, Indian Institute of Science, Bangalore, India; M.S., 1955, and Ph.D. (Electrical Engineering), 1957, University of Wisconsin, Madison, Wisconsin; AT&T Bell Laboratories, 1962—. Before joining AT&T Bell Laboratories, Mr. Sondhi worked for over a year at the Avionics division of John Oster Manufacturing Company, Racine, Wisconsin; for a year at the Central Electronics Engineering Research Institute, Pilani, India; and taught for a year at the University of Toronto. At AT&T Bell Laboratories his research has included work on speech signal processing, echo cancellation, adaptive filtering, modeling of auditory and visual processes, acoustical inverse problems, and HMM of speech. From 1971 to 1972, Mr. Sondhi was a guest scientist at the Royal Institute of Technology, Stockholm, Sweden.

Maximum-Likelihood Estimation for Mixture Multivariate Stochastic Observations of Markov Chains

By B.-H. JUANG*

(Manuscript received November 15, 1984)

In this paper we discuss parameter estimation by means of the reestimation algorithm for a class of multivariate mixture density functions of Markov chains. The scope of the original reestimation algorithm is expanded and the previous assumptions of log concavity or ellipsoidal symmetry are obviated, thereby enhancing the modeling capability of the technique. Reestimation formulas in terms of the well-known forward-backward inductive procedure are also derived.

I. INTRODUCTION

Hidden Markov models, which use probabilistic functions of Markov chains to model random processes, have been found to be extremely useful for stock market behavior, ecology,¹⁻² and more recently, speech recognition.³⁻⁵ The effectiveness of this model class lies in its ability to deal with nonstationarity that often appears in the observed data sequences. The general structure of such a class of models may be briefly described as follows.

Consider a first-order N -state Markov chain governed by an $N \times N$ transition probability matrix $\mathbf{A} = [a_{ij}]$, and an initial probability vector $\mathbf{u}^t = [u_1 u_2 \cdots u_N]$. Obviously, $\sum_{j=1}^N a_{ij} = 1$ for any $i = 1, 2, \dots, N$, and $\sum_{j=1}^N u_j = 1$. a_{ij} is the probability of making a transition from state

* AT&T Bell Laboratories.

Copyright © 1985 AT&T. Photo reproduction for noncommercial use is permitted without payment of royalty provided that each reproduction is done without alteration and that the Journal reference and copyright notice are included on the first page. The title and abstract, but no other portions, of this paper may be copied or distributed royalty free by computer-based and other information-service systems without further permission. Permission to reproduce or republish any other portion of this paper must be obtained from the Editor.

i to state j given that the current state is i . For any integer state sequence $\Theta = (\theta_0, \theta_1, \theta_2, \dots, \theta_T)$, where $\theta_t \in \{1, 2, \dots, N\}$, the probability of Θ being generated by the Markov source can be easily calculated by

$$\Pr(\Theta | \mathbf{A}, \mathbf{u}) = u_{\theta_0} a_{\theta_0 \theta_1} \cdots a_{\theta_{T-1} \theta_T}. \quad (1)$$

Now, suppose Θ cannot be directly observed. Instead, we assume that what we observe is a stochastic process $\mathbf{S} = (\mathbf{s}_1, \mathbf{s}_2, \dots, \mathbf{s}_T)$, produced by an underlying (stochastic) state sequence $(\theta_1, \theta_2, \dots, \theta_T)$. Each state, say i , manifests itself through a probability density function $f_i(s)$, $\int f_i(s) ds = 1$. We use $F = \{f_i(\cdot)\}$ to denote such a set of density functions. The probability density of $\mathbf{S} = S \triangleq (s_1, s_2, \dots, s_T)$, given a specific state sequence Θ generated by the Markov chain with transition probability matrix \mathbf{A} , and initial probability vector \mathbf{u} is thus

$$f(S | \Theta, \mathbf{A}, \mathbf{u}, F) = \prod_{t=1}^T f_{\theta_t}(s_t). \quad (2)$$

It then follows that the density of \mathbf{S} , given \mathbf{A} , \mathbf{u} and F , is

$$f(S | \mathbf{A}, \mathbf{u}, F) = \sum_{\text{all } \Theta} u_{\theta_0} \prod_{t=1}^T a_{\theta_{t-1} \theta_t} f_{\theta_t}(s_t). \quad (3)$$

The triple $(\mathbf{A}, \mathbf{u}, F) \triangleq \lambda$ is called a (hidden) Markov model source and we write $f(S | \lambda) \triangleq f(S | \mathbf{A}, \mathbf{u}, F)$, for simplicity.

Given an observation sequence S , the objective in maximum-likelihood estimation is thus to maximize $f(S | \lambda)$ over all parameters in λ . Such a maximization problem is clearly nontrivial. To solve this problem, a reestimation algorithm—developed by Baum et al.¹ in 1970—that guarantees monotonic increase in the likelihood as the algorithm iterates, is often used. An auxiliary function, based upon the Kullback-Leibler number,⁶ serves as the basis of Baum's optimization procedure, in which parameter estimates are characterized as the critical point of the auxiliary function. However, the development in Ref. 1 encounters difficulties when the densities $\{f_i(\cdot)\}$ are not log concave. The Cauchy density $f(s) = \pi^{-1}(1 + s^2)^{-1}$, which is only concave for $3s^2 \leq 1$, was cited as one such problematic example.

More than a decade later, in an effort to obviate the log-concavity limitation in Baum's algorithm, Liporace⁷ invoked a representation theorem by Fan⁸ to redefine the auxiliary function and then successfully extended the reestimation algorithm to accommodate a class of elliptically symmetric, multivariate distributions. As a result, each $f_i(s) \in F$ is allowed to assume the form

$$|\mathbf{R}_i|^{-1/2} h_i(g_i(s)), \quad (4)$$

where $g_i(s)$ is positive definite quadratic,

$$g_i(s) = (s - \eta_i)^* \mathbf{R}_i^{-1} (s - \eta_i).$$

The asterisk denotes the transpose of a vector or matrix as we, following Liporace, will be dealing with vector observations from this point on. The matrix \mathbf{R}_i is positive definite and symmetric, and the location vector η_i is an arbitrary point in the observation space that is d -dimensional Euclidean.

While Liporace's results are significant in expanding the scope of the reestimation algorithm, the requirements that the observation densities be elliptically symmetric are in many real situations still very restrictive. In particular, useful parametrizations of speech signals, such as reflection coefficients and autocorrelation, have been shown by Gray and Markel⁹ and Rabiner et al.,¹⁰ respectively, not to exhibit the desired symmetry. This lack of symmetry is often observed even within each state because of the arbitrariness in choosing the number of states for modeling the given process. It is thus the purpose of this paper to further obviate the ellipsoidal symmetry assumption so that an even more versatile statistical modeling technique than the previous ones is obtainable. Levinson also reported the same effort.¹¹

The class of densities $F = \{f_i(\cdot)\}$ we consider in this paper is the class of mixtures of general, strictly log-concave, and/or elliptically symmetric densities, having the form

$$f_i(s) = \sum_{k=1}^M c_{ik} b_{ik}(s), \quad (5)$$

where $b_{ik}(s)$ is general strictly log concave and/or elliptically symmetric and c_{ik} satisfies

$$\sum_{k=1}^M c_{ik} = 1 \quad \text{for } i = 1, 2, \dots, N. \quad (6)$$

As required in Liporace's results,⁷ one extra assumption for elliptically symmetric $b_{ik}(s)$ is necessary: the density $b_{ik}(s)$ also satisfies the consistency conditions of Kolmogorov (see Ref. 12, p. 10) so that $b_{ik}(\cdot)$ has the representation

$$b_{ik}(s) = \int_0^\infty \mathcal{N}(s; \eta_{ik}, \nu \mathbf{R}_{ik}) dG(\nu) \quad (7)$$

for some probability distribution G on $[0, \infty)$. In (7), the expression $\mathcal{N}(s; \eta_{ik}, \nu \mathbf{R}_{ik})$ is the multivariate Gaussian density with mean vector η_{ik} and covariance matrix $\nu \mathbf{R}_{ik}$. Clearly, $\{f_i(s)\}$, as expressed in (5), is very general and may serve better in the modeling of many complex but realistic observations than unimodal, symmetric density functions.

This paper is organized as follows. The main body of the theory is presented in Section II, where the auxiliary function is redefined and the reestimation formula for all the parameters is derived. In Section

III, applications of the theory to familiar probability densities are discussed. Furthermore, for computational convenience, parameter reestimation using the forward-backward inductive procedure is also provided.

II. REESTIMATION

2.1 Joint density

For mathematical clarity, the following definitions are necessary.

Let Λ be an open subset of Euclidean p space. A hidden Markov model λ is a point in Λ and to each $\lambda \in \Lambda$ we have a smooth assignment $\lambda \rightarrow (\mathbf{A}(\lambda), \mathbf{u}(\lambda), F(\lambda))$. One trivial assignment is that dimensions in Λ are one-to-one, corresponding to the parameters defining the triple $(\mathbf{A}, \mathbf{u}, F)$, and thus p is the total number of model parameters.

Define the state alphabet $\Omega_s \triangleq \{1, 2, \dots, N\}$. Let Ω_s^{T+1} be the $(T + 1)$ th Cartesian product of Ω_s . The state sequence space is denoted by Ω_s^{T+1} , and $\Theta \in \Omega_s^{T+1}$ means $\Theta = (\theta_0, \theta_1, \dots, \theta_T)$, where every $\theta_t \in \Omega_s$.

We further define the branch alphabet $\Omega_b \triangleq \{1, 2, \dots, M\}$. Similarly, Ω_b^T is the set of all T -tuples $K = (k_1, k_2, \dots, k_T)$, where every $k_t \in \Omega_b$. K is called a branch sequence.

The global density function of (3) with state density defined by (5) can be written as

$$f(S|\lambda) = \sum_{\text{all } \Theta \in \Omega_s^{T+1}} u_{\theta_0} \prod_{t=1}^T \left[a_{\theta_{t-1}\theta_t} \cdot \sum_{k=1}^M c_{\theta_t k} b_{\theta_t k}(s_t) \right]. \quad (8)$$

The summand in (8) over all $\Theta \in \Omega_s^{T+1}$ is, in fact, the joint density $f(S, \Theta|\lambda)$, which can be expressed as

$$\begin{aligned} f(S, \Theta|\lambda) &= u_{\theta_0} \prod_{t=1}^T a_{\theta_{t-1}\theta_t} \sum_{k=1}^M c_{\theta_t k} b_{\theta_t k}(s_t) \\ &= \sum_{k_1=1}^M \sum_{k_2=1}^M \cdots \sum_{k_T=1}^M \left[u_{\theta_0} \prod_{t=1}^T a_{\theta_{t-1}\theta_t} b_{\theta_t k_t}(s_t) \right] \\ &\quad \cdot c_{\theta_1 k_1} c_{\theta_2 k_2} \cdots c_{\theta_T k_T}. \end{aligned} \quad (9)$$

We further define

$$f(S, \Theta, K|\lambda) = u_{\theta_0} \prod_{t=1}^T a_{\theta_{t-1}\theta_t} b_{\theta_t k_t}(s_t) c_{\theta_t k_t}. \quad (10)$$

Therefore, the joint density of the truncated stochastic process \mathbf{S} is

$$f(S|\lambda) = \sum_{\Theta \in \Omega_s^{T+1}} \sum_{K \in \Omega_b^T} f(S, \Theta, K|\lambda). \quad (11)$$

An interpretation of (11) is that there are N^{T+1} possible stochastic state sequences that may lead to the observation S , with each possible state sequence being a superposition of M^T branch layers.

2.2 Auxiliary function and an inequality

For more general theoretical interest, let $\Omega = \Omega_s^{T+1} \times \Omega_b^T$ be a totally finite measure space with measure $\mu(\Theta, K)$. The joint density of (11) then has the following general form:

$$f(S|\lambda) = \int_{\Omega} f(S, \Theta, K|\lambda) d\mu(\Theta, K).$$

Following the concept of the Kullback-Leibler statistic, we define an auxiliary function $Q(\lambda, \lambda')$ of two model points, λ and λ' , in Λ , given an observation S :

$$Q(\lambda, \lambda') \triangleq \int_{\Omega} f(S, \Theta, K|\lambda) \log f(S, \Theta, K|\lambda') d\mu(\Theta, K). \quad (12)$$

We now have the following theorem:

Theorem 1: If $Q(\lambda, \lambda') \geq Q(\lambda, \lambda)$ then $f(S|\lambda') \geq f(S|\lambda)$. The inequality is strict unless $f(S, \Theta, K|\lambda) = f(S, \Theta, K|\lambda')$ almost everywhere $d\mu(\Theta, K)$.

Proof: Similar to Baum et al.,¹ $\log x$ is strictly concave for $x > 0$. Hence,

$$\begin{aligned} \log \frac{f(S|\lambda')}{f(S|\lambda)} &= \log \int_{\Omega} \frac{f(S, \Theta, K|\lambda')}{f(S|\lambda)} d\mu(\Theta, K) \\ &= \log \int_{\Omega} \frac{f(S, \Theta, K|\lambda)}{f(S|\lambda)} d\mu(\Theta, K) \frac{f(S, \Theta, K|\lambda')}{f(S, \Theta, K|\lambda)} \\ &\geq \int_{\Omega} \frac{f(S, \Theta, K|\lambda)}{f(S|\lambda)} \left[\log \frac{f(S, \Theta, K|\lambda')}{f(S, \Theta, K|\lambda)} \right] d\mu(\Theta, K) \\ &= [f(S|\lambda)]^{-1} [Q(\lambda, \lambda') - Q(\lambda, \lambda)] \geq 0 \end{aligned}$$

by hypothesis. The inequality above is due to Jensen's inequality for the measure $d\zeta(\Theta, K|\lambda) = f(S, \Theta, K|\lambda)d\mu(\Theta, K)/f(S|\lambda)$. This inequality is strict unless $f(S, \Theta, K|\lambda')/f(S, \Theta, K|\lambda)$ is constant almost everywhere $d\zeta(\Theta, K|\lambda)$, hence unless $f(S, \Theta, K|\lambda') = f(S, \Theta, K|\lambda)$ almost everywhere $d\mu(\Theta, K)$.

The significance of Theorem 1 will be discussed below. For simplicity, we often use the expression of (11) for the joint density and define the auxiliary function as

$$Q(\lambda, \lambda') = \sum_{\theta \in \Omega_T^{T+1}} \sum_{K \in \Omega_T^T} f(S, \theta, K | \lambda) \log f(S, \theta, K | \lambda') \quad (13)$$

as long as the key result of Theorem 1 is held valid.

2.3 Reestimation algorithm

Theorem 1 is one of the bases of Baum's reestimation algorithm that is sketched below for self-containedness. For a given observation S , the reestimation algorithm starts with an initial guess of the model λ . The parameter reestimates are then defined to be those that maximize $Q(\lambda, \lambda')$ as a function of λ' ; that is, the model reestimate $\bar{\lambda}$ stemming from the current model λ is $\bar{\lambda} = \mathcal{T}(\lambda) \in \{\hat{\lambda} \in \Lambda \mid Q(\lambda, \hat{\lambda}) = \max_{\lambda' \in \Lambda} Q(\lambda, \lambda')\}$. The transformation $\mathcal{T}: \Lambda \rightarrow \Lambda$ is called the reestimation transformation. If Q has a unique global maximum as a function of λ' , the set $\{\hat{\lambda}\}$ has only one element $\bar{\lambda}$. Then $\bar{\lambda}$ plays the role of λ as before and new reestimates are determined. The procedure iterates until some criterion is met.

Due to Theorem 1 and the following theorem, the above iterative procedure produces a sequence of reestimates that guarantee monotonic increase in the likelihood $f(S | \lambda)$ unless it reaches a critical point of the likelihood.

Theorem 2: Let $f(S, \theta, K | \lambda)$ be continuously differentiable in λ for almost all $(\theta, K) \in \Omega$. Let \mathcal{T} be a continuous map of $\Lambda \rightarrow \Lambda$ such that for each fixed λ , $\bar{\lambda} = \mathcal{T}(\lambda)$ is a critical point of $Q(\lambda, \lambda')$ as a function of λ' . Then all fixed points of the reestimation transformation \mathcal{T} are critical points of $f(S | \lambda)$, and if $f(S | \bar{\lambda}) > f(S | \lambda)$, unless $\bar{\lambda} = \lambda$, all limit points of $\mathcal{T}^n(\lambda_0) \triangleq \mathcal{T}(\mathcal{T}(\mathcal{T} \dots (\mathcal{T}(\lambda_0)) \dots))$ are fixed points of \mathcal{T} for any $\lambda_0 \in \Lambda$.

Proof: Let ∇_λ be the gradient vector.

$$\begin{aligned} \nabla_\lambda f(S | \lambda) |_\lambda &= \nabla_\lambda \int_\Omega f(S, \theta, K | \lambda) d\mu(\theta, K) \\ &= \int_\Omega \nabla_\lambda f(S, \theta, K | \lambda) d\mu(\theta, K) \\ &= \int_\Omega f(S\theta, K | \lambda) [\nabla_\lambda \log f(S, \theta, K | \lambda)] d\mu(\theta, K) \\ &= \nabla_{\lambda'} Q(\lambda, (\lambda, \lambda')) |_{\lambda'=\lambda}. \end{aligned}$$

Thus $\nabla_\lambda f(S | \lambda) |_{\lambda=\bar{\lambda}} = 0$ if and only if $\nabla_{\lambda'} Q(\lambda, \lambda') |_{\lambda'=\lambda} = 0$ at $\lambda = \bar{\lambda}$. The rest of the proof follows Baum et al.¹

Theorems 1 and 2 thus guarantee that after each iteration, the new reestimate $\bar{\lambda}$ improves the likelihood, i.e., $f(S | \bar{\lambda}) > f(S | \lambda)$, unless $\bar{\lambda}$ is a fixed point of the transformation. On the other hand, the trans-

formation will converge to a fixed point, or equivalently, a critical point of the likelihood, if an increase in the likelihood is maintained after each iteration and if the limit $\lim_{n \rightarrow \infty} \mathcal{T}^n(\lambda_0)$ exists, regardless of what the initial guess $\lambda_0 (\in \Lambda)$ is. If $f(S|\lambda)$ has finitely many critical points, $\mathcal{T}^n(\lambda_0)$ approaches a critical point of $f(S|\lambda)$ that is at least a local maximum.

The transformation as previously defined requires maximization of the auxiliary function. Difficulties encountered in the maximization process would directly translate into difficulties in obtaining the maximum-likelihood estimate. We next show that if every $b_{ij}(\cdot)$, $i = 1, 2, \dots, N$ and $j = 1, 2, \dots, M$ is strictly log concave or elliptically symmetric with the representation (7), $Q(\lambda, \lambda')$ has a unique global maximum as a function of λ' , and thus the transformation exists and is single valued. The reestimation algorithm is thus guaranteed to work for the joint density of (8).

2.4 Maximization of the auxiliary function

The auxiliary function for the joint density (8) with mixture densities is defined in (12). The following decomposition can be easily seen:

$$\begin{aligned} \log f(S, \Theta, K|\lambda') &= \log \mu'_{\theta_0} + \sum_{t=1}^T \log a'_{\theta_{t-1}\theta_t} + \sum_{t=1}^T \log b'_{\theta_t k_t}(s_t) + \sum_{t=1}^T \log c'_{\theta_t k_t}. \quad (14) \end{aligned}$$

The next theorem suggests that maximization of the likelihood by way of reestimation can be accomplished on individual parameter sets due to the separability shown in (14), if the following assumptions hold. Suppose for almost all (Θ, K) , $\log f(S, \Theta, K|\lambda) = \sum_{i=1}^q \log f^{(i)}(S, \Theta, K|\lambda_i)$, where for each i and almost all (Θ, K) $\log f^{(i)}(S, \Theta, K|\lambda_i)$ has a unique global maximum as a function of λ_i . Note that $\lambda = \{\lambda_i\}$ and q is the number of parameter sets after separation. Define $Q_i(\lambda, \lambda'_i)$ by

$$Q_i(\lambda, \lambda'_i) = \int_{\Omega} f(S, \Theta, K|\lambda) \log f^{(i)}(S, \Theta, K|\lambda_i) d\mu(\Theta, K). \quad (15)$$

Then for λ fixed, $Q_i(\lambda, \lambda'_i)$ as a function of λ'_i has a unique global maximum $\bar{\lambda}_i$ that is a critical point of $Q_i(\lambda, \lambda'_i)$. The reestimation transformation \mathcal{T} is thus defined as $\mathcal{T}: \lambda \rightarrow \bar{\lambda} = \{\bar{\lambda}_i\}$. We further define $\mathcal{T}_i: \lambda \rightarrow \tilde{\lambda}_i = \{\lambda_1, \lambda_2, \dots, \bar{\lambda}_i, \dots, \lambda_q\}$.

Theorem 3: Under the above assumptions, for all $\lambda \in \Lambda$, and every i , $f(S|\mathcal{T}_i(\lambda)) \geq f(S|\lambda)$ with equality if and only if λ_i is a critical point of $f(S|\lambda)$ with respect to λ_i or, equivalently, $\tilde{\lambda}_i$ is a fixed point of \mathcal{T}_i and furthermore, $f(S|\mathcal{T}(\lambda)) \geq f(S|\lambda)$ with equality if and only if λ is a critical point of $f(S|\lambda)$ or, equivalently, a fixed point of \mathcal{T} .

Proof:

$$\begin{aligned}
 Q(\lambda, \tilde{\lambda}_i) &= \sum_{\substack{j=1 \\ j \neq i}}^q Q_j(\lambda, \lambda_j) + Q_i(\lambda, \bar{\lambda}_i) \\
 &\geq \sum_{j=1}^q Q_j(\lambda, \lambda_j) = Q(\lambda, \lambda),
 \end{aligned}$$

so Theorem 1 implies $f(S | \tilde{\lambda}_i) \geq f(S | \lambda)$. Since $Q_i(\lambda, \lambda'_i)$ has a unique global maximum as a function of λ'_i , the inequality $Q(\lambda, \tilde{\lambda}_i) \geq Q(\lambda, \lambda)$ is strict unless $\bar{\lambda}_i = \lambda_i$. Furthermore,

$$Q(\lambda, \bar{\lambda}) = \sum_{i=1}^q Q_i(\lambda, \bar{\lambda}_i) \geq \sum_{i=1}^q Q_i(\lambda, \lambda_i) = Q(\lambda, \lambda),$$

the second half of the theorem is thus true.

The separation of (14) is seen to be the key to the increased versatility of the reestimation algorithm in accommodating mixture-observation densities. Let \mathbf{b}_{jk} be the parameter set defining the density $b_{jk}(s)$. Obviously, if $b_{jk}(s)$ is multivariate Gaussian, $\mathbf{b}_{jk} = (\eta_{jk}, \mathbf{R}_{jk})$, where η_{jk} is the mean vector and \mathbf{R}_{jk} is the covariance matrix. We now write the auxiliary function in a separated form using the simplified expression of (13) without loss of generality.

$$\begin{aligned}
 Q(\lambda, \lambda') &\triangleq \sum_{\Theta} \sum_K f(S, \Theta, K | \lambda) \log f(S, \Theta, K | \lambda') \\
 &= \sum_{\Theta} \sum_K f(S, \Theta, K | \lambda) \left\{ \log u'_{\theta_0} + \sum_{t=1}^T \log a_{\theta_{t-1}\theta_t} \right. \\
 &\quad \left. + \sum_{t=1}^T \log b'_{\theta_t k_t}(s_t) + \sum_{t=1}^T \log c'_{\theta_t k_t} \right\} \\
 &= Q_u(\lambda, \mathbf{u}') + \sum_{i=1}^N Q_{a_i}[\lambda, \{a'_{ij}\}_{j=1}^N] \\
 &\quad + \sum_{j=1}^N \sum_{k=1}^M Q_b(\lambda, \mathbf{b}'_{jk}) + \sum_{j=1}^N Q_{c_j}[\lambda, \{c'_{jk}\}_{k=1}^M], \quad (16)
 \end{aligned}$$

where

$$\begin{aligned}
 Q_u(\lambda, \mathbf{u}') &= \sum_{\Theta} \sum_K f(S, \Theta, K | \lambda) \log u'_{\theta_0} \\
 &= \sum_{i=1}^N \sum_K f(S, \theta_0 = i, K | \lambda) \log u'_i \quad (17)
 \end{aligned}$$

$$\begin{aligned}
Q_{a_i}[\lambda, \{a'_{ij}\}_{j=1}^N] &= \sum_{\Theta} \sum_K f(S, \Theta, K | \lambda) \sum_{t=1}^T \log a'_{\theta_{t-1} \theta_t} \delta(\theta_{t-1} - i) \\
&= \sum_{j=1}^N \sum_{t=1}^T \sum_K f(S, \theta_{t-1} = i, \theta_t = j, K | \lambda) \log a'_{ij} \quad (18)
\end{aligned}$$

$$\begin{aligned}
Q_b(\lambda, \mathbf{b}'_{jk}) &= \sum_{\Theta} \sum_K f(S, \Theta, K | \lambda) \\
&\quad \cdot \sum_{t=1}^T \log b'_{\theta_t k_t}(s_t) \delta(\theta_t - j) \delta(k_t - k) \\
&= \sum_{t=1}^T f(S, \theta_t = j, k_t = k | \lambda) \log b'_{jk}(s_t), \quad (19)
\end{aligned}$$

and

$$\begin{aligned}
Q_{c_j}(\lambda, \{c'_{jk}\}_{k=1}^M) &= \sum_{\Theta} \sum_K f(S, \Theta, K | \lambda) \sum_{t=1}^T \log c'_{\theta_t k_t} \delta(\theta_t - j) \\
&= \sum_{k=1}^M \sum_{t=1}^T f(S, \theta_t = j, k_t = k | \lambda) \log c'_{jk}. \quad (20)
\end{aligned}$$

The above expression $\delta(\cdot)$ is the Kronecker delta function.

Individual maximization of Q_u , Q_{a_i} and Q_{c_i} for $i = 1, 2, \dots, N$ subject to the constraints

$$\begin{aligned}
1. \quad &\sum_{j=1}^N u_j = 1, \quad u_j \geq 0 \\
2. \quad &\sum_{j=1}^N a_{ij} = 1, \quad a_{ij} \geq 0 \quad \text{for all appropriate } i \text{ and } j \\
3. \quad &\sum_{j=1}^M c_{ij} = 1, \quad c_{ij} \geq 0, \quad (21)
\end{aligned}$$

respectively, is well known.^{13,14} These individual auxiliary functions have the same form $\sum_{j=1}^N w_j \log y_j$, which as a function of $\{y_j\}_{j=1}^N$, subject to the constraints $\sum_{j=1}^N y_j = 1$ and $y_j \geq 0$, attains a global maximum at the single point

$$y_j = \frac{w_j}{\sum_{i=1}^N w_i} \quad j = 1, 2, \dots, N. \quad (22)$$

The result has been proved in many ways.¹⁴

When $b_{jk}(s)$ is strictly log concave in \mathbf{b}_{jk} and $\lim_{|\mathbf{b}_{jk}| \rightarrow \infty} \log b_{jk}(s) = -\infty$, it is easily seen that for λ fixed $Q_b(\lambda, \mathbf{b}'_{jk})$ has a unique global maximum that is a critical point of $Q_b(\lambda, \mathbf{b}'_{jk})$. When $b_{jk}(s)$ is elliptically symmetric, the following theorem due to Liporace⁷ is applicable.

Theorem 4: If (i) $b_{jk}(s)$ has the representation of eq. (7), and (ii) there

are among $s_1, s_2, \dots, s_T, d + 1$ observations, any d (the dimension of each observation vector) of which are linearly independent, for fixed λ , $Q_b(\lambda, \mathbf{b}'_{jk})$ has a unique global maximum as a function of $\mathbf{b}'_{jk} = (\eta'_{jk}, \mathbf{R}'_{jk})$, and this maximum is the one and only critical point of $Q_b(\lambda, \mathbf{b}'_{jk})$.

Proof of this theorem is easily obtained by following the Appendix in Ref. 7.

The reestimation algorithm has thus been extended to accommodate the hidden Markov joint density (8) with mixture observation densities.

III. APPLICATIONS

We now explicitly derive the reestimation transformation. By applying eq. (22), we can easily calculate $\bar{\mathbf{u}}, \bar{\mathbf{A}}$, and $\{\bar{c}_{ik}\}_{k=1}^M$ for $i = 1, 2, \dots, n$, the reestimates that for fixed λ maximize $Q_u(\lambda, \mathbf{u}')$, $Q_{a_i}(\lambda, \{a'_{ij}\}_{j=1}^N)$ and $Q_{c_i}(\lambda, \{c'_{ik}\}_{k=1}^M)$ for $i = 1, 2, \dots, N$, as a function of $\mathbf{u}', \{a'_{ij}\}_{j=1}^N$ and $\{c'_{ik}\}_{k=1}^M$, respectively.

1. Initial probability:

$$Q_u(\lambda, \mathbf{u}') \triangleq \sum_{j=1}^N \sum_K f(S, \theta_0 = i, K | \lambda) \log u'_j.$$

Hence, for $i = 1, 2, \dots, N$,

$$\begin{aligned} \bar{u}_i &= \sum_{K \in \Omega_f^i} f(S, \theta_0 = i, K | \lambda) \bigg/ \sum_{K \in \Omega_f^i} f(S, K | \lambda) \\ &= f(S, \theta_0 = i | \lambda) / f(S | \lambda). \end{aligned} \quad (23)$$

2. Transition probability:

For every $i = 1, 2, \dots, N$,

$$Q_{a_i}(\lambda, \{a'_{ij}\}_{j=1}^N) = \sum_{j=1}^N \sum_{t=1}^T \sum_K f(S, \theta_{t-1} = i, \theta_t = j, K | \lambda) \log a'_{ij}.$$

Therefore, for $i, j = 1, 2, \dots, N$,

$$\begin{aligned} \bar{a}_{ij} &= \sum_{t=1}^T \sum_K f(S, \theta_{t-1} = i, \theta_t = j, K | \lambda) \bigg/ \\ &\quad \cdot \sum_{t=1}^T \sum_K f(S, \theta_{t-1} = i, K | \lambda) \\ &= \sum_{t=1}^T f(S, \theta_{t-1} = i, \theta_t = j | \lambda) \bigg/ \sum_{t=1}^T f(S, \theta_{t-1} = i | \lambda). \end{aligned} \quad (24)$$

3. Branch probability:

For every $i = 1, 2, \dots, N$,

$$Q_{c_i}(\lambda, \{c'_{ik}\}_{k=1}^M) = \sum_{k=1}^M \sum_{t=1}^T f(S, \theta_t = i, k_t = k | \lambda) \log c'_{ij}.$$

Then obviously, for $i = 1, 2, \dots, N, k = 1, 2, \dots, M,$

$$\bar{c} = \frac{\sum_{t=1}^T f(S, \theta_t = i, k_t = k | \lambda)}{\sum_{t=1}^T f(S, \theta_t = i | \lambda)}. \quad (25)$$

4. Branch density:

For every $i = 1, 2, \dots, N,$ and $k = 1, 2, \dots, M,$

$$Q_b(\lambda, \mathbf{b}'_{ik}) = \sum_{t=1}^T f(S, \theta_t = i, k_t = k | \lambda) \log b'_{ik}(s_t).$$

Maximization of $Q_b(\lambda, \mathbf{b}'_{ij})$ with respect to \mathbf{b}'_{ik} is well known for many familiar density functions. The solution to the maximization problem is, in general, obtained through differentiation; i.e., we find $\bar{\mathbf{b}}_{ik}$ that satisfies

$$\begin{aligned} \nabla_{\mathbf{b}'_{ik}} Q_b(\lambda, \mathbf{b}'_{ik}) \Big|_{\mathbf{b}'_{ik} = \bar{\mathbf{b}}_{ik}} \\ &= \sum_{t=1}^T f(S, \theta_t = i, k_t = k | \lambda) \frac{\nabla_{\mathbf{b}'_{ik}} b'_{ik}(s_t)}{b'_{ik}(s_t)} \Big|_{\mathbf{b}'_{ik} = \bar{\mathbf{b}}_{ik}} \\ &= 0. \end{aligned} \quad (26)$$

For strictly log concave $b_{ik}(s),$ the solution can be easily found. For elliptically symmetric $b_{ik}(s),$

$$b_{ik}(s) = |\mathbf{R}_{ik}|^{-1/2} h_{ik}(g_{ik}(s)),$$

where

$$g_{ik}(s) = (s - \eta_{ik})^* \mathbf{R}_{ik}^{-1} (s - \eta_{ik}),$$

with representation (7), Liporace's results apply.⁷ In particular, the solution to (26), i.e., reestimates $\bar{\eta}_{ik}$ and $\bar{\mathbf{R}}_{ik},$ is given by

$$\bar{\eta}_{ik} = \frac{\sum_{t=1}^T f(S, \theta_t = i, k_t = k | \lambda) \cdot s_t}{\sum_{t=1}^T f(S, \theta_t = i, k_t = k | \lambda)} \quad (27)$$

$$\bar{\mathbf{R}}_{ik} = \frac{\sum_{t=1}^T f(S, \theta_t = i, k_t = k | \lambda) \cdot (s_t - \eta_{ik})(s_t - \eta_{ik})^*}{\sum_{t=1}^T f(S, \theta_t = i, k_t = k | \lambda)}. \quad (28)$$

Note that if $b_{ik}(s)$ is multivariate Gaussian, the reestimates $\bar{\eta}_{ik}$ and $\bar{\mathbf{R}}_{ik}$ above are readily applicable. It is also easy to see that each $\bar{\mathbf{R}}_{ik}$ is positive definite. If s is any d -dimensional vector,

$$s^* \bar{\mathbf{R}}_{ik} s = \sum_{t=1}^T x_{ik}(t) [s^*(s_t - \eta_{ik})]^2 \geq 0, \quad (29)$$

where

$$x_{ik}(t) = f(S, \theta_t = i, k_t = k | \lambda) \bigg/ \sum_{t=1}^T f(S, \theta_t = i, k_t = k | \lambda) \geq 0.$$

The inequality (29) is strict provided for any η_{ik} the vectors $\{s_t - \eta_{ik}\}$ span the d -dimensional observation space, i.e., the observation process $S = (s_1, s_2, \dots, s_T)$ satisfies the condition laid out in Theorem 4.

The above reestimates can be conveniently calculated with the forward-backward inductive procedure. Define "forward probabilities" $\alpha_0(i) = u_i, i = 1, 2, \dots, N$, and

$$\begin{aligned} \alpha_t(i) &= f(s_1, s_2, \dots, s_t, \theta_t = i | \lambda) \\ &= \sum_{j=1}^N \alpha_{t-1}(j) a_{ji} f_i(s_t), \end{aligned} \quad (30)$$

for $i = 1, 2, \dots, N$ and $t = 1, 2, \dots, T$. Branch densities $f_i(s)$ are defined in (5). Similarly, define "backward probabilities"

$$\begin{aligned} \beta_t(i) &= f(s_{t+1}, s_{t+2}, \dots, s_T | \theta_t = i, \lambda) \\ &= \sum_{j=1}^N \beta_{t+1}(j) a_{ij} f_j(s_{t+1}), \end{aligned} \quad (31)$$

and $\beta_T(i) = 1$, for $i = 1, 2, \dots, N$ and $t = T - 1, T - 2, \dots, 0$. Further define "branch probability" $\gamma_t(i, k)$

$$\begin{aligned} \gamma_t(i, k) &= f(s_1, s_2, \dots, s_t, \theta_t = i, k_t = k | \lambda) \\ &= \sum_{j=1}^N \alpha_{t-1}(j) a_{ji} c_{ik} b_{ik}(s_t), \end{aligned} \quad (32)$$

for $i = 1, 2, \dots, N, k = 1, 2, \dots, M$, and $t = 1, 2, \dots, T$. Then,

$$f(S, \theta_t = i | \lambda) = \alpha_t(i) \beta_t(i), \quad (33)$$

which leads to

$$f(S | \lambda) = \sum_{i=1}^N \alpha_t(i) \beta_t(i), \quad (34)$$

and in particular at $t = T$,

$$f(S|\lambda) = \sum_{i=1}^N \alpha_T(i). \quad (35)$$

Furthermore,

$$\begin{aligned} f(S, \theta_{t-1} = i, \theta_t = j|\lambda) &= \alpha_{t-1}(i) a_{ij} f_j(s_t) \beta_t(j) \\ &= \alpha_{t-1}(i) a_{ij} \left[\sum_{k=1}^M c_{jk} b_{jk}(s_t) \right] \beta_t(j), \end{aligned} \quad (36)$$

and

$$\begin{aligned} f(S, \theta_t = i, k_t = k|\lambda) &= \gamma_t(i, k) \beta_t(i) \\ &= \sum_{j=1}^N \alpha_{t-1}(j) a_{ji} c_{ik} b_{ik}(s_t) \beta_t(i). \end{aligned} \quad (37)$$

As a result, the reestimates are expressed in terms of the forward and backward probabilities:

1. Initial Probability:

$$\begin{aligned} \bar{u}_i &= \alpha_0(i) \beta_0(i) \Big/ \sum_{j=1}^N \alpha_0(j) \beta_0(j) \\ &= \alpha_0(i) \beta_0(i) \Big/ \sum_{j=1}^N \alpha_T(j) \end{aligned} \quad (38)$$

2. Transition probability:

$$\bar{a}_{ij} = \frac{\sum_{t=1}^T \alpha_{t-1}(i) a_{ij} \left[\sum_{k=1}^M c_{jk} b_{jk}(s_t) \right] \beta_t(j)}{\sum_{t=1}^T \alpha_{t-1}(i) \beta_{t-1}(i)} \quad (39)$$

3. Branch probability:

$$\bar{c}_{ik} = \frac{\sum_{t=1}^T \sum_{j=1}^N \alpha_{t-1}(j) a_{ji} c_{ik} b_{ik}(s_t) \beta_t(i)}{\sum_{t=1}^T \alpha_t(i) \beta_t(i)} \quad (40)$$

4. Branch density:

$$\bar{\eta}_{ik} = \frac{\sum_{t=1}^T \sum_{j=1}^N \alpha_{t-1}(j) a_{ji} c_{ik} b_{ik}(s_t) \beta_t(i) \cdot s_t}{\sum_{t=1}^T \sum_{j=1}^N \alpha_{t-1}(j) a_{ji} c_{ik} b_{ik}(s_t) \beta_t(i)} \quad (41)$$

and

$$\bar{\mathbf{R}}_{ik} = \frac{\sum_{t=1}^T \sum_{j=1}^N \alpha_{t-1}(j) a_{ji} c_{ik} b_{ik}(s_t) \beta_t(i) \cdot (s_t - \eta_{ik})(s_t - \eta_{ik})^*}{\sum_{t=1}^T \sum_{j=1}^N \alpha_{t-1}(j) a_{ji} c_{ik} b_{ik}(s_t) \beta_t(i)} \quad (42)$$

Note that the results of (41) and (42) apply to the case of mixture of elliptically symmetric densities with the representation (7). Mixtures of multivariate Gaussian densities, of course, fall into such a category. For other strictly log-concave densities, (26) applies.

Note that the above results can be easily applied to conventional parametric estimation of mixture distributions by setting the number of states, N , to unity.

IV. CONCLUSIONS

We have extended the reestimation algorithm to accommodate a broad class of mixtures of strictly log-concave or elliptically symmetric multivariate distributions. The algorithm is particularly useful in modeling nonstationary stochastic processes with multimodal non-symmetric probabilistic functions of Markov chains that could not be dealt with previously. Explicit reestimates in terms of the well-known forward-backward inductive probabilities are derived for computational ease. Due to the greatly expanded capability of the reestimation method, more accurate modeling of sophisticated signals and thus improvements in various applications such as speech recognition are expected.

REFERENCES

1. L. E. Baum et al. "A Maximization Technique Occurring in the Statistical Analysis of Probabilistic Functions of Markov Chains," *Ann. Math. Statist.*, 41 (1970), pp. 164-71.
2. L. E. Baum and J. A. Eagon, "An Inequality With Applications to Statistical Estimation for Probabilistic Functions of Markov Processes and to a Model for Ecology," *Bull. Amer. Math. Soc.*, 73 (1967), pp. 360-3.
3. J. K. Baker, "The DRAGON System—An Overview," *IEEE Trans. Acoust., Speech, Signal Processing, ASSP-23* (February 1975), pp. 24-9.
4. F. Jelinek, "Continuous Speech Recognition By Statistical Methods," *Proc. IEEE*, 64 (April 1976), pp. 532-56.
5. L. R. Rabiner, S. E. Levinson, and M. M. Sondhi. "On the Application of Vector Quantization and Hidden Markov Models to Speaker-Independent Isolated Word Recognition," *B.S.T.J.* 62, No. 4, Part 1 (April 1983), pp. 1075-106.

6. S. Kullback and R. A. Leibler, "On Information and Sufficiency," *Ann. Math. Statist.*, 22 (March 1951), pp. 79-86.
7. L. R. Liporace, "Maximum Likelihood Estimation for Multivariate Observations of Markov Sources," *IEEE Trans. Inform. Theory*, *IT-28* (September 1982), pp. 729-34.
8. K. Fan, "Les Fonctions Définies—Positives et les Fonctions Complètement Monotones," *Mémoires des Sciences Math.*, 114, 1950.
9. A. H. Gray and J. D. Markel, "Quantization and Bit Allocation in Speech Processing," *IEEE Trans. Acoust., Speech, Signal Processing*, *ASSP-24* (December 1976), pp. 459-73.
10. L. R. Rabiner, J. G. Wilpon, and J. G. Ackenhuisen, "On the Effects of Varying Analysis Parameters on an LPC-Based Isolated Word Recognizer," *B.S.T.J.*, 60 (July-August 1981), pp. 893-911.
11. S. E. Levinson, private communication.
12. J. L. Doob, *Stochastic Processes*, New York; Wiley, 1953.
13. L. E. Baum, "An Inequality and Associated Maximization Technique in Statistical Estimation for Probabilistic Functions of Markov Processes," *Inequalities*, 3 (1972), pp. 1-8.
14. S. E. Levinson, L. R. Rabiner, and M. M. Sondhi, "An Introduction to the Application of the Theory of Probabilistic Functions of a Markov Process in Automatic Speech Recognition," *B.S.T.J.*, 62, No. 4, Part 1 (April 1983), pp. 1035-74.

AUTHOR

Biing-Hwang Juang, B.Sc. (Electrical Engineering), 1973, National Taiwan University, Republic of China; M.Sc. and Ph.D. (Electrical and Computer Engineering), University of California, Santa Barbara, 1979 and 1981, respectively; Speech Communications Research Laboratory (SCRL), 1978; Signal Technology, Inc., 1979-1982; AT&T Bell Laboratories, 1982; AT&T Information Systems Laboratories, 1983; AT&T Bell Laboratories, 1983—. Before joining AT&T Bell Laboratories, Mr. Juang worked on vocal tract modeling at the Speech Communications Research Laboratory, and on speech coding and interference suppression at Signal Technology, Inc. Presently, he is a member of the Acoustics Research Department, where he is researching speech communications techniques and stochastic modeling of speech signals.

Some Properties of Continuous Hidden Markov Model Representations

By L. R. RABINER, B.-H. JUANG, S. E. LEVINSON, and
M. M. SONDHI*

(Manuscript received January 14, 1985)

Many signals can be modeled as probabilistic functions of Markov chains in which the observed signal is a random vector whose probability density function (pdf) depends on the current state of an underlying Markov chain. Such models are called Hidden Markov Models (HMMs) and are useful representations for speech signals in terms of some convenient observations (e.g., cepstral coefficients or pseudolog area ratios). One method of estimating parameters of HMMs is the well-known Baum-Welch reestimation method. For continuous pdf's, the method was known to work only for elliptically symmetric densities. We have recently shown that the method can be generalized to handle mixtures of elliptically symmetric pdf's. Any continuous pdf can be approximated to any desired accuracy by such mixtures, in particular, by mixtures of multivariate Gaussian pdf's. To effectively make use of this method of parameter estimation, it is necessary to understand how it is affected by the amount of training data available, the number of states in the Markov chain, the dimensionality of the signal, etc. To study these issues, Markov chains and random vector generators were simulated to generate training sequences from "toy" models. The model parameters were estimated from these training sequences and compared to the "true" parameters by means of an appropriate distance measure. The results of several such experiments show the strong sensitivity of the method to some (but not all) of the model parameters. A procedure for getting good initial parameter estimates is, therefore, of considerable importance.

* Authors are employees of AT&T Bell Laboratories.

I. INTRODUCTION

The theory of signal representation based on Hidden Markov Models (HMMs) is well established and has been applied to text analysis,¹ coding theory,² ecology,³ and most recently, speech processing.⁴⁻⁶ The form of the HMM that we are considering is sketched in Fig. 1. The Markov chain has N states, and transitions between states are governed by a stochastic transition matrix, \mathbf{A} , with elements a_{ij} , where

$$a_{ij} = \text{probability of making a transition to state } j, \\ \text{given currently in state } i.$$

In a given state, j , the observed output of the model is a random vector with a probability density function (pdf) b_j .

Given the model of Fig. 1, it is necessary to be able to estimate the model parameters (i.e., the transition matrix, \mathbf{A} , and the pdf's b_j) from training data consisting of observations of output sequences generated by the model. One very useful method of parameter estimation for HMMs is the Baum-Welch reestimation procedure.⁷ For the case of continuous pdf's of interest here, the method was originally shown to be valid for log-concave densities.⁷ This restriction was relaxed by Liporace,⁸ who extended the applicability of the method to elliptically symmetric densities. However, this class of densities is still too restrictive for many interesting problems (e.g., measured densities of various

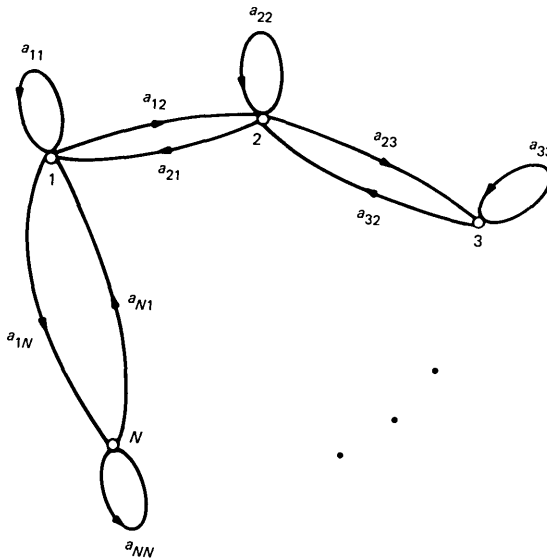


Fig. 1—Markov model with N states.

speech parameters). Therefore, we consider a more general representation of the density—a finite mixture of the form

$$b_j(\mathbf{x}) = \sum_{m=1}^M c_{jm} \mathcal{N}[\mathbf{x}, \boldsymbol{\mu}_{jm}, \mathbf{U}_{jm}] \quad j = 1, N, \quad (1)$$

where \mathcal{N} may be any log-concave or elliptically symmetric density, and is assumed to be Gaussian in our present study. The vector \mathbf{x} is the observation vector. The vector $\boldsymbol{\mu}_{jm}$ and the matrix \mathbf{U}_{jm} are, respectively, the mean vector and the covariance matrix for the m th mixture component in state j . The coefficients, c_{jm} , are the mixture gains, and satisfy the stochastic constraint

$$\sum_{m=1}^M c_{jm} = 1, \quad c_{jm} \geq 0, \quad (2)$$

so that

$$\int_{-\infty}^{\infty} b_j(\mathbf{x}) d\mathbf{x} = 1, \quad j = 1, N. \quad (3)$$

The representation of eq. (1) can be used to approximate arbitrarily closely any finite, continuous density function; hence its appropriateness to a wide range of problems. It has recently been shown⁹ that the reestimation procedure of Refs. 7 and 8 can be extended to cover the mixture representation of eq. (1).

To understand the properties of such HMMs, and to study the sensitivity of the parameter estimates to the details of the estimation procedure, we have simulated several “toy” models and examined the effects of sample size, initial parameter estimates, model inconsistencies, etc., on the corresponding estimated models. In this paper we present the results of our simulations. Since we have studied only a few, carefully selected cases, we make no claims about specific sample sizes, range of initial parameter values, etc. Instead, it is intended that the examples presented allow the reader to understand the nature of the representation, and thereby use it appropriately for his or her particular application.

The outline of this paper is as follows. In Section I we show how a toy model or HMM sequence generator can be implemented to provide appropriate training sequences for estimating model parameters. In Section II we review the continuous density HMM. In Section III we describe a series of experiments designed to study the sensitivities and properties of the HMM signal representation. Finally, in Section IV we review the key results and discuss their implications for practical problems.

II. REVIEW OF THE CONTINUOUS HMM

Consider an N -state Markov chain where we label the states q_1, q_2, \dots, q_N . The Markov chain is characterized by its state transition matrix $\mathbf{A} = [a_{ij}]$. Each state q_j is characterized by a continuous multivariate, probability density function $b_j(\mathbf{x})$, where \mathbf{x} is a K -dimensional observation vector.

Given a sequence of observations, $\mathbf{O} = O_1, O_2, \dots, O_T$, where each O_t is a K -dimensional vector, we can calculate the likelihood of \mathbf{O} , given a model \mathbf{M} . We denote the likelihood as $\mathcal{L}(\mathbf{O} | \mathbf{M})$. Following Baum,¹⁰ we can define a set of forward and backward likelihoods, $\alpha_t(i)$ and $\beta_t(j)$ respectively, where, for $1 \leq i, j \leq N$, and $1 \leq t \leq T$,

$$\alpha_t(i) = \mathcal{L}(O_1, O_2, \dots, O_t \text{ and } q_i \text{ at time } t | \mathbf{M}) \quad (4)$$

and

$$\beta_t(j) = \mathcal{L}(O_{t+1} O_{t+2} \dots O_T | q_j \text{ at time } t \text{ and } \mathbf{M}). \quad (5)$$

Baum has shown that $\alpha_t(i)$ and $\beta_t(j)$ can be computed recursively. Assuming that we start in q_1 , whereby $\alpha_0(1) = 1$, $\alpha_0(i) = 0$, $2 \leq i \leq N$, and $\beta_T(j) = 1$, $1 \leq j \leq N$, then for $1 \leq t \leq T$ we get

$$\alpha_t(j) = \left[\sum_{i=1}^N \alpha_{t-1}(i) a_{ij} \right] b_j(O_t), \quad (6)$$

and for $T-1 \geq t \geq 0$,

$$\beta_t(i) = \sum_{j=1}^N a_{ij} b_j(O_{t+1}) \beta_{t+1}(j). \quad (7)$$

Thus, $\mathcal{L}(\mathbf{O} | \mathbf{M})$ can be efficiently evaluated as

$$\mathcal{L}(\mathbf{O} | \mathbf{M}) = \sum_{i=1}^N \sum_{j=1}^N \alpha_t(i) a_{ij} b_j(O_{t+1}) \beta_{t+1}(j), \quad (8)$$

for $0 \leq t \leq T-1$. The parameters of the HMM are estimated by finding some \mathbf{M} that is a local maximum of $\mathcal{L}(\mathbf{O} | \mathbf{M})$ for a given observation sequence \mathbf{O} .

Using the mixture density of eq. (1) as the parameterized pdf's $b_j(\mathbf{x})$, the model \mathbf{M} is specified by the following:

- N = number of states in the model
- M = number of mixture densities for each distribution
- K = number of dimensions of each observation vector
- $\mathbf{A} = [a_{ij}]$ = state transition matrix
- $\mathbf{C} = [c_{jm}]$, where c_{jm} = mixture gains for m th mixture in state j
- $\boldsymbol{\mu} = [\mu_{jmk}]$, where μ_{jmk} = the k th component of the mean vector $\boldsymbol{\mu}_{jm}$ for m th mixture in state j

$\mathbf{U} = [U_{jmk}],$ where $U_{jmk} =$ the (k, l) th entry of the covariance matrix for the m th mixture in state j .

Given the values chosen for $N, M,$ and $K,$ and a set of initial guesses for $\mathbf{A}, \mathbf{C}, \boldsymbol{\mu},$ and $\mathbf{U},$ a set of reestimation formulas is available⁹ for optimizing $\mathcal{L}(\mathbf{O} | \mathbf{M}),$ for a given training set of observations $\mathbf{O}.$

There are two general cases of the model that are of interest, namely the *ergodic* case in which the Markov chain is ergodic (i.e., all states are aperiodic and recurrent nonnull) and the *left-to-right* case in which a transition from state q_i to state q_j is possible only if $j \geq i$ (i.e., there is a sequential progression through states of the model). Both general cases are of interest for real-world applications.

2.1 Toy Markov model generator

In order to investigate the behavior of the parameter estimation algorithms for the continuous HMM, a toy Markov model generator was implemented. Its function was to generate an observation sequence (for the ergodic case), or a set of observation sequences (for the left-to-right case), for an input model specification $\mathbf{M}_{in}.$ Each observation generated by the model was a K -dimensional vector according to the probability density $b_j(\mathbf{x})$ for the j th state.

The algorithm used to generate the observation sequences is the following:

1. Set the state index, $j = 1$ and the time index, $t = 1.$
2. Partition the unit interval proportionally to $c_{jm}, 1 \leq m \leq M.$ Generate $x,$ a random number uniform on $[0, 1].$ Select the mixture density, $l,$ according to the subinterval in which x falls.
3. Decompose \mathbf{U}_{jl} into $\mathbf{Q}\boldsymbol{\Lambda}\mathbf{Q}',$ where \mathbf{Q} is the matrix of eigenvectors of \mathbf{U}_{jl} and $\boldsymbol{\Lambda}$ is the diagonal matrix of eigenvalues of $\mathbf{U}_{jl}.$
4. Generate a K -dimensional normal deviate, $\mathbf{y},$ of zero mean and covariance $\boldsymbol{\Lambda}.$
5. Set $\mathbf{O}_t = \mathbf{Q}\mathbf{y} + \boldsymbol{\mu}_{jl}.$
6. Partition the unit interval proportionally to $a_{jk}, 1 \leq k \leq N.$ Generate $x,$ a random deviate uniform on $[0, 1]$ and select the next state, $i,$ according to the subinterval in which x falls.
7. Increment $t.$
8. If $t \leq T$ go to 2; else, stop.

The Markov model generator was specified by a model $\mathbf{M}_{in},$ and by a limit on the number of observations $T,$ or on the number of sequences Q (for the left-to-right case). Each individual sequence, in the left-to-right case, started in state q_1 (at observation 1) and terminated in state q_N (at observation T), with the property that it had to have been in state q_N for at least L observations. (Typically L was 5 to 10.)

III. EXPERIMENTAL EVALUATION OF THE REESTIMATION PROCEDURE

A series of experimental evaluations of the reestimation procedure were made to determine the sensitivities of the algorithm—and hence the resulting HMMs—to aspects of the observation sequence used to train the model. Using the toy Markov model generators, several input source models were defined (i.e., the model parameters were specified) and several sets of observation sequences were generated from the models. For each input source model, the reestimation algorithm was used to obtain locally optimal model parameters based on the generated sequences and initial estimates. The resulting model \mathbf{M} was compared with the source model using a probabilistic distance measure¹¹ of the form

$$D(\mathbf{M}_{in}, \mathbf{M}) = \frac{\log[\mathcal{L}(\mathbf{O}_{M_{in}} | \mathbf{M}_{in})] - \log[\mathcal{L}(\mathbf{O}_{M_{in}} | \mathbf{M})]}{T_{in}}, \quad (9)$$

where $\mathbf{O}_{M_{in}}$ was a set of observations generated by the toy model \mathbf{M}_{in} , and T_{in} was the total number of observations in this set. The distance measure of eq. (9) gives the normalized difference in log likelihoods of the observation sequence coming from the true toy model, and of the likelihood of its coming from the estimated model, where the normalization is the number of observations in $\mathbf{O}_{M_{in}}$. Previous experience with D has shown that this measure is very effective for comparing HMMs.¹¹

3.1 Correlation of model distance to changes in model parameters

Before investigating the sensitivities of the reestimation procedure to various model parameters and initial conditions, a preliminary experiment was run to measure the correlation of model distance to changes in model parameters. For this experiment, the initial (ergodic) model had the specifications

$$\begin{aligned} M &= N = K = 2 \\ \mathbf{A} &= \begin{bmatrix} 0.8 & 0.2 \\ 0.3 & 0.7 \end{bmatrix}, & \mathbf{C} &= \begin{bmatrix} 0.75 & 0.25 \\ 0.35 & 0.65 \end{bmatrix} \\ \boldsymbol{\mu}_{1..} &= \begin{bmatrix} 1. & 5. \\ 3. & 4. \end{bmatrix}, & \boldsymbol{\mu}_{2..} &= \begin{bmatrix} 5. & 9. \\ 8. & 2. \end{bmatrix} \\ \mathbf{U}_{11..} &= \begin{bmatrix} 4 & 2 \\ 2 & 4 \end{bmatrix}, & \mathbf{U}_{21..} &= \begin{bmatrix} 7 & 3 \\ 3 & 7 \end{bmatrix}, & \mathbf{U}_{12..} &= \begin{bmatrix} 10 & 2 \\ 2 & 10 \end{bmatrix} \\ \mathbf{U}_{22..} &= \begin{bmatrix} 8 & 1 \\ 1 & 8 \end{bmatrix}. \end{aligned}$$

A new model was created in which all model parameters remained the same except for one set, in which the columns of the corresponding matrix or matrices were reversed, i.e., a_{ij} became a_{ji} , or c_{jm} became c_{mj} , etc. In this manner we could study the effects of changing only a single parameter set on the model distance. A smooth interpolation between the parameter set for the initial model and the reversed parameter set was made by changing the parameter set in steps, and then measuring model distance at each step. In particular, if we denote the matrix in the initial model by \mathbf{X} and the reversed matrix in the new model by \mathbf{X}' , the intermediate matrices \mathbf{X}'' were formed by

$$\mathbf{X}'' = \frac{1}{1 + \delta} \mathbf{X} + \frac{\delta}{1 + \delta} \mathbf{X}',$$

where the deviation factor $\delta = \epsilon, 2\epsilon, \dots, 2^{12}\epsilon$ and $\epsilon = 0.016$.

The results of this preliminary experiment are shown in Fig. 2, which gives a series of plots of model distance D , versus signal-to-noise ratio γ , defined as

$$\gamma = 10 \log_{10} \frac{\|\mathbf{X}\|^2}{\|\mathbf{X} - \mathbf{X}''\|^2},$$

where $\|\cdot\|$ denotes matrix norm ($\|\mathbf{X}\|^2 = \sum_i \sum_j x_{ij}^2$ for $\mathbf{X} = [x_{ij}]$) for changes in \mathbf{A} , \mathbf{C} , and μ . (Curves similar to that for μ can be obtained for changes in \mathbf{U} .) It can be seen that perturbed models are far more

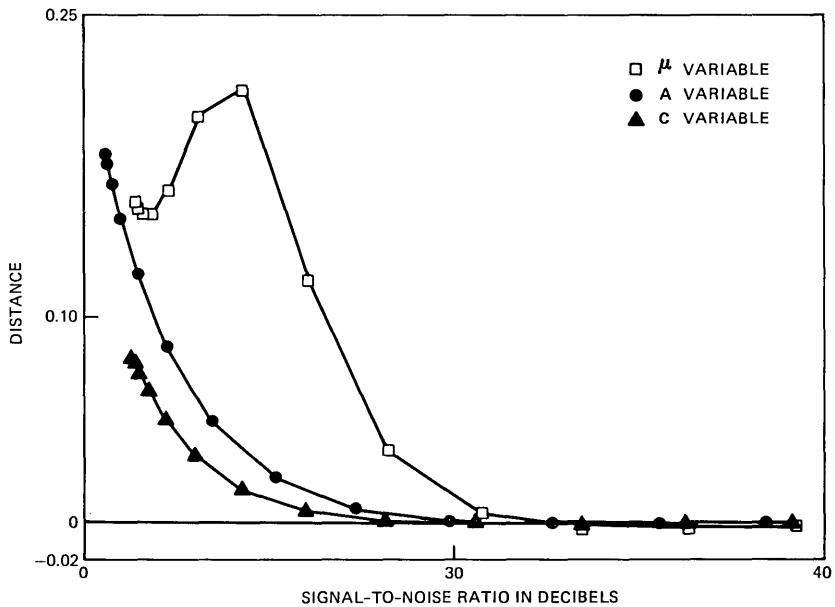


Fig. 2—Distance as a function of parameter deviation for changes in μ , \mathbf{A} , and \mathbf{C} .

distant (in the probabilistic distance sense) from the initial models when μ is perturbed than when the transition probability or the mixture gain parameters are perturbed. In general, the HMMs are indeed much more sensitive to small errors in μ values than to small errors in C or A values unless the variances are extremely large. The exact sensitivity will depend on the precise relationships among means and the associated variances.

The effects of the detailed relationships among means and the associated variances can be seen from the nonmonotonic behavior of the distance curve pertaining to μ in Fig. 2. In this particular case, the mean vectors moved from (1,5) to (5,1), (3,4) to (4,3), (5,9) to (9,5), and (8,2) to (2,8) as the signal-to-noise ratio decreased from about 38.6 dB to 2.6 dB. Thus, as seen in Fig. 2, when γ drops below 8 dB, the probabilistic distance for μ deviations actually decreases. One may observe that in some section along the perturbation path from (8,2) to (2,8), the perturbed mean moves *closer* to the original mean locations (1,5) and (3,4), and thus results in a decrease rather than increase in the probabilistic distance.

We should point out that if we arbitrarily increase the number of mixture components in modeling a given density, then, with proper choice of the initial estimate, the obtained mixture weights become proportional to sample values of the density function at the mean locations of the mixtures. When this happens, the variance in each mixture density, as well as the spacing of the means, decreases and, asymptotically, the observation density is mainly characterized by the mixture gains and the mean vectors. Thus, there is a continuum in the observation of relative model sensitivities as the number of mixture terms varies.

3.2 Sensitivities of the reestimation procedure to parameter inaccuracies and to the training sequence

Based on the results given in the previous section, a series of experiments were performed to investigate the sensitivities of the reestimation procedure to initial parameter estimates and to the length of the training sequence.

The first experiment used a left-to-right source model with the characteristics

$$N = 5, \quad M = 3, \quad K = 5$$

$$\mathbf{A} = \begin{bmatrix} .8 & .15 & .05 & 0 & 0 \\ 0 & .8 & .15 & .05 & 0 \\ 0 & 0 & .8 & .15 & .05 \\ 0 & 0 & 0 & .8 & .2 \\ 0 & 0 & 0 & 0 & 1. \end{bmatrix}, \quad \mathbf{C} = \begin{bmatrix} .6 & .3 & .1 \\ .6 & .3 & .1 \\ .6 & .3 & .1 \\ .6 & .3 & .1 \\ .6 & .3 & .1 \\ .6 & .3 & .1 \end{bmatrix}$$

$$\mu_{1..} = \begin{bmatrix} 1 & 1 & 1 & 1 & 1 \\ 1.5 & 1.5 & 1.5 & 1.5 & 1.5 \\ 2 & 2 & 2 & 2 & 2 \end{bmatrix}, \quad \mu_{2..} = \begin{bmatrix} 3 & 3 & 3 & 3 & 3 \\ 3.5 & 3.5 & 3.5 & 3.5 & 3.5 \\ 4 & 4 & 4 & 4 & 4 \end{bmatrix},$$

$$\mu_{3..} = \begin{bmatrix} 5 & 5 & 5 & 5 & 5 \\ 5.5 & 5.5 & 5.5 & 5.5 & 5.5 \\ 6 & 6 & 6 & 6 & 6 \end{bmatrix}$$

$$\mu_{4..} = \begin{bmatrix} 7 & 7 & 7 & 7 & 7 \\ 7.5 & 7.5 & 7.5 & 7.5 & 7.5 \\ 8 & 8 & 8 & 8 & 8 \end{bmatrix}, \quad \mu_{5..} = \begin{bmatrix} 9 & 9 & 9 & 9 & 9 \\ 9.5 & 9.5 & 9.5 & 9.5 & 9.5 \\ 10 & 10 & 10 & 10 & 10 \end{bmatrix}$$

$$U_{jmkk} = \begin{cases} .5 & m = 1 \\ .2 & m = 2 \\ .1 & m = 3 \end{cases} \text{ for } k = 1, 2, \dots, 5, \text{ and}$$

$$U_{jmk l} = 0.01 \text{ for all } k \neq l.$$

The initial guess of the model parameters was random for \mathbf{A} and \mathbf{C} , and identity matrices for \mathbf{U} . For μ , the initial guess had the form

$$\mu' = (1 - z \cdot \alpha)\mu, \quad (10)$$

where α is a random variable uniformly distributed on $(0,2)$, and z is a user-specified error bound, which limits the maximum possible deviation of μ' from μ in the source model.

The source generated Q random sequences according to the specified model, where Q varied from 10 to 100 (in steps of 10) and initial estimates with values of $z = 0.0, 0.2, 0.4,$ and 0.6 were used. For each set of observations, and for each initial estimate, the reestimation procedure was iterated until a stationary point was found. At this point, both the average (negative) log likelihood for the estimated model \mathbf{M} and the model distance (from the source to the estimated model) were calculated. Figure 3 shows a series of plots of the average (negative) log likelihood, and the model distance, as a function of the total number of observations in the Q training sequences, for the four values of z . For values of $z = 0$ and 0.2 , for sufficiently long training sequences (i.e., 20 sets of observations or about 400 observations), the model distances were reasonably small (less than 0.25). As z got bigger, thereby making the initial estimates of μ poorer, the resulting models had distances on the order of 0.4 or larger. It is clearly shown that the accuracy of the estimated model depends on the initial estimate from which the iterative reestimation procedure starts. A converged model estimate is only a local optimum and, in general, has a lower likelihood than the global optimum.

Figure 3 also shows the correlation between the log likelihood and the model distance. For sufficiently long observations, the model distance is a good predictor of the relative log likelihood for the

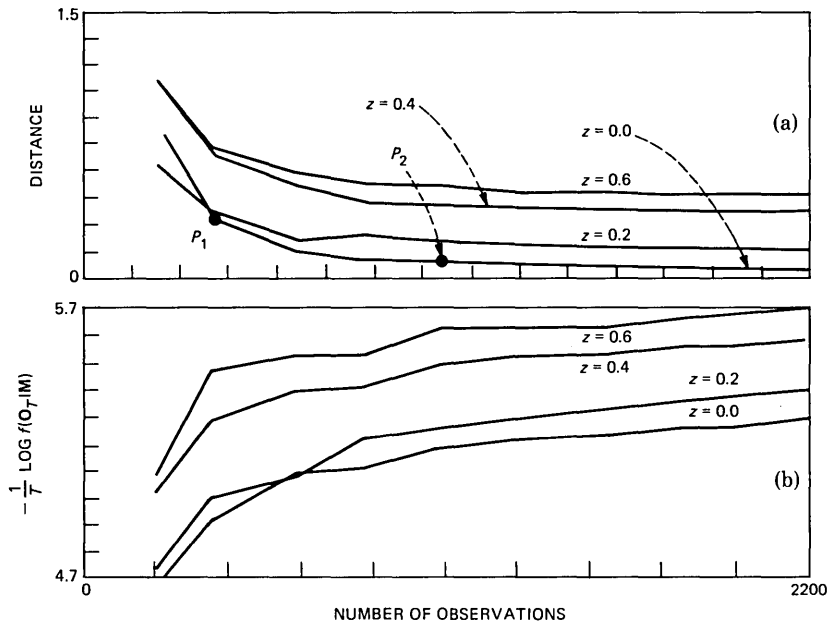


Fig. 3—(a) Distance and (b) average log likelihood as a function of the number of observations in the training sequence, and as a function of the initial estimation deviation, z .

estimated model. When a smaller number of observations is generated for estimation, the statistical characteristics of the source become less well represented in the generated observation sequences, and hence, the estimated model is more data specific, resulting in greater variations in the log likelihood. This can be more easily seen from the behavior of distance for a specific set of training sequences as the reestimation procedure iterates to a stable solution. Such a plot is given in Fig. 4 for $Q = 20$ sequences (part a) and for $Q = 50$ sequences (part b). (Note that these two curves show the distance behavior of the model reestimate as it converges to the solution corresponding to the two particular points, P_1 and P_2 , in the upper curve of Fig. 3, respectively.) For $Q = 20$ sequences, the training set does not provide a good characterization of the source model—it is too short; hence the model distance decreases for a couple of iterations and then increases as the local estimated parameters are adjusted to match those of the specific observation sequence rather than those of the true generating model. For $Q = 50$ sequences, the distance between the estimated model and the true source model steadily decreases.

3.3 Sensitivity of model reestimation to evaluation of the density function

Because of the wide dynamic range of the density function, $b_j(\mathbf{x})$, of

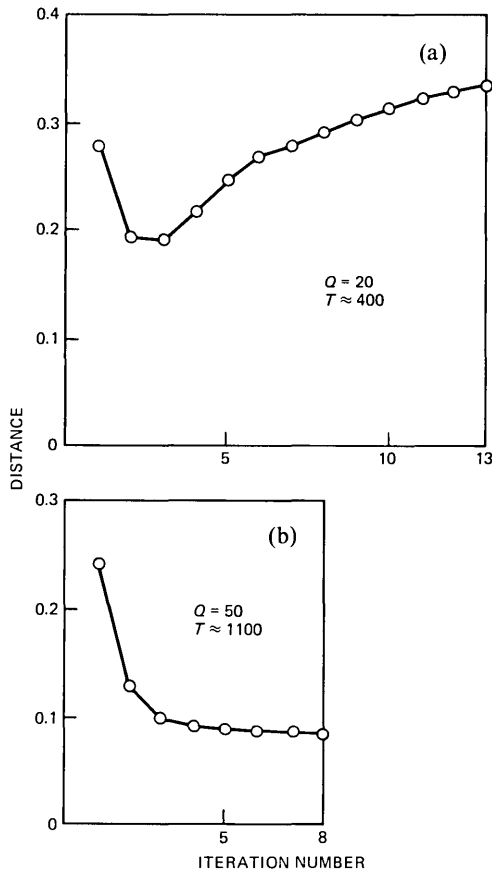


Fig. 4—(a) Distance for $Q = 20$ sequences training and (b) $Q = 50$ sequences training as a function of the iteration number.

eq. (1)—especially when the estimates of μ and U are in error—a minimum value clipping level, f_{CLIP} , is usually required to avoid potential underflow and singularity problems. In our study, whenever $b_j(\mathbf{x})$ was less than $10^{-f_{\text{CLIP}}}$, it was artificially clamped at $10^{-f_{\text{CLIP}}}$; otherwise $b_j(\mathbf{x})$ was kept as computed. This, in effect, injects certain noise components into the observations. To understand the effect of f_{CLIP} on the resulting model estimates, a left-to-right, four-state, one-mixture, two-dimensional model was used, with the specification

$$N = 4, \quad M = 1, \quad K = 2$$

$$\mathbf{A} = \begin{bmatrix} .8 & .15 & .05 & 0 \\ 0 & .8 & .15 & .05 \\ 0 & 0 & .8 & .2 \\ 0 & 0 & 0 & .1 \end{bmatrix}, \quad \mathbf{C} = \begin{bmatrix} 1 \\ 1 \\ 1 \\ 1 \end{bmatrix}$$

$$\mu_1. = [0 \ 0], \quad \mu_2. = [4 \ 4], \quad \mu_3. = [8 \ 8], \quad \mu_4. = [12 \ 12]$$

$$U_{j1,k,l} = \begin{cases} 1, & k = l, \text{ all } j \\ .1, & k \neq l, \text{ all } j. \end{cases}$$

The value of f_{CLIP} was varied from 70—which is essentially full precision on the Data General MV8000 32-bit computer—down to 10—severe clipping—and initial estimates of μ' were generated as in eq. (10). For each value of f_{CLIP} and z , the distance between the model resulting from the reestimation procedure and the original source model was computed, and the results are plotted in Fig. 5. For all runs, the number of observation sequences used in training was 50; hence there was an adequate number of observations for the parameter estimates to converge to the true model. The results given in Fig. 5 show that for $z = 0$ the distance is insensitive to values of f_{CLIP} over the entire range. For $z = 0.2$, the distance is much larger for $f_{\text{CLIP}} = 10$ than for all other values of f_{CLIP} . The differences in distance between the results for $z = 0.2$ and those for $z = 0.0$ are insignificant except for those at $f_{\text{CLIP}} = 10$. For $z = 0.4$, the model estimates yield larger distances than for $z = 0$ or $z = 0.2$ for all values of f_{CLIP} . The differences for f_{CLIP} values of less than 50 are primarily due to the sensitivity of the reestimation procedure to the initial μ estimates as discussed previously. The differences for f_{CLIP} in the range 10 to 40 are due to sensitivities of the reestimation procedure to the clipping itself. To understand this sensitivity, consider Fig. 6, which shows a Gaussian with a clipping threshold $10^{-f_{\text{CLIP}}}$. In the case that initial estimates of μ (and U) are very close to the true value, the density function will rarely, if ever, be clipped; hence until $10^{-f_{\text{CLIP}}}$ approaches the peak of the density function, the clipping has little effect on the model estimate. In the case where initial estimates of μ are far from the true value, a large percentage of the density computations will be clipped and the reestimation procedure will be unable to improve the parameter estimates because the density function is essentially flat in the region of the clipping. For such cases, very poor estimates of μ result and large model distances are obtained. The results point out an important consideration in practical implementations of the estimation algorithm, where finite precision is inevitable.

3.4 Modeling correlated processes by mixtures of uncorrelated processes

The mixture form of eq. (1) is a very versatile and flexible representation of the pdf in each state. For example, a complicated multivariate pdf may be approximated by a mixture of Gaussian multivariate densities with full covariance matrices, or, by increasing the number of mixture components, a mixture of Gaussian multivariate densities with only diagonal covariance matrices (i.e., vector elements are un-

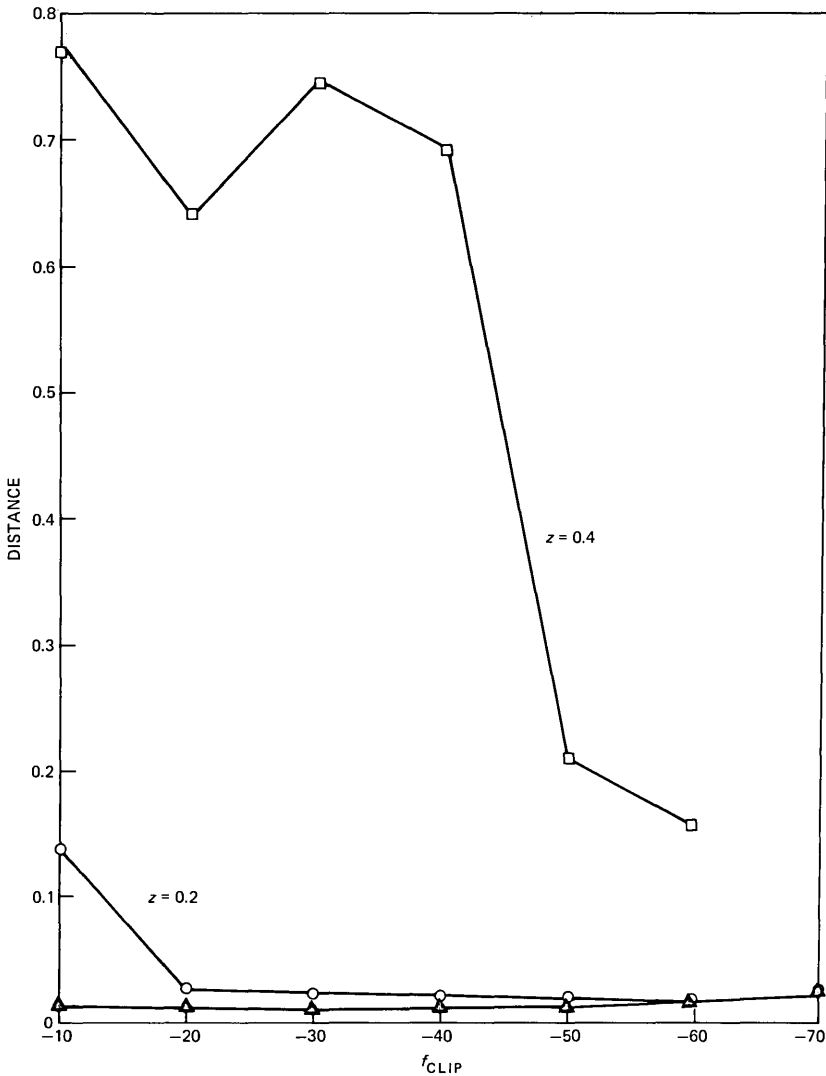


Fig. 5—Distance as a function of the density clipping threshold for $z = 0, 0.2,$ and 0.4 .

correlated). To better understand this concept, we studied the trade-off between the degree of correlation and the number of mixture components in the representation by modeling correlated multivariate densities with different numbers of uncorrelated multivariate densities using the HMM framework.

The source model used for these studies had the following specifications:

$$N = 4, \quad M = 1, \quad K = 2$$

$$\mathbf{A} = \begin{bmatrix} .8 & .15 & .05 & 0 \\ 0 & .8 & .15 & .05 \\ 0 & 0 & .8 & .2 \\ 0 & 0 & 0 & 1.0 \end{bmatrix}, \quad \mathbf{C} = \begin{bmatrix} 1 \\ 1 \\ 1 \\ 1 \end{bmatrix}$$

$$\mu_1. = [0 \ 0], \quad \mu_2. = [4 \ 4], \quad \mu_3. = [8 \ 8], \quad \mu_4. = [12 \ 12]$$

$$\mathbf{U}_{jkl} = \begin{cases} 1, & k = l \\ \rho, & k \neq l, \end{cases}$$

where ρ varied from 0 to 0.9 (in steps of 0.1). Thus, the source model had a full two-dimensional covariance matrix with correlation ρ between components of each vector.

We considered two separate HMMs for matching the observation sequences of the full covariance source model. The first model used an $M = 1$ (a single) mixture with a diagonal covariance matrix; the second model used an $M = 5$ mixture, where each component density again had a diagonal covariance matrix. Since we were interested only in the capabilities of the models—and not in the concomitant problems

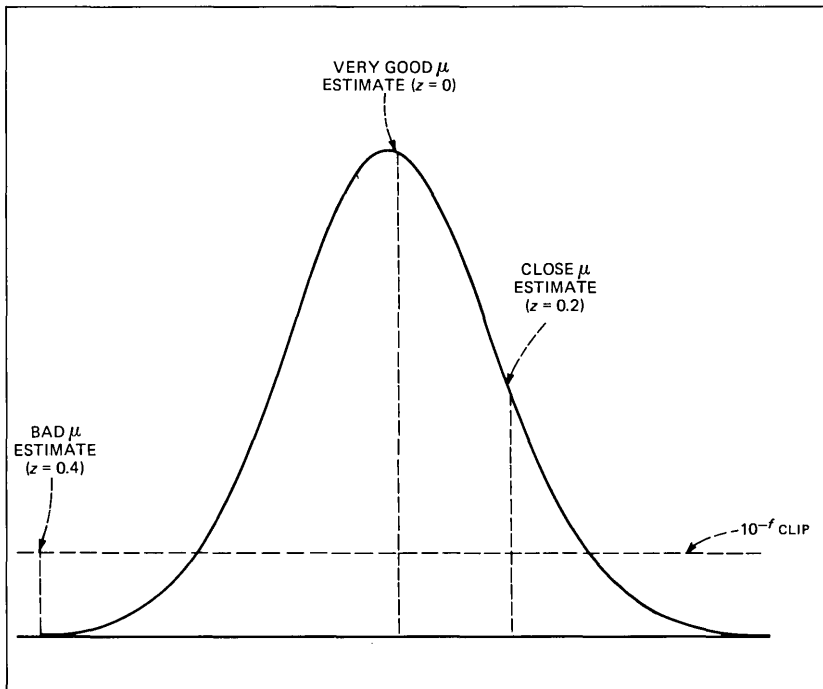


Fig. 6—Explanation of the sensitivity of the reestimation algorithm to the density clipping threshold for different values of z .

of reestimation—the initial estimates of the model parameters were selected to optimize the match. Thus for the $M = 1$ model, the initial estimates were identical to those of the source, except the off-diagonal covariance terms were set to 0. For the $M = 5$ model, the initial estimates of μ and U were adjusted in order to best match the full covariance with correlation ρ by the $M = 5$ mixtures. The procedure used is illustrated in Fig. 7, which shows a K equals a two-dimensional correlation in the (x_1, x_2) plane (part a), and a one-dimensional slice (part b). The initial estimates of μ for the $M = 5$ case are shown by the center dots of the five circles in part a. The mixture gains and the mixture covariances were chosen to provide good initial fits to the correlated covariance as shown in both parts a and b.

The results of estimating optimum models for the $M = 1$ and $M = 5$ cases are shown in Fig. 8, which gives plots of model distance versus ρ . For $M = 1$, the model fits have distances less than or equal to 0.1 only for $\rho \leq 0.35$, and have distances less than or equal to 0.2 for $\rho \leq 0.5$. For $M = 5$, the model fits have distances less than or equal to 0.1 for $\rho \leq 0.7$, and have distances less than or equal to 0.2 for ρ up to 0.9. Thus, for this case, the $M = 5$ mixture models without correlations provide excellent approximations to models with correlated random variables up to correlations of 0.9.

The results presented above show that it is possible to model a K -dimensional ($K = 2$) correlated random process by a mixture of M -uncorrelated, K -dimensional, Gaussian random processes. The question that remains is why one would be interested in using such an approximation. There are two possible reasons that readily come to mind. First, there is the possibility that more reliable estimates can be made of the set of $2M \cdot K$ means and variances for the M -mixture uncorrelated processes case, than for the set of $K(K + 3)/2$ means and correlations for the one-mixture correlated process. If this is the case the trade-off is between the increased error in the approximation process and the increased reliability in the estimation process. The second possible reason for using the M -mixture uncorrelated process instead of the one-mixture correlated process is the potential for a decrease in the number of parameters that need to be estimated. To see when this can occur, we define P_c as the number of parameters for the one-mixture correlated density, and P_μ as the number of parameters in the M -mixture uncorrelated density case. Then, assuming K -dimensional vectors, we get

$$P_c = \frac{K(K + 3)}{2}$$

and

$$P_\mu = M(2K + 1).$$

For $P_\mu \leq P_c$ we require

$$M \leq \frac{K(K+3)}{2(2K+1)}.$$

Thus, for $K \leq 5$, the largest M can be is 1, for $9 \geq K \geq 6$, the largest M can be is 2, and for $13 \geq K \geq 10$, the largest M can be is 3 to realize

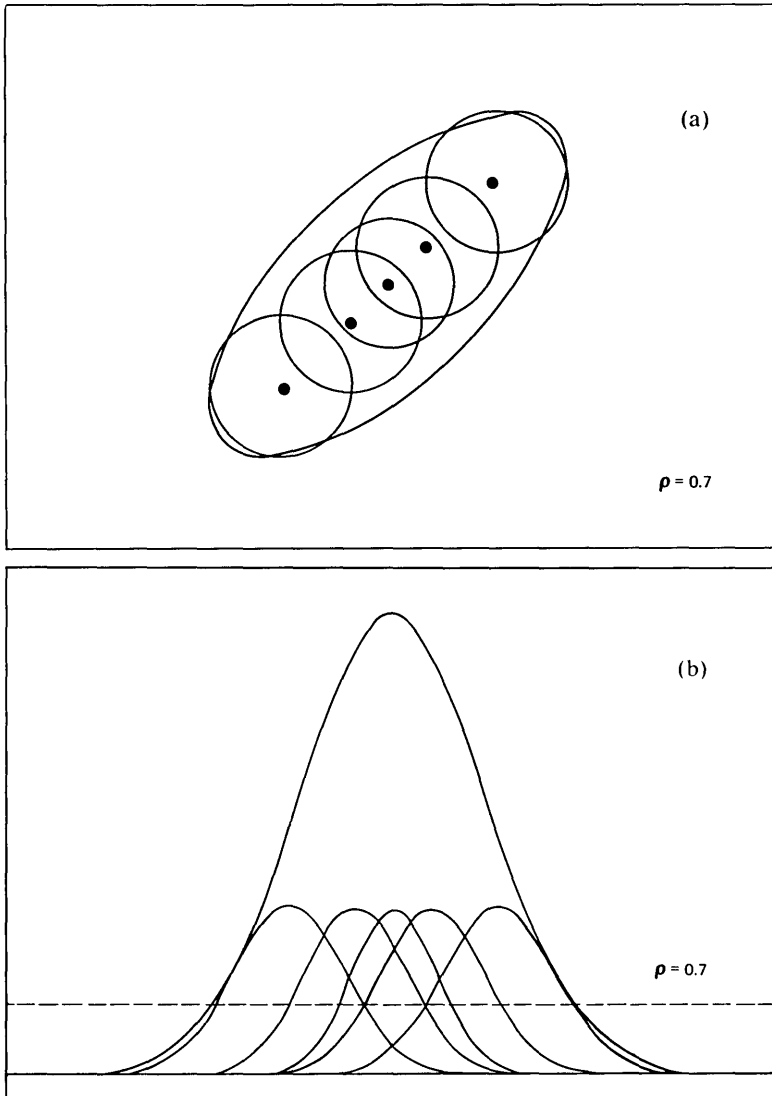


Fig. 7—(a) Observation region in the (x_1, x_2) plane for highly correlated vector components along with initial estimates of μ for $M = 5$ model; (b) interpretation of initial estimates along a one-dimensional projection of the (x_1, x_2) plane.

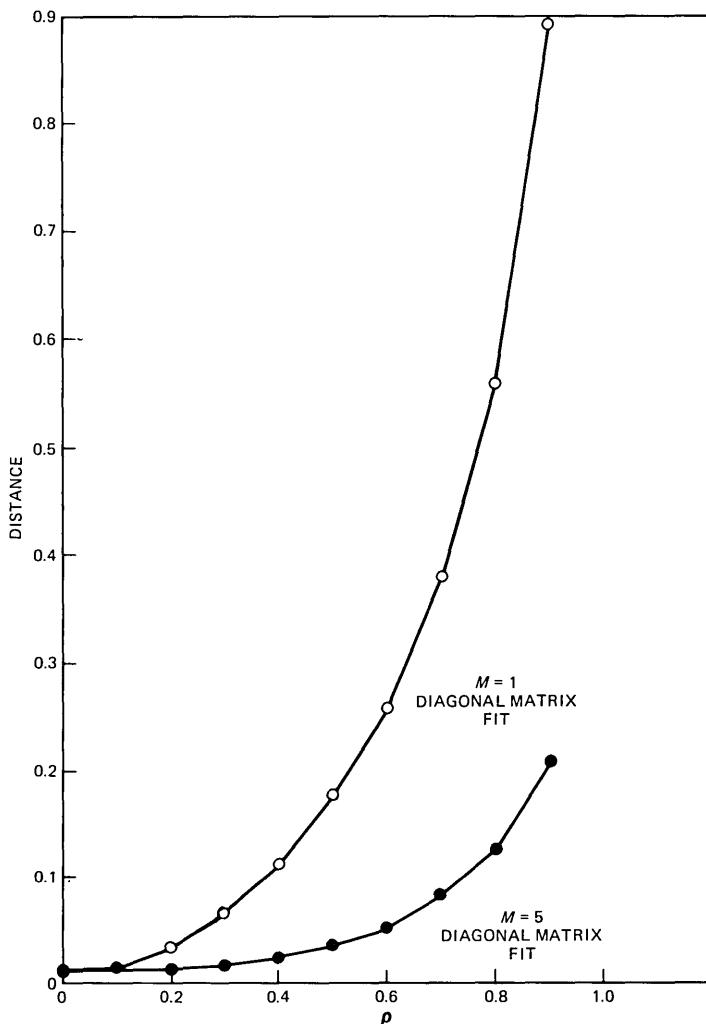


Fig. 8—Distance versus ρ for $M = 1$ and $M = 5$ mixture fits using diagonal covariance matrices.

any reduction in the number of variables to be estimated. For speech-recognition applications, we generally use $K \approx 10$; hence values of $M \leq 3$ could be considered. Whether or not the model is adequately represented with this many diagonal mixtures depends heavily on the specific application. The purpose of the above discussion is to point out the possibilities of the alternative method.

IV. DISCUSSION

The results presented in the previous section have shown the following:

1. Continuous HMMs characterized by mixture densities are most sensitive to estimation errors in the locations of the means of each mixture density. If the error in the initial estimate of the mean becomes sufficiently large, then the reestimation procedure has very little chance of giving good model parameter estimates.

2. The sensitivity of the models to errors in initial covariance estimates is less than that due to errors in the initial mean estimates.

3. The sensitivity of the models to errors in either transition matrix coefficients, or mixture gains, is low. Hence, good model estimates can be obtained even with poor initial estimates of these parameters, as long as the distribution does not contain singularities.

4. We have found that observations on the order of 500 to 1000 are adequate for models that are typical of many applications in speech processing (e.g., models with $N = 10$, $K = 10$, $M = 3$).

5. Good initial parameter estimates become critical in the reestimation procedure when word precision for the evaluation of the density function is limited—an inevitable situation in practical implementations.

6. Mixture density models with diagonal covariance matrices for each mixture can be used to approximate full covariance models.

The most important conclusion from our experiments is that it is absolutely mandatory to have a good initial guess of the means of the density functions to obtain good HMMs. With a good initial guess of the means, the parameter reestimation procedure is capable of yielding good models even if other model parameters have poor initial estimates.

V. SUMMARY

Several interesting properties of continuous density HMMs have been discussed. These include model sensitivity to initial parameter estimates, to evaluation of the density function, and to size and type of training sequence. We have shown how a mixture density of uncorrelated variables can successfully represent a model with highly correlated variables, as long as enough mixtures are used. The results presented here can be applied to a variety of real-world problems.

REFERENCES

1. R. L. Cave and L. P. Neuwirth, "Hidden Markov Models for English," *Hidden Markov Models for Speech*, J. Ferguson, ed., IDA-CRD, 1980, pp. 16–56.
2. L. R. Bahl et al., "Optimizing Decoding of Linear Codes for Minimizing Symbol Error Rate," *IEEE Trans. on Inform. Theory*, *IT-20*, No. 2 (March 1984), pp. 284–7.
3. L. E. Baum and J. A. Eagon, "An Inequality with Applications to Statistical Estimation for Probabilistic Functions of Markov Processes and to a Model for Ecology," *Bull. Amer. Math. Soc.*, *73* (1967), pp. 360–3.
4. J. K. Baker, "The Dragon System—An Overview," *IEEE Trans. on Acoust., Speech, Signal Processing*, *ASSP-23*, No. 1 (February 1975), pp. 24–9.

5. L. R. Bahl, F. Jelinek, and R. L. Mercer, "A Maximum Likelihood Approach to Continuous Speech Recognition," *IEEE Trans. Pattern Analysis Mach. Intell., PAM 1-5*, No. 2 (March 1983), pp. 179-90.
6. L. R. Rabiner, S. E. Levinson, and M. M. Sondhi, "On the Application of Vector Quantization and Hidden Markov Models to Speaker Independent, Isolated Word Recognition," *B.S.T.J.*, 62, No. 4 (April 1983), pp. 1075-106.
7. L. E. Baum, T. Petrie, G. Soules, and N. Weiss, "A Maximization Technique Occurring in the Statistical Analysis of Probabilistic Functions of Markov Chains," *Ann. Math. Statist.*, 41 (1970), pp. 164-71.
8. L. R. Liporace, "Maximum Likelihood Estimation for Multivariate Observations of Markov Sources," *IEEE Trans. Inform. Theory*, IT-28 (September 1982), pp. 729-34.
9. B. H. Juang, S. E. Levinson, and M. M. Sondhi, unpublished work.
10. L. E. Baum, "An Inequality and Associated Maximization Technique in Statistical Estimation for Probabilistic Functions of a Markov Process," *Inequalities*, 3 (1977), pp. 1-8.
11. B. H. Juang and L. R. Rabiner, "A Probabilistic Distance Measure for Hidden Markov Models," 64, No. 2 (February 1985), pp. 391-408.

AUTHORS

Biing-Hwang Juang, B.Sc. (Electrical Engineering), 1973, National Taiwan University, Republic of China; M.Sc. and Ph.D. (Electrical and Computer Engineering), University of California, Santa Barbara, 1979 and 1981, respectively; Speech Communications Research Laboratory (SCRL), 1978; Signal Technology, Inc., 1979-1982; AT&T Bell Laboratories, 1982; AT&T Information Systems Laboratories, 1983; AT&T Bell Laboratories, 1983—. Before joining AT&T Bell Laboratories, Mr. Juang worked on vocal tract modeling at the Speech Communications Research Laboratory, and on speech coding and interference suppression at Signal Technology, Inc. Presently, he is a member of the Acoustics Research Department, where he is researching speech communications techniques and stochastic modeling of speech signals.

Stephen E. Levinson, B.A. (Engineering Sciences), 1966, Harvard; M.S. and Ph.D. (Electrical Engineering), University of Rhode Island, Kingston, Rhode Island, 1972 and 1974, respectively; General Dynamics, 1966-1969; Yale University, 1974-1976; AT&T Bell Laboratories, 1976—. From 1966 to 1969, Mr. Levinson was a design engineer at Electric Boat Division of General Dynamics in Groton, Connecticut. From 1974 to 1976, he held a J. Willard Gibbs Instructorship in Computer Science at Yale University. In 1976, he joined the technical staff at AT&T Bell Laboratories, where he is pursuing research in the areas of speech recognition and cybernetics. Member, Association for Computing Machinery, Acoustical Society of America, editorial board of *Speech Technology*; associate editor, *IEEE Transactions on Acoustics, Speech and Signal Processing*.

Lawrence R. Rabiner, S.B. and S.M., 1964, Ph.D., 1967 (Electrical Engineering), The Massachusetts Institute of Technology; AT&T Bell Laboratories, 1962—. Presently, Mr. Rabiner is engaged in research on speech communications and digital signal processing techniques. He is coauthor of *Theory and Application of Digital Signal Processing* (Prentice-Hall, 1975), *Digital Processing of Speech Signals* (Prentice-Hall, 1978), and *Multirate Digital Signal Processing* (Prentice-Hall, 1983). Member, National Academy of Engineering, Eta Kappa Nu, Sigma Xi, Tau Beta Pi. Fellow, Acoustical Society of America, IEEE.

Man Mohan Sondhi, B.Sc. (Physics), Honours degree, 1950, Delhi University, Delhi, India; D.I.I.Sc. (Communications Engineering), 1953, Indian Institute of Science, Bangalore, India; M.S., 1955 and Ph.D. (Electrical Engineering), 1957, University of Wisconsin; AT&T Bell Laboratories, 1962—. Before joining AT&T Bell Laboratories, Mr. Sondhi worked for a year at the Central Electronics Engineering Research Institute, Pilani, India, and taught for a year at the University of Toronto. At AT&T Bell Laboratories his research has included work on speech signal processing, echo cancellation, adaptive filtering, modeling of auditory and visual processes, and acoustical inverse problems. From 1971 to 1972, Mr. Sondhi was a guest scientist at the Royal Institute of Technology, Stockholm, Sweden.

Variable-Length Packetization of μ -Law PCM Speech*

By R. STEELE[†] and F. BENJAMIN[‡]

(Manuscript received October 31, 1984)

A variable-length packetization process is proposed for logarithmic Pulse Code Modulation (log-PCM)-encoded speech signals. Blocks of W log-PCM words are reduced in size by discarding words on the basis that the receiver can recover the speech with a signal-to-noise ratio (s/n) that is, in general, above a specified value. Specifically, blocks of two hundred fifty-six, 8-bit, μ -law PCM words are left unchanged or reduced to either 214, 205, 192, 171, or 128 words. These blocks are then formulated into packets. The discarded samples at the dispatching terminal are replaced at the receiver by means of adaptive interpolation. We found that by specifying the s/n of the decoded speech in each variable-length packet to be above 27 dB, the reduction in the transmitted speech data was 25 percent, while the recovered speech signal had negligible perceptual degradation.

I. INTRODUCTION

Speech signals are inherently bursty. Indeed, conversational speech is composed of speech segments sandwiched between variable durations of silences and interword pauses, as well as intraword gaps. Even during a speech utterance, the information rate is not constant and can exhibit surges. Stated simply, the statistical properties of speech are nonstationary, and our speech encoders are designed to exploit in

* Most of this work was conducted when the authors were members of AT&T Bell Laboratories.

[†] University of Southampton, England. [‡] Perkin-Elmer Corporation, Tinton Falls, New Jersey.

Copyright © 1985 AT&T. Photo reproduction for noncommercial use is permitted without payment of royalty provided that each reproduction is done without alteration and that the Journal reference and copyright notice are included on the first page. The title and abstract, but no other portions, of this paper may be copied or distributed royalty free by computer-based and other information-service systems without further permission. Permission to reproduce or republish any other portion of this paper must be obtained from the Editor.

various degrees this nonstationarity. However, the majority of existing speech encoders¹⁻³ generate data at a fixed rate, and as the information content of the speech source is varying, so is the recovered speech quality. If we stipulate that the speech quality should be maintained above a specified level, then the variation in the information content of the speech signal causes the bit rate to vary. Earlier attempts at variable-bit-rate encoding have usually employed a buffer to convert the variable bit rate generated by the encoder to a fixed rate for transmission over the channel. Such arrangements suffer from long delays in the recovered speech signal and are often susceptible to transmission errors. However, when the transmission medium can accommodate many channels, variable-rate digitized speech can be used with advantage. By converting this variable data rate into packets of varying length, we are able to reduce the overall data rate for a given number of speech channels. These packets are amenable to statistical multiplexing, which is essentially a generalization of digital-speech interpolation. By employing packet switching,⁴ we can conveniently combine statistical multiplexing with switching and routing procedures. Thus, the line of enquiry to be followed here is concerned with the formulation of packetized digital speech, and, in particular, variable-length packets that utilize the time-varying statistics of speech signals.

It is interesting to observe that there are many speech-encoding algorithms that operate on blocks of speech samples.¹⁻³ The resulting blocks of digital speech are eminently suited to packetization. All that is required to yield packets of digital speech is the addition of suitable headers and flags to the blocks. These additions enable the multiplexer and the switching and routing network to identify the beginning and termination of the packets, and give the receiver access to any decoding commands. Although the number of digital encoders conceived are legion, only a few types are employed in the networks. Foremost is logarithmic Pulse Code Modulation (log-PCM),⁵ which is formidably entrenched in the international networks. Adaptive differential pulse code modulation is now being introduced⁶ on trunk networks, and adaptive delta modulation⁷ has been used in a limited way in subscriber loops and over satellite links. In this discourse we will focus on the variable-length packetization of log-PCM speech.

In Section II we review the adaptive interpolation procedures to be used in our variable-length packetized μ -law PCM-encoded speech system. The technique of determining the packet length is described in Section III. For each packet we ensure that the recovered speech quality at the receiver is, in general, above a minimum specified value. In Section IV we discuss our results. The final section deliberates on the properties and ramifications of the proposed packetization method.

II. APPLICATION OF ADAPTIVE INTERPOLATION TO REDUCE THE TRANSMITTED DATA RATE

Starting with blocks of W speech samples, it is possible to reject certain samples at the transmitter with the knowledge that the receiver is able to replace the discarded samples with virtually an imperceptible degradation. The replacement technique⁸ employs adaptive interpolation. Thus, we commence with a block of W speech samples, discard some samples prior to transmission, and at the receiver reinsert the missing samples to yield speech that is acceptable according to a simple objective criterion. For a given recovered speech quality criterion, the number of samples discarded in any block is dependent on the correlative properties of its W speech samples. When the samples are highly correlated more samples are rejected prior to transmission, and vice versa when the samples are relatively uncorrelated. This is because of the nature of the interpolation procedure. In general, the W samples in each block are reduced in number. We may, therefore, think of packets having W speech samples converted to packets containing fewer speech samples. The length of the packet, i.e., the number of samples in the packet, depends upon the ability to discard samples in the confident knowledge that the receiver will reproduce W samples with a speech quality that is above a specified value. However, in our deliberations we will not be concerned with variable-length packetization of samples, but with log-PCM speech data. This matter will be dealt with in Section III.

Next we will briefly review the adaptive procedure used to replace the discarded samples. This procedure is cardinal in controlling the length of the transmitted packet.

The method is fully described in Ref. 8 and only a brief review will be presented here. Essentially, speech is sampled at or above the Nyquist rate to give the sequence $\{x_k\}$. Operating on a block containing W contiguous samples of this sequence, we reject every n th member in order to achieve a reduction in the speech data. The discarded samples are replaced by

$$\hat{z}_r; \quad r = n, 2n, \dots, W - n, W$$

to give the recovered sequence,

$$x_1, \dots, x_{n-1}, \hat{z}_n, x_{n+1}, \dots, x_{2n-1}, \hat{z}_{2n}, x_{2n+1}, \dots, x_{W-1}, \hat{z}_W.$$

The interpolated samples are

$$\hat{z}_r = \sum_{i=-(n-1)}^{n-1} a_i x_{r+i}, \quad (1)$$

where a_i are the interpolation coefficients, $a_0 = 0$. The set of interpo-

	1	$R(-5,-6)$	$R(-4,-6)$	$R(-3,-6)$	$R(-2,-6)$	$R(-1,-6)$	$R(1,-6)$	$R(2,-6)$	$R(3,-6)$	$R(4,-6)$	$R(5,-6)$	$R(6,-6)$
$R(-6,-5)$	1	$R(-4,-5)$	$R(-3,-5)$	$R(-2,-5)$	$R(-1,-5)$	$R(1,-5)$	$R(2,-5)$	$R(3,-5)$	$R(4,-5)$	$R(5,-5)$	$R(6,-5)$	
$R(-6,-4)$	$R(-5,-4)$	1	$R(-3,-4)$	$R(-2,-4)$	$R(-1,-4)$	$R(1,-4)$	$R(2,-4)$	$R(3,-4)$	$R(4,-4)$	$R(5,-4)$	$R(6,-4)$	
$R(-6,-3)$	$R(-5,-3)$	$R(-4,-3)$	1	$R(-2,-3)$	$R(-1,-3)$	$R(1,-3)$	$R(2,-3)$	$R(3,-3)$	$R(4,-3)$	$R(5,-3)$	$R(6,-3)$	
$R(-6,-2)$	$R(-5,-2)$	$R(-4,-2)$	$R(-3,-2)$	1	$R(-1,-2)$	$R(1,-2)$	$R(2,-2)$	$R(3,-2)$	$R(4,-2)$	$R(5,-2)$	$R(6,-2)$	
$R(-6,-1)$	$R(-5,-1)$	$R(-4,-1)$	$R(-3,-1)$	$R(-2,-1)$	1	$R(1,-1)$	$R(2,-1)$	$R(3,-1)$	$R(4,-1)$	$R(5,-1)$	$R(6,-1)$	
$R(-6,1)$	$R(-5,1)$	$R(-4,1)$	$R(-3,1)$	$R(-2,1)$	$R(-1,1)$	1	$R(2,1)$	$R(3,1)$	$R(4,1)$	$R(5,1)$	$R(6,1)$	
$R(-6,2)$	$R(-5,2)$	$R(-4,2)$	$R(-3,2)$	$R(-2,2)$	$R(-1,2)$	$R(1,2)$	1	$R(3,2)$	$R(4,2)$	$R(5,2)$	$R(6,2)$	
$R(-6,3)$	$R(-5,3)$	$R(-4,3)$	$R(-3,3)$	$R(-2,3)$	$R(-1,3)$	$R(1,3)$	$R(2,3)$	1	$R(4,3)$	$R(5,3)$	$R(6,3)$	
$R(-6,4)$	$R(-5,4)$	$R(-4,4)$	$R(-3,4)$	$R(-2,4)$	$R(-1,4)$	$R(1,4)$	$R(2,4)$	$R(3,4)$	1	$R(5,4)$	$R(6,4)$	
$R(-6,5)$	$R(-5,5)$	$R(-4,5)$	$R(-3,5)$	$R(-2,5)$	$R(-1,5)$	$R(1,5)$	$R(2,5)$	$R(3,5)$	$R(4,5)$	1	$R(6,5)$	
$R(-6,6)$	$R(-5,6)$	$R(-4,6)$	$R(-3,6)$	$R(-2,6)$	$R(-1,6)$	$R(1,6)$	$R(2,6)$	$R(3,6)$	$R(4,6)$	$R(5,6)$	1	

Fig. 1—Matrix A for $n = 2, 3, \dots, 6$.

lation coefficients that minimizes the mean-square interpolation error

$$e_r = x_r - \hat{z}_r; \quad r = n, 2n, \dots, W, \quad (2)$$

is

$$\alpha = [a_{1-n}, a_{2-n}, \dots, a_{-1}, a_1, \dots, a_{n-2}, a_{n-1}]^T \quad (3)$$

and is found from

$$\alpha = \mathbf{A}^{-1}\mathbf{C}, \quad (4)$$

where

$$\mathbf{C} = [R(0, 1 - n), R(0, 2 - n), \dots, R(0, -1), R(0, 1), \dots, R(0, n - 2), R(0, n - 1)]^T. \quad (5)$$

The superscripts -1 and T represent inverse and transpose operations, respectively. The matrix \mathbf{A} for $n = 2, 3, \dots, 6$ is shown in Fig. 1, where the innermost dotted enclosure, the next dotted enclosure, and so on, and the complete matrix refer to $n = 2, 3, \dots, 6$, respectively. We will not perform adaptive interpolation with $n > 6$ for the reasons stated in Section 3.1. The elements in the matrix \mathbf{A} , and in the vector \mathbf{C} given by eq. (5), are

$$R(k, j) = \frac{\sum_{r=n}^W x_{r+k} x_{r+j}}{\sum_{r=n}^W x_{r+j}^2}$$

$$k = \pm 1, \pm 2, \dots, \pm n - 1$$

$$j = \pm 1, \pm 2, \dots, \pm n - 1$$

$$r = n, 2n, \dots, W. \quad (6)$$

Observe that

$$a_{-p} \neq a_p, \quad p = 1, 2, \dots, n - 1 \quad (7)$$

and, therefore, that the number of interpolation coefficients to be computed is twice that required when the simple correlation coefficient

$$R(\tau) = \frac{\sum_{r=1}^{W-\tau} x_r x_{r+\tau}}{\sum_{r=1}^W x_r^2}, \quad r = 1, 2, \dots, W \quad (8)$$

is employed. The use of $R(\tau)$ yields significantly greater interpolation errors than does the use of $R(k, j)$.⁸

III. VARYING n TO DEMAND A BLOCK SIGNAL-TO-NOISE RATIO ABOVE A SPECIFIED LEVEL

In the previous subsection, we summarized (1) the procedure for removing every n th sample in a block of W speech samples and (2) the reinsertion of these discarded samples at the receiver by using adaptive interpolation based on the transmitted samples. Thus, the interpolated sample \hat{z}_r , given by eq. (1), is the weighted sum of $2(n - 1)$ neighboring speech samples that were transmitted. In the original paper⁸ the value of n was a constant, although the effect of varying n was studied. When the signal-to-noise ratio (s/n), computed over a block of length W samples, was plotted as a function of block number during a sentence of speech, it exhibited huge variations.

For example, for $W = 256$, $n = 4$, the s/n in a block could have been as small as 4 dB and as large as 58 dB, while the average of these block s/n's, the segmental s/n, was 35 dB. This implies that when the block s/n was low, the speech was relatively uncorrelated and n should have been significantly in excess of 4. By contrast, a high-block s/n meant that the speech correlation was so high that more samples could have been discarded, and a value of $n = 2$ might have still yielded an acceptable block s/n. To attempt to guarantee a minimum block s/n, we must be prepared to vary n , even allowing for n to be infinity, i.e., no samples rejected, when the speech is very uncorrelated. The value of n clearly determines the number of samples in the transmitted block, being as large as W when n is infinity and as small as $W/2$ when n is 2. As blocks are virtually synonymous with packets, we are led to the notion of variable-length packets.

3.1 Generation of variable-length packets

So far our discussion of adaptive interpolation has involved the processing of analog speech samples. We will not, however, be con-

cerned with the transmission of samples. Rather, we will describe the packetizing of μ -law PCM-encoded speech. The packets are formulated at a transmitting terminal, gathering the encoded speech words as they are produced. (Alternatively, the packetization may operate at a node in the network, converting a 64-kb/s data stream into a sequence of variable-length packets and thereby reducing the overall data rate.)

Figure 2 shows the system arrangement for the creation of variable-length packets when packets are created at the subscriber's packet network terminal or interface. Figure 3 is the similar system on the receiver side. The input speech sequence is μ -law PCM encoded, and the resulting words are stored in buffer 3. The μ -law PCM-encoded speech is locally decoded to give quantized speech samples that are directed into buffer 1. While this is in progress the sequence of previously decoded samples $\{x_k\}$ is removed from buffer 2 for processing. Buffers 1 and 2 are of length W samples. Buffer 3 holds the contents of buffers 1 and 2, but in the μ -law format. Starting with $n = 2$, every other sample in $\{x_k\}$ is discarded to yield the sequence $\{z_k\}$. The two interpolation coefficients a_{-1} and a_1 are computed from $\{x_k\}$ using eq. (4). These coefficients must be encoded for transmission, so they are scaled by a factor K to ensure that the largest coefficient will not exceed the range of the quantizer. The quantized coefficients are binary encoded and, if selected for transmission, are conveyed to the multiplexer (MUX). The coefficients are also locally descaled by $1/K$ to give the decoded coefficients \hat{a}_{-1} , \hat{a}_1 that a receiver would have to use, assuming they would be regenerated without error. Operating on $\{z_k\}$ and $\{\hat{a}_k\}$, the discarded samples are reinserted using the adaptive interpolation procedure described in Section II. The locally recovered sequence $\{\hat{z}_k\}$ and the corresponding block of input speech samples $\{\tilde{x}_k\}$ are then used to calculate the block s/n:

$$(s/n)_n = 10 \log_{10} \left[\frac{\sum_{k=1}^W \tilde{x}_k^2}{\sum_{k=1}^W (\tilde{x}_k - \hat{z}_k)^2} \right]. \quad (9)$$

This block s/n, $(s/n)_n$, is compared with a reference s/n, $(s/n)_{\text{ref}}$, and if

$$(s/n)_n \geq s/n_{\text{ref}}; \quad n \text{ accepted}, \quad (10)$$

then the value of $n = 2$ is accepted. Otherwise, the process is repeated using the next higher value of n , namely, 3. Should this later condition prevail, the coefficients \hat{a}_{-2} , \hat{a}_{-1} , \hat{a}_1 , \hat{a}_2 , are calculated, and this time $\{z_k\}$ has every third sample missing. The new $\{\hat{z}_k\}$ is formulated, the $(s/n)_3$ computed, and inequality (10) tested. If this inequality is not

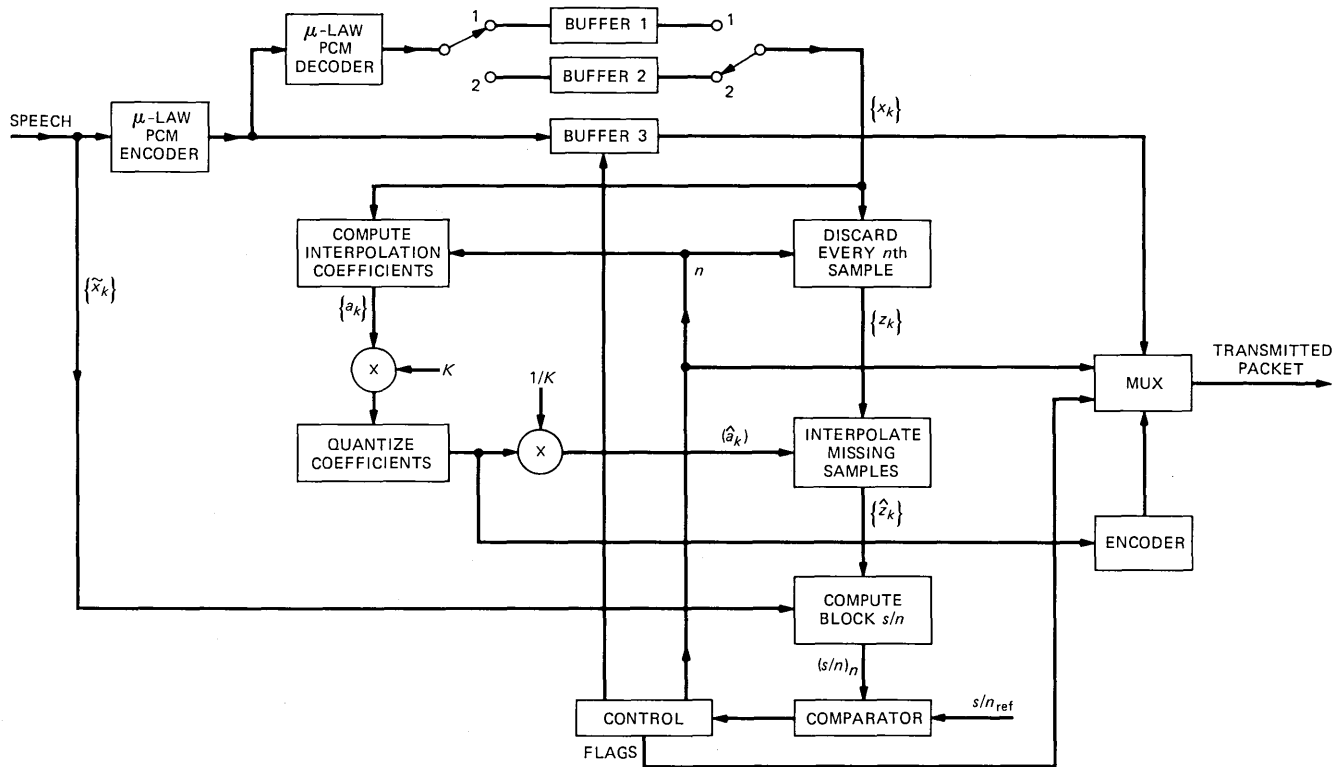


Fig. 2—System for generating variable-length packet speech.

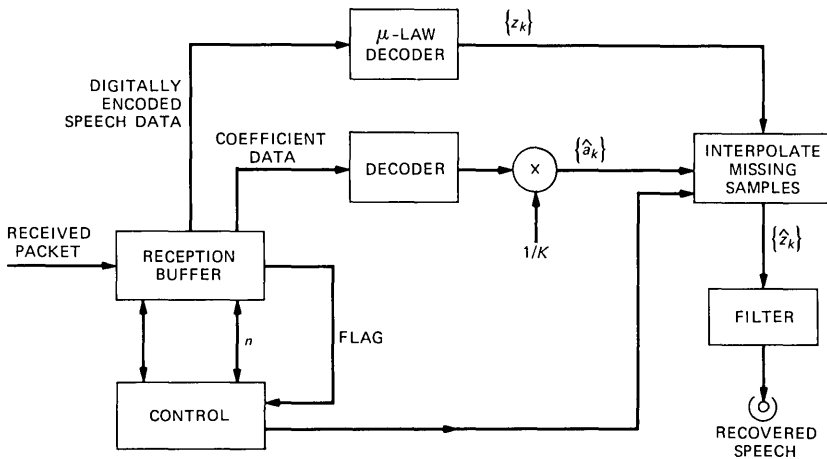


Fig. 3—System for decoding variable-length packet speech.

satisfied, n is increased to 4 and another iteration is performed, and so on. Should $n = 6$ fail to satisfy inequality (10), the iteration ceases because the packet size reduction with $n > 6$ is insufficient to justify the increase in processing time and system complexity. In this situation the entire block of μ -law PCM speech data is transmitted.

Observe that in computing $(s/n)_n$ we formulate the overall error [see the denominator of eq. (9)], which includes the effects of both quantization and interpolation. Thus, when inequality (10) is satisfied the overall s/n for the block of W speech samples is guaranteed to be above the specified minimum value of s/n_{ref} . However, we note that if s/n_{ref} is sufficiently high there will be some blocks where the quantization noise due to μ -law PCM encoding prevents inequality (10) from being satisfied, even though no samples are discarded. In this situation we do no worse than the performance of the μ -law PCM encoder, i.e., the s/n for the block is only dependent on the encoder noise, and the number of code words transmitted in the block remains unchanged at W .

The packetization scheme shown in Fig. 2 causes the original block of W speech samples, namely, $\{\tilde{x}_k\}$, to be processed to yield a data sequence where words have lengths of

$$L = \begin{cases} W \left(\frac{n-1}{n} \right); & n = 2, \dots, 6 \\ W; & n = \infty. \end{cases} \quad (11)$$

This μ -law PCM data sequence is removed from buffer 3, with words discarded where appropriate, and conveyed to the multiplexer. These L μ -law PCM words are the digitized-speech data that are formulated

into the packet at the multiplexer. To these data must be added the header, which consists of a 3-bit binary number for n , followed by an 8-bit representation of each interpolation coefficient, and a system flag. The end of the packet is signified by another system flag. These flags are dependent on the switching arrangements for a particular network, and because of the myriad of possible switching systems, we will refrain from detailing the properties of the flags. The number of channel-protection bits for n and $\{\hat{a}_k\}$ is dependent on the bit error rate specified for the network. Again we will not concern ourselves with the numerous network scenarios. We can state that (1) if n is represented by an 8-bit word—i.e., it is equivalent in length to one μ -law PCM word—the combination of L data words and the part of the header needed by the receiver to decode the speech data is

$$L_r = \begin{cases} L + 1 + 2n; & n = 2, \dots, 6 \\ L + 1; & n = \infty \end{cases} \quad (12)$$

because $2n$ words are required for the transmission of the interpolation coefficients when every n th word is discarded; and (2) when $n = \infty$ only one extra word is required to inform the receiver of the situation. It is not necessary that the end of packet be conveyed, because a knowledge of n specifies the length of the packet. By employing an end-of-packet flag, we are allowing for errors in the reception of n .

3.2 Decoding the variable-length packets

The received packet enters a buffer. The flag at the front end of the packet causes the control system to remove the data word representing n . Armed with this information, the coefficient data and digital-speech data are extracted from the buffer and subsequently decoded. The sequences $\{\hat{a}_k\}$ and $\{z_k\}$ are formed (see Fig. 3), and the samples that were rejected at the transmitter are reinserted by adaptive interpolation to yield $\{\hat{z}_k\}$. Speech is decoded in successive packets such that although there are L elements in $\{z_k\}$, where L is a function of n , there are always W samples in the recovered sequence $\{\hat{z}_k\}$. Thus, speech samples are presented to the final filter at the same rate at which they were originally generated.

IV. RESULTS

The sentences "Live wires should be kept covered," spoken by a male, and "To reach the end he needs much courage," enunciated by a female, were concatenated, bandlimited from 0.3 to 3.2 kHz, and sampled at 8 kHz to yield the input speech sequence. This sequence was 8-bit, μ -law PCM encoded, $\mu = 255$, to provide the input digital-speech sequence.

Figure 2 shows the block diagram of the variable-length packetization system. The μ -law PCM data stream was decoded, and the resulting samples were directed into either buffer 1 or 2, as described in Section 3.1. The selection of W was 256, a value that had been found to provide a reasonable recovered s/n for the range of n values considered here.⁸ This choice of W also ensured that the amount of header information to convey the interpolation coefficients was insignificant compared with the number of data words in the packet and that the delay in the recovered speech signal at the receiving terminal due to the block size was not excessive. The duration of these blocks of 256 speech samples was 32 ms.

The coefficients $\{a_k\}$ were quantized using, for convenience, an 8-bit, μ -law quantizer, $\mu = 255$. The scaling factor K was determined as follows. The system of Fig. 2 was operated as described in Section 3.1, but without the interpolation coefficients $\{a_k\}$ being quantized. However, the value of K for each block was noted as

$$K_{\max} = \frac{V}{|a_{(\cdot)}|_{\max}}, \quad (13)$$

where V was the maximum range of the quantizer, namely, 4079 arbitrary units, and $|a_{(\cdot)}|_{\max}$ was the coefficient with the maximum magnitude. Although we considered quantizing each value of K with an 8-bit word and transmitting it as part of the header, we opted in favor of a fixed value of K . Accordingly, we set k to be the maximum value of K , namely, 7969, observed in the 152 blocks of input data used in our experiments. With this fixed K we commenced our packetization properly, quantizing the interpolation coefficients and employing them in our adaptive interpolation procedures. The same fixed K was used at the receiver.

The value of n used in our experiments was either 2, 3, 4, 5, 6, or infinity, depending on the minimum s/n, s/n_{ref} , stipulated. The block s/n for a particular value of n , namely, $(s/n)_n$, was computed using the input speech samples $\{\tilde{x}_k\}$ and $\{\hat{z}_k\}$. The latter sequence contained the original speech samples contaminated by both quantization and interpolation noise. Thus, the $(s/n)_n$ values employed in our simulations are indicative of the quality of the recovered speech. To visually emphasize, in Fig. 4, those occasions when n was infinity, we arranged for the block s/n to "hit the stops," namely, an arbitrary number of 50 dB. These large excursions in s/n dramatically underline those times when the system was unable to reject any samples and thereby effect a reduction in the transmitted data rate. In our calculations of segmental s/n⁹ (shown in Fig. 5) we, of course, used the original input speech sequence and the recovered speech sequence at the output of the receiver. We note that those blocks for which n equaled infinity

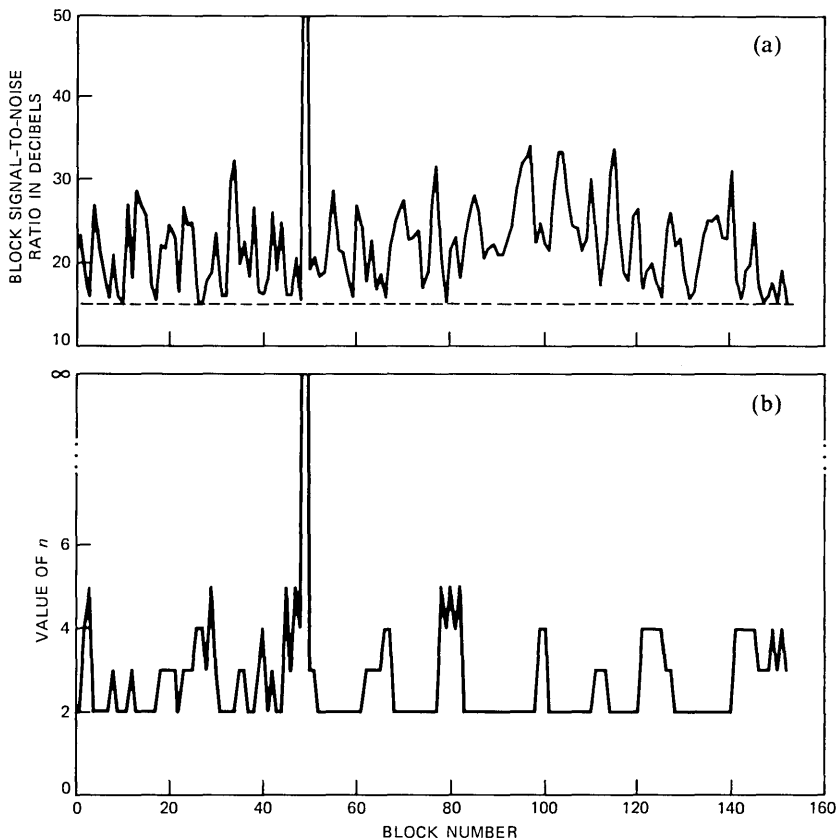


Fig. 4—Variation of block s/n and parameter n as a function of block number. (a) and (b) Block s/n and n , respectively, for s/n_{ref} of 15 dB. (Cont.)

had an s/n that was the signal-to-quantization noise ratio of the μ -law PCM speech.

Figures 4a, c, e, and g show the variation of block s/n , i.e., the $(s/n)_n$ for the final value of n used in the iteration, as a function of block number when s/n_{ref} was 15, 20, 25, and 30 dB, respectively. The corresponding profiles of the value of n used in the packetization process are displayed in Figs. 4b, d, f, and h, respectively. For s/n_{ref} of only 15 dB, $n = 2$ occurred most frequently, and only in one block was the system unable to reject any samples. By contrast, when $s/n_{\text{ref}} = 30$ dB, the guaranteed speech quality was so high that the most frequent decision was not to discard any speech samples in the block. This situation occurred because the block s/n of 8-bit, μ -law PCM was often below 30 dB.

Observe that for every 256 data words received, 128, 85, 64, 51, 42,

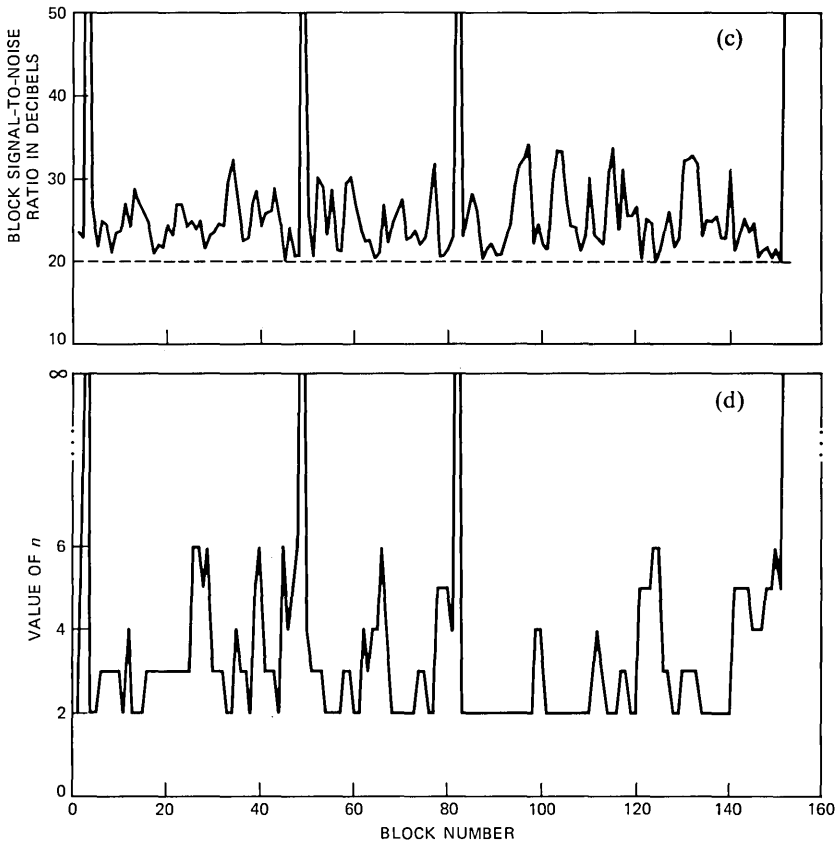


Fig. 4—(c) and (d) Block s/n and n , respectively, for s/n_{ref} of 20 dB. (Cont.)

and 0 words were discarded for transmitted packets associated with n of 2, 3, 4, 5, 6, and infinity, respectively. Clearly, the lower the value of n , the greater the data reduction. However, the value of n selected for a given block of W speech samples was dependent on s/n_{ref} , such that the lower the s/n_{ref} , the more probable the occurrence of a low value of n . Thus, as expected, the savings in the transmitted bit rate were at the expense of speech quality.

The histograms of n for different values of s/n_{ref} are displayed in Fig. 6. When a low recovered speech quality is acceptable, such as that obtained with $s/n_{\text{ref}} = 15$ dB, we found that $n = 2$ was the most frequently selected value of n and that $n > 4$ was rarely used. The reduction in the packetized data was found to be 41 percent. As the s/n_{ref} was increased, there was an increase in the frequency of occurrence of the higher values of n and a diminution in the rate at which lower n values occurred. The reduction in the data due to variable-

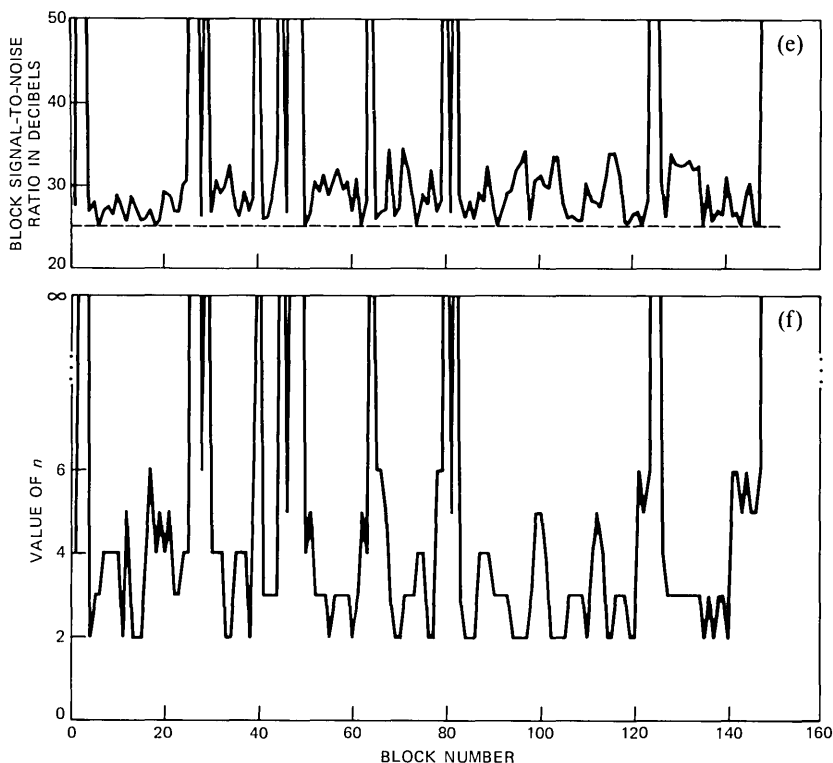


Fig. 4—(e) and (f) Block s/n and n , respectively for s/n_{ref} of 25 dB. (Cont.)

length packetizing was found to be 36, 28, and 20 percent for segmental s/n of 22.5, 25.5, and 33 dB, respectively. These reductions are displayed graphically in Fig. 5 as a function of our control parameter s/n_{ref} . Categorizing speech quality from segmental s/n is always contentious. However, when we included our informal listening experiences, we achieved a close approximation to toll quality speech with a data reduction of some 25 percent.

Figures 7a and b show a segment of the speech signal having a duration of 360 ms and its spectrogram. The corresponding error waveform and its spectrogram for 8-bit, μ -law PCM encoding are displayed in Figs. 7c and d. As expected with log-PCM, the quantization noise power was approximately proportional to the speech-signal power, and the error spectrum was relatively constant over the message band. When the variable-length packetizing of the speech signal was performed, the error in the recovered speech signal was composed of the quantization noise and interpolation noise components. The error magnitudes were, therefore, increased as shown in Figs. 7e and f, where

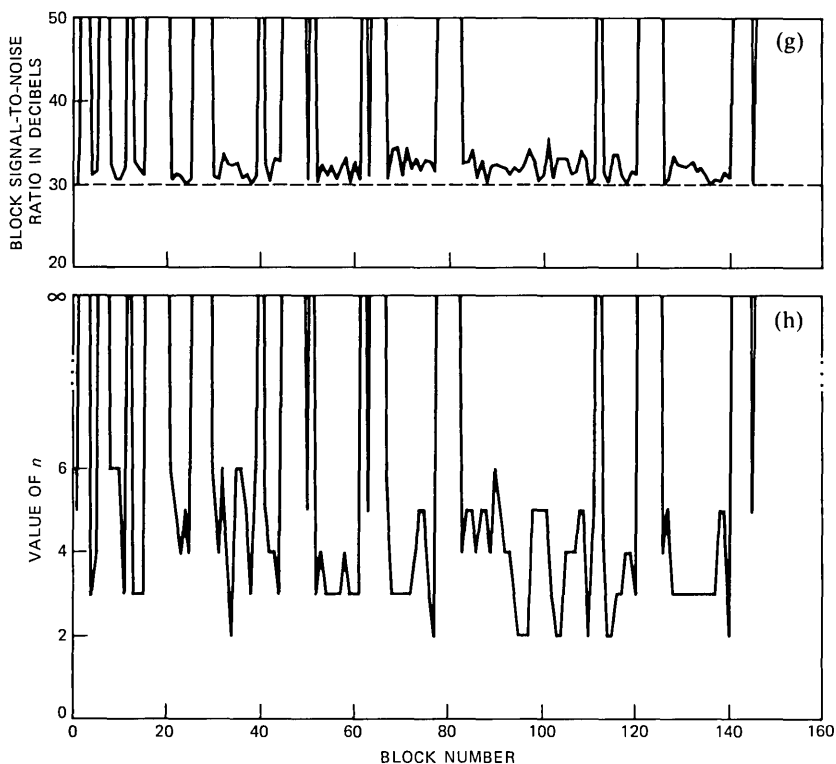


Fig. 4—(g) and (h) Block s/n and n , respectively, for s/n_{ref} of 30 dB.

$s/n_{\text{ref}} = 25$ dB. The spectral magnitudes in Figs. 7d and f have the same arbitrary units.

Figure 8a shows variations of the error signal for μ -law PCM over the entire speech signal, while the corresponding waveform for the recovered packetization speech is displayed in Fig. 8b. The waveforms of Figs. 8a and b are drawn to the same scale and provide a visual guide to the magnitude and location of the increase in error due to the packetization process. We observe that there is considerable correspondence between the variations in signal amplitudes in Figs. 8a and b. These variations also closely correspond to those in the original speech signal (not shown). This is to be expected, as the quantization noise is approximately proportional to the speech signal, and so is the interpolation noise because of the control exhibited by s/n_{ref} .

V. DISCUSSION

A variable-length packetization scheme has been proposed for 8-bit, μ -law PCM-encoded speech. By the aid of our control parameter

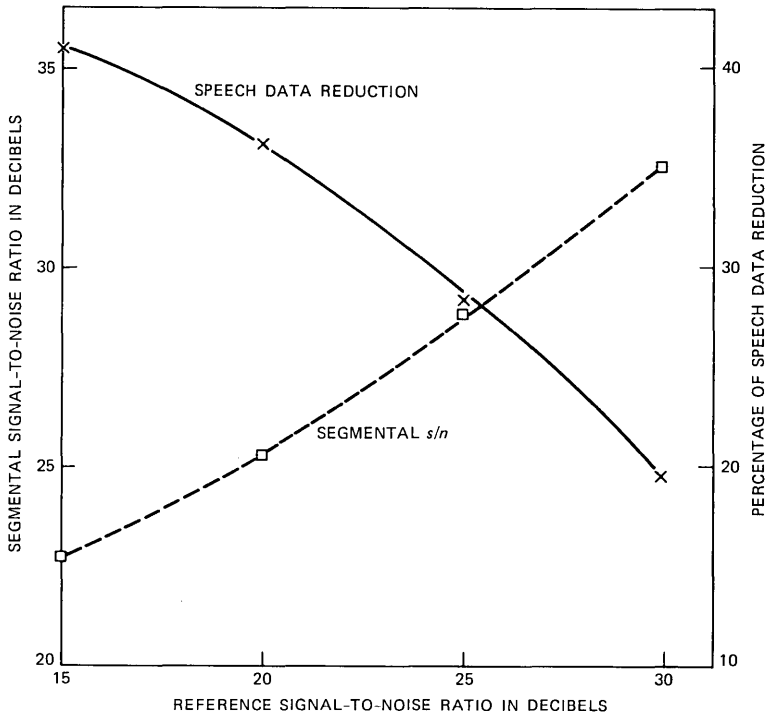


Fig. 5—Variation of segmental s/n , and percentage of speech data reduction, as a function of s/n_{ref} .

reference s/n we obtained a reduction in encoded speech data of 25 percent, while the segmental s/n exceeded 30 dB, i.e., the recovered speech displayed negligible perceptual impairments. An important feature of the system is that the s/n of the recovered speech in each packet is required to exceed an s/n_{ref} . Accepting s/n as a crude guide to quality, particularly for the relatively high s/n values employed here, our system endeavors to generate packets of variable length such that when they are decoded the speech will be maintained above a certain quality.

In the scheme proposed here the length of the packets varies. The number of μ -law PCM words in the packets could be either 256, 214, 205, 192, 171, or 128, where the original block of speech contained 256 words. While these packets can be transmitted as variable length with suitable headers and flags, they can also be transmitted as fixed-length packets, where the discarded speech data can be replaced with other types of data, such as that arising from computer traffic.

In our proposal the packet lengths are determined for a given speech signal by the selection of the s/n_{ref} , which acts as a quality control

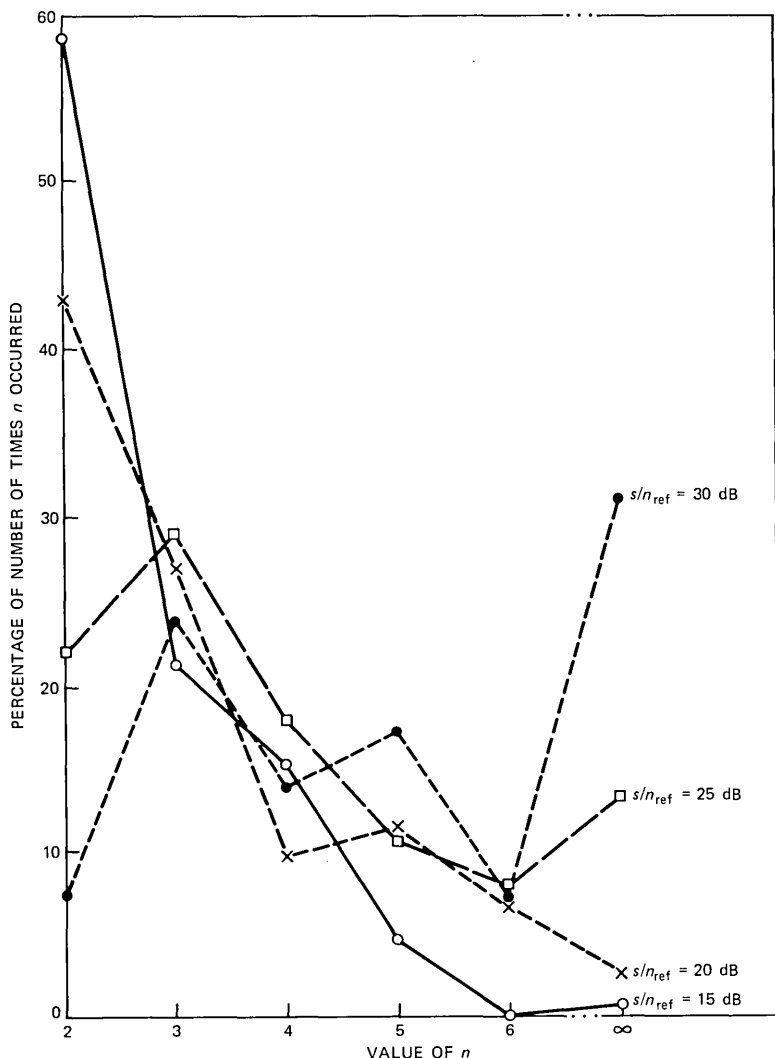


Fig. 6—Variation of the percentage of time the parameter n was used as a function of n for different s/n_{ref} .

mechanism. If the multiplexer is allowed to vary the s/n_{ref} , it can determine the length of the packets required for multiplexing. Thus, as more packets access the highways, the multiplexer control can discard more μ -law PCM words. Because the selection of those words to be discarded for a given s/n_{ref} is related to the interpolation algorithm, the degradation in recovered speech quality with increased user capacity is relatively smooth.

The packetization process need not be at the user's interface or

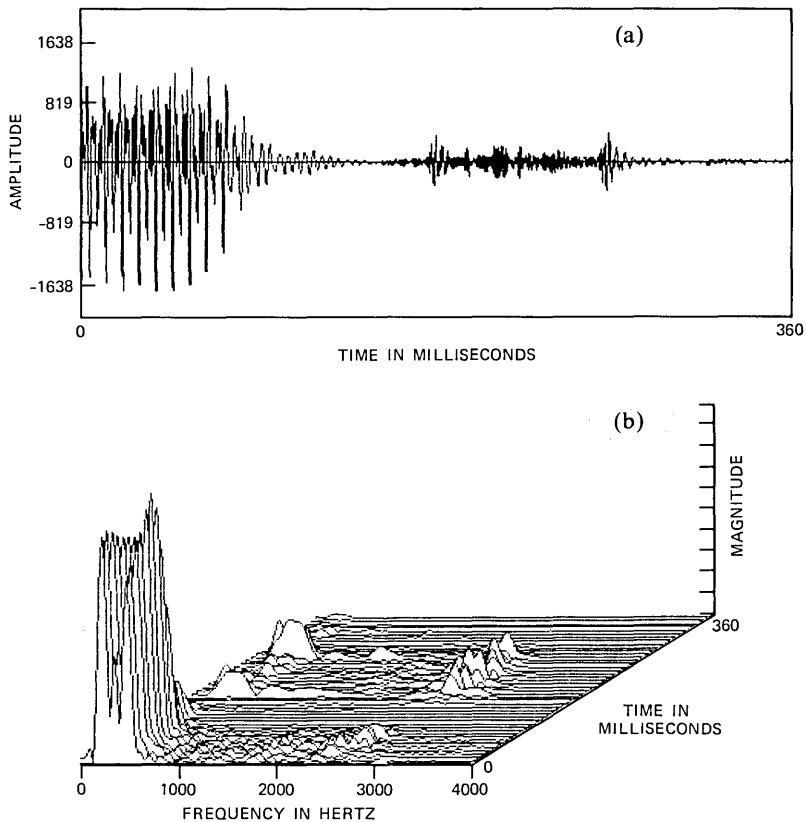


Fig. 7—Speech waveforms and spectrograms. (a) and (b) Segment of the speech signal and its spectrogram. (Cont.)

terminal; it can be located at a node in the network converting successive groups of W μ -law PCM words into variable-length packets. Thus, time-division-multiplexed μ -law PCM channels can be statistically multiplexed using the packetization scheme and thereby achieve a significant diminution in the data rate. Alternatively, a limited-capacity output port from the network node can accommodate more μ -law PCM traffic by employing the packetization procedure.

However, packetizing μ -law PCM at a node in the network requires a different s/n_{ref} compared with when the packetization occurs at the user's interface. In Fig. 2 we observe that the block s/n , namely $(s/n)_n$, is computed using $\{\hat{z}_k\}$ and $\{\tilde{x}_k\}$. The packetization equipment at a node in the network would not have access to the original speech sequence $\{\tilde{x}_k\}$ and would have to employ $\{x_k\}$. In this situation, when no samples are discarded in a block, i.e., n is infinity, $(s/n)_n$ would also be infinity because the sequences $\{\hat{z}_k\}$ and $\{x_k\}$ are identical. Thus,

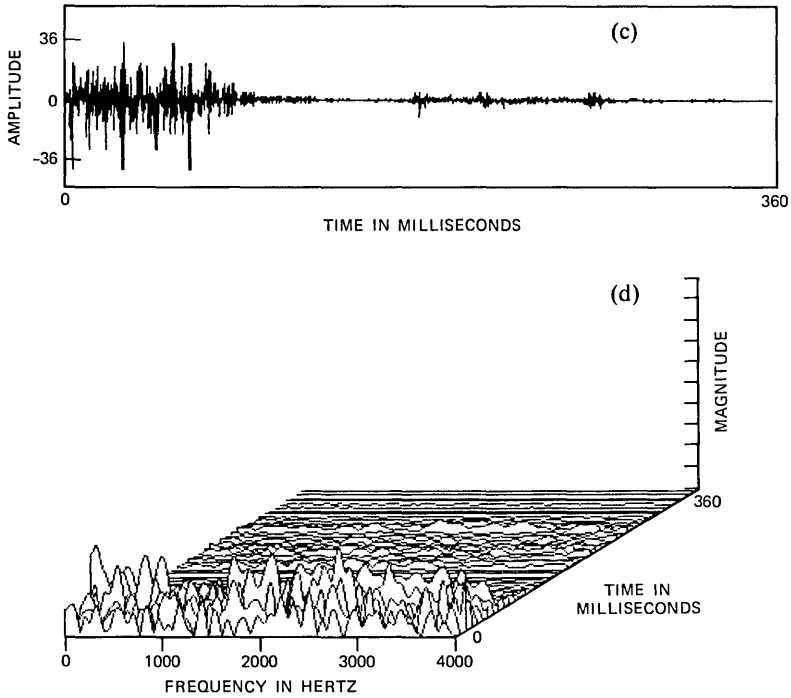


Fig. 7—(c) and (d) Corresponding error waveform and its spectrogram for 8-bit, μ -law PCM-encoded speech, $\mu = 255$. (Cont.)

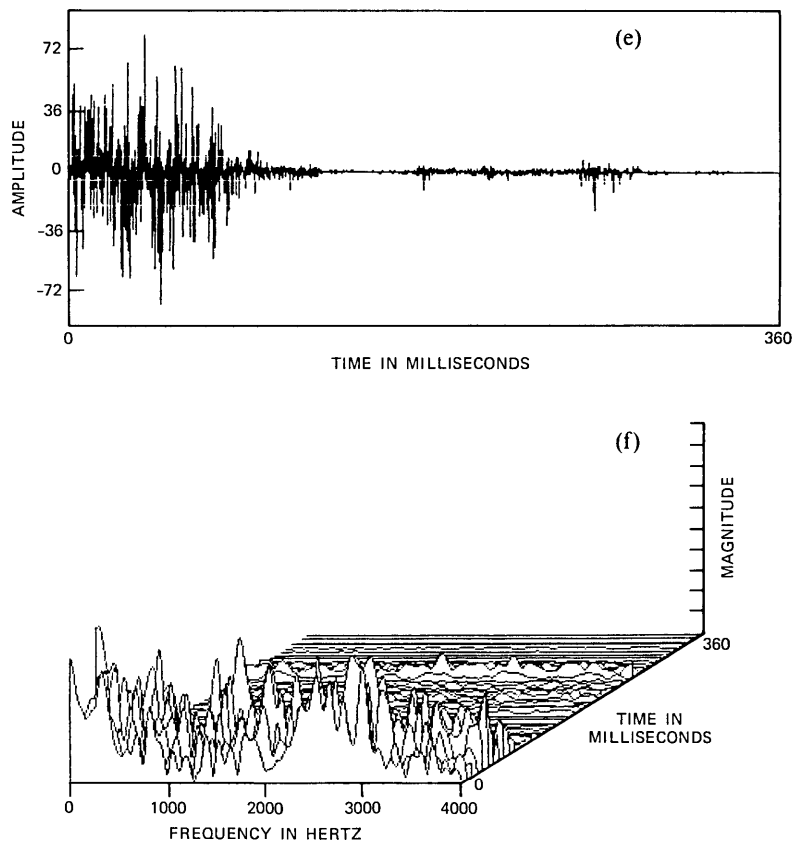


Fig. 7—(e) and (f) Corresponding error waveform and its spectrogram when the variable-length packetized speech system was employed.

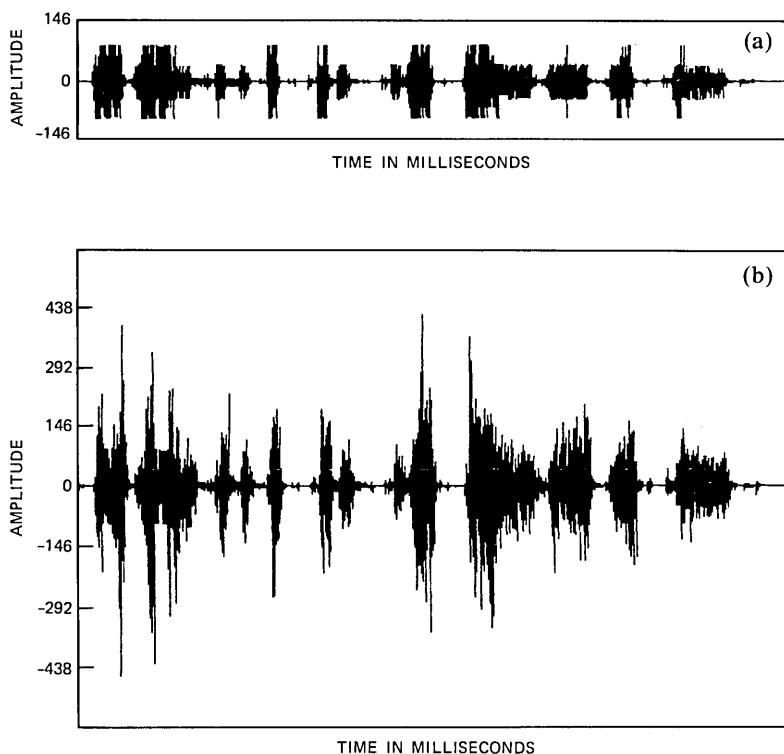


Fig. 8—Error waveforms for the speech signal. (a) Eight-bit, μ -law PCM speech. (b) Variable-length packetized speech.

$(s/n)_n$ computed at a node in the network is the signal-to-interpolation noise ratio, and for a given n this ratio is higher than that obtained for the arrangement shown in Fig. 2. Consequently, if s/n_{ref} is specified in terms of packetizing at the subscriber's interface, a higher value of s/n_{ref} is required when the packetization occurs at a node in the network. The important point to note, however, is that s/n_{ref} is a control parameter, and it is a simple procedure to increase it in order to achieve the required minimum block s/n performance, or a required average value of n .

Finally, we note that controlling packet length with spectral distance measures, and other measures more closely related to perception, should reduce the average transmitted bit rate per channel, but at the expense of added complexity.

VI. ACKNOWLEDGMENT

The authors are grateful to D. J. Goodman for his constructive criticism of this work.

REFERENCES

1. J. L. Flanagan, M. R. Schroeder, B. A. Atal, R. E. Crochiere, N. S. Jayant, and J. M. Tribolet, "Speech Coding," *IEEE Trans. Commun.*, *COM-27* (April 1979), pp. 710-37.
2. B. G. Haskell and R. Steele, "Audio and Video Bit-Rate Reduction," *Proc. IEEE*, *69*, No. 2 (February 1981), pp. 252-62.
3. N. S. Jayant and P. Noll, *Digital Coding of Waveforms*, Englewood Cliffs, N.J.: Prentice-Hall, 1984.
4. J. S. Turner and L. F. Wyatt, "A Packet Network Architecture for Integrated Services," *IEEE Globecom '83*, San Diego, Calif., November 18-December 1, 1983, pp. 45-50.
5. K. W. Cattermole, *Principles of Pulse Code Modulation*, London: Iliffe, 1969.
6. CCITT Study Group XVIII, Draft Recommendation G.7zz, "32 kbits s Adaptive Differential Pulse Code Modulation (ADPCM)," Geneva, November 21-25, 1983.
7. R. Steele, *Delta Modulation Systems*, London: Pentech Press, 1975.
8. R. Steele and F. Benjamin, "Sample Reduction and Subsequent Adaptive Interpolation of Speech Signals," *B.S.T.J.*, *62*, No. 6 (July-August 1983), pp. 1365-98.
9. R. Steele and D. Vitello, "Simultaneous Transmission of Speech and Data Using Code-Breaking Techniques," *B.S.T.J.*, *60*, No. 9 (November 1981), pp. 2081-105.

AUTHORS

Frank Benjamin, B.A. (Music Education), 1980; B.S. (Electronic Engineering), 1983, Valedictorian (both cum laude), Monmouth College, West Long Branch, N.J.; AT&T Bell Laboratories, 1981-1983; Perkin-Elmer Corp., 1983—. In 1980 he was appointed at Monmouth College as laboratory instructor in the Electronic Engineering Department and served as acoustical consultant to the Department of Physics on a publication for General Physics (Dr. Robert Smith, Chairman/author). Later in 1980 he joined United Telecontrol Electronics, Asbury Park, N.J., where he helped develop a missile guidance control system for the Navy. In 1981 he joined AT&T Bell Laboratories as a member of the Communications Methods Research Department, Crawford Hill, Holmdel, N.J., developing and writing software simulation systems for speech companding and interpolation techniques. In 1983 Mr. Benjamin joined Perkin-Elmer Corporation/Data Systems Group as a Member of Technical Staff hardware/software engineer in the Computer Processor/Memory Development Department, where he is currently designing and developing processor diagnostic equipment and computer graphics systems. President, college honor society Lambda Sigma Tau (1979-81). Member, national engineering society Eta Kappa Nu; national physics and mathematics honor societies. Nominee, Who's Who Among Students in American Colleges and Universities. New Jersey State Teacher's Certificate.

Raymond Steele, B.Sc. (Electrical Engineering), 1959, Durham University, Durham, England; Ph.D. (Delta Modulation Systems), 1975, and D.Sc. (Digital Encoding, Methods for Combatting Transmission Errors, and other Communication Techniques), 1983, Loughborough University of Technology, Loughborough, England. Prior to his enrollment at Durham University, he was an indentured apprenticed Radio Engineer. After research and development posts at E. K. Cole Ltd., Cossor Radar and Electronics Ltd., and The Marconi Company, all in Essex, England, he joined the lecturing staff at the Royal Naval College, Greenwich, London, England. Here he lectured in telecommunications to NATO and the External London University degree courses. His next post was as Senior Lecturer in the Electronic and Electrical Engineering Department of Loughborough University, Loughborough, Leics., England, where he directed a research group in digital encoding of speech and

television signals. In 1975 his book, *Delta Modulation Systems* (London: Pentech Press), was published. He was a consultant to the Acoustics Research Department at Bell Laboratories in the summers of 1975, 1977, and 1978, and in 1979 he joined the company's Communications Methods Research Department, Crawford Hill Laboratory, Holmdel, N.J. In 1983 he became Professor of Communications in the Electronics Department at the University of Southampton, England and nonexecutive Director of Plessey Electronic Systems Research Limited, England. Senior member, IEEE. Member, IEE.

PAPERS BY AT&T BELL LABORATORIES AUTHORS

COMPUTING/MATHEMATICS

- Assmann S. F., Johnson D. S., Kleitman D. J., Leung J. Y. T., **On a Dual Version of the One-Dimensional Bin Packing Problem.** *J Algorithm* 5(4):502-525, Dec 1984.
- Burman D. Y., Lehoczky J. P., Lim Y., **Insensitivity of Blocking Probabilities in a Circuit-Switching Network.** *J Appl Prob* 21(4):850-859, Dec 1984.
- Calderbank R., Mazo J. E., **A New Description of Trellis Codes.** *IEEE Info T* 30(6):784-791, Nov 1984.
- Chung M. J. et al., **Polynomial-Time Algorithms for the Min Cut Problem on Degree Restricted Trees.** *SIAM J Comp* 14(1):158-177, Feb 1985.
- Conway J. H., Sloane N. J. A., **A Lower Bound on the Average Error of Vector Quantizers (Letter).** *IEEE Info T* 31(1):106-109, Jan 1985.
- Craig R. J., **Normal Family Distribution Functions—FORTRAN and Basic Programs.** *J Qual Tech* 16(4):232-236, Oct 1984.
- Derman E., Vanwyk C. J., **A Simple Equation Solver and Its Application to Financial Modeling.** *Software* 14(12):1169-1181, Dec 1984.
- Fishburn P. C., **Paradoxes of Two-Length Interval Orders.** *Discr Math* 52(2-3):165-175, Dec 1984.
- Flatto L., Odlyzko A. M., Wales D. B., **Random Shuffles and Group Representations.** *Ann Probab* 13(1):154-178, Feb 1985.
- Ganapathy S., **Decomposition of Transformation Matrices for Robot Vision.** *Patt Rec L* 2(6):401-412, Dec 1984.
- Goodman J. B., Massey W. A., **The Non-Ergodic Jackson Network.** *J Appl Prob* 21(4):860-869, Dec 1984.
- Graham R. L., Hell P., **On the History of the Minimum Spanning Tree Problem.** *Ann Hist C* 7(1): 43-57, Jan 1985.
- Hohenberg P. C., **Convection Patterns in Large Aspect Ratio Systems.** *Lect N Phys* 210:127-128, 1984.
- Huang A., **Impact of Technological Advances and Architectural Insights on the Design of Optical Computers.** *Phi T Roy A* 313(1525):205-211, Dec 18 1984.
- Hwang F. K., **Robust Group Testing.** *J Qual Tech* 16(4):189-195, Oct 1984.
- Hwang F. K., Korner J., Wei V. K. W., **Selecting Non-Consecutive Balls Arranged in Many Lines.** *J Comb Th A* 37(3):327-336, Nov 1984.
- Hwang F. K., Sun J., Yao E. Y., **Optimal Set Partitioning.** *SIAM J Alg* 6(1):163-170, Jan 1985.
- Jewell J. L. et al., **Optical Logic on a Single Etalon.** *Phi T Roy A* 313(1525):375-380, Dec 18 1984.
- Johnson D. S., **The NP-Completeness Column—An Ongoing Guide.** *J Algorithm* 5(4):595-609, Dec 1984.
- Knapp G. R., Stark A. A., Wilson R. W., **The Global Properties of the Galaxy. 3. Maps of the ¹²CO Emission in the First Quadrant of the Galaxy.** *Astronom J* 90(2):254-301, Feb 1985.
- Lagarias J. C., **The 3X + 1 Problem and Its Generalizations.** *Am Math Mo* 92(1):3-23, Jan 1985.
- Lagarias J. C., **The Computational Complexity of Simultaneous Diophantine Approximation Problems.** *SIAM J Comp* 14(1):196-209, Feb 1985.
- Lagarias J. C., Odlyzko A. M., **Solving Low-Density Subset Sum Problems.** *J ACM* 32(1):229-246, Jan 1985.
- Mitchell J. S., **Subject Access to Microcomputer Software.** *Lib Res Tec* 29(1): 66-72, Jan-Mar 1985.
- Moon A., **The Graphs G(N, K) of the Johnson Schemes Are Unique for N ≥ 20.** *J Comb Th B* 37(2):173-188, Oct 1984.
- Morrison J. A., **Response-Time Distribution for a Processor-Sharing System.** *SIAM J A Ma* 45(1):152-167, Feb 1985.

- Odlyzko A. M., Richmond L. B., **On the Unimodality of High Convolutions of Discrete Distributions.** *Ann Probab* 13(1):299-306, Feb 1985.
- Perry M. W., Reinold G. A., Yeisley P. A., **Physical Design of the SL Repeater.** *J Lightw T* 2(6):863-869, Dec 1984.
- Selfridge P. G., Derr M. A., **Some Experiments in Distributed Vision.** *P Soc Photo* 521:384-391, 1985.
- Serfozo R. F., **Rarefactions of Compound Point Processes.** *J Appl Prob* 21(4):710-719, Dec 1984.
- Tukey J. W., **More Intelligent Statistical Software and Statistical Expert Systems—Future Directions—Comment.** *AM Statistn* 39(1):12-14, Feb 1985.
- Wang Y. C., Vandendorpe J., Evens, M., **Relational Thesauri in Information Retrieval.** *J Am S Info* 36(1):15-27, Jan 1985.
- Zave P., **A Distributed Alternative to Finite-State-Machine Specifications.** *ACM T Progr* 7(1):10-36, Jan 1985.

ENGINEERING

- Abidi A. A., **Gigahertz Transresistance Amplifiers in Fine Line NMOS.** *IEEE J Soli* 19(6):986-994, Dec 1984.
- Adl A., Chien T. M., Chu T. C., **Design and Testing of the SL Cable.** *J Lightw T* 2(6):824-832, Dec 1984.
- Agrawal G. P., **Chirp Minimization and Optimum Biasing for Current-Modulated Coupled-Cavity Semiconductor Lasers.** *Optics Lett* 10(1):10-12, Jan 1985.
- Aloisio C. J., Lenahan T. A., Taylor C. R., **Coating Optical Fibers With Dual Dies Separated by a Pressurized Chamber.** *Fiber In Op* 5(1):81-97, 1984.
- Anderson C. D., Keller D. L., **The SL Supervisory System.** *J Lightw T* 2(6):991-997, Dec 1984.
- Antler M., **Effect of Fretting on the Contact Resistance of Palladium Electroplate Having a Gold Flash, Cobalt-Gold Electroplate, and DG-R156.** *IEEE Compon* 7(4):363-369, Dec 1984.
- Bayruns R. J., Johnston R. L., Fraser D. L., Fang S. C., **Delay Analysis of Si NMOS Gbit/s Logic Circuits.** *IEEE J Soli* 19(5):755-764, Oct 1984.
- Becker J. A., Shive J. N., **The Transistor—A New Semiconductor Amplifier (Reprinted From Electrical Engineering, 68, pp. 215-21, 1949).** *P IEEE* 72(12):1696-1703, Dec 1984.
- Besomi P., Wilson R. B., Nelson R. J., **Investigation of Melt Carry-Over During Liquid-Phase Epitaxy. 2. Growth of Indium Gallium Arsenic Phosphide Double Heterostructure Material Lattice Matched to Indium Phosphide.** *J Elchem So* 132(1):176-179, Jan 1985.
- Bodeep G. E., **Temperature-Measurement System for Optical-Fiber Preform Fabrication.** *Rev Sci Ins* 55(12):1957-1959, Dec 1984.
- Bosch F., Palmer G. M., Sallada C. D., Swan C. B., **Compact 1.3- μ m Laser Transmitter for the SL Undersea Lightwave System.** *J Lightw T* 2(6):952-959, Dec 1984.
- Boulnois J. L., **Gas-Flow-Induced Controlled Unidirectional Operation of a CO₂ Ring Laser.** *Optics Lett* 10(1):7-9, Jan 1985.
- Buswell G., Hoadley B., **QMP-USP—A Modern Alternative to MIL-STD-105D.** *Nav Res Log* 32(1):95-111, Feb 1985.
- Campbell J. C., **Photodetectors and Compatible Low-Noise Amplifiers for Long-Wavelength Light-Wave Systems.** *Fiber In Op* 5(1):1-21, 1984.
- Candy J. C., **A Use of Double Integration in Sigma Delta Modulation.** *IEEE Commun* 33(3):249-258, Mar 1985.
- Celler G. K., Robinson M., Trimble L. E., Lischner D. J., **Dielectrically Isolated Thick Si Films by Lateral Epitaxy From the Melt.** *J Elchem So* 132(1):211-219, Jan 1985.
- Chang J. J., Julesz B., **Cooperative Phenomena in Apparent Movement Perception of Random-Dot Cinematograms.** *Vision Res* 24(12):1781-1788, 1984.

- Chen C. Y., Cho A. Y., Garbinski P. A., **A New Ga_{0.47}In_{0.53}As Field-Effect Transistor With a Lattice-Mismatched GaAs Gate for High-Speed Circuits.** IEEE Elec D 6(1):20-21, Jan 1985.
- Chen C. Y., Cho A. Y., Olsson N. A., Garbinski P. A., **Reduction of Fall Times in Ga_{0.47}In_{0.53}As Photoconductive Receivers Through Back Gating.** Appl Phys L 46(3):296-298, Feb 1 1985.
- Chen C. Y., Kasper B. L., Cox H. M., Plourde J. K., **2-Gb/s Sensitivity of a Ga_{0.47}In_{0.53}As Photoconductive Detector/GaAs Field-Effect Transistor Hybrid Photoreceiver.** Appl Phys L 46(4):379-831, Feb 15 1985.
- Cheung N. K., Davidow S., Duff D. G., **A 90-Mb/s Transmission Experiment in Single-Mode Fibers Using 1.5- μ m Multi-Longitudinal-Mode InAsGaP/InP Lasers.** J Lightw T 2(6):1034-1039, Dec 1984.
- Cheung N. K., Tomita A., Glodis P. F., **Observation of Modal Noise in Single-Mode-Fibre Transmission Systems.** Electr Lett 21(1):5-7, Jan 3 1985.
- Chu S. N. G., Macrander, A. T., Stregge K. E., Johnston W. D., **Misfit Stress in InGaAs/InP Heteroepitaxial Structures Grown by Vapor-Phase Epitaxy.** J Appl Phys 57(2):249-257, Jan 15 1985.
- Coldren L. A., Koch T. L., **External-Cavity Laser Design.** J Lightw T 2(6):1045-1051, Dec 1984.
- Coldren L. A., Koch T. L., Bridges T. J., Burkhardt E. G., Miller B. I., Rentschler J. A., **Etched-Groove Coupled-Cavity Vapor-Phase-Transported Window Lasers at 1.55 μ m.** Appl Phys L 46(1): 5-7, Jan 1 1985.
- Cooper J. A., Thornber K. K., **Screened-Space-Charge Transferred-Electron Oscillators.** IEEE Elec D 6(1):50-53, Jan 1985.
- Dawson S. W., Riera J. R., Stafford E. K., **CTNE Undersea Lightwave Inter-Island System.** J Lightw T 2(6):773-778, Dec 1984.
- Deimel P. P., **Calculations for Integral Lenses on Surface-Emitting Diodes.** Appl Optics 24(3):343-348, Feb 1 1985.
- Dragone C. **A Rectangular Horn of Four Corrugated Plates.** IEEE Antenn 33(2):160-164, Feb 1985.
- Dunlop A. E., Kernighan B. W., **A Procedure for Placement of Standard-Cell VLSI Circuits.** IEEE Comp A 4(1):92-98, Jan 1985.
- Dupuis R. D., Temkin H., Hopkins L. C., **InGaAsP/InP Double Heterostructure Lasers Grown by Atmospheric-Pressure MOCVD.** Electr Lett 21(2):60-62, Jan 17 1985.
- Dutta N. K., Napholtz S. G., Yen R., Brown R. L., Shen T. M., Olsson N. A., Craft D. C., **Fabrication and Performance Characteristics of InGaAsP Multiquantum Well Double Channel Planar Buried Heterostructure Lasers.** Appl Phys L 46(1):19-21, Jan 1 1985.
- Dyer C. K., **Improved Cathodes for Industrial Electrolytic Hydrogen Production.** Int J Hyd E 9(12):993-995, 1984.
- Dyer C. K., **Improved Nickel Anodes for Industrial Water Electrolyzers.** J Elchem So 132(1):64-67, Jan 1985.
- Feldman R. D., Hart R. M., Oron M., Lum R. M., Ballman A. A., **Effects of Zinc Doping of the Antireflect Layer on 1.55 μ m InGaAsP/InP Lasers.** J Appl Phys 57(3):723-726, Feb 1 1985.
- Fromme J. L., Tremblay M. D., **Terminal Transmission Equipment (TTE) for the SL Undersea Lightwave System.** J Lightw T 2(6):1002-1006, Dec 1984.
- Gallagher P. K., **Temperature Calibration of a Mass Spectrographic Evolved Gas-Analysis System.** Thermoc Act 82(2):325-334, Dec 15 1984.
- Gibbs H. M. et al., **Semiconductor Nonlinear Etalons.** Phi T Roy A 313(1525):245-248, Dec 18 1984.
- Goodman D. J., Sundberg C. E., **The Effect of Channel Coding on the Efficiency of Cellular Mobile Radio Systems (Letter).** IEEE Commun 33(3):288-291, Mar 1985.
- Greenberger A. J., **Digital Transversal Filter Architecture.** Electr Lett 21(3):86-88, Jan 31 1985.
- Hegarty J., Jackson K. A., **High-Speed Modulation and Switching With Gain in a GaAlAs Traveling-Wave Optical Amplifier.** Appl Phys L 45(12):1314-1316, Dec 15 1984

- Henry C. H., Kazarinov R. F., Logan R. A., Yen R., **Observation of Destructive Interference in the Radiation Loss of Second-Order Distributed Feedback Lasers.** IEEE J Q El 21(2):151-154, Feb 1985.
- Hill D. D., **ICON—A Tool for Design at Schematic, Virtual Grid, and Layout Levels.** IEEE Des T 1(4):53-60, Nov 1984.
- Ihm J., **Urbach Tails and the Structure of Chalcogenide Glasses.** Sol St Comm 53(3):293-296, Jan 1985.
- Kaufman S., Reynolds R.L., Loeffler G. C., **An Optical Switch for the SL Undersea Lightwave System.** J Lightw T 2(6):975-979, Dec 1984.
- Kazarinov R. F., Henry C. H., **Second-Order Distributed Feedback Lasers With Mode Selection Provided by First-Order Radiation Losses.** IEEE J Q El 21(2):144-150, Feb 1985.
- Kazovsky L. G., **An Optical Rain Gauge Based on Forward Scattering.** IEEE Geosci 23(2):124-131, Mar 1985.
- Kiehl R. A., Gossard A. C., **Complementary P-MODFET and n-HB MESFET (Al, Ga) as Transistors.** IEEE Elec D 5(12):521-523, Dec 1984.
- Kim O. K., Dutt B. V., McCoy R. J., Zuber J. R., **A Low Dark-Current, Planar InGaAs P-I-N Photodiode With a Quaternary InGaAsP Cap Layer.** IEEE J Q El 21(2):138-143, Feb 1985.
- Koch T. L., Coldren L. A., **Optimum Coupling Junction and Cavity Lengths for Coupled-Cavity Semiconductor Lasers.** J Appl Phys 57(3):740-754, Feb 1 1985.
- Koehler B. G., Bowers, J. E., **In-Line Single-Mode Fiber Polarization Controllers at 1.55, 1.30, and 0.63 μm .** Appl Optics 24(3):349-353, Feb 1 1985.
- Lee C. M., Soukup H., **An Algorithm for CMOS Timing and Area Optimization.** IEEE J Soli 19(5):781-787, Oct 1984.
- Lee T. P., Burrus C. A., Wilt D. P., **Measured Spectral Linewidth of Variable-Gap Cleaved-Coupled-Cavity Lasers.** Electr Lett 21(2):53-54, Jan 17 1985.
- Lefevre B. G. et al., **Intermetallic Compound Growth on Tin and Solder Platings on Cu Alloys.** Wire J Int 18(1):66-71, Jan 1985.
- Levine B. F., Bethea C. G., Campbell J. C., **Room-Temperature 1.3- μm Optical-Time Domain Reflectometer Using a Photon-Counting InGaAs/InP Avalanche Detector.** Appl Phys L 46(4):333-335, Feb 15 1985.
- Levine B. F., Bethea C. G., Cohen L. G., Campbell J. C., Morris G. D., **Optical-Time Domain Reflectometer Using a Photon-Counting InGaAs/InP Avalanche Photodiode at 1.3 μm .** Electr Lett 21(2): 83-84, Jan 17 1985.
- Lieneweg U., Bean J. C., **Space-Charge Behavior of Thin-MOS Diodes With MBE-Grown Silicon Films.** Sol St Elec 27(10):867-880, Oct 1984.
- Lin C., Eisenstein G., Burrus C. A., Tucker R. S., **Fine Structure of Frequency Chirping and FM Sideband Generation in Single-Longitudinal-Mode Semiconductor Lasers Under 10-GHz Direct Intensity Modulation.** Appl Phys L 46(1):12-14, Jan 1 1985.
- Lu N. C. C., Lu C. Y., **IV Characteristics of Polysilicon Resistors at High Electric Field and the Non-Uniform Conduction Mechanism.** Sol St Elec 27(8-9):797-805, Aug-Sep 1984.
- Magnea N., Petroff P. M., Capasso F., Logan R. A., Foy P. W., **Microplasma Characteristics in InP-In_{0.53}Ga_{0.47}As Long Wavelength Avalanche Photodiodes.** Appl Phys L 46(1):66-68, Jan 1 1985.
- Manalio A. A., **Simulation of the Steady-State Behavior of Crystal-Controlled Oscillators Using the Watand Computer-Aided-Design Program.** IEEE Instr 34(1):47-51, Mar 1985.
- Marcuse D., **Computer Simulation of Laser Photon Fluctuations—Coupled-Cavity Lasers.** IEEE J Q El 21(2):154-161, Feb 1985.
- Marcuse D., **Computer-Simulation of Laser Photon Fluctuations—DFB Lasers.** IEEE J Q El 21(2):161-167, Feb 1985.
- McCaughan L., **Recent Results With Long Wavelength Ti-LiNbO₃ Directional Coupler Optical Switches and Switch Arrays.** P Soc Photo 517:246-248, 1985.
- McNulty J. J., **A 150-km Repeaterless Undersea Lightwave System Operating at 1.55 μm .** J Lightw T 2(6):787-791, Dec 1984.
- Michejda J., Kim S. K., **A Precision CMOS Bandgap Reference.** IEEE J Soli 19(6):1014-1021, Dec 1984.

- Miller L. E., **Ultrahigh-Reliability Ultrahigh-Speed Silicon Integrated Circuits for Undersea Optical Communications Systems.** *J Lightw T* 2(6):939-944, Dec 1984.
- Minkoff J., **The Role of AM-to-PM Conversion in Memoryless Nonlinear Systems.** *IEEE Commun* 33(2):139-144, Feb 1985.
- Olsson N. A., Hegarty J., Logan R. A., Johnson L. F., Walker K. L., Cohen L. G., Kasper B. L., Campbell J. C., **68.3-km Transmission With 1.37-Tbit/km/s Capacity Using Wavelength Division Multiplexing of Ten Single-Frequency Lasers at 1.5 μ m.** *Electr Lett* 21(3):105-106, Jan 31 1985.
- Penna T., Tell B., Liao A. S. H., Bridges T. J., Burkhardt G., **Ion Implantation of Si and Se Donors in $\text{In}_{0.53}\text{Ga}_{0.47}\text{As}$.** *J Appl Phys* 57(2):351-354, Jan 15 1985.
- Perry M. W., Reinold G. A., Yeisley P. A., **Physical Design of the SL Branching Repeater.** *J Lightw T* 2(6):889-894, Dec 1984.
- Phillips J. C., Thorpe M. F., **Constraint Theory, Vector Percolation and Glass Formation.** *Sol St Comm* 53(8):699-702, Feb 1985.
- Pierce J. R., Kompfner R., **Trans-Oceanic Communication by Means of Satellites (Reprinted From Proc. IRE, 47, pp. 372-80, 1959).** *P IEEE* 72(12):1705-1713, Dec 1984.
- Pinczuk A., **Light-Scattering by Two-Dimensional Electron Systems in Semiconductors.** *J Physique* 45(NC-5):477-487, Apr 1984.
- Rosenberg R. L., Chamzas C., Fishman D. A., **Timing Recovery With Saw Transversal Filters in the Regenerators of Undersea Long-Haul Fiber Transmission Systems.** *J Lightw T* 2(6):917-925, Dec 1984.
- Ross D. G., Paski R. M., Ehrenberg D. G., Homsey G. M., **A Highly Integrated Regenerator for 295.6-Mbit/s Undersea Optical Transmission.** *J Lightw T* 2(6):895-900, Dec 1984.
- Runge P. K., Trischitta P. R., **The SL Undersea Lightwave System.** *J Lightw T* 2(6):744-753, Dec 1984.
- Sabnani K., Schwartz M., **Multidestination Protocols for Satellite Broadcast Channels.** *IEEE Commun* 33(3):232-240, Mar 1985.
- Shimer J. A., Holbrook W. R., Reynolds C. L., Thompson C. W., Olsson N. A., Temkin H., **Self-Aligned Rib-Waveguide Large Optical Cavity AlGaAs Laser for High-Power Single-Mode Operation.** *J Appl Phys* 57(3):727-731, Feb 1 1985.
- Snodgrass M. L., Klinman R., **A High-Reliability High-Sensitivity Lightwave Receiver for the SL Undersea Lightwave System.** *J Lightw T* 2(6):968-974, Dec 1984.
- Swartzlander E. E., Young W. K. W., Joseph S. J., **A Radix 4 Delay Commutator for Fast Fourier Transform Processor Implementation.** *IEEE J Soli* 19(5):702-709, Oct 1984.
- Szymanski T. G., **Dogleg Channel Routing is NP-Complete.** *IEEE Comp A* 4(1):31-41, Jan 1985.
- Tamari N. et al., **Characteristics of Tin and Cadmium Doping in Liquid-Phase Epitaxial Grown InGaAsP.** *J Appl Phys* 57(2):310-317, Jan 15 1985.
- Tomita A., Lemaire P. J., **Hydrogen-Induced Loss Increases in Germanium-Doped Single-Mode Optical Fibers—Long-Term Predictions.** *Electr Lett* 21(2):71-72, Jan 17 1985.
- Tsang W. T., Logan R. A., Olsson N. A., Johnson L. F., Henry C. H., **Heteroepitaxial Ridge Overgrown Distributed Feedback Laser at 1.5 μ m.** *Appl Phys L* 45(12):1272-1274, Dec 15 1984.
- Vonseggern H., **Improved Surface Voltage Uniformity on Electrets Obtained by Modified Corona Charging Method.** *IEEE Ind Ap* 20(6):1623-1626, Nov-Dec 1984.
- Wagner R. E., **Future 1.55- μ m Undersea Lightwave Systems.** *J Lightw T* 2(6):1007-1015, Dec 1984.
- Wang Y. T., Morris R. J. T., **Load Sharing in Distributed Systems.** *IEEE Comput* 34(3):204-218, Mar 1985.
- Williams L. M., **Plasma Enhanced Chemical Vapor Deposition of Titanium Dioxide Films.** *Appl Phys L* 46(1):43-45, Jan 1 1985.
- Wilson R. B., Besomi P., Nelson R. J., **Investigation of Melt Carry-Over During Liquid-Phase Epitaxy. 1. Growth of Indium Phosphide.** *J Elchem So* 132(1):172-176, Jan 1985.

Wood T. H., Burrus C. A., Miller D. A. B., Chemla D. S., Damen T. C., Gossard A. C., Wiegmann W., **131 PS Optical Modulation in Semiconductor Multiple Quantum Wells (MQWS) (Letter)**. *IEEE J Q El* 21(2):117-118, Feb 1985.

MANAGEMENT/ECONOMICS

Fishburn P. C., Willig R. D., **Transfer Principles in Income Redistribution**. *J Public Ec* 25(3):323-328, Dec 1984.

Ross I. M., **R and D for a Competitive Edge**. *Res Manag* 28(1):6-8, Jan-Feb 1985.

PHYSICAL SCIENCES

Aeppli G., Hauser J. J., Shirane G., Uemura Y. J., **Spin Correlations in a Concentrated Metallic Spin Glass**. *Phys Rev L* 54(8):843-846, Feb 25 1985.

Agrawal G. P., Dutta N. K., **Polarization Characteristics of Distributed Feedback Semiconductor Lasers**. *Appl Phys L* 46(3):213-214, Feb 1 1985.

Alferness R. C., Joyner C. H., Divino M. D., Buhl L. L., **InGaAsP/InP Wave-Guide Grating Filters for $\lambda = 1.5 \mu\text{m}$** . *Appl Phys L* 45(12):1278-1280, Dec 15 1984.

Andrews L., Bondybey V. E., English J. H., **FTIR Spectra of (HF)_n Species in Solid Neon**. *J Chem Phys* 81(8):3452-3457, Oct 15 1984.

Axe J. D. et al., **Neutron-Scattering Study of the Pressure-Induced Phase-Transformation in ReO₃**. *Phys Rev B* 31(2):663-667, Jan 15 1985.

Azbel M. Y., **Dehaas-VanAlphen, Quantized Hall and Meissner Effects**. *Sol St Comm* 53(2):147-150, Jan 1985.

Baker G. L., Bates F. S., **Synthesis of Polyacetylene Block Graft Copolymers**. *Macromolec* 17(12):2619-2626, Dec 1984.

Bates F. S., **Block Copolymers Near the Microphase Separation Transition. 2. Linear Dynamic Mechanical Properties**. *Macromolec* 17(12):2607-2613, Dec 1984.

Bedeaux D., Weeks J. D., **Correlation Functions in the Capillary Wave Model of the Liquid Vapor Interface**. *J Chem Phys* 82(2):972-979, Jan 15 1985.

Belfiore L. A., Schilling F. C., Tonelli A. E., Lovinger A. J., Bovey F. A., **Magic Angle Spinning C-13 NMR Spectroscopy of 3 Crystalline Forms of Isotactic Poly(1-Butene)**. *Macromolec* 17(12):2561-2565, Dec 1984.

Bishop D. J., Batlogg B., Varma C. M., Bucher E., Fisk Z., Smith J. L., **Ultrasonic Attenuation and Sound Velocity in UPt₃**. *Physica B&C* 126(1-3):455-456, Nov 1984.

Bloembergen N., Zou Y. H., Rothberg L. J., **Collision-Induced Hanle Resonances of KiloHertz Width in Phase-Conjugate Four-Wave Light Mixing**. *Phys Rev L* 54(3):186-188, Jan 21 1985.

Bondybey V. E., English J. H., **Laser-Induced Fluorescence of the Calcium Dimer in Supersonic Jet—The Red Spectrum of Ca²**. *Chem P Lett* 111(3):195-200, Nov 2 1984.

Bovey F. A., Jelinski L. W., **The Observation of Chain Motion in Macromolecules by C-13 and H₂ Nuclear Magnetic-Resonance Spectroscopy**. *J Phys Chem* 89(4):571-583, Feb 14 1985.

Bowers J. E., Tsang W. T., Koch T. L., Olsson N. A., Logan R. A., **Microwave Intensity and Frequency Modulation of Heteroepitaxial-Ridge-Overgrown Distributed Feedback Lasers**. *Appl Phys L* 46(3):233-365, Feb 1 1985.

Brand H. R. et al., **Codimension-2 Bifurcations for Convection in Binary Fluid Mixtures**. *Phys Rev A* 30(5):2548-2561, Nov 1984.

Brand H. R., Cladis P. E., Finn P. L., **Helioelectric-Ferroelectric Transition Mediated by a Tilt-Suppressing Intermediate Phase in Liquid Crystals**. *Phys Rev A* 31(1):361-365, Jan 1985.

Bruch M. D., Bovey F. A., Cais R. E., **Microstructure Analysis of Poly(Vinyl Fluoride) by Flurine-19 Two-Dimensional J-Correlated NMR Spectroscopy**. *Macromolec* 17(12):2547-2551, Dec 1984.

- Cais R. E., Kometani J. M., **Synthesis of Pure Head-to-Tail Poly(Trifluoroethylenes) and Their Characterization by 470-MHz F-19 NMR.** *Macromolec* 17(10):1932-1939, Oct 1984.
- Carroll P. J. et al., **The Distribution of Relaxation Frequencies From Photon-Correlation Spectroscopy Near the Glass Transition.** *J Chem Phys* 82(1):9-13, Jan 1 1985.
- Cava R. J., Rietman E. A., **Ionic Conductivity of Beta-AgI.** *Phys Rev B* 30(12):6896-6902, Dec 15 1984.
- Chabal Y. J., Patel C. K. N., **Infrared-Absorption in A-Si-H—First Observation of the Gas-Solid Transition of Occluded Molecular H₂.** *Physica B&C* 126(1-3):461-462, Nov 1984.
- Chiu T. H., Tsang W. T., Chu S. N. G., Shah J., Ditzenberger J. A., **Molecular-Beam Epitaxy of GaSb_{0.5}As_{0.5} and Al_xGa_{1-x}Sb_yAs_{1-y} Lattice Matched to InP.** *Appl Phys L* 46(4):408-410, Feb 15 1985.
- Citrin P. H., **Bond Lengths and Coordination Numbers From L2,3-Edge Versus K-Edge Surface Extended X-Ray-Absorption Fine-Structure.** *Phys Rev B* 31(2):700-721, Jan 15 1985.
- Comin F., Incochia L., Lagarde P., Rossi G., Citrin P. H., **Local Atomic Structure of a Clean Surface by Surface Extended X-Ray Absorption Fine-Structure-Amorphized Si.** *Phys Rev L* 54(2):122-125, Jan 14 1985.
- Cross M. C., Bhatt R. N., **Diagonalization of an Exchange Hamiltonian for 16 He-3 Spins.** *J L Temp Ph* 57(5-6):573-587, Dec 1984.
- Derby J. J., Brown R. A., Geyling F. T., Jordan A. S., Nikolakopoulou G. A., **Finite-Element Analysis of a Thermal-Capillary Model for Liquid Encapsulated Czochralski Growth.** *J Elchem So* 132(2):470-482, Feb 1985.
- Dicenzo S. B., Bennett P. A., Tribula D., Thiry P., Wertheim G. K., Rowe J. E., **Structure of Sn/Ge(111) From Low-Energy Electron Diffraction and Photoemission Studies.** *Phys Rev B* 31(4):2330-2337, Feb 15 1985.
- Downey P. M., Martin R. J., Nahory R. E., Lorimor O. G., **High-Speed, Ion Bombarded InGaAs Photoconductors.** *Appl Phys L* 46(4):396-398, Feb 15 1985
- Dudderar T. D., Gilbert J. A., **Real-Time Holographic Interferometry Through Fiber Optics.** *J Phys E* 18(1):39-43, Jan 1985.
- Dyer C. K. **New Electrochemical Process for Making Ni/Ni Hydroxide Battery Electrodes.** *J Elchem So* 132(1):13-18, Jan 1985.
- Eisenstein J. P., Stormer H. L., Narayanamurti V., Gossard A. C., Wiegmann W., **Effect of Inversion Symmetry on the Band Structure of Semiconductor Heterostructures.** *Phys Rev L* 53(27):2579-2582, Dec 31 1984.
- Fisanick G. J., Gross M. E., Hopkins J. B., Fennell M. D., Schnoes K. J., Katzir A., **Laser-Initiated Microchemistry in Thin Films—Development of New Types of Periodic Structure.** *J Appl Phys* 57(4):1139-1142, Feb 15 1985.
- Fisher D. S., **Sliding Charge-Density Waves as a Dynamic Critical Phenomenon.** *Phys Rev B* 31(3):1396-1427, Feb 1 1985.
- Fleming R.M., Schneemeyer L. F., Moncton D.E., **Commensurate-Incommensurate Transition in the Charge-Density-Wave State of K_{0.30}MOO₃.** *Phys Rev B* 31(2):899-903, Jan 15 1985.
- Frerking M. A., Langer W. D., Wilson R. W., **Structure and Dynamics of the BOK Globule B335.** *Icarus* 61(1):22-26, Jan 1985.
- Gibson J. M., Treacy M. M. J., **The Effect of Elastic Relaxation on the Local Structure of Lattice-Modulated Thin Films.** *Ultramicros* 14(4):345-349, 1984.
- Girvin S. M., MacDonald A. H., Platzman P. M., **Collective-Excitation Gap in the Fractional Quantum Hall-Effect.** *Phys Rev L* 54(6):581-583, Feb 11 1985.
- Goldsmith P. F., **Bipolar Outflows in Dark Clouds.** *Astrophys J* 286(2):599-608, Nov 15 1984.
- Gooden R., Hellman M. Y., Hutton R. S., Winslow F. H., **Solid-State Photochemistry of Poly(Ethylene-Co-Carbon Monoxide)—Model Studies of Polyethylene Photochemistry.** *Macromolec* 17(12):2830-2837, Dec 1984.
- Graebner J. E., Allen L. C., Golding B., **Solid H₂ in a-Si-H at Low Temperatures.** *Phys Rev B* 31(2):904-912, Jan 15 1985.
- Griffiths J. E., Malyj M., Espinosa G. P., Remeika J. P., **Nonstoichiometric Selenium Rich Si_xSe_{1-x} Films.** *Sol St Comm* 53(7):587-590, Feb 1985.

- Haavasoja T., Narayanamurti V., Chin M. A., **Comment on Anomalous Dispersion and Scattering Rates for Multiphonon Spontaneous Decay in HE-II.** *J L Temp Ph* 57(1-2):55-59, Oct 1984.
- Haddon R. C., Roth H. D., **Homoconjugation in Radical Cations.** *Croat Chem* 57(5):1165-1176, 1984.
- Harris T. D., Williams A. M., **Fundamental Detection Limits in Spectrophotometric Analysis.** *Appl Spectr* 39(1):28-32, Jan-Feb 1985.
- Hasegawa A., **Plasma Heating by Alfvén Waves—Kinetic Properties of Magneto-hydrodynamic Disturbances.** *IAU Symp* (107):381-389, 1985.
- Hauser J. J., **Conductivity (ac and dc) in III-V Amorphous Semiconductors and Chalcogenide Glasses.** *Phys Rev B* 31(4):2133-2139, Feb 15 1985.
- Hilinski E. F., Masnovi J. M., Kochi J. K., Rentzepis P. M., **Role of Ion-Pairs in the Photochemistry of Electron-Donor Acceptor Complexes—Picosecond Spectroscopic Studies of Arene Tetracyanoethylene Systems.** *J Am Chem S* 106(26):8071-8077, Dec 26 1984.
- Kaufman S., Reynolds R. L., Loeffler G. C., **A Mechanical Optical Switch.** *P Soc Photo* 517:275-280, 1985.
- Kennel C.F. et al., **Perspectives on Space and Astrophysical Plasma Physics.** *IAU Symp* (107):537-552, 1985.
- Kevan S. D., Stoffel N. G., Smith N. V., **High-Resolution Angle-Resolved Photoemission Studies of the Surface States on Al(111) and Al(001).** *Phys Rev B* 31(4):1788-1795, Feb 15 1985.
- Klauder J. R. et al., **Universality of the Continuum Limit of Lattice Quantum Theories.** *Z Phys C* 26(1):149-155, 1984.
- Knoell R. V., Murarka S. P., **Epitaxial-Growth Induced by Phosphorus Tribromide Doping of Polycrystalline Silicon Films on Silicon.** *J Appl Phys* 57(4):1322-1327, Feb 15 1985.
- Kramer L., Hohenberg P. C., **Effect of Boundaries on Periodic Patterns.** *Lect N Phys* 210:63-74, 1984.
- Kuo C. Y., Kerl R. J., Patel N. D., Patel C. K. N., **Nonradiative Relaxation of Excited Vibrational States of Solid Hydrogen.** *Phys Rev L* 53(27):2575-2578, Dec 31 1984.
- Lake G., Pudritz R. E., **Ultrahigh Energy Cosmic-Ray Production by Current Disruption in Active Galactic Nuclei.** *IAU Symp* (107):471-473, 1985.
- Levinson M., Stavola M., Besomi P., Bonner W. A., **MFE Center—A Configurationally Bistable Defect in InP-Fe.** *Phys Rev E* 30(10):5817-5821, Nov 15 1984.
- Levy R. A. et al. **Properties of LPCVD Aluminum Films Produced by Disproportionation of Aluminum Monochloride.** *J Elchem So* 132(2):457-463, Feb 1985.
- Logan R. A., Temkin H., Merritt F. R., Mahajan S., **GaInAsP-InP Buried Heterostructure Formation by Liquid-Phase Epitaxy.** *Appl Phys L* 45(12):1275-1277, Dec 15 1984.
- Lum R. M., Glass A. M., Ostermayer F. W., Kohl P. A., Ballman A. A., Logan R. A., **Holographic Photoelectrochemical Etching of Diffraction Gratings in N-InP and n-GAInAsP for Distributed Feedback Lasers.** *J Appl Phys* 57(1):39-44, Jan 1 1985.
- Luryi S., **Hot-Electron Memory Effect in Double-Layered Heterostructures.** *Appl Phys L* 45(12):1294-1296, Dec 15 1984.
- Macrander A. T., Long J. A., Riggs V. G., Bloemeke A. F., **Electrical Characterization of Fe-Doped Semi-insulating InP Grown by Metalorganic Chemical Vapor Deposition.** *Appl Phys L* 45(12):1297-1298, Dec 15 1984.
- Martinez O. E., **Linear Measurement of Ultrashort Light Pulses by Phase-Contrast Optical Sweep.** *J Opt Soc B* 2(2):327-330, Feb 1985.
- Matsuoka S., **Prediction of Stress Strain Relationships in Glassy and Crystalline Polymers.** *Polym J* 17(1):321-335, 1985.
- McCrorry-Joy C., **Electrolytic and Chemical Precipitation of Germanium Dioxide From Oxalate Solution.** *Electr ACT* 30(1):51-55, Jan 1985.
- McRae E. G., **Structure of Si(111)-7 × 7.** *Surf Sci* 147(2-3):663-684, Nov 1984.
- McRae E. G., Petroff P. M., **Tests of Si(111)-7 × 7 Structural Models by Comparison With Transmission Electron-Diffraction Patterns.** *Surf Sci* 147(2-3):385-395, Nov 1984.

- Mills A. P., Crane W. S., **Beam-Foil Production of Fast Positronium.** *Phys Rev A* 31(2):593-597, Feb 1985.
- Nassau K., Levy R. A., Chadwick D. L. **Modified Phosphosilicate Glasses for VLSI Applications.** *J Elchem So* 132(2):409-415, Feb 1985.
- Nuzzo R. G., Dubois L. H., **The Chemisorption and Catalytic Properties of Nickel Intermetallic Compounds—Studies of Single Crystalline and High Surface-Area, Supported Materials.** *Appl Surf S* 19(1-4):407-413, Nov 1984.
- Porter J. D., Heller A., Aspnes D. E., **Experiment and Theory of Transparent Metal Films.** *Nature* 313(6004):664-666, Feb 21 1985.
- Powers L., Sessler J. L., Woolery G. L., Chance B., **CO Bond Angle Changes in Photolysis of Carboxymyoglobin.** *Biochem* 23(23):5519-5523, Nov 6 1984.
- Pregibon D., **Data Analytic Methods for Matched Case Control Studies.** *Biometrics* 40(3):639-651, Sep 1984.
- Reents W. D., Wood D. L., Mujse A. M., **Impurities in Silicon Tetrafluoride Determined by Infrared Spectrometry and Fourier-Transform Mass Spectrometry.** *Analyt Chem* 57(1):104-109, Jan 1985.
- Reichmanis E., Smith B. C., Gooden R., **Ortho-Nitrobenzyl Photochemistry—Solution vs. Solid-State Behavior.** *J Pol Sc PC* 23(1):1-8, Jan 1985.
- Reimann C. T., Boring J. W., Johnson R. E., Garrett J. W., Farmer K. R., Brown W. L., Marcantonio K. J., Augustyniak W. M., **Ion-Induced Molecular Ejection From D₂O Ice.** *Surf Sci* 147(1):227-240, Nov 1984.
- Ridge D. P. et al., **Relationship Between Structure and Reactivity for Metal Clusters Formed in Ion Molecule Reactions in Decacarbonyldirhenium.** *J Phys Chem* 89(4):612-617, Feb 14 1985.
- Rosamilia J. M. et al., **Coupled Photovoltaic Junction-Metal Dissolution Elements Under Mass and Light-Flux Variation.** *J Phys Chem* 89(4):677-681, Feb 14 1985.
- Rosamilia J. M., Miller B., **Maximum Power Spectroscopy of N-Type A-Si-H, C-Si, CdSe, and InP in Nonaqueous Photoelectrochemical Cells.** *J Elchem So* 132(2):349-353, Feb 1985.
- Rosenbaum T. F., Field S. B., Nelson D. A., Littlewood P. B., **Magnetic-Field-Induced Localization Transition in HgCdTe.** *Phys Rev L* 54(3): 241-244, Jan 21 1985.
- Rossetti R., Hull R., Gibson J. M., Brus L. E., **Excited Electronic States and Optical-Spectra of ZnS and CdS Crystallites in the Approximately 15 to 50Å^o Size Range—Evolution From Molecular to Bulk Semiconducting Properties.** *J Chem Phys* 82(1):552-559, Jan 1 1985.
- Seidel T. E., Lischner D. J., Pai C. S., Lau S. S., **Temperature Transients in Heavily Doped and Undoped Silicon Using Rapid Thermal Annealing.** *J Appl Phys* 57(4):1317-1321, Feb 15 1985.
- Shen T. M., **Temperature Behavior of Optical-Absorption in InGaAsP Lasers.** *Appl Phys L* 45(12):1262-1264, Dec 15 1984.
- Skolnick M. S., Harris T. D., Tu C. W., Brennan T.M., Sturge M. D., **Strongly Polarized Bound Exciton Luminescence From GaAs Grown by Molecular-Beam Epitaxy.** *Appl Phys L* 46(4):427-429, Feb 15 1985.
- Starnes W. H. et al., **Polyvinyl-Chloride Structural Segments Derived From Azobis(Isobutyronitrile).** *Macromolec* 17(12):2507-2512, Dec 1984.
- Stavola M., Dexter D. L., Knox R. S., **Electron-Hole Pair Excitation in Semiconductors via Energy Transfer From an External Sensitizer.** *Phys Rev B* 31(4):2277-2289, Feb 15 1985.
- Stillinger F. H., **Structural Equilibration in Condensed Phases.** *J Phys Chem* 88(26):6494-6499, Dec 20 1984.
- Sunil K. K., Jordan K. D., Raghavachari K., **The Importance of F-Functions and 3D Electron Correlation Effects in the Bonding in Cu₂.** *J Phys Chem* 89(3):457-459, Jan 31 1985.
- Svensson C., Abrahams S. C., **Large-Amplitude Molecular and Inversion Center Displacements in Ferroelastic 9-Hydroxy-1-Phenalenone at 298K.** *J Appl Crys* 17(Dec):459-463, Dec 1 1984.
- Tarascon J. M., Disalvo F. J., Waszczak J. V., Hull G. W., **Synthesis and Peculiar Properties of InMo₆S_{8-x}Se_x, TiMo₆S_{8-x}Se_x, and HgYMo₆S_{8-x}Se_x.** *Phys Rev B* 31(2):1012-1021, Jan 15 1985.

- Tarascon J. M., Waszczak J. V., Disalvo F. J., Johnson D. C., **Composition and Temperature-Induced Instabilities in the Chevrel Phases $\text{InMo}_6\text{S}_{8-x}\text{Se}_x$** . *Sol St Comm* 53(10):849-855, Mar 1985.
- Tersoff J., Hamann D. R., **Theory of the Scanning Tunneling Microscope**. *Phys Rev B* 31(2):805-813, Jan 15 1985.
- Tsang W. T., Chiu T. H., Kisker D. W., Ditzenberger J. A., **Molecular-Beam Epitaxial Growth of $\text{In}_{1-x}\text{Ga}_x\text{As}_{1-y}\text{Sb}_y$ Lattice Matched to GaSb**. *Appl Phys L* 46(3):283-285, Feb 1 1985.
- Vannice F. L. et al., **Light Scattering From Solubilized Polyacetylene**. *Macromolec* 17(12):2626-2629, Dec 1984.
- Venugopalan S., Dutta M., Ramdas A. K., Remeika J. P., **Magnetic and Vibrational Excitations in Rare-Earth Ortho-Ferrites—A Raman-Scattering Study**. *Phys Rev B* 31(3):1490-1497, Feb 1 1985.
- Wayda A. L., Dye J. L., Rogers R. D., **Divalent Lanthanoid Synthesis in Liquid-Ammonia. 1. The Synthesis and X-Ray Crystal Structure of $(\text{C}_5\text{ME}_5)_2\text{Yb}(\text{NH}_3)(\text{THF})$** . *Organometal* 3(11):1605-1610, Nov 1984.
- Weber T. A., Stillinger F. H., **Local Order and Structural Transitions in Amorphous Metal-Metalloid Alloys**. *Phys Rev B* 31(4):1954-1963, Feb 15 1985.
- Weinberg S. L., Carroll J. D., Cohen H. S., **Confidence Regions for INDSCAL Using the Jackknife and Bootstrap Techniques**. *Psychometri* 49(4):475-491, Dec 1984.
- Wertheim G. K., Dizenzo S. B., Buchanan D. N., Bennett P. A., **Core Electron-Binding Energy Shifts in Metal Clusters—Tin on Amorphous Carbon**. *Sol St Comm* 53(4):377-381, Jan 1985.
- Wescott L. D., **Molecular Structure and Polymerization Mechanism of Polyvinyl Chloride-Co-Carbon Monoxide**. *Macromolec* 17(12):2501-2507, Dec 1984.
- Wudl F. et al., **Reactions of Dimethylselenadiazole and Alkyltin Derivatives**. *J Orgmet Ch* 280(2):197-201, Jan 29 1985.
- Zirngibl E. et al., **Direct Observation of Intraionic and Interconfigurational Excitations in an Intermediate-Valence Compound by Raman Spectroscopy**. *Phys Rev L* 54(3):213-216, Jan 21 1985.

SOCIAL AND LIFE SCIENCES

- Suh S. Y., Craighead H. G., **Optical Writing Mechanism of Textured Media**. *Appl Optics* 24(2):208-214, Jan 15 1985.
- Wilkinson L. C., Wilkinson A. C., Spinelli F., Chiang C. P., **Metalinguistic Knowledge of Pragmatic Rules in School-Age Children**. *Child Dev* 55(6):2130-2140, Dec 1984.

SPEECH/ACOUSTICS

- Fahey P. F., Allen J. B., **Nonlinear Phenomena as Observed in the Ear Canal and at the Auditory Nerve**. *J Acoust So* 77(2):599-612, Feb 1985.
- Holtzman J. M., **Automatic Speech Recognition Error No Decision Tradeoff Curves (Letter)**. *IEEE Acoust* 32(6):1232-1235, Dec 1984.

AT&T TECHNICAL JOURNAL is abstracted or indexed by *Abstract Journal in Earthquake Engineering, Applied Mechanics Review, Applied Science & Technology Index, Chemical Abstracts, Computer Abstracts, Current Contents/Engineering, Technology & Applied Sciences, Current Index to Statistics, Current Papers in Electrical & Electronic Engineering, Current Papers on Computers & Control, Electronics & Communications Abstracts Journal, The Engineering Index, International Aerospace Abstracts, Journal of Current Laser Abstracts, Language and Language Behavior Abstracts, Mathematical Reviews, Science Abstracts (Series A, Physics Abstracts; Series B, Electrical and Electronic Abstracts; and Series C, Computer & Control Abstracts), Science Citation Index, Sociological Abstracts, Social Welfare, Social Planning and Social Development, and Solid State Abstracts Journal*. Reproductions of the Journal by years are available in microform from University Microfilms, 300 N. Zeeb Road, Ann Arbor, Michigan 48106.

